Control of Wnt Trans-Synaptic Signaling by Secreted Extracellular Regulators

By

Danielle Lauren Kopke

Dissertation

Submitted to the Faculty of the

Graduate School of Vanderbilt University

in partial fulfillment of the requirements

for the degree of

DOCTOR OF PHILOSOPHY

in

Biological Sciences

February 29, 2020

Nashville, Tennessee

Approved:

Kendal Broadie, Ph.D.

Katherine Friedman, Ph.D.

Ethan Lee, Ph.D.

Douglas McMahon, Ph.D.

Maulik Patel, Ph.D.

PREFACE

I didn't do that well in high school biology class, so I figured science just wasn't my "thing". Fast forward to college application time. I didn't know what subject I wanted to study so I applied to a few colleges in Michigan (where I had lived all my life). I decided on Central Michigan University, where my parents fell in love (with the school and each other). Freshman year I took an assortment of introductory classes to obtain a smattering of knowledge about each subject, hoping that I would find my passion. Among the list of classes included "Intro to Painting", where I was the only non-art major. I had to work very hard in that class and spent late nights in the studio only to obtain my worst grade all year. I enjoyed the process of using my creativity, working hard, and seeing the end result come to life. However, I ruled out art as my major because, once again, I thought that I was bad at it. Sophomore year came and went. I felt so lost that I did an internship in Disney World to get away for a semester. Upon my return to college, it was junior year…and the deadline to sign a major was looming. I opened the school bulletin and started crossing off majors that I was definitely not interested in. I came across biology and thought back to that high school experience and figured I'd give it another go. I signed up for the intro biology class/lab and ended up doing well and liking it. I scheduled a meeting with my academic advisor to sign a biology major. My advisor asked, "which one?" and I thought "Uh oh…another decision!?" The options were general biology, pre-medicine, microscopy, and ecology. I tried to sign for general biology but my advisor said I should pick something more unique/specialized. I was not interested in pre-medicine, and what the heck is microscopy? Ecology it is! I signed up for an ecology class but I didn't enjoy it and by this time I was panicking. I went back to my advisor and told him that I would try this "microscopy" thing. He took me down to the "dungeon" (basement) where the electron microscopes were housed and he introduced me to the Imaging Facility Director, Phil Oshel. Phil said there was one spot left for the "Transmission Electron Microscopy" class if I wanted to try it. In case you don't know – electron microscopy is a technique that uses

an electron beam (instead of light) to obtain high resolution **pictures** of organisms and fine structures to **answer biological questions**. It's ART and SCIENCE combined! The decision to enroll in this course changed the direction of my life. Needless to say, I fell in love with microscopy and majored in it. The unique skillset landed me several graduate school interviews and ultimately led me to the laboratory of Dr. Kendal Broadie at Vanderbilt University to use microscopy to study neuronal signaling using the best model organism, *Drosophila melanogaster*.

ACKNOWLEDGEMENTS

I want to start by thanking my undergraduate science professors and mentors from Central Michigan University (CMU). I credit Philip Oshel with all of my electron microscopy knowledge. He could see details in micrographs like nobody else could and I am grateful to have had his guidance. I would like to also acknowledge Dr. Joanne Dannenhoffer, Dr. Philip Hertzler, Dr. Stephen Juris, Dr. Eric Linton, Dr. Lori Reyna, Dr. Jennifer Schisa and Dr. Michelle Steinhilb for igniting my passion for science. Lastly, my mentor Dr. Stephen Roberts, who took me under his wing. For a microscopy class final project, I went door-to-door to faculty in the biology department asking if anybody needed electron microscopy imaging performed, and he said "Well…sure! I've been meaning to image these bumble bee muscles". The project earned me experience with microscopy and got me interested in studying insects while ultimately leading to my images getting published in a reference book. Dr. Roberts allowed me to work in his lab as an undergraduate on *Drosophila melanogaster* and let me start the Master's program at CMU while supporting my transition into a PhD program at Vanderbilt University (VU).

Here at VU, I would like to acknowledge my advisor, Dr. Kendal Broadie, as well as the entire Broadie laboratory, for their endless encouragement and motivation. I would like to specifically thank Emma Rushton, Cheryl Gatto, Caleb Doll, Patty Jumbo, Jim Sears, Neil Dani, Mary Lynn Dear, Tyler Kennedy, Shannon Leahy, Will Parkinson, Chunzhu Song, Dominic Vita, Darius Booth, Qing Xia Chen, Josh Mitchell, Sofia Lima, Anish Raman, Jarrod Shilts and Jacob Vest. There were many times that I did not believe in myself and I am thankful that I was surrounded by people that would remind me that I was beyond capable. I am grateful to Dr. R. Jason Pitts, with whom I taught alongside as a Teaching Assistant for three semesters, for his mentorship and enthusiasm for teaching science. We made a great teaching team. I would like to thank my Director of Graduate Studies and Thesis Committee Chair, Kathy Friedman, for being my role model as a woman in science. I am thankful to my Thesis Committee members Doug

McMahon, Maulik Patel, and Ethan Lee for the scientific guidance during my time as a graduate student. I would not have successfully navigated graduate school without the help of administrators in the Biological Sciences office including Alicia Goostree, Carol Wiley, and LaDonna Smith. I would like to thank everybody who has funded the experiences to aid my growth as a scientist. This includes the Biological Sciences Department, Gisela Mosig for the generous gift for traveling to conferences, the Graduate School gift for traveling to present my research, the Vanderbilt College of Arts and Science Summer Research Award to travel to another lab to learn a new technique and the National Institutes of Mental Health for money to support my graduate student stipend. I want to thank my mom Laura, dad Dave, and sister Kayla, though they don't fully understand why I put myself through this tough PhD program, they have supported my efforts and dreams in more ways than I can truly thank them for. Last but not least, I would like to thank my lab mate and life mate, Randy Golovin, for his unwavering support. My PhD research was enriched thanks to you, and my life is better because of you! Thank you so much, everyone, for believing in me.

FUNDING

This work was supported by:

National Institutes of Health R01 MH096832 to K.B. and F31 MH111144 to D.L.K.

PUBLICATIONS

1. **Kopke DL**, Leahy SN, Vita DJ, Lima SC, Zachary NL, Broadie K (2019) Carrier of Wingless (Cow) Regulation of *Drosophila* Neuromuscular Junction Development. Under Review.
2. Kim N, Kim S, Nahm M, **Kopke D**, Kim J, Cho E, Lee MJ, Lee M, Kim SH, Broadie K, Lee S (2019) BMP-dependent synaptic development requires Abi-Abl-Rac signaling of BMP receptor macropinocytosis. Nat Commun 10(1):684.
3. **Kopke DL**, Broadie K (2018) FM Dye Cycling at the Synapse: Comparing High Potassium Depolarization, Electrical and Channelrhodopsin Stimulation. J Vis Exp 135.
4. **Kopke DL**, Lima SC, Alexandre C, Broadie K (2017) Notum coordinates synapse development via extracellular regulation of Wingless trans-synaptic signaling. Development 144(19):3499-3510.
5. Jumbo-Lucioni PP, Parkinson WM, **Kopke DL**, Broadie K (2016) Coordinated movement, neuromuscular synaptogenesis and trans-synaptic signaling defects in Drosophila galactosemia models. Hum Mol Genet 25(17):3699-3714.

Table of Contents

Page

LIST OF FIGURES

Figure Page

LIST OF TABLES

Table Page

LIST OF SUPPLEMENTARY FIGURES

LIST OF ABBREVIATIONS

Ala	Alanine
ANOVA	Analysis of Variance
APC	Adenomatous polyposis coli
Arm	Armadillo
Arr	Arrow
Asn	Asparagine
Axin	Axis inhibition
AZ	Active zone
Brp	Bruchpilot
BMP	Bone morphogenic protein
$CaCl_2$	Calcium chloride
CaMKII	Ca^{2+}/Calmodulin-Dependent Protein Kinase II
CK1	Casein kinase 1
Co-IP	Co-immunoprecipitation
Cow	Carrier of Wingless
Cttn	Cortactin
Cys	Cysteine
Dkk	Dickkopf
DLG	Discs-large
Dlp	Dally-like protein
Drl	Derailed
Dsh	Dishevelled
Dvl	Dishevelled
ECM	Extracellular matrix

EJC	Excitatory junctional current
EJP	Excitatory junctional potential
Elav	Embryonic lethal abnormal vision
ER	Endoplasmic reticulum
Evi	Evenness interrupted
exWg	Extracellular Wg
FGF	Fibroblast growth factor
FNI	Frizzled nuclear import
Fz2	Frizzled 2
Fz2-C	Frizzled 2 C-terminus
GAG	Glycosaminoglycan
GECI	Genetically encoded calcium indicator
GluR	Glutamate receptor
GOF	Gain-of-function
GOI	Gene of interest
GPCR	G-protein couple receptor
GPI	Glycosylphosphatidylinositol
GRIP	Glutamate receptor interacting protein
GSK-3β	Glycogen Synthase Kinase 3 Beta
HEPES	4-(2-hydroxyethyl)-1-piperazineethanesulfonic acid
Hh	Hedgehog
HRP	Horse radish peroxidase
HS	Heparan sulfate
HSPG	Heparan sulfate proteoglycan
IGFBP-4	Insulin-like growth-factor binding protein 4
IP3	Inositol Triphosphate

JNK	c-Jun N-terminal Kinase
KCl	Potassium chloride
LAR	Leukocyte common antigen-related
LOF	Loss-of-function
LRP5/6	Low-density lipoprotein receptor-related protein 5/6
Magi	Membrane associated guanylate kinase
MAP1B	Microtubule Associated Protein 1B
MBOAT	Membrane-bound *O*-acyltransferase
ME	Microelectrode
mEJC	miniature EJC
mEJP	miniature EJP
$MgCl_2$	Magnesium chloride
MMP	Metalloproteinase
MMTV	Mouse mammary tumor virus
NaCl	Sodium chloride
Nesp1	Nesprin1
NLS	Nuclear localization sequence
NMJ	Neuromuscular junction
NRT	Neurotactin
PBS	Phosphate buffered saline
Pcan	Perlecan
PDE	Phosphodiesterase
PFA	Paraformaldehyde
PI-PLC	Phosphatidylinositol-specific phospholipase-C
PKG	Protein Kinase G
Por	Porcupine

PSD-95	Post synaptic density 95
PTM	Post-translational modification
Rac	Ras-related C3 botulinum toxin substrate 1
Rho	Rhodopsin
RNP	Ribonucleoprotein
RNAi	RNA interference
ROCK	Rho-associated Coiled-coil-containing Kinase 1
RPTP	Receptor protein tyrosine phosphatase
RSPO	R-spondin
SEM	Standard error of the mean
Ser	Serine
Sens	Senseless
Sfl	Sulfateless
SFRPs	Secreted frizzled-related proteins
Sgg	Shaggy
SOSTDC1	Sclerostin domain-containing 1
SP	Signal peptide
SPARC	Secreted protein acidic and rich in cysteine
Srt	Sprinter
SSR	Subsynaptic reticulum
SV	Synaptic vesicle
TEM	Transmission electron microscopy
TEVC	Two-electrode voltage clamp
Trol	Terribly reduced optic lobes
Vglut	Vesicular glutamate transporter
VNC	Ventral nerve cord

WB	Western Blot
Wg	Wingless
WIF-1	Wnt-inhibitory factor 1
Wls	Wntless
Wnt	Wingless-type MMTV integration site
WT	Wildtype

Chapter I

Introduction

Drosophila Neuromuscular Junction

The *Drosophila* larval neuromuscular junction (NMJ) is an exquisite model system for studying structural and functional synaptogenesis for a multitude of reasons, including relative stereotypical connectivity, ease of visualization, genetic malleability and conservation of genetic programs (Broadie and Bate, 1995). The neuromuscular system in abdominal segments A2-A7 consists of a 3-layered array of 30 named multinucleate muscle fibers in each hemisegment (Bate, 1990). 36 motoneurons project into each abdominal hemisegment via dorsal and ventral nerves (Landgraf and Thor, 2006). Each neuron makes a consistent muscle target choice, making the NMJ pattern invariant from animal to animal. The NMJ axon terminals contain large varicosities (termed synaptic boutons) that house the molecular machinery for glutamate neurotransmission. On the muscle side, the Discs-large (DLG) scaffold, *Drosophila* homolog of the mammalian postsynaptic density scaffolding protein (PSD-95), and two ionotropic glutamate receptor (GluR) classes, cluster at postsynaptic sites in elaborate membrane folds called the subsynaptic reticulum (SSR; Guan et al., 1996; Menon et al., 2013; Schuster et al., 1991). This NMJ pattern is first formed in the late embryo, but grows ~100-fold by the mature third instar, with the muscle size and synaptic bouton number scaling accordingly. This process of growth and functional development, termed synaptogenesis, involves the elegant orchestration of interwoven genetically programmed events that leads to the proper synaptic architecture and neurotransmission strength of the NMJ (Menon et al., 2013).

Drosophila NMJ Structure

In a stereotypical fashion, motor neuron axonal projections emanate from soma located in the ventral nerve cord (VNC), fasciculate to form peripheral bundled nerves, defasciculate at specified branch points, and synapse onto specific target muscle fibers (Fig. 1). The axonal terminals form synaptic boutons grouped into 3 classes (Type I, II and III) based on morphology, neurotransmitter type and degree of SSR elaboration (Menon et al., 2013). Type I boutons innervate all syncytial muscle fibers in a 1-to-1 fashion, and function by fast chemical synaptic transmission mediated by glutamate (Jan and Jan, 1976). Type II boutons contain both glutamate and the biogenic amine octopamine, and multiply innervate the body wall muscles (Monastirioti et al., 1995). Type III boutons contain neuropeptides such as proctolin, leucokinin I and insulin-like peptide (Anderson et al., 1988; Cantera and Nässel, 1992; Gorczyca et al., 1993). Type I boutons are further divided based on size into Ib (big) and Is (small). Each motor neuron terminal contains only one bouton class, but more than one terminal class can innervate a given muscle. My work focuses on type Ib glutamatergic NMJs on ventral longitudinal muscles 6/7 (muscles 6/7 share a single NMJ) and lateral longitudinal muscle 4 in the mature larval (wandering) third instar stage, when each NMJ arbor has a characteristic NMJ area, branch number and bouton number (Fig. 1). Therefore, these quantitative measurements are frequently used as a read-out for structural synaptogenesis. The commonly used horse radish peroxidase (HRP) antibody recognizes extracellular fucosylated N-glycans associated with the presynaptic neural membrane (Jan and Jan, 1982). The commonly used DLG antibody is used to visualize the postsynaptic SSR (Lahey et al., 1994). Together, these antibodies mark type Ib boutons allowing for the precise and reliable quantification of NMJ synaptic regions.

Mature type Ib boutons are fairly consistent in size and contain both HRP and DLG. Boutons can form at the end of an axon branch, or between two pre-existing boutons via asymmetric budding of a parent bouton, by symmetric division of a pre-existing mature bouton, or *de novo* from the axonal membrane (Zito et al., 1999). Despite the overall stereotypy of the

NMJ, boutons can appear with a variety of morphologies that point toward an aberrant developmental process or genetic perturbation. During normal development, dynamic filopodia-like projections (termed synaptopods) form, which can only be visualized via live imaging because they are too delicate to withstand fixation (Ataman et al., 2008). Developing terminals shed presynaptic debris (Fuentes-Medel et al., 2009), form immature ghost boutons (Ataman et al., 2006) and developmentally transient satellite boutons (Torroja et al., 1999), and manifest postsynaptic footprints lacking boutons (Eaton et al., 2002). Neuronal activity increases both presynaptic shedding/debris generation and ghost bouton formation (Ataman et al., 2008). Ghost boutons contain only HRP and either develop to become stabilized mature boutons (recruit DLG), or get eliminated (Ataman et al., 2008). Satellite boutons contain both HRP and DLG, but are much smaller than mature boutons (Torroja et al., 1999). Satellites most often bud off from a parent terminal bouton, but are also seen budding from the axon shaft. Footprints contain only DLG and represent presynaptic retractions that have not yet disassembled the postsynaptic compartment (Eaton et al., 2002). Synaptopods, ghosts, satellites and footprints are observed at a very low frequency at wildtype (WT) NMJs. Therefore, if they are observed at a high frequency in a mutant this provides information that a specific gene product is involved in a particular stage of NMJ structural synaptogenesis.

Synaptic bouton features at the ultrastructural level can be studied using transmission electron microscopy (TEM). TEM provides the resolution to visualize T-bar active zone (AZ) sites of synaptic vesicle (SV) fusion, with docked SVs clustered around (Dear et al., 2016). Synaptic ultrastructural features of note include AZ number/distribution, SV number/distribution, the proximity of readily releasable pool (RRP) SVs to AZ T-bars, the number/size/length of apposing postsynaptic SSR folds, and the distance of the SSR to the presynaptic membrane (Packard et al., 2002; Kamimura et al., 2013). The neuronal membrane is normally closely and directly juxtaposed to the SSR muscle membrane folds to enable rapid communication across the

synaptic cleft. In some mutants, there is extra space between the two membranes, termed "postsynaptic pockets" (Packard et al., 2002).

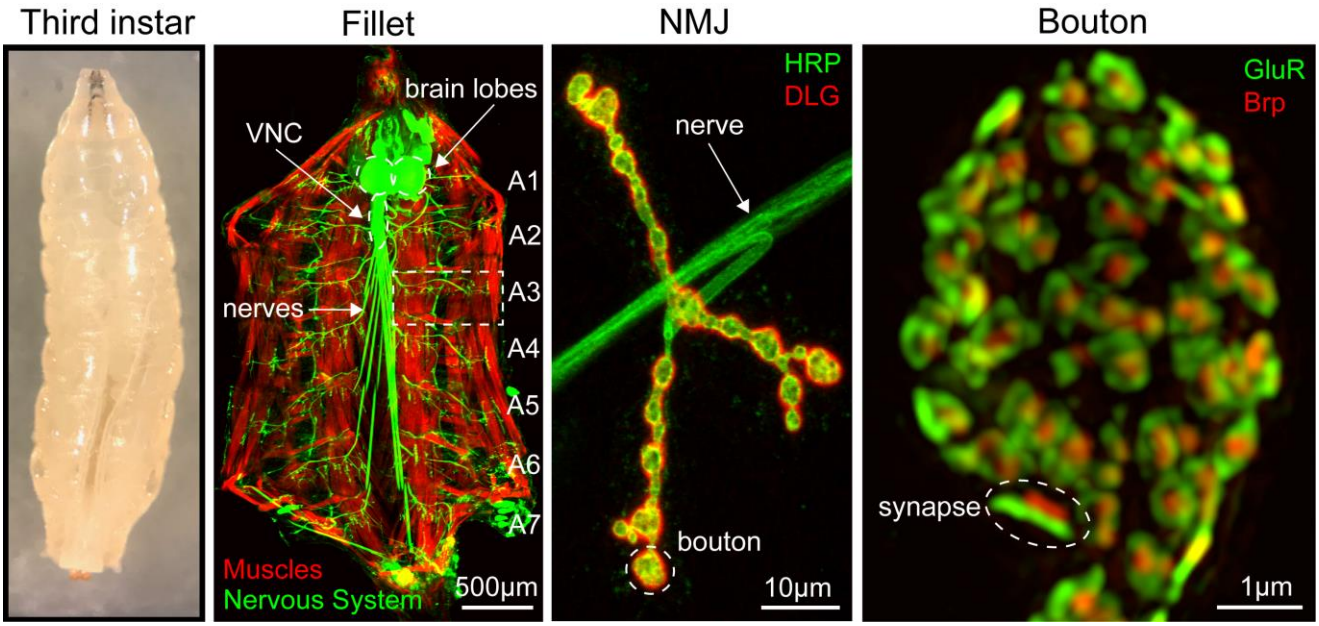

Fig. 1: *Drosophila* Larval NMJ Model Synapse

A third instar can be filleted to reveal the musculature and nervous system. The central nervous system (CNS) consists of two brain lobes and a ventral nerve cord (VNC), with nerve bundles emanating out to the periphery to form neuromuscular junctions (NMJs). The muscles are reiterated in 8 abdominal segments (A1-8). An NMJ consists of axonal varicosities (boutons), with presynaptic Bruchpilot (Brp) active zone (AZ) juxtaposed to postsynaptic glutamate receptors (GluRs) to form glutamatergic synapses.

Drosophila NMJ Function

At presynaptic AZs, the Bruchpilot (Brp) scaffold clusters Ca^{2+} channels and tethers SVs leading up to vesicular exocytosis (Kittel et al., 2006; Hallermann et al., 2010). SVs are separated into functionally distinct vesicle pools: readily releasable, recycling and reserve pools (Rizzoli and Betz, 2005). Vesicles in the ready pool are docked and primed for release, fusing rapidly upon the arrival of an action potential. The recycling pool consists of SVs that fuse and recycle more slowly upon physiological stimulation, typically comprising 10-20% of all vesicles (Denker and Rizzoli, 2010). The reserve pool contains vesicles that are least likely to fuse and are therefore only recruited upon high-frequency stimulation (HFS) after the recycling pool has been depleted (Rizzoli and Betz, 2005). Several SV recycling mechanisms are proposed including kiss-and-run, full fusion, bulk endocytosis and endosomal sorting. Kiss-and-run endocytosis is a mechanism where the vesicle fuses only transiently though a small protein pore (Stevens and Williams, 2000). Full fusion represents complete SV exocytosis by fully collapsing into the plasma membrane. Bulk endosomes, large membrane infoldings, form after HFS to compensate for the loss of many SVs released in quick succession (Clayton and Cousin, 2009). Lastly, endosomal sorting is when recently endocytosed SVs fuse with a sorting endosome from which new SVs will bud (Hoopmann et al, 2010). The SV pools are investigated with techniques such as FM dye loading (Kopke and Broadie, 2018). FM dyes are water-soluble, lipophilic dyes that are less fluorescent until they become bound to the outer leaflet of the cell membrane and become brightly fluorescent (Betz et al., 1992). If you bathe a synaptic terminal with FM dye and induce neural activity, neurotransmitter is released, FM dye is internalized in recycling SVs and boutons become brightly labeled (Fig. 15). Non-specific plasma membrane dye can be washed away, and the trapped dye then imaged to visualize “loaded” SVs. The terminal can be induced to release dye and imaged again to visualize “unloaded” SVs (Fig. 15). The unloaded/loaded ratio reveals SV cycling rate, and specific temporal paradigms can be used to study specific SV pools and/or types of SV recycling (Verstreken et al., 2008).

On the postsynaptic side, the muscle SSR houses both the glutamate receptor (GluR) and voltage-gated ion channels necessary for neurotransmission and amplification, respectively (Menon et al., 2013). Precise apposition of presynaptic AZs to postsynaptic GluR clusters is necessary for rapid and efficient glutamatergic signaling. *Drosophila* NMJ GluRs are non-N-methyl-D-aspartate (NMDA)-like heterotetrameric clusters containing GluRIIC/III, D and E subunits, and either GluRIIA or GluRIIB (Qin et al., 2005). GluRIIA and GluRIIB are both non-selective cation channels with high permeability to Ca^{2+}, but display distinct channel kinetics (DiAntonio et al., 1999; Han et al., 2015). To assess differences between these two receptor classes, double mutants were made and then rescued with either gene alone (DiAntonio et al., 1999). GluRIIA/B double mutants are embryonic lethal, but either receptor is sufficient for viability. Solely GluRIIA-expressing NMJs had a significantly larger SV quantal size than GluRIIB-expressing synapses (i.e. response to the spontaneous release of a single vesicle), but the response from the GluRIIA-type synapses was similar to WT (DiAntonio et al., 1999). Solely GluRIIA-expressing NMJs had a desensitization time course similar to WT at <20msec, whereas GluRIIB- synapses were nearly 10X faster, with a decay of ~2msec. Tinkering with the expression level of just one GluR class (A or B) in either a WT background or an otherwise *glurII* null background caused changes in SV quantal size, indicating that receptor density and subtype composition are determinants of quantal size (DiAntonio et al., 1999). Several genes have been shown to independently regulate GluRIIA vs. GluRIIB to cause changes in NMJ function.

GluR mobilization, localization and function are modulated by postsynaptic scaffolds as well as auxiliary channel subunits. For the scaffolds, PDZ domains play a key role in anchoring receptors in the membrane to underlying cytoskeletal filaments. The DLG scaffold was found to regulate GluR clustering, albeit not directly, as GluRs do not precisely localize with DLG and do not contain a PDZ-binding motif (Chen and Featherstone, 2005; Kim et al., 2012). In *dlg* mutants, the postsynaptic SSR develops more slowly and is less complex (Lahey et al., 1994). To best test synaptic functional changes, two-electrode voltage-clamp (TEVC) electrophysiology is used

(Guan et al., 2013). In this recording configuration, motor nerves are cut at the VNC and two microelectrodes (ME) are placed into a muscle cell. The muscle is clamped at a particular voltage (command voltage; V_C), with one ME sensing membrane voltage (V_m) while the other ME injects current to maintain the V_C (Guan et al., 2013). To measure the amplitude of nerve-evoked neurotransmission, the motor nerve is stimulated using a suction electrode to elicit an action potential-driven excitatory junctional current (EJC). The frequency and amplitude of miniature EJC (mEJC) events indicates spontaneous Ca^{2+}-independent single SV fusions in the absence of an action potential. An unchanged mEJC amplitude (quantal size) along with a change in EJC amplitude has classically been interpreted as a modification in presynaptic release properties, whereas a change in mEJC amplitude results from a postsynaptic receptor modification (Dudel and Kuffler, 1961). Functionally, *dlg* mutants have larger EJC amplitudes but no changes in mEJCs, indicating a change in the number of SVs released during stimulus (quantal content) (Budnik et al., 1996). Another way to study NMJ functional properties is using fluorescent Ca^{2+} reporters (Koldenkova and Nagai, 2013). For example, GCaMP reporters are genetically-encoded calcium indicator (GECI) fusion proteins of green fluorescent protein (GFP), calmodulin (CaM), and a M13 myosin light chain peptide (Wang et al., 2008). GCaMP has low basal fluorescence with a Ca^{2+}-dependent intramolecular conformational change that results in increased fluorescent intensity (Wang et al., 2008). GCaMP targeted to the postsynaptic NMJ has been used to study the functional properties of type I boutons (Newman et al., 2017). One huge advantage of GCaMP is spatial information of SV fusion events.

Using *Drosophila* to find genes regulating NMJ structure and function

The *Drosophila* NMJ is genetically tractable via an extensive and ever-growing genetic toolkit, including the recent use of the clustered regularly interspaced short palindromic repeat (CRISPR) gene editing technique (Bassett et al., 2013; Gratz et al., 2013), the transgenic binary

GAL4/UAS system (Fischer et al., 1988; Brand and Perrimon, 1993), and the use of live imaging reporter transgenes usually based on green fluorescent protein (GFP; Wang and Hazelrigg, 1994). CRISPR is a fairly new technology hijacked from prokaryotic organisms that allows for target-specific genome editing (Gilbert et al., 2013). Although CRISPR is a huge step forward, random mutagenesis *Drosophila* screens have provided us with most knowledge over the last several decades, and served as the basis for discovering many genes involved in structural and functional synaptogenesis, and will ever remain the primary means of discovery-based progress. The GAL4/UAS binary system allows for targeted expression of genes in a select cell or tissue. GAL4 encodes a yeast transcription factor that binds to an upstream activating sequence (UAS) promoter. In the "driver line", GAL4 is inserted downstream of a tissue-specific promoter from a gene of interest (GOI), and thus GAL4 is only expressed when/where that GOI is normally expressed (Brand and Perrimon, 1993). In the "responder line", UAS is inserted upstream of a construct to be expressed (e.g. an RNA interference (RNAi) construct; Montgomery et al., 1991). In this way, genes can be knocked down (KD) or overexpressed (OE) with tight spatiotemporal control. GFP is a protein that fluoresces when exposed to a specific wavelength of light, and can thus be used to transgenically tag a gene to visualize protein localization (Shimomura et al., 1962; Tsien, 1998). Using a combination of these genetic approaches, molecular pathways identified at the *Drosophila* NMJ have been repeatedly shown to be directly conserved in mammalian synapses. Indeed, most components of mammalian excitatory central brain synapses are present at *Drosophila* NMJs. In particular, the *Drosophila* glutamatergic NMJ contains many components conserved with mammalian glutamatergic brain synapses, including cell adhesion molecules (CAMs), membrane scaffolds, endocytic machinery, channels/receptors and *trans*-synaptic signaling pathways involved in directing the assembly of these diverse synaptic molecules (Menon et al., 2013). Of particular focus for this thesis are the Wnt ligands; a family of secreted cysteine-rich glycoproteins with roles in tissue patterning, cell proliferation, tissue homeostasis and synapse development (Steinhart and Angers, 2018). With a multitude of diverse functions,

misregulated Wnt signaling underlies many disease states spanning from cancers to developmental neurological disorders (Nusse and Clevers, 2017).

Wnt Signaling Ligands

The Wnt family was discovered in *Drosophila* (Sharma, 1973; Sharma and Chopra, 1976), with the first Wnt (mammalian Wnt-1) named *wingless* (*wg*). In a *wg* hypomorph, dorsal thorax (i.e. Notum) structures are duplicated, at the expense of the wings. In 1982, a *wg* homolog was discovered in mammals (Varmus and Nusse, 1982), but was not identified as such until several years later (Rijsewijk et al., 1987). The locus was found using a provirus, which can integrate at many sites in host genomes to cause tumor induction by retroviruses without oncogenes, and this strategy was therefore used to isolate novel oncogenes. A putative oncogene was found on mouse chromosome 15 via integration of the proviral mouse mammary tumor virus (MMTV), and the integration locus was named *int*-1 (Nusse et al., 1984). It was later realized that *int*-1 encodes a glycoprotein conserved with the previously identified *Drosophila wg* gene product, and the family of genes were therefore renamed Wnt (a mnemonic of “wingless” + “integration”; Nusse et al., 1991). Since then, numerous other Wnt family members have been discovered in both *Drosophila* and mammals (Nusse and Varmus, 2012).

In comparison to the 19 Wnts in mammals, *Drosophila* have 7 Wnts; *Wnt-1* (aka *wg*), *Wnt2*, *Wnt4*, *Wnt5*, *Wnt6*, *Wnt8* (aka *wntD*) and *Wnt10* (Miller, 2001; Table 1). Wnts are reliant on the multipass transmembrane protein Wntless (Wls)/Evenness interrupted (Evi)/Sprinter (Srt) for trafficking to the plasma membrane (Bänziger et al., 2006; Bartscherer et al., 2006; Goodman et al., 2006). To date, only Wnt5, Wnt2 and Wg have reported roles at the *Drosophila* NMJ (Liebl et al., 2008; Liebl et al., 2010; Packard et al., 2002). Wg is expressed presynaptically in motor neurons (Packard et al., 2002), and also in NMJ-associated glia (Kerr et al., 2014), and secreted into the extracellular space of the synaptic cleft (synaptomatrix) to bind the Frizzled-2 (Fz2)

receptor in both autocrine and anterograde signaling. Wg signaling positively regulates NMJ growth, presynaptic bouton formation and expression/localization of postsynaptic GluRs (Packard et al., 2002). In contrast, Wnt2 is expressed postsynaptically by the muscle and secreted as a retrograde signal to bind an unknown receptor to regulate presynaptic structural development, such as NMJ branch number, as well as molecular differentiation, such as active zone (AZ) assembly localization regulating neurotransmission strength (Liebl et al., 2010). Finally, Wnt5 is likely secreted from neurons to signal through the Derailed (Drl) receptor expressed in postsynaptic muscle, and positively regulates NMJ growth and synapse density (Liebl et al., 2008). By far, the most widely studied Wnt is Wingless (Wg), which is the particular focus of this thesis, and will therefore be described in more detail in the following section.

Wg *Trans*-synaptic Signaling

The role of Wg *trans*-synaptic signaling in *Drosophila* NMJ structural synaptogenesis was first reported nearly 20 years ago (Packard et al., 2002), with several follow-up studies later indicating an importance for functional synaptogenesis as well (Ataman et al., 2008; Kerr et al., 2014). Canonical Wnt signaling components include Axis inhibition (Axin), Adenomatous polyposis coli (APC), Casein kinase 1 (CK1), Dishevelled (Dvl; Dsh in *Drosophila*), Glycogen synthase kinase 3β (GSK3β) and β-catenin, which in the absence of Wnt, form a "destruction complex" in the cytosol (Stamos and Weis, 2013). In the "off state", GSK3β phosphorylates β-catenin, which targets it to the proteosome for degradation. In the "on state", Wnt binds to the Fz2 receptor and a Low-density lipoprotein receptor-related protein 5/6 (LRP5/6) co-receptor to recruit Axin and Dvl to the membrane, while other components dissociate from the destruction complex (Stamos and Weis, 2013). β-catenin is then stabilized in the cytosol and translocates to the nucleus where it acts as a transcription factor to influence the expression of many genes. Interestingly, components of the canonical Wnt signaling pathway are not present at the NMJ, most notably the *Drosophila* homolog of β-catenin (Armadillo; Arm), which led to the discovery of

the 1) presynaptic divergent canonical pathway and 2) postsynaptic non-canonical pathway of Frizzled Nuclear Import (FNI; Fig. 2).

Presynaptically, Wg binding to Fz2 receptor results in synaptic bouton differentiation (Ataman et al., 2008; Franco et al., 2004). The *Drosophila* GSK3β homolog Shaggy (Sgg) was found in a screen to identify genes that control NMJ structure (Franco et al., 2004). Since GSK3β is a part of the canonical Wnt pathway, other proteins in that pathway were tested for at the NMJ via antibody or transgenic fluorescent labeling, and it was found that the *Drosophila* LRP5/6 homolog Arrow (Arr) and Dvl were also present (Miech et al., 2008). However, with the absence of Arm, the signaling cascade involving GSK3β could not be via a canonical pathway. Sgg is concentrated at the presynaptic side of the NMJ, and negatively regulates NMJ growth (Franco et al., 2004). Inhibition of Sgg led to an increase in the number of microtubule loops in the presynaptic terminal, suggesting a function inhibiting NMJ growth involving regulation of microtubule cytoskeletal dynamics. Indeed, epistasis experiments show that the Microtubule Associated Protein 1B (MAP1B) *Drosophila* homolog Futsch acts downstream of Sgg function (Franco et al., 2004). Thus, the presynaptic divergent canonical pathway involves Wg binding to the Fz2 receptor, activating Dvl to inhibit the Sgg GSK3β, and causing changes in synaptic microtubule dynamics via Futsch regulation to enable new bouton growth (Fig. 2).

Postsynaptically, Wg binding to Fz2 causes internalization of the receptor modulated by Shank-dependent cleavage of the C-terminus (Fz2-C; Harris et al., 2016; Mathew et al., 2005), by a currently unknown protease, and import of Fz2-C into the nucleus by Importin-β11 and -α2 (Mosca and Schwarz, 2010). This unusual mechanism was discovered when antibodies were made to both the Fz2 N-terminus (Fz2-N) and C-terminus (Fz2-C). Upon immunostaining with Fz2-C, punctae were seen inside muscle nuclei, were enriched in nuclei closest to the NMJ, and were largely excluded from regions of transcriptionally inactive DNA (Mathew et al., 2005). To test whether Fz2 is cleaved, *Drosophila* S2 cells were cultured with full-length Fz2, and lysates run on a Western blot were labeled for Fz2-N or Fz2-C. Two distinct protein bands were detected when

labeling with Fz2-C; a small 8-kD band and larger 83-kD band (Mathew et al., 2005). Importantly, when labeling with Fz2-N, the smaller band was not detected. A combination of *in vivo* internalization assays and blocking of endocytosis/retrograde transport mechanisms provided strong evidence that Fz2 is internalized from the plasma membrane, with Fz2-C carried by retrograde transport to the muscle nucleus (Mathew et al., 2005). Wg overexpression resulted in an increase in Fz2-C nuclear punctae, and Wg knockdown caused a decrease in these punctae (Mathew et al., 2005; Mosca and Schwarz 2010). To test whether Wg is required for the nuclear import of Fz2, Fz2-transfected S2 cells were treated with and without Wg-conditioned media. Fz2-C nuclear punctae were present only in cells treated with Wg (Mathew et al., 2005). In summary, Wg binds to Fz2 receptors in the postsynaptic muscle causing internalization of the receptor. Endocytosed vesicles travel toward a nearby nucleus, while the Fz2 C-terminus is cleaved and undergoes retrograde transport into the nucleus (Fig. 2). Since this discovery, the Fz2-C antibody has been used in numerous NMJ studies as a read-out for postsynaptic Wg signaling (Dani et al., 2012; Friedman et al., 2013; Kopke et al., 2017; Parkinson et al., 2016).

In numerous follow up studies, more molecular players in this Wg signaling pathway have been discovered. The Fz2-C receptor fragment is trafficked to the postsynaptic muscle nucleus via the PDZ protein glutamate receptor-interacting protein (GRIP; Ataman et al., 2006). Decreasing GRIP levels prevents the transport of endocytosed Fz2 receptors to the muscle nucleus, and co-immunoprecipitation (co-IP) studies show Fz2 interacts directly with PDZ domains of the GRIP protein (Ataman et al., 2006). The Fz2C nuclear foci contain large ribonucleoprotein (RNP) granules harboring synaptic transcripts, which export from the nucleus through nuclear envelope budding (Speese et al., 2012). Of the 19 mRNAs tested, 7 were present in the RNP particles including the PDZ proteins Partitioning defective 6 (Par6) and Membrane associated guanylate kinase (Magi), but excluding GluRIIC and Dlg (Speese et al., 2012). F-actin associated Nesprin1 (Nesp1) forms “railroad tracks” from the muscle nucleus to the NMJ for polarized transport of mRNAs to postsynaptic regions for local translation (Packard and Jokhi et

al., 2015). Polyribosomes have been observed in the SSR and local translation of GluRIIA has been suggested (Sigrist et al., 2000). In summary, the postsynaptic FNI pathway involves Wg binding to Fz2, a ligand-receptor complex being internalized, the C-terminus cleaved and imported into the nucleus, where it binds mRNAs to form RNPs (Fig. 2). The RNPs travel back to the membrane and may mediate local translation to facilitate the development and plasticity of synapses.

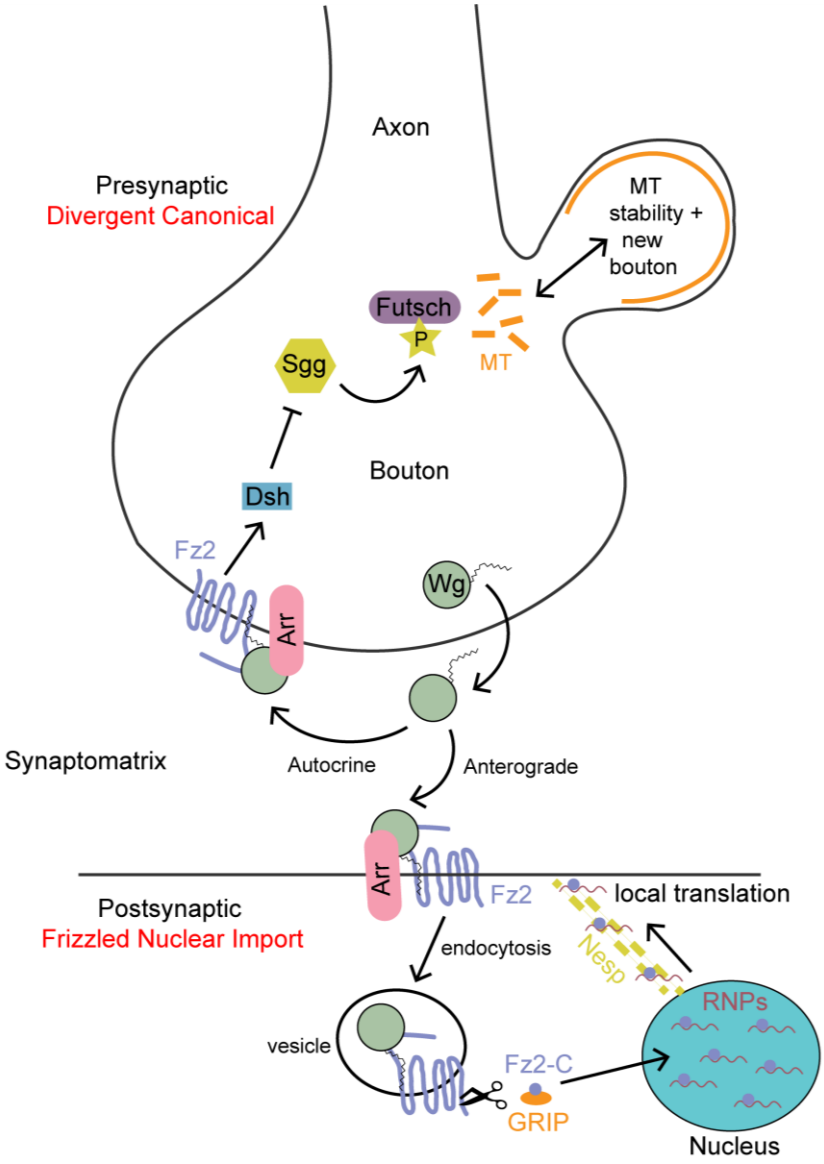

Fig. 2: Wg *trans*-synaptic signaling at the *Drosophila* NMJ

Wg is secreted from the presynaptic terminal and signals in both autocrine and anterograde fashions. The autocrine signaling is termed the "divergent canonical pathway" and involves Wg binding to receptor Frizzled-2 (Fz2) and co-receptor Arrow (Arr) to activate Dishevelled (Dsh), inhibit Shaggy (Sgg) and phosphorylate microtubule-associated Futsch to regulate synaptic microtubules in a dynamic fashion to control new bouton formation. The anterograde signaling is termed the "frizzled nuclear import pathway" (FNI), with Wg binding to Fz2 causing endocytosis of the ligand-receptor complex. The Fz2 C-terminus (Fz2-C) is then cleaved, and travels to the nucleus dependent on glutamate receptor interacting protein (GRIP). Nuclear Fz2-C binds to mRNAs to form ribonucleoprotein (RNP) particles, which travel towards postsynaptic sites along Nesprin1 (Nesp) "railroad tracks" containing F-actin. At NMJs, the mRNAs are thought to undergo local translation to drive the development of synaptic connections.

Wg Post-translational Modifications

Wnt ligands share a signature motif (C-K-C-H-G-(LIVMT)-S-G-*X*-C), 23-25 conserved cysteines, many highly charged amino acid residues, and several potential glycosylation sites (Zhai et al., 2004). Based on amino acid sequences alone, Wnt proteins should be soluble glycoproteins (Willert and Nusse, 2012). Historically, Wnts did not exhibit the properties expected of hydrophilic proteins, which led to the discovery of post-translational modifications (PTMs) rendering Wnts highly hydrophobic and strongly membrane-associated. All known Wnts (except Wnt8) undergo palmitoylation (Ching et al., 2008). The function of these modifications (0-2 lipidations and 2-4 glycosylations) differ among Wnts, but I focus here on Wg. Wg has two N-glycosylation sites at Asparagine residues Asn103 and Asn414 (Tanaka et al., 2002). To test the importance of these glycosylation events, Wg mutants were made with single or double amino acid substitutions, WgN103Q (N103 converted to Gln), WgN414S (N414 converted to Ser) and WgNN (combination; Tang et al., 2012). Wg activity was first measured in *Drosophila* S2 cells using a luciferase reporter. WgNN had ~20% decrease in autocrine signaling and ~40% decrease in paracrine signaling, considered relatively mild defects (Tang et al., 2012). To test *in vitro* findings, transgenic *Drosophila* expressing GAL4-inducible WT Wg or mutant Wg were generated. Glycosylation-deficient Wg proteins (both single and double mutants) were capable of patterning the embryonic epidermis (autocrine signaling) and cuticle (paracrine signaling). Moreover, WgNN induced downstream gene expression of the short-range Wg target Senseless (Sens) to levels similar to WT in the *Drosophila* wing disc (Tang et al., 2012). Therefore, Wg glycosylation *in vivo* does not appear important for secretion or signaling.

Two acyl groups can be attached to Wg in the endoplasmic reticulum (ER): palmitate at the first conserved cysteine residue (Cys93) near the N-terminus, and palmitoleic acid at an internal serine residue (Ser239) (Takada et al., 2006; Willert et al., 2003). These lipidation events are controlled by the ER-resident membrane-bound *O*-acyltransferase (MBOAT) Porcupine (Por; Kadowaki et al., 1996; Zhai et al., 2004). Single and double amino acid substitutions were made

to produce acyl-deficient Wg mutants: WgC93A (C93 converted to Ala), WgS239A (S239 converted to Ala) and WgCS (combination; Tang et al., 2012). Both single mutants are produced and glycosylated normally. Using similar assays as above, WgC93A was able to induce cell-autonomous and cell-non-autonomous signaling. Furthermore, it could induce target gene expression to similar levels as WT Wg. In contrast, WgS239A mutants showed a severe reduction of signaling activity in all assays (Tang et al., 2012). The poor signaling could be caused by a reduction in secretion or a reduction in affinity for the Fz2 receptor. Following WgS239A expression in the wing disc, extracellular Wg was detected and Wg could be retrieved from the media of WgS239A transfected S2 cells (Tang et al., 2012). These results strongly indicate that WgS239A is still secreted. Co-IP and Western blots were used to examine complex formation between WgS239A and Fz2 to reveal a 90% reduction in receptor binding. The WgCS double mutant failed to signal in every assay. Upon closer examination, WgCS did not reach the surface of the wing disc and was absent from S2 cell media (Tang et al., 2012). Therefore, Wg lipidation is essential for secretion, but single lipidation at either C93 or S239 is sufficient. In conclusion, N-glycosylation at Asn103 and Asn414 are dispensable for Wg secretion and signaling, either single lipidation of Wg is required for secretion, and lipidation at S239 increases Wg affinity for the Fz2 receptor.

Wnt Transport

Once secreted into the aqueous extracellular environment, the movement of Wnt is severely limited due to its hydrophobicity. Therefore, Wnt proteins can only signal to neighboring cells, or utilize transport methods to travel further afield (Routledge and Scholpp, 2019). Indeed, Wnt proteins form aggregates in the ECM unless stabilized (Fuerer et al., 2010). Several mechanisms to explain the intercellular movement of Wnts have been proposed, including lipoproteins, exosomes, Wnt-binding chaperone proteins and cytonemes. Lipoproteins are

globular complexes typically used for transporting hydrophobic lipids and proteins. Wg co-purifies with lipophorins, the *Drosophila* homolog of lipoproteins. Knockdown of lipophorins reduces Wg extracellular gradients, supporting a role of liphophorins in Wg transport/spreading (Panáková et al., 2005). Exosomes are cell-derived vesicles that form after progression of early endosomes into multivesicular bodies (MVBs). As they are trafficked through the endosomal compartments, exosomes are loaded with cargo proteins and then secreted from cells through MVB fusion with the plasma membrane (Hessvik and Llorente, 2018). Exosomes then travel through the ECM to deliver proteins to other cells, mediating intercellular communication. A role for exosomes in transporting Wnt proteins was first reported at the *Drosophila* NMJ (Korkut et al., 2009). Wg is reportedly carried across the synaptic cleft by Wls-containing exosomes to influence synaptic growth, function and plasticity. Wg-binding transport proteins include the *Drosophila* Secreted Wingless-interacting molecule (Swim), which was suggested to facilitate long-range Wg transport by maintaining solubility in the ECM and thus aiding transport to Wg-receiving cells (Mulligan et al., 2012). In humans, secreted Afamin was similarly shown to enhance secretion of 12 Wnt proteins, potentially by increasing solubility via interaction with a hydrophobic binding pocket (Mihara et al., 2016; Naschberger et al., 2017). First described in *Drosophila* imaginal wing discs, cytonemes are specialized actin-based filopodia that extend protrusions to neighboring cells to transport signaling components (Ramírez-Weber and Kornberg, 1999). Similarly, a vertebrate Wnt has been observed being transported from producing to receiving cells via cytonemes (Stanganello et al., 2015). Depletion of the glypicans Dally or Dally-like protein (Dlp) significantly reduces the expansion of cytonemes, with cytonemes rarely detected in *dally/dlp* double mutants (González-Méndez et al., 2017). Interestingly, Dally and Dlp are members of the heparan sulfate proteoglycan (HSPG) protein family, which also mediate Wnt signaling by stabilization/localization/lateral diffusion of the extracellular ligand (Baeg et al., 2001; Yan et al., 2009).

Heparan Sulfate Proteoglycans

Heparan sulfate proteoglycans (HSPGs) are a family of proteins in which heparan sulfate (HS) glycosaminoglycan (GAG) chains are covalently attached to serine resides of the core protein (Sarrazin et al., 2011). HS GAG chains are linear polysaccharides consisting of repeating disaccharide units of uronic acid linked to glucosamine (Fig. 3). Formation of HS chains begins with the addition of a xylose residue to a serine of the core protein, followed by a tetrasaccharide linker (xylose-galactose-galactose-glucuronic acid; Sarrazin et al., 2011). Subsequent addition of an *N*-acetylglucosamine (GlcNAc) commits the chain to HS biosynthesis (Grobe, 2014). The nascent precursor chain consists of glucuronic acid (GlcA) and GlcNAc, which can be further modified in the Golgi through the action of a number of enzymes (Fig. 3). For example, the *N*-deacetylase/*N*-sulfotransferase (NDST) family of enzymes are bifunctional: *N*-deacetylase activity first removes acetyl groups from GlcNAc residues, generating free amino groups, which are then sulfated to GlcNS residues through *N*-sulfotransferase enzyme activity (Kjellén et al., 1992). The *Drosophila* genome contains a single NDST ortholog named *sulfateless* (sfl; Lin and Perrimon, 1999). Following *N*-sulfation of GlcNAc, heparan sulfate C5-epimerase (Hsepi in *Drosophila)* can then epimerize GlcA to iduronic acid (IdoA; Grobe, 2014). Other sulfotransferases are present that add sulfates to GlcA or IdoA (Hs2st) and to GlcNAc (Hs6st). In the final HS chain, highly modified IdoA/GlcNS domains (*N*-sulfated; NS) alternate with largely unmodified GlcA/GlcNAc domains (*N*-acetylated; NA; Sarrazin et al., 2011). Thus, the number of sugar residues, sulfate groups and uronic acids can vary enormously, leading to tremendous heterogeneity in HSPG size/molecular weight (i.e. polydispersity) and conferring distinct ligand binding specificities.

The functional importance of NDST (Sfl) in generating ligand-binding HS domains was first described in *Drosophila*, where the loss of Sfl was shown to affect the ability to transduce Wg signaling (Lin and Perrimon, 1999). At the NMJ, muscle-specific knockdown of Sfl reduced the muscle size (Kamimura et al., 2013). Functionally, *sfl* mutants exhibited increased stimulation-evoked excitatory junction potentials (EJPs) and decreased miniature EJP (mEJP) frequency

(Ren et al., 2009). Ultrastructurally, *sfl* mutant boutons were surrounded by a normal SSR but had a reduction of larger 70nm vesicles (not SVs) and, interestingly, enlarged postsynaptic pockets (a *wg* phenotype). Behaviorally, the mutant larvae had reduced locomotion (Ren et al., 2009). Mutations in Hs6st also affect NMJ structure and function (Dani et al., 2012). Reduction or removal of Hs6st caused a large increase in NMJ synaptic bouton number and decrease in EJC amplitude. Dlp abundance was decreased in this *Hs6st* mutant (Dani et al., 2012). Since Wg is known to interact with Dlp, Wg expression was measured and the Wg extracellular ligand was found to be consistently increased in *Hs6st* mutants (Dani et al., 2012). Furthermore, the downstream postsynaptic FNI pathway was also increased, as visualized with Fz2-C antibody nuclear labeling. In summary, these results suggest that the sulfation state of HSPGs is important for Wg ligand localization and can therefore affect downstream NMJ signaling and synaptic molecular assembly, ultimately altering the behavior of the animal.

Overall, HSPGs are present in virtually every cell in vertebrates and invertebrates (Grobe, 2014). Mammalian cells express 17 HSPGs that are separated into groups according to their location: membrane HSPGs (such as glypicans and syndecans), secreted extracellular matrix (ECM) HSPGs (such as agrin, perlecan and type XVIII collagen), and the secretory vesicle serglycin (Sarrazin et al., 2011). HSPGs have a multitude of functions including providing structure to basement membranes, packaging contents in secretory vesicles, binding cytokines/growth factors/morphogens to establish a gradient, binding and protecting ligands from degradation, acting as receptors for proteases, functioning as co-receptors, facilitating the cell-ECM attachment, and acting as endocytic receptors for the clearance of bound ligands (Sarrazin et al., 2011). *Drosophila* have a simplified array of HSPGs, which are described in more detail below with a focus on synaptic roles.

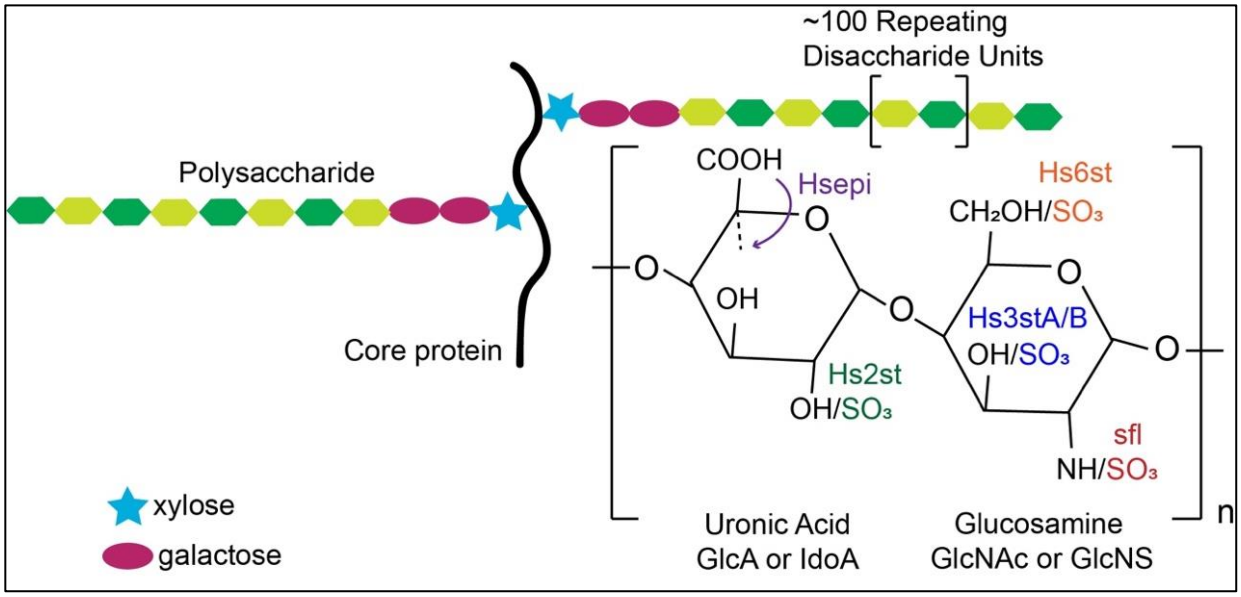

Fig. 3: The structure of an HS GAG chain

Heparan sulfate (HS) polysaccharide chains are covalently linked to a core protein via a tetrasaccharide linker (xylose-galactose-galactose-glucuronic acid), and contain ~100 repeating disaccharide residues of uronic acid and glucosamine. The residues can be modified via sulfotransferase (Hs2st, Hs3stA/B, Hs6st, sfl) or epimerase (Hsepi) enzymes to generate an enormous diversity of ligand-binding structures.

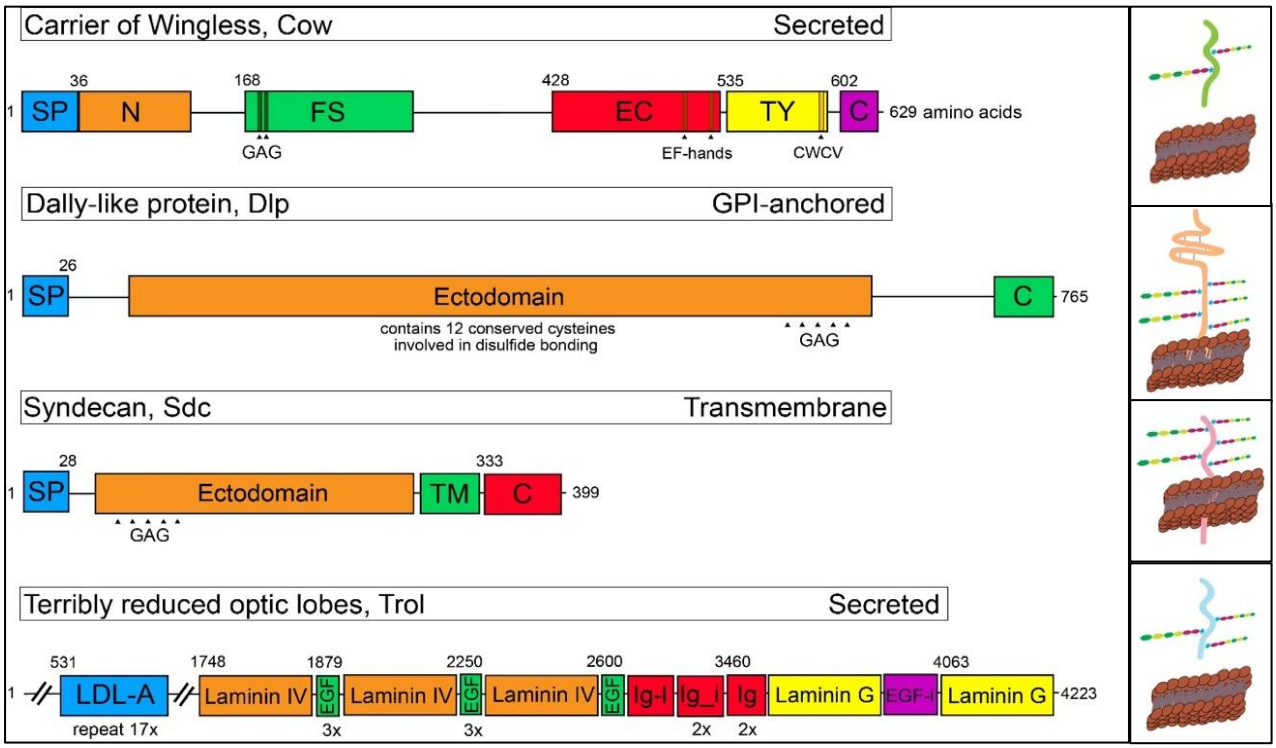

Fig. 4: HSPGs present at the *Drosophila* NMJ

HSPG amino acids are shown with colored characterized protein domains. A schematic of the protein and plasma membrane are shown to the right. Domains: SP=signal peptide, N=N-terminus, FS=follistatin-like, EC=extracellular calcium (Ca^{2+}) binding with 2 EF-hand motifs, TY=thyroglobulin-like with a CWCV motif, C=C-terminus, TM=transmembrane, LDL-A=low-density lipoprotein receptor A, EGF=Laminin epidermal growth factor, Ig-I=immunoglobulin-like, Ig_i=immunoglobulin I-set, Ig=immunoglobulin, EGF-I=EGF-like.

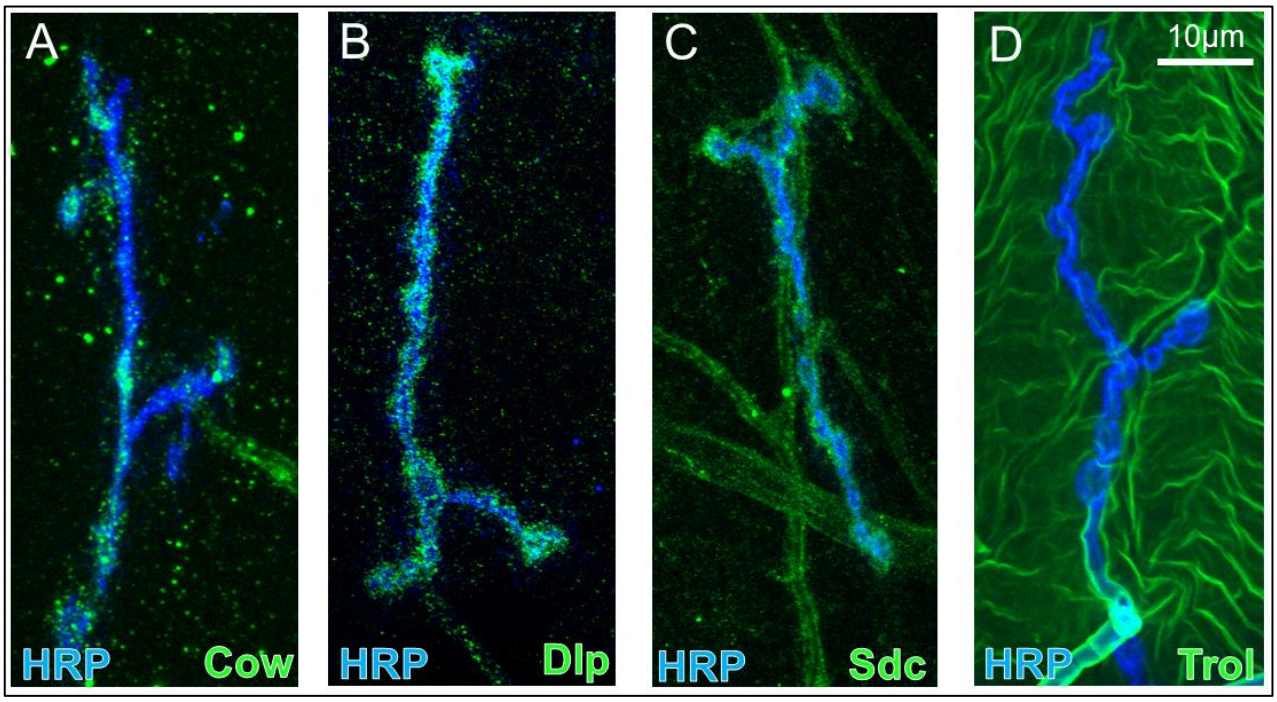

Fig. 5: Immunohistochemistry of HSPGs at the *Drosophila* NMJ

Antibody labeling of **A**) Carrier of Wingless (Cow), **B**) Dally-like Protein (Dlp), **C**) Syndecan (Sdc) and **D**) Terribly reduced optic lobes (Trol), all co-stained with anti-HRP to label presynaptic neuronal membranes.

HSPG Glypicans

HSPG glypicans are tethered to the cell surface via a glycosylphosphatidylinositol (GPI) anchor with an ectodomain containing 12 conserved cysteines and 5 GAG-binding sites (Fig. 4). The mammalian genome encodes 6 glypicans (GPC1-6), whereas *Drosophila* have only 2 (Dally and Dally-like protein; Dlp) (Nakato et al., 1995; Baeg et al., 2001). The main function of glypicans is to regulate extracellular ligand distribution and function. Depending on the concentration, glypicans can have either a stimulatory or inhibitory effect on signaling (Filmus et al., 2008). For example, Glypican-3 has been shown to bind Fz receptors to stimulate the formation of signaling complexes between Wnt and Fz, but very high concentrations of Glypican-3 reduce this stimulatory activity, presumably in a competitive-inhibitory manner (Capurro et al., 2014). *Drosophila* glypican mutants have defective Hedgehog (Hh), Bone morphogenic protein (BMP), Fibroblast growth factor (FGF) and Wnt signaling in different tissues, highlighting the importance of glypicans in regulating ligand localization and function. Both Dally and Dlp have been shown to bind and stabilize Wg at the cell surface (Strigini and Cohen, 2000; Baeg et al., 2001). In wing discs, Dlp has a biphasic function; it represses short-range Wg signaling, but activates long-rang signaling. Importantly, the transition from Wg signaling activator to repressor is determined by the relative expression levels of Dlp and Fz2 (Yan et al., 2009). The core protein of Dlp can interact with Wg, and the HS GAG chains enhance this interaction. In summary, the main function of Dlp is to retain Wg at the cell surface, to either compete with the Fz receptor or provide Wg to the receptor as a facilitating co-receptor depending on the ratio of Wg, Fz2 and Dlp; a mechanism termed the ‘exchange factor model’ (Yan et al., 2009).

Dally is not known to be expressed in the nervous system, and only Dlp is present at the *Drosophila* NMJ. Dlp is expressed mostly by the postsynaptic muscle and is observed in punctate structures surrounding type Ib boutons (Fig. 5). Structurally, *dlp* mutants reportedly have bouton numbers comparable to WT at the NMJ innervating muscles 6/7; however, pre- or post-synaptic Dlp OE is sufficient to reduce bouton number at the same NMJs (Johnson et al., 2006).

Contradictory to this, bouton number was shown to be increased upon postsynaptic OE of Dlp in a different study (Friedman et al., 2013). Functionally, Dlp LOF results in increased evoked EJP amplitude, with no change in spontaneous mEJP amplitude, and thus the elevated neurotransmission likely results from an increase in SV quantal content (Johnson et al., 2006). Ultrastructurally, *dlp* mutant AZs were reportedly significantly smaller than WT, yet the density of AZs was 2-fold increased. Dlp was found to bind the receptor protein tyrosine phosphatase (RPTP) Leukocyte common antigen-related (LAR) and antagonize its signaling function. Knockdown of LAR caused a significant increase in the phosphorylation of the LAR substrate Enabled (Ena; Johnson et al., 2006). Knockdown of Dlp caused the opposite effect on Ena phosphorylation, consistent with a model that Dlp antagonizes LAR activity. To test if Dlp acts upstream in a LAR-dependent fashion, both LAR and Dlp were knocked down at the same time. The LAR phenotype was found to be epistatic to Dlp; that is, it exhibited the LAR phenotype (Johnson et al., 2006). In summary, Dlp regulates Ena phosphorylation via inhibition of LAR activity to limit AZ morphogenesis and SV quantal content at the NMJ. More recently, it was shown that Dlp expression at the NMJ is activity-dependent (Dear et al., 2017). After an acute exogenous increase in synaptic activity, Dlp was increased >60% surrounding synaptic boutons. Interestingly, Wg secretion is also activity-dependent (Ataman et al., 2008), and Dlp can bind Wg (Yan et al., 2009), thus the two might interact to facilitate synaptic plasticity.

HSPG Syndecans

Syndecans are HSPGS with a single transmembrane domain and several GAG-binding sites in the ectodomain (Fig. 4). They were first discovered in vertebrates, with a role in linking the cytoskeleton to the interstitial matrix (Saunders et al., 1989). The mammalian genome encodes 4 syndecans (Sdc1-4), whereas *Drosophila* has only a single gene (*sdc*; Spring et al., 1994). Syndecans have roles in cellular proliferation, differentiation, adhesion and migration

(Leonova and Galzitskaya, 2013). *Drosophila* Sdc is expressed in embryonic tissues consistent with the analogous mammalian Syndecan (Spring et al., 1994; Table 1). Sdc genetically interacts with the Slit signaling ligand and its receptor Roundabout (Robo) to control midline crossing of embryonic neuronal axons (Steigemann et al., 2004). A follow-up biochemical study showed that Sdc participates directly in a complex with both Slit and Robo (Johnson et al., 2004). Sdc was subsequently discovered as a ligand for the RPTP LAR, and this interaction is essential during motor axon guidance in *Drosophila* (Fox and Zinn, 2005). At the NMJ, Sdc is expressed by presynaptic boutons and is observed in domains surrounding type Ib boutons (Fig. 5). Sdc binding to LAR promotes the formation of NMJ synaptic boutons (Johnson et al., 2006).

Both Dlp and Syndecan are upregulated in a *Drosophila* model of Fragile X Syndrome (FXS; Friedman et al., 2013), the most common heritable cause of intellectual disability and autism spectrum disorder, causing changes in structure and function of the NMJ. Wg ligand levels were also highly upregulated in the FXS disease model. Despite increased extracellular Wg ligand levels, the postsynaptic FNI pathway was found significantly downregulated (Friedman et al., 2013). This result can be explained by the exchange factor model (Yan et al., 2009); high levels of HSPG sequestering Wg away from Fz2 receptors to result in depressed signaling. Importantly, reducing the levels of Dlp and Sdc in the FXS disease model reduced Wg and increased FNI to near WT levels (Friedman et al., 2013). Correcting Dlp levels in the FXS background was sufficient to restore NMJ synaptic architecture, but both Dlp and Sdc had to be corrected to restore functional synaptic neurotransmission. These results indicate that HSPG elevation in the FXS disease model is causal for the changes in Wg *trans*-synaptic signaling, which can explain the excess synaptic structure and function in this disease state.

HSPG Perlecans

Perlecan/Trol is a very large, multi-domain, secreted HSPG (Fig. 4). In *Drosophila*, *trol* mutants were isolated several decades ago (Judd et al., 1972), but were renamed ‘terribly

reduced optic lobes' due to loss of the third instar larval brain lobes (Datta and Kankel, 1992) owing to a role in activating neuroblast proliferation (Datta, 1995). Perlecan binds multiple growth factors and basement membrane components, including laminin and collagen IV (Battaglia et al., 1992). A synaptic involvement has been characterized, with Perlecan required for localizing secreted acetylcholinesterase at the mouse NMJ (Arikawa-Hirasawa et al., 2002). At the *Drosophila* NMJ, Trol is expressed by postsynaptic muscle and is clearly expressed on muscle surfaces (Fig. 5). Immunoelectron microscopy analysis revealed that Trol accumulates in the postsynaptic SSR (Kamimura et al., 2013). Structurally, *trol* mutants have smaller muscles and abnormal NMJ boutons, with elevated ghost and satellite boutons. Functionally, the frequency and amplitude of miniature neurotransmission events are decreased in mutants (Kamimura et al., 2013). The *trol* mutants also show a reduction in SSR area and complexity, enlarged postsynaptic pockets, and a reduction in GluRIIA receptor levels. Since many of the phenotypes described for *trol* mutants are phenocopied by *wg* LOF, Trol regulation of Wg signaling was investigated (Kamimura et al., 2013). The postsynaptic FNI pathway was reduced in *trol* mutants, and genetically correcting FNI in an otherwise *trol* mutant background corrected most of the NMJ phenotypes observed in the mutant alone (ghost boutons, SSR area, and postsynaptic pockets). In contrast, the presynaptic Wg signaling pathway was increased (Kamimura et al., 2013), with satellite boutons observed at *trol* mutant NMJs. Genetically correcting presynaptic signaling in an otherwise *trol* mutant background suppressed the satellite bouton phenotype. In summary, Trol reportedly regulates the bidirectional activity of Wg by distributing the appropriate levels of Wg pre- or postsynaptically. Trol normally serves to bind and sequester Wg in the SSR so in a *trol* mutant, more of the Wg travels to the presynaptic membrane causing an increase in presynaptic signaling (overproliferation of boutons) and a concomitant decrease in postsynaptic signaling (SSR development, GluRs).

HSPG Carrier of Wingless

The most recent HSPG characterized in *Drosophila* is Carrier of Wingless (Cow; Chang and Sun, 2014). Cow was first identified in a GOF screen and shown to belong to the Testican family of secreted HSPGs (Tsou et al., 2003), with a signal peptide (SP) and conserved domains including kazal, thyroglobulin type 1 and extracellular calcium binding domains. Cow is expressed throughout the developing wing disc (Chang and Sun, 2014). To test secretion, a Flag-tagged Cow was transfected into S2 cells and an anti-Flag antibody detected two protein bands in the culture supernatant; with (~100 kDa) and without (~75 kDa) HS chains. Mutants of the HS-glucosamine N-sulfotransferase sulfateless (*sfl*) probed with anti-Cow showed a significantly reduced 100-kDa band (Chang and Sun, 2014). Moreover, when the two Cow HS sites were mutated, the 100-kDa band was again significantly reduced. RNAi knockdown of Cow levels resulted in phenotypes similar to *wg* mutants, including embryonic denticle belt fusion and defects in chemosensory bristles along the wing margin (Chang and Sun, 2014). Genetic tests suggested that Cow regulates Wg at a step upstream of the Fz2 receptor. In the wing disc, Wg is expressed in a stripe of a few rows of cells at the D-V boundary, but affects the expression of target genes many cell diameters away. Neuralized (Neur) is a short-range target requiring high Wg signaling, while Distalless (Dll) is a long-range target requiring low Wg signaling (Zecca et al., 1996). Cow knockdown had a biphasic effect on these target genes, suggesting Cow promotes Wg transport; if Cow is removed, Wg builds up at the source and causes Wg OE phenotypes for the short-range Neur target and Wg KD phenotypes for the long-range Dll target (Chang and Sun, 2014).

To understand how Cow regulates Wg, Cow was overexpressed in the *Drosophila* wing disc, which resulted in a significant increase in extracellular Wg (exWg; Chang and Sun, 2014). Furthermore, secreted Wg from transfected S2 cells added to control or *Cow-dsRNA* S2 cells showed a small Wg decrease in the supernatant of control cells and large decrease in *Cow-dsRNA* cells, suggesting Cow may stabilize exWg. Using Co-IP, it was shown that Cow can physically interact with Wg with only the 100kD band present, indicating that Wg can only interact

with HS-modified Cow. A tethered version of Cow (Cow-GPI) was shown to restrict Wg movement *in vivo* (Chang and Sun, 2014). GFP-Wg was transiently expressed in the presence or absence of co-expressed Cow, and the movement of Wg was followed over time. In wing discs where Cow and Wg were co-expressed, the mobility of GFP-Wg increased 40-50%. These results suggest Cow binds to Wg and serves as a carrier to increase the speed of exWg movement, perhaps by shielding the hydrophobic lipids of Wg to encourage movement from cell membranes. Importantly, it was shown that the human homolog Testican-2 (Table 1) can also bind to Wnt extracellularly, showing an evolutionarily conserved role (Chang and Sun, 2014). Testicans have been studied for their roles in cell adhesion, migration and proliferation (Ruoslahti, 1988; Yang et al., 2016), but have not been much studied in the nervous system, despite *testican-2* mRNA being highly expressed in the brains of both mice and humans (Marr et al., 1997; Vannahme et al., 1999). Testican-2 has been shown to cause a significant decrease in neurite outgrowth in cultured neurons (Schnepp et al., 2005). I address in this thesis work whether the secreted HSPG Cow regulates Wg at *Drosophila* NMJ synapses *in vivo*.

Wnt deacylase Notum

Notum (a.k.a. *wingful* because of its role as a negative feedback regulator of *wingless*) was first identified via a GOF mutant screen that caused loss of the wing and duplication of the dorsal thorax (i.e. the notum; Mata et al., 2000), resembling defects seen with loss of Wg (Sharma and Chopra, 1976). Notum was characterized a few years later by two different groups (Gerlitz and Basler, 2002; Giráldez et al., 2002), who both concluded that Notum is an enzyme from the α/β-hydrolase superfamily that acts as a negative feedback inhibitor of Wg signaling. Ectopic expression of Wg induced ectopic Notum expression, reducing Notum increased the level and broadened the distribution of Wg, and increasing Notum activity blocked Wg signaling (Giráldez et al., 2002). Thus, high levels of Wg induce Notum, which in turn serves as a Wg antagonist.

Phylogenetic analyses showed *Drosophila*, mouse and human Notum orthologs have a distinctive conserved block of residues flanking a serine (G-X-S-X-G) active site (Giráldez et al., 2002). Protein structural modeling suggested Notum could be a α/β-hydrolase superfamily member, which includes peptidases, lipases, esterases and other hydrolytic enzymes with a conserved active site motif of the Ser/Asp/His catalytic triad (Nardini and Dijkstra, 1999; Fig. 6). One superfamily member, pectin acetylesterase, acts as a secreted enzyme to deacetylate pectins in plant cell walls (Philippe et al., 2017). Pectins are composed of galacturonic acid groups, some of which are methylated or acetylated, and pectin acetylesterases hydrolyze the ester bond linking acetyl groups to galacturonic acid. In comparison, HSPGs consist of repeating GlcA and GlcNAc disaccharide residues. Although GAGs and pectins differ in structure, the similarity of Notum to pectin acetylesterases raised the hypothesis that Notum interacts with HSPG GAG side chains. To address this possibility, Notum and the glypican Dally were co-expressed in S2 cells, which reduced the amount of Dally recovered in S2 lysates (Giráldez et al., 2002). Normally, Dlp appears as 2 prominent bands on Western blots (+HS and -HS chains), but when Notum and Dlp were co-expressed, the smaller band was increased, suggesting Notum modifies the HS chains of Dlp (Giráldez et al., 2002).

In a follow-up study, the 5 putative GAG-addition sites of Dlp were deleted or mutated, and the Dlp mutants were co-expressed with Notum in S2 cells (Kreuger et al., 2004). If Notum serves as a GAG-modifying enzyme, then it was hypothesized that Notum could not modify the GAG-less Dlp. Surprisingly, the co-expression caused a large shift in the electrophoretic mobility of Dlp to a faster migrating species. Therefore, it was hypothesized that Notum may act as a phospholipase to cleave the GPI anchor of Dlp. Consistently, treatment with phosphatidylinositol-specific phospholipase-C (PI-PLC) caused a mobility shift similar to that caused by Notum (Kreuger et al., 2004), although curiously the shift in molecular weight was larger than would be expected from the weight of a GPI anchor alone. Dlp GPI mutants were made (either by mutating the GPI anchor site or fusing to a transmembrane protein) and Notum appeared insensitive to

either form of Dlp lacking a GPI anchor, indicating that Notum cleaves the GPI anchor of Dlp (Kreuger et al., 2004). The faster migrating form of Dlp (i.e. the cleaved form) was recovered from the culture media, suggesting Notum-processed Dlp can be released from the cell surface. Over-expressing Dlp resulted in the binding and sequestering of Wg ligand (Baeg et al., 2001). Over-expressing Dlp or Notum alone caused a mild reduction of Wg signaling, while co-expression lead to a severe reduction, suggesting that Notum enhances the ability of Dlp to reduce Wg signaling. These observations led to the attractive model that Notum can release Dlp (bound to Wg) from the cell surface, therefore reducing the level of Wg available for signaling (Kreuger et al., 2004). In other words, it was concluded that Notum could convert Dlp from a membrane-tethered Wg co-receptor to a secreted Wg ligand antagonist. An additional study showed that Notum induces the release of GPI-anchored proteins from the cell surface of mammalian cells (Traister et al., 2008).

One glaring issue with Notum being a phospholipase is how it could confer specificity to Wg regulation, since glypicans also regulate many other signaling pathways including Hh, Dpp and FGF (Capurro et al., 2008; Grisaru et al., 2001; Hayashi et al., 2009). Yet, Notum seems to only to be activated by Wnt signaling, and selectively suppresses Wnt signaling in many organisms (Flowers et al., 2012; Giráldez et al., 2002; Gerlitz and Basler, 2002; Petersen and Reddien, 2011; Torisu et al., 2008). Moreover, a more recent study published in Nature could not replicate the above *in vitro* or *in vivo* results, and concluded that Notum is not a glypican-specific phospholipase (Kakugawa et al., 2015). Notum does bind Dlp to regulate signaling. Over-expressing Notum led to a reduction of Wg signaling, as assayed by suppression of the Wg target Sens (Kakugawa et al., 2015). In the absence of Dlp, the suppression was significantly reduced. Moreover, re-expressing a Dlp-CD8 transgene in which the GPI anchor was replaced with a transmembrane domain restored the ability of Notum to suppress Wg signaling, indicating the GPI anchor is not important for Notum to act (Kakugawa et al., 2015). In the presence of Sfl knockdown, Notum OE could not suppress Wg signaling. Therefore, HSPG sulfation is necessary for Notum to act. Interestingly, Notum did not accumulate in the presence of Sfl knockdown, and

Notum was also depleted from the surface of *dally dlp* double-mutants (Kakugawa et al., 2015). Overall, these experiments demonstrate the importance of HSPG glypicans in Notum function, specifically their HS chains, but not their GPI anchor, with the likely function to retain Notum at the cell surface.

To finally resolve the tricky question of Notum enzymatic activity, the crystal structures of both the *Drosophila* (dNotum) and human (hNotum) Notum proteins were recently determined (Kakugawa et al., 2015). An extensive GAG-binding patch was found, which supports the notion that Notum binds to Dlp. However, the catalytic triad of Notum, Ser-Asp-His, is quite distant from this patch suggesting that Notum does not enzymatically act on HSPGs. The putative active site exhibits a canonical α/β-hydrolase fold and structure-based homologs indicate that it belongs to the family of carboxylesterases (Kakugawa et al., 2015). It was shown that hNotum could act on a carboxylesterase substrate, but not on other substrates of the α/β-hydrolase superfamily. How does Notum confer specificity to Wnt proteins? Carboxylesterases can target carboxy-oxoester and carboxy-thioester bonds, and the linkage between Wnt and palmitoleic acid is the former. Wg was treated with recombinant hNotum and Wnt was inactivated irreversibly and in a time-dependent manner (Kakugawa et al., 2015). Surprisingly, the Notum crystal structures revealed a hydrophobic pocket adjacent to the catalytic triad that could accommodate long-chain fatty acids up to 16 carbon atoms (e.g. palmitoleic acid is 16 carbons long). Finally, it was shown that Notum can directly deacylate Wnt proteins, including Wg (Kakugawa et al., 2015). The specificity of Notum comes from the shape of the active site hydrophobic pocket, which can only accommodate *cis*-unsaturated fatty acids, such as myristoleate and palmitoleate, and the nature of its enzymatic activity (i.e. carboxyl-oxoesterase). These two characteristics ensure that Notum only acts on Wnt proteins, the only known secreted proteins to be *O*-palmitoleoylated on a serine residue (Kakugawa et al., 2015). The serine lipidation of Wnts is known to contribute directly to Fz receptor binding (Janda et al., 2012). In summary, Notum can remove the Wnt/Wg palmitoleic acid

lipidation at the conserved serine residue, rendering Wg less able to bind Fz2. I address in this thesis work whether Notum acts as a negative regulator of Wg signaling at NMJ synapses *in vivo*.

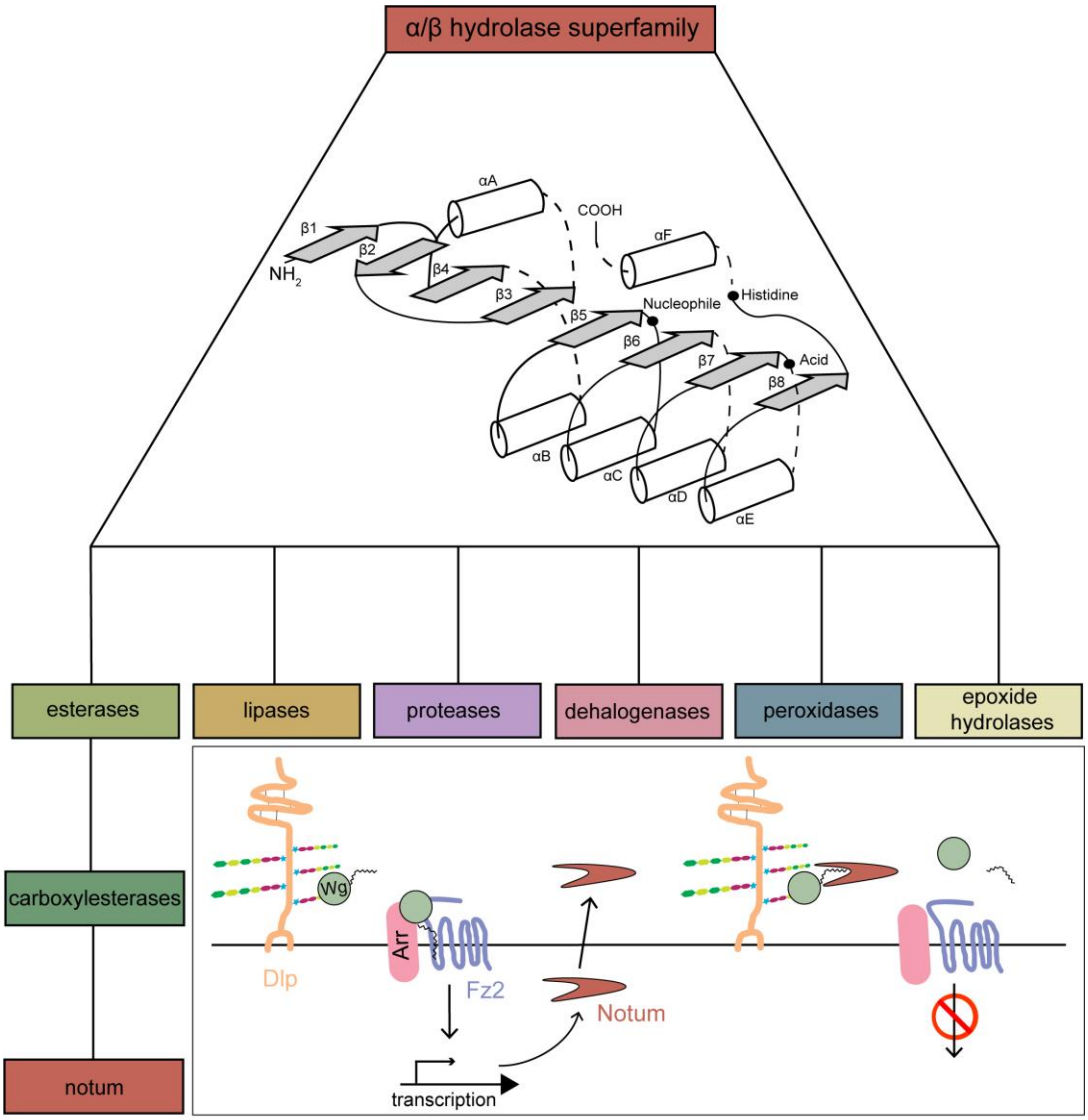

Fig 6: The α/β hydrolase superfamily members and summarized Notum function

The Notum carboxylesterase is a member of the α/β hydrolase superfamily, which is defined by the "Nucleophile-His-Acid" catalytic triad. Dlp helps to localize Wg near Fz2 receptors. The lipid moiety attached to Wg facilitates its interaction with Fz2 and co-receptor Arrow (Arr). Notum transcription is induced upon Wg signaling. Notum is then secreted and cleaves the lipid from Wg in a glypican-assisted fashion, leaving Wg less able to bind Fz2 and therefore reduces signaling. Figure adapted from Nardini and Dijkstra (1999) and Kakugawa et al. (2015).

***Drosophila* gene**	**Human homolog**	**Also known as**	**% identity *Drosophila* gene identical to target human gene (Reference: ensembl.org)**
HSPGs			
Cow	*SPOCK2*	*Testican-2*	29.72
dally	*GPC5*		24.65
dlp	*GPC6*		38.02
sdc	*SDC2*		38.31
trol	*HSPG2*	*PRCAN, SJS1, perlecan*	23.50
Wnts			
Wnt1 or wg	*WNT1*		54.05
Wnt2	*WNT7B*		48.14
Wnt4	*WNT16*		32.88
Wnt5	*WNT5A/WNT5B*		46.58/47.91
Wnt6	*WNT6*		44.38
Wnt8 or wntD	*WNT8*		
Wnt10	*WNT10A/WNT10B*		41.01/43.45
Other			
brp	*Erc1*	*ELKS/Rab6-interacting/CAST family member 1*	
dlg1	*PSD-95*	*SAP-90, DLG4*	37.81
Notum	*Notum*		

Table 1: List of vertebrate genes and *Drosophila* homologs with % identity.

References

Anderson MS, Halpern ME, Keshishian H (1988) Identification of the neuropeptide transmitter proctolin in Drosophila larvae: characterization of muscle fiber-specific neuromuscular endings. J Neurosci 8(1):242-55.

Andreae LC, Burrone J (2018) The role of spontaneous neurotransmission in synapse and circuit development. J Neurosci Res 96(3):354-59.

Arikawa-Hirasawa E, Rossi SG, Rotundo RL, Yamada Y (2002) Absence of acetylcholinesterase at the neuromuscular junction of perlecan-null mice. Nat Neurosci 5:119-23.

Ataman B, Ashley J, Gorczyca D, Gorczyca M, Mathew D, Wichmann C, Sigrist SJ, Budnik V (2006) Nuclear trafficking of Drosophila Frizzled-2 during synapse development requires the PDZ protein dGRIP. PNAS 103(20):7841-46.

Ataman B, Ashley J, Gorczyca M, Ramachandran P, Fouquet W, Sigrist SJ, Budnik V (2008) Rapid Activity-Dependent Modifications in Synaptic Structure and Function Require Bidirectional Wnt Signaling. Neuron 57(5):705-18.

Baeg GH, Lin X, Khare N, Baumgartner S, Perrimon N (2001) Heparan sulfate proteoglycans are critical for the organization of the extracellular distribution of Wingless. Development 128(1):87-94.

Bänziger C, Soldini D, Schütt C, Zipperlen P, Hausmann G, Basler K (2006) Wntless, a conserved membrane protein dedicated to the secretion of Wnt proteins from signaling cells. Cell 125(3):509-22.

Bartscherer K, Pelte N, Ingelfinger D, Boutros M (2006) Secretion of Wnt ligands requires Evi, a conserved transmembrane protein. Cell 125(3):523-33.

Bassett AR, Tibbit C, Ponting CP, Liu JL (2013) Highly Efficient Targeted Mutagenesis of *Drosophila* with the CRISPR/Cas9 System. Cell Rep 4(1):220-8.

Bate M (1990) The embryonic development of larval muscles in Drosophila. Development 110(3):791-804.

Battaglia C, Mayer U, Aumailley M, Timpl R (1992) Basement-membrane heparan sulfate proteoglycan binds to laminin by its heparan sulfate chains and to nidogen by sites in the protein core. Eur J Biochem 208(2):359-66.

Betz WJ, Mao F, Bewick GS (1992) Activity-dependent fluorescent staining and destaining of living vertebrate motor nerve terminals. J Neurosci 12(2):363-75.

Brand AH, Perrimon N (1993) Targeted gene expression as a means of altering cell fates and generating dominant phenotypes. Development 118(2):401-15.

Broadie K, Bate M (1995) The *Drosophila* NMJ: a genetic model system for synapse formation and function. Semin Cell Dev Biol 6(3):221-31.

Budnik V, Koh YH, Guan B, Hartmann B, Hough C, Woods D, Gorczyca M (1996) Regulation of Synapse Structure and Function by the Drosophila Tumor Suppressor Gene *dlg*. Neuron 17(4):627-40.

Capurro MI, Xu P, Shi W, Li F, Jia A, Filmus J (2008) Glypican-3 inhibits Hedgehog signaling during development by competing with patched for Hedgehog binding. Dev Cell 14(5):700-11.

Capurro M, Martin T, Shi W, Filmus J (2014) Glypican-3 binds to Frizzled and plays a direct role in the stimulation of canonical Wnt signaling. J Cell Sci 127:1565-75.

Cantera R, Nässel DR (1992) Segmental peptidergic innervation of abdominal targets in larval and adult dipteran insects revealed with an antiserum against leucokinin I. Cell Tissue Res 269(3):459-71.

Chang Y-H, Sun YH (2014) Carrier of Wingless (Cow), a Secreted Heparan Sulfate Proteoglycan, Promotes Extracellular Transport of Wingless. PLoS ONE 9(10):e111573.

Chen K, Featherstone DE (2005) Discs-large (DLG) is clustered by presynaptic innervation and regulates postsynaptic glutamate receptor subunit composition in *Drosophila.* BMC Biol 3(1).

Ching W, Hang HC, Nusse R (2008) Lipid-independent Secretion of a *Drosophila* Wnt Protein. J Biol Chem 283(25):17092-8.

Clayton EL, Cousin MA (2009) The molecular physiology of activity-dependent bulk endocytosis of synaptic vesicles. J Neurochem 111:901-14.

Clayton EL, Evans GJO, Cousin MA (2008) Bulk synaptic vesicle endocytosis is rapidly triggered during strong stimulation. J Neurosci 28:6627-32.

Dani N, Nahm M, Lee S, Broadie K (2012) A targeted glycan-related gene screen reveals heparan sulfate proteoglycan sulfation regulates WNT and BMP trans-synaptic signaling. PLoS Genet 8:e1003031.

Datta S, Kankel DR (1992) *l(1)trol* and *l(1)devl*, Loci Affecting the Development of the Adult Central Nervous System in *Drosophila melanogaster*. Genetics 130:523-37.

Datta S (1995) Control of proliferation activation in quiescent neuroblasts of the Drosophila central nervous system. Development 121(4):1173-82.

Dear ML, Dani N, Parkinson W, Zhou S, Broadie K (2016) Two classes of matrix metalloproteinases reciprocally regulate synaptogenesis. Development 143:75-87.

Dear ML, Shilts J, Broadie K (2017) Neuronal activity drives FMRP- and HSPG-dependent matrix metalloproteinase function required for rapid synaptogenesis. Sci Signal 10(504).

Denker A, Rizzoli SO (2010) Synaptic Vesicle Pools: An Update. Front Synaptic Neurosci 2:135.

DiAntonio A, Peterson SA, Heckmann M, Goodman CS (1999) Glutamate Receptor Expression Regulates Quantal Size and Quantal Content at the *Drosophila* Neuromuscular Junction. J Neurosci 19(8):3023-32.

Doubravska L, Krausova M, Gradl D, Vojtechova M, Tumova L, Lukas J, Valenta T, Posphichalova V, Fafilek B, Plachy J, Sebesta O, Korinek V (2011) Fatty acid modification of Wnt1 and Wnt3a at serine is prerequisite for lipidation at cysteine and is essential for Wnt signaling. Cell Signal 23(5):837-48.

Dudel J, Kuffler SW (1961) Presynaptic inhibition at the crayfish neuromuscular junction. J Physiol 155:543-62.

Eaton BA, Fetter RD, Davis GW (2002) Dynactin is Necessary for Synapse Stabilization. Neuron 34(5):729-41.

Filmus J, Capurro M, Rast J (2008) Glypicans. Genome Biol 9(5):224.

Fischer JA, Giniger E, Maniatis T, Ptashne M (1988) GAL4 activates transcription in Drosophila. Nature 332:853–856.

Flowers GP, Topczewska JM, Topczewski J (2012) A zebrafish Notum homolog specifically blocks the Wnt/β-catening signaling pathway. Development 139:2416-25.

Fox AN, Zinn K (2005) The heparan sulfate proteoglycan syndecan is an in vivo ligand for the Drosophila LAR receptor tyrosine phosphatase. Curr Biol 15(19):1701-11.

Franco B, Bogdanik L, Bobinnec Y, Debec A, Bockaert J, Parmentier M-L, Grau Y (2004) Shaggy, the Homolog of Glycogen Synthase Kinase 3, Controls Neuromuscular Junction Growth in Drosophila. J Neurosci 24(29):6573-7.

Friedman SH, Dani N, Rushton E, Broadie K (2013) Fragile X mental retardation protein regulates trans-synaptic signaling in *Drosophila*. Dis Model Mech 6:1400-13.

Fuentes-Medel Y, Logan MA, Ashley J, Ataman B, Budnik V, Freeman MR (2009) Glia and Muscle Sculpt Neuromuscular Arbors by Engulfing Destabilized Synaptic Boutons and Shed Presynaptic Debris 7(8):e1000184.

Fuerer C, Habib SJ, Nusse R (2010) A study on the interactions between Heparan Sulfate Proteoglycans and Wnt proteins. Dev Dyn 239(1):184-90.

Gerlitz O, Basler K (2002) Wingful, an extracellular feedback inhibitor of Wingless. Genes Dev 16:1055-59.

Gilbert LA, Larson MH, Morsut L, Liu Z, Brar GA, Torres SE, Stern-Ginossar N, Brandman O, Whitehead EH, Doudna JA, Lim WA, Weissman JS, Qi LS (2013) CRISPR-mediated modular RNA-guided regulation of transcription in eukaryotes. Cell 154(2):441-51.

Giráldez AJ, Copley RR, Cohen SM (2002) HSPG modification by the secreted enzyme notum shapes the wingless morphogen gradient. Dev Cell 2:667-76.

González-Méndez L, Seijo-Barandiarán I, Guerrero I (2017) Cytoneme-mediated cell-cell contacts for Hedgehog reception. eLIFE 6:e24045.

Goodman RM, Thombre S, Firtina Z, Gray D, Betts D, Roebuck J, Spana EP, Selva EM (2006) Sprinter: a novel transmembrane protein required for Wg secretion and signaling. Development 133(24):4901-11.

Gorczyca M, Augart C, Budnik V (1993) Insulin-like receptor and insulin-like peptide are localized at neuromuscular junctions in Drosophila. J Neurosci 13(9):3692-704.

Grisaru S, Cano-Gauci D, Tee J, Filmus J, Rosenblum ND (2001) Glypican-3 modulates BMP- and FGF-mediated effects during renal branching morphogenesis. Dev Biol 231(1):31-46.

Grobe K (2014) N-Deacetylase/N-Sulfotransferase (Heparan Glucosaminyl) 1 (NDST1). Handbook of Glycosyltransferases and Related Genes 2:1091-103.

Gratz SJ, Cummings AM, Nguyen JN, Hamm DC, Donohue LK, Harrison MM, Wildonger J, O'Connor-Giles KM (2013) Genome engineering of Drosophila with the CRISPR RNA-guided Cas9 nuclease. Genetics 194(4):1029-35.

Guan B, Hartmann B, Kho YH, Gorczycz M, Budnik V (1996) The *Drosophila* tumor suppressor gene, *dlg*, is involved in structural plasticity at a glutamatergic synapse. Curr Biol 6(6):695-706.

Guan B, Chen X, Zhang H (2013) Two-electrode voltage clamp. Methods Mol Biol 998:79-89.

Hallermann S, Kittel RJ, Wichmann C, Weyhersmüller A, Fouquet W, Mertel S, Owald D, Eimer S, Depner H, Schwärzel M, Sigrist SJ, Heckmann M (2010) Naked Dense Bodies Provoke Depression. J Neurosci 30(43):14340-45.

Han TH, Dharkar P, Mayer ML, Serpe M (2015) Functional reconstitution of *Drosophila melanogaster* NMJ glutamate receptors. PNAS 112(19):6182-7.

Harris KP, Akbergenova Y, Cho RW, Baas-Thomas MS, Littleton JT (2016) Shank Modulates Postsynaptic Wnt Signaling to Regulate Synaptic Development. J Neurosci 36(21):5820-32.

Hayashi Y, Kobayashi S, Nakato H (2009) *Drosophila* glypicans regulate the germline stem cell niche. JCB 187(4):473.

Hessvik NP, Llorente A (2018) Current knowledge on exosome biogenesis and release. Cell Mol Life Sci 75(2):193-208.

Hoopmann P, Punge A, Barysch SV, Westphal V, Bückers J, Opazo F, Bethani I, Lauterbach MA, Hell SW, Rizzoli SO. (2010) Endosomal sorting of readily releasable synaptic vesicles. Proc Natl Acad Sci USA 107(44):19055-60.

Jan LY, Jan YN (1976) L-Glutamate as an excitatory transmitter at the *Drosophila* larval neuromuscular junction. J Physiol 262:215-36.

Jan LY, Jan YN (1982) Antibodies to horseradish peroxidase as specific neuronal markers in Drosophila and in grasshopper embryos. Proc Natl Acad Sci 79(8):2700-4.

Janda CY, Waghray D, Levin AM, Thomas C, Garcia KC (2012) Structural basis of Wnt recognition by Frizzled. Science 337(6090):59-64.

Johnson KG, Ghose A, Epstein E, Lincecum J, O'Connor MB, Van Vactor D (2004) Axonal heparan sulfate proteoglycans regulate the distribution and efficiency of the repellent slit during midline axon guidance. Curr Biol 14(6):499-504.

Johnson KG, Tenney AP, Ghose A, Duckworth AM, Higashi ME, Parfitt K, Marcu O, Heslip TR, Marsh JL, Schwarz TL, Flanagan JG, Van Vactor D (2006) The HSPGs Syndecan and Dallylike bind the receptor phosphatase LAR and exert distinct effects on synaptic development. Neuron 49(4):517-31.

Judd BH, Shen MW, Kaufman TC (1972) The Anatomy and Function of a Segment of the X Chromosome of *Drosophila melanogaster.* Genetics 71(1):139-56.

Kadowaki T, Wilder E, Klingensmith J, Zachary K, Perrimon N (1996) The segment polarity gene porcupine encodes a putative multitransmembrane protein involved in Wingless processing. Genes Dev 10(24):3116-28.

Kakugawa S, Langton PF, Zebisch M, Howell SA, Chang TH, Liu Y, Feizi T, Bineva G, O'Reilly N, Snijders AP, Jones EY, Vicent JP (2015) Notum deacylates Wnt proteins to suppress signalling activity. Nature 519:187-92.

Kamimura K, Ueno K, Nakagawa J, Hamada R, Saitoe M, Maeda N (2013) Perlecan regulates bidirectional Wnt signaling at the *Drosophila* neuromuscular junction. J Cell Biol 200:219-33.

Kerr KS, Fuentes-Medel Y, Brewer C, Barria R, Ashley J, Abruzzi KC, Sheehan A, Tasdemir-Yilmaz OE, Freeman MR, Budnik V (2014) Glial Wingless/Wnt regulates glutamate receptor clustering and synaptic physiology at the *Drosophila* neuromuscular junction. J Neurosci 34:2910-20.

Kim YJ, Bao H, Bonanno L, Zhang B, Serpe M (2012) *Drosophila* Neto is essential for clustering glutamate recetprso at the neuromuscular junction. Genes and Dev 26:974-87.

Kittel RJ, Wichmann C, Rasse TM, Fouquet W, Schmidt M, Schmid A, Wagh DA, Pawlu C, Kellner RR, Willig KI, Hell SW, Buchner E, Heckmann M, Sigrist SJ (2006) Bruchpilot promotes active zone assembly, Ca^{2+} channel clustering, and vesicle release. Science 312:1051-4.

Kjellén L, Pettersson I, Unger E, Lindahl U (1992) Two Enzymes in One: N-Deacetylation and N-Sulfation in Heparin Biosynthesis are Catalyzed by the Same Protein. Heparin and Related Polysaccharides 313:107-11.

Koldenkova VP, Nagai T (2013) Genetically encoded Ca^{2+} indicators: Properties and evaluation. Biochim Biophys Acta 1833(7):1787-97.

Kopke DL, Lima SC, Alexandre C, Broadie K (2017) Notum coordinates synapse development via extracellular regulation of Wingless trans-synaptic signaling. Development 144:3499-510.

Kopke DL, Broadie K (2018) FM Dye Cycling at the Synapse: Comparing High Potassium Depolarization, Electrical and Channelrhodopsin Stimulation. J Vis Exp 135.

Korkut C, Ataman B, Ramachandran P, Ashley J, Barria R, Cherbesi N, Budnik V (2009) Trans-Synaptic Transmission of Vesicular Wnt Signals through Evi/Wntless. Cell 139(2):393-404.

Kreuger J, Perez L, Giraldez AJ, Cohen SM (2004) Opposing activities of Dally-like glypican at high and low levels of Wingless morphogen activity. Dev Cell 7(4):503-12.

Lahey T, Gorczyca M, Jia X-X, Budnik V (1994) The drosophila tumor suppressor gene dlg is required for normal synaptic bouton structure. Neuron 13(4):823-35.

Landgraf M, Thor S (2006) Development of Drosophila motoneurons: specification and morphology. Semin Cell Dev Biol 17(1):3-11.

Leonova EI, Galzitskaya OV (2013) Structure and Functions of Syndecans in Vertebrates. Biochem (Mosc) 78(10):1373-90.

Liebl FLW, Wu Y, Featherstone DE, Noordermeer JN, Fradkin L, Hing H (2008) Derailed regulates development of the Drosophila neuromuscular junction. Dev Neurobiol 68:152-65.

Liebl FLW, McKeown C, Yao Y, Hing HK (2010) Mutations in Wnt2 alter presynaptic motor neuron morphology and presynaptic protein localization at the Drosophila neuromuscular junction. PLoS ONE 5:e12778.

Lin X, Perrimon N (1999) Dally cooperates with *Drosophila* Frizzled 2 to transduce Wingless signaling. Nature 400:281-84.

Lin X, Buff EM, Perrimon N, Michelson AM (1999) Heparan sulfate proteoglycans are essential for FGF receptor signaling during Drosophila embryonic development. Development 126:3715–3723.

Marr HS, Basalamah MA, Edgell C-JS (1997) Endothelial Cell Expression of Testican mRNA. Endothelium 5:209-19.

Mata J, Curado S, Ephrussi A, Rorth P (2000) Tribbles coordinates mitosis and morphogenesis in Drosophila by regulating string/CDC25 proteolysis. Cell 101(5):511-22.

Mathew D, Ataman B, Chen J, Zhang Y, Cumberledge S, Budnik V (2005) Wingless signaling at synapses is through cleavage and nuclear import of receptor DFrizzled2. Science 310:1344-47.

Miech C, Pauer HU, He X, Schwarz TL (2008) Presynaptic local signaling by a canonical wingless pathway regulates development of the *Drosophila* neuromuscular junction. J Neurosci 28:10875-84.

Mihara E, Hirai H, Yamamoto H, Tamura-Kawakami K, Matano M, Kikuchi A, Sato T, Takagi J (2016) Active and water-soluble form of lapidated Wnt protein is maintained by a serum glycoprotein afamin/α-albumin. eLIFE 5:e11621.

Miller JR (2001) The Wnts. Genome Biol 3(1):3001.1-3001.15.

Monastirioti M, Gorczyca M, Rapus J, Eckert M, White K, Budnuk V (1995) Octopamine immunoreactivity in the fruit fly Drosophila melanogaster. J Comp Neurol 356(2):275-87.

Montgomery MK, Xu S, Fire A (1998) RNA as a target of double-stranded RNA-mediated genetic interference in *Caenorhabditis elegans*. PNAS 95(26):15502-7.

Mosca TJ, Schwarz TL (2010) The nuclear import of Frizzled2-C by Importins β11 and α2 promotes postsynaptic development. Nat Neurosci 13:935-43.

Mulligan KA, Fuerer C, Ching W, Fish M, Willert K, Nusse R (2012) Secreted Wingless-interacting molecule (Swim) produces long-range signaling by maintaining Wingless solubility. Proc Natl Acad Sci USA 109(2):370-7.

Nakato H, Futch TA, Selleck SB (1995). The division abnormally delayed (dally) gene: a putative integral membrane proteoglycan required for cell division patterning during

postembryonic development of the nervous system in Drosophila. Development 121(11):3687-702.

Nardini M, Dijkstra BW (1999) Alpha/beta hydrolase fold enzymes: the family keeps growing. Curr Opin Struct Biol 9(6):732–7.

Naschberger A, Orry A, Lechner S, Bowler MW, Nurizzo D, Novokmet M, Keller MA, Oemer G, Seppi D, Haslbeck M, Pansi K, Dieplinger H, Rupp B (2017) Structural Evidence for a Role of the Multi-functional Human Glycoprotein Afamin in Wnt Transport. Structure 25(12):1907-15.

Newman ZL, Hoagland A, Aghi K, Worden K, Levy SL, Son JH, Lee LP, Isacoff EY (2017) Input-Specific Plasticity and Homeostasis at the Drosophila Larval Neuromuscular Junction. Neuron 93(6):1388-404.

Nusse R, Varmus HE (1982) Many tumors induced by the mouse mammary tumor virus contain a provirus integrated in the same region of the host genome. Cell 31(1):99-109.

Nusse R, van Ooyen A, Cox D, Fung YK, Varmus H (1984) Mode of proviral activation of a putative mammary oncogene (int-1) on mouse chromosome 15. Nature 307(5947):131-6.

Nusse R, Brown A, Papkoff J, Scambler P, Shackleford G, McMahon A, Moon R, Varmus H (1991) A new nomenclature for int-1 and related genes: the Wnt gene family. Cell 64(2):231.

Nusse R, Varmus H (2012) Three decades of Wnts: a personal perspective on how a scientific field developed. EMBO J 31(12):2670-84.

Nusse R, Clevers H (2017) Wnt/β-Catenin Signaling, Disease, and Emerging Therapeutic Modalities. Cell 169(6):985-99.

Packard M, Koo ES, Gorczyca M, Sharpe J, Cumberledge S, Budnik V (2002) The *Drosophila* Wnt, Wingless, provides an essential signal for pre- and postsynaptic differentiation. Cell 111:319-30.

Packard M, Jokhi V, Ding B, Ruiz-Cañada C, Ashley J, Budnik V (2015) Nucleus to Synapse Nesprin1 Railroad Tracks Direct Synapse Maturation Through RNA Localization. Neuron 86(4):1015-28.

Panáková D, Sprong H, Marois E, Thiele C, Eaton S (2005) Lipoprotein particles are required for Hedgehog and Wingless signaling. Nature 435:58-65.

Parkinson WM, Dookwah M, Dear ML, Gatto CL, Aoki K, Tiemeyer M, Broadie K (2016) Synaptic roles for phosphomannomutase type 2 in a new *Drosophila* congenital disorder of glycosylation disease model. Dis Model Mech 9:513-27.

Petersen CP, Reddien PW (2011) Polarized notum activation at wounds inhibits Wnt function to promote planarian head regeneration. Science 332(6031):852-5.

Philippe F, Pelloux J, Rayon C (2017) Plant pectin acetylesterase structure and function: new insights from bioinformatic analysis. BMC Genomics 18:456.

Qin G, Schwarz T, Kittel RJ, Schmid A, Rasse TM, Kappei D, Ponimaskin E, Heckmann M, Sigrist SJ (2005) Four different subunits are essential for expressing the synaptic glutamate receptor at neuromuscular junctions of Drosophila. J Neurosci 25(12):3209-18.

Ramírez-Weber FA, Kornberg TB (1999) Cytonemes: cellular processes that project to the principal signaling center in Drosophila imaginal discs. Cell 97(5):599-607.

Ren Y, Kirkpatrick CA, Rawson JM, Sun M, Selleck SB (2009) Cell Type-Specific Requirements for Heparan Sulfate Biosynthesis at the Drosophila Neuromuscular Junction:

Effects on Synapse Function, Membrane Trafficking, and Mitochondondrial Localization. J Neurosci 29(26):8539-50.

Rijsewijk F, Schuermann M, Wagenaar E, Parren P, Weigel D, Nusse R (1987) The Drosophila homolog of the mouse mammary oncogene int-1 is identical to the segment polarity gene wingless. Cell 50(4):649-57.

Rizzoli SO, Betz WJ (2005) Synaptic vesicle pools. Nat Rev Neurosci 6(1):57-69.

Routledge D, Scholpp S (2019) Mechanisms of intercellular Wnt transport. Development 146(10):dev176073.

Ruoslahti E (1988) Structure and Biology of Proteoglycans. Ann Rev Cell Biol 4:229-55.

Sarrazin S, Lamanna WC, Esko JD (2011). Heparan Sulfate Proteoglycans. Cold Spring Harb Perspect Biol 3(7):a004952.

Saunders S, Jalkanen M, O'Farrell S, Bernfield M (1989) Molecular cloning of syndecan, an integral membrane proteoglycan. J Cell Biol 108(4):1547.

Schnepp A, Komp Lindgren P, Hülsmann H, Kröger S, Paulsson M, Hartmann U (2005) Mouse testican-2. Expression, glycosylation, and effects on neurite outgrowth. 280(12):11274-80.

Schuster CM, Ultsch A, Schloss P, Cox JA, Schmitt B, Betz H (1991) Molecular cloning of an invertebrate glutamate receptor subunit expressed in Drosophila muscle. Science 254(5028)112-4.

Sharma RP (1973) Wingless – a new mutant in *D. melanogaster*. DIS 50:134.

Sharma RP, Chopra VL (1976) Effect of the wingless (wg1) mutation on wing and haltere development in Drosophila melanogaster. Dev Biol 48(2):461-65.

Shimomura O, Johnson FH, Saiga Y (1962) Extraction, purification and properties of aequorin, a bioluminescent protein from the luminous hydromedusan, Aequorea. J Cell Comp Physiol 59:223-39.

Sigrist SJ, Thiel PR, Reiff DF, Lachance PE, Lasko P, Schuster CM (2000) Postsynaptic translation affects the efficacy and morphology of neuromuscular junctions. Nature 405(6790):1062-5.

Speese SD, Ashley J, Jokhi V, Nunnari J, Barria R, Li Y, Ataman B, Koon A, Chang YT, Li Q, Moore MJ, Budnik V (2012) Nuclear envelope budding enables large ribonucleoprotein particle export during synaptic Wnt signaling. Cell 149:832-46.

Spring J, Paine-Saunders SE, Hynes RO, Bernfield M (1994) Drosophila syndecan: conservation of a cell-surface heparan sulfate proteoglycan. Proc Natl Acad Sci 91(8):3334-8.

Stamos JL, Weis WI (2013) The β-catenin destruction complex. Cold Spring Harb Perspect Biol 5(1):a007898.

Stanganello E, Hagemann AIH, Mattes B, Sinner C, Meyen D, Weber S, Schug A, Raz E, Scholpp S (2015) Filopodia-based Wnt transport during vertebrate tissue patterning. Nat Commun 6:5846.

Steigemann P, Molitor A, Fellert S, Jäckle H, Vorbrüggen G (2004) Heparan sulfate proteoglycan syndecan promotes axonal and myotube guidance by slit/robo signaling. Curr Biol 14(3):225-30.

Steinhart Z, Angers S (2018) Wnt signaling in development and tissue homeostasis. Development 145(11):dev146589.

Stevens CF, Williams JH (2000) “Kiss and run” exocytosis at hippocampal synapses. Proc Natl Acad Sci USA 97(23):12828-33.

Strigini M, Cohen SM (2000) Wingless gradient formation in the Drosophila wing. Curr Biol 10:293–300.

Swarup S, Verheyen EM (2012) Wnt/Wingless Signaling in *Drosophila.* Cold Spring Harb Perspect Biol 4(6):a007930.

Tanaka K, Kitagawa Y, Kadowaki T (2002) *Drosophila* Segment Polarity Gene Product Porcupine Stimulates the Posttranslational *N*-Glycosylation of Wingless in the Endoplasmic Reticulum. J Biol Chem 277(15):12816-23.

Tang X, Wu Y, Belenkaya TY, Huang Q, Ray L, Qu J, Lin X (2012) Roles of N-glycosylation and lipidation in Wg secretion and signaling. Dev Biol 364(1):32-41.

Torisu Y, Watanabe A, Nonaka A, Midorikawa Y, Makuuchi M, Shimamura T, Sugimura H, Niida A, Akiyama T, Iwanari H, Kodama T, Zeniya M, Aburatani H (2008) Human homolog of NOTUM, overexpressed in hepatocellular carcinoma, is regulated transcriptionally by beta-catenin/TCF. Cancer Sci 99(6):1139-46.

Torroja L, Packard M, Gorczyca M, White K, Budnik V (1999) The Drosophila ß-Amyloid Precursor Protein Homolog Promotes Synapse Differentiation at the Neuromuscular Junction. J Neurosci 19(18):7793-803.

Traister A, Shi W, Filmus J (2008) Mammalian Notum induces the release of glypicans and other GPI-anchored proteins from the cell surface. Biochem J 410:503-11.

Tsien RY (1998) The Green Fluorescent Protein. Annu Rev Biochem 67:509-44.

Tsou AP, Chuang YC, Su JY, Yang CW, Liao YL, Liu WK, Chiu JH, Chou CK (2003) Overexpression of a novel imprinted gene, *PEG10*, in human hepatocellular carcinoma and in regenerating mouse livers. J Biomed Sci 10(6):625-35.

Vannahme C, Schübel S, Herud M, Gösling S, Hülsmann H, Paulsson M, Hartmann U, Maurer P (1999) Molecular Cloning of Testican-2: Defining a Novel Calcium-Binding Proteoglycan Family Expressed in Brain. J Neurochem 73(1):12-20.

Verstreken P, Ohyama T, Bellen HJ (2008) FM 1-43 Labeling of Synaptic Vesicle Pools at the Drosophila Neuromuscular Junction. Methods Mol Biol 440:349-69.

Wang S, Hazelrigg T (1994) Implications for *bcd* mRNA localization from spatial distribution of *exu* protein in *Drosophila* oogenesis. Nature 369(6479):400-3.

Wang Q, Shui B, Kotlikoff MI, Sondermann H (2008) Structural basis for Calcium Sensing by GCaMP2. Structure 16(12):1817-27.

Willert K, Brown JD, Danenberg E, Duncan AW, Weissman IL, Reya T, Yates Jr III, Nusse R (2003) Wnt proteins are lipid-modified and can act as stem cell growth factors. Nature 423(6938):448-52.

Willert K, Nusse R (2010) Wnt proteins. Cold Spring Harb Perspect Biol 4(9):a007864.

Yan D, Wu Y, Feng Y, Lin S-C, Lin X (2009) The core protein of glypican Dally-like determines its biphasic activity in wingless morphogen signaling. Dev Cell 17:470-81.

Yang J, Yang Q, Yu J, Li X, Yu S, Zhang X (2016) SPOCK1 promotes the proliferation, migration and invasion of glioma cells through PI3K/AKT and Wnt/β-catenin signaling pathways. Oncol Rep 35(6):3566-76.

Zecca M, Basler K, Struhl G (1996) Direct and Long-Range Action of a Wingless Morphogen Gradient. Cell 87(5):833-44.

Zhai L, Chaturvedi D, Cumberledge S (2004) *Drosophila* Wnt-1 Undergoes a Hydrophobic Modification and Is Targeted to Lipid Rafts, a Process That Requires Porcupine. J Biol Chem 279(32):33220-7.

Zito K, Parnas D, Fetter RD, Isacoff EY, Goodman CS (1999) Watching a synapse grow: noninvasive confocal imaging of synaptic growth in Drosophila. Neuron 22(4):719-29.

Chapter II

Notum Coordinates Synapse Development via Extracellular Regulation of Wingless Trans-synaptic Signaling

Danielle L. Kopke[1], Sofia C. Lima[1], Cyrille Alexandre[2], Kendal Broadie[1]

[1]Department of Biological Sciences, Kennedy Center for Research on Human Development, Vanderbilt University, Nashville, TN 37235, USA

[2]Francis Crick Institute, 1 Midland Road, London, NW1 1AT, UK

This paper is published under the same title in the journal Development, 2017.

- **Competing interests**

  The authors declare no competing or financial interests.

- **Author contributions**

  Conceptualization: D.L.K., K.B.; Methodology: D.L.K., S.C.L., C.A., K.B.; Validation: D.L.K., S.C.L., C.A.; Formal analysis: D.L.K.; Investigation: D.L.K., S.C.L., C.A.; Resources: D.L.K., C.A., K.B.; Writing - original draft: D.L.K.; Writing - review & editing: D.L.K., S.C.L., C.A., K.B.; Visualization: D.L.K., K.B.; Supervision: D.L.K., K.B.; Project administration: D.L.K., K.B.; Funding acquisition: K.B.

- **Funding**

  This work was fully supported by a National Institutes of Health grant (MH096832 to K.B.).

- **Supplementary information**

  Supplementary information available online at http://dev.biologists.org/lookup/doi/10.1242/dev.148130.supplemental

- Received December 14, 2016.
- Accepted August 10, 2017.
-

Abstract

Synaptogenesis requires orchestrated communication between pre- and postsynaptic cells via coordinated trans-synaptic signaling across the extracellular synaptomatrix. The first Wnt signaling ligand discovered, *Drosophila* Wingless (Wg; Wnt1 in mammals), plays crucial roles in synaptic development, regulating synapse architecture as well as functional differentiation. Here, we investigate synaptogenic functions of the secreted extracellular deacylase Notum, which restricts Wg signaling by cleaving an essential palmitoleate moiety. At the glutamatergic neuromuscular junction (NMJ) synapse, we find that Notum secreted from the postsynaptic muscle acts to strongly modulate synapse growth, structural architecture, ultrastructural development and functional differentiation. In *Notum* null flies, we find upregulated extracellular Wg ligand and nuclear trans-synaptic signal transduction, as well as downstream misregulation of both pre- and postsynaptic molecular assembly. Structural, functional and molecular synaptogenic defects are all phenocopied by Wg overexpression, suggesting that Notum acts solely by inhibiting Wg trans-synaptic signaling. Moreover, these synaptic development phenotypes are suppressed by genetically correcting Wg levels in *Notum* null mutants, indicating that Notum normally functions to coordinate synaptic structural and functional differentiation via negative regulation of Wg trans-synaptic signaling in the extracellular synaptomatrix.

Introduction

In the developing nervous system, Wnt signaling ligands act as potent regulators of multiple stages of neuronal connectivity maturation, stabilization and synaptogenesis, including sculpting structural architecture and determining neurotransmission strength (Packard et al., 2002; Ataman et al., 2008; Miech et al., 2008). The founding Wnt ligand, *Drosophila* Wingless (Wg), is secreted from presynaptic neurons (Packard et al., 2002) and glia (Kerr et al., 2014) at the developing glutamatergic neuromuscular junction (NMJ) (Jan and Jan, 1976) to bind Frizzled 2 (Fz2) receptors in both anterograde and autocrine signaling (Packard et al., 2002). In the postsynaptic muscle, Wg binding to Fz2 activates the Frizzled Nuclear Import (FNI) signaling pathway, which involves Fz2 endocytosis followed by Fz2 cleavage and Fz2 C-terminus (Fz2-C) nuclear import (Mathew et al., 2005). Fz2-C trafficked in nuclear ribonucleoprotein (RNP) granules regulates translation of synaptic mRNAs, thereby driving expression changes that modulate synapse structural and functional differentiation (Speese et al., 2012). In the presynaptic neuron, Wg binding to Fz2 activates a divergent canonical pathway inhibiting the glycogen synthase kinase 3β (GSK3β) homolog Shaggy (Sgg) to regulate microtubule cytoskeleton dynamics via the microtubule-associated protein 1B (MAP1B) homolog Futsch (Miech et al., 2008). Futsch binding to microtubules regulates architectural changes in synaptic branching and bouton formation. Such multifaceted Wg functions require tight management throughout synaptic development.

A highly conserved extracellular Wg regulator is the secreted deacylase Notum. The *Notum* gene was discovered in a *Drosophila* gain-of-function (GOF) mutant screen targeting wing development (Mata et al., 2000). Under *scalloped*-Gal4 control, *Notum* GOF causes loss of the wing and duplication of the dorsal thorax (Giráldez et al., 2002). In the developing wing disc, Notum acts as a secreted, extracellular feedback inhibitor of Wg signaling (Gerlitz and Basler, 2002). Notum was recently re-defined as a carboxylesterase that cleaves an essential Wg lipid moiety (palmitoleic acid attached to a conserved serine), leaving it unable to bind to Fz2 and activate downstream signaling (Kakugawa et al., 2015). This Wnt palmitoleate moiety is similarly

cleaved by human Notum acting as a highly conserved secreted feedback antagonist in the extracellular space to inactivate Wnt signaling (Kakugawa et al., 2015; Langton et al., 2016). At the *Drosophila* NMJ, we have found that extracellular regulation of Wg trans-synaptic signaling plays key roles in synaptogenesis (Dani and Broadie, 2012; Parkinson et al., 2013). For example, extracellular matrix metalloproteinase (MMP) enzymes cleave heparan sulfate proteoglycan (HSPG) co-receptors to regulate the Wg trans-synaptic signaling that controls structural and functional synaptic development (Dear et al., 2016). Impairment of this mechanism is causative for fragile X syndrome (FXS) synaptogenic defects (Friedman et al., 2013). Similarly, misregulated extracellular mechanisms impair Wg trans-synaptic signaling in both congenital disorder of glycosylation (CDG) and galactosemia disease states, causing NMJ synaptogenic defects that result in disorders of coordinated movement (Jumbo-Lucioni et al., 2014, 2016; Parkinson et al., 2016). Given these insights, we wished to investigate the putative roles for Notum as a secreted Wg antagonist regulating synaptogenesis.

In the current study, we utilize the well-characterized *Drosophila* NMJ glutamate synapse model (Harris and Littleton, 2015; Keshishian et al., 1996; Menon et al., 2013) to study Notum requirements in synaptic development. We find that Notum secreted from muscle and glia is resident in the extracellular space surrounding developing synaptic boutons, where it negatively regulates Wg trans-synaptic signaling. In *Notum* mutants, extracellular Wg ligand levels and downstream Wg signaling are elevated. Null mutants display increased synapse number and strength, altered synaptic vesicle cycling, and synaptic ultrastructural defects including a decrease in subsynaptic reticulum (SSR)/bouton ratio, decreased synaptic vesicle density and an increase in the size of vesicular organelles. Cell-targeted RNAi studies reveal both postsynaptic and perisynaptic requirements, with muscle and glial *Notum* knockdown resulting in overelaborated NMJ architecture, but neuronal-driven *Notum* knockdown causing no detectable effects on synaptogenesis. Null *Notum* defects are all phenocopied by neuronal Wg overexpression, suggesting that synaptogenic phenotypes arise from lack of Wg inhibition. Consistently,

genetically correcting Wg levels at the synapse in *Notum* nulls alleviates synaptogenic phenotypes, demonstrating that Notum functions solely as a negative regulator of Wg signaling. Taken together, these results identify Notum as a secreted Wnt inhibitor resident in the extracellular synaptomatrix with crucial functions regulating trans-synaptic Wnt signaling to coordinate structural and functional synaptogenesis.

Results

Secreted Notum limits Wg levels and downstream trans-synaptic signaling

At the *Drosophila* NMJ, Wg secreted from neurons and glia regulates structural and functional synaptogenesis (Kerr et al., 2014; Packard et al., 2002), and this Wg signaling is tightly regulated within the extracellular synaptomatrix (Dear et al., 2016; Parkinson et al., 2016). Our goal was to test whether secreted Notum contributes to Wg trans-synaptic signaling control as a palmitoleate deacylase in this extracellular space (Kakugawa et al., 2015). We first tested Notum expression using a CRISPR/Cas9 HA tag in the endogenous *Notum* locus (Notum-HA; Fig. S1A-C). Introduction of Notum-HA does not detectably perturb Notum function, and the NMJ shows normal architectural development (Fig. S2A,B) and functional differentiation (Fig. S2C-F) compared with the w^{1118} genetic background control. At the NMJ, we used anti-HA to detect Notum and anti-Discs Large (DLG; Dlg1) to mark postsynaptic scaffolding (Dear et al., 2016; Jumbo-Lucioni et al., 2016). We find that Notum is localized at the NMJ and enriched at synaptic boutons (Fig. 7A). Detergent-free extracellular labeling shows that Notum is secreted into the external synaptomatrix surrounding individual synaptic boutons (Fig. S1D-F). Notum expression is similar to the dynamic Wg pattern at the NMJ (Dear et al., 2016; Jumbo-Lucioni et al., 2016). Extracellular Notum and Wg both surround synaptic boutons, and colocalize around a variable subset of boutons (Fig. S1G). This colocalization shows that Notum and Wg are in close proximity in the extracellular synaptomatrix, allowing Notum the opportunity to deacylate Wg and thus

decrease trans-synaptic signaling. In the absence of Notum, Wg signaling is expected to increase at the synapse.

We used the combination of a *Notum* knockout null mutation (*Notum*^{KO}) and two characterized *UAS-Notum:RNAi* lines to test synaptic Notum roles in the regulation of Wg trans-synaptic signaling (Kakugawa et al., 2015; Perkins et al., 2015). Extracellular Wg ligand levels were assayed using detergent-free immunocytochemical labeling to reveal only secreted Wg (Dear et al., 2016). Anti-horseradish peroxidase (HRP) was used to label the NMJ by binding to extracellular fucosylated N-glycans associated with the presynaptic membrane (Parkinson et al., 2013). We first compared *Notum*^{KO} with the *w*^{1118} genetic background control and found that Wg is strikingly increased in *Notum* mutants, with elevated expression levels and an expanded spatial domain in the extracellular space surrounding NMJ synaptic boutons (Fig. 7B, left). Comparing *Notum* RNAi knockdown (*UH1*-Gal4>UAS-*Notum*:*RNAi*) with the transgenic driver alone control (*UH1*-Gal4/+) reveals a similar, but more modest, increase in extracellular Wg ligand levels at the NMJ synapse (Fig. 7B, right). In quantified measurements, decreasing Notum significantly increases Wg levels in parallel (mean±s.e.m.: normalized *UH1*-Gal4/+, 1.0±0.10 versus *UH1>Notum:RNAi*, 1.37±0.12; n=16, P=0.022; Fig. 7E). Completely eliminating Notum in null mutants results in a very strong Wg elevation by >70% compared with controls (*w*^{1118}, 1.0±0.11 versus *Notum*^{KO}, 1.71±0.16; n=16, P=0.001; Fig. 7E). These results show that Notum greatly limits Wg expression in the extracellular synaptomatrix.

We next investigated the roles of Notum in Wg trans-synaptic signaling. Presynaptically, Wg binding to Fz2 receptor regulates the MAP1B homolog Futsch to modulate microtubule dynamics (Miech et al., 2008). We therefore assayed Futsch labeling in *Notum* mutants (Fig. S3A), but observed no discernible difference in quantified comparisons (Fig. S3B). In the muscle, Wg binding drives postsynaptic Fz2 receptor endocytosis, cleavage and Fz2-C fragment transportation into muscle nuclei (FNI signaling pathway) to drive expression changes modifying NMJ structural and functional development (Mathew et al., 2005; Speese et al., 2012). We

therefore next tested Fz2 receptor expression at the neuronal membrane in the absence of Notum (Fig. 7C) using the Fz2-C antibody. In *Notum*^{KO} null mutants, we find a clear decrease in the intensity of Fz2-C punctae surrounding synaptic boutons, consistent with the highly increased Wg ligand levels (Fig. 7B,C). In quantified measurements, Fz2-C receptors are very significantly reduced in *Notum* mutants compared with controls (*w*^{1118}, 1.0±0.04 versus *Notum*^{KO}, 0.81±0.03; *n*=23, *P*=0.0001; Fig. 7F, left). We next tested the downstream import of Fz2-C into postsynaptic muscle nuclei (Fig. 7D). Comparing *Notum* RNAi knockdown (*UH1*-Gal4>UAS-*Notum*:*RNAi*) with transgenic driver alone controls (*UH1*-Gal4/+), there is a striking increase in the number of Fz2-C punctae in muscle nuclei with loss of Notum function (Fig. 7D). In quantified measurements, nuclear Fz2-C intensity in mutants is increased by 40% compared with controls (*UH1*-Gal4/+, 1.0±0.06 versus *UH1>Notum:RNAi*, 1.40±0.09; *n*=10 nuclei, *P*=0.001; Fig. 7F, right). These results show that Notum strongly limits Wg trans-synaptic signaling at the developing NMJ.

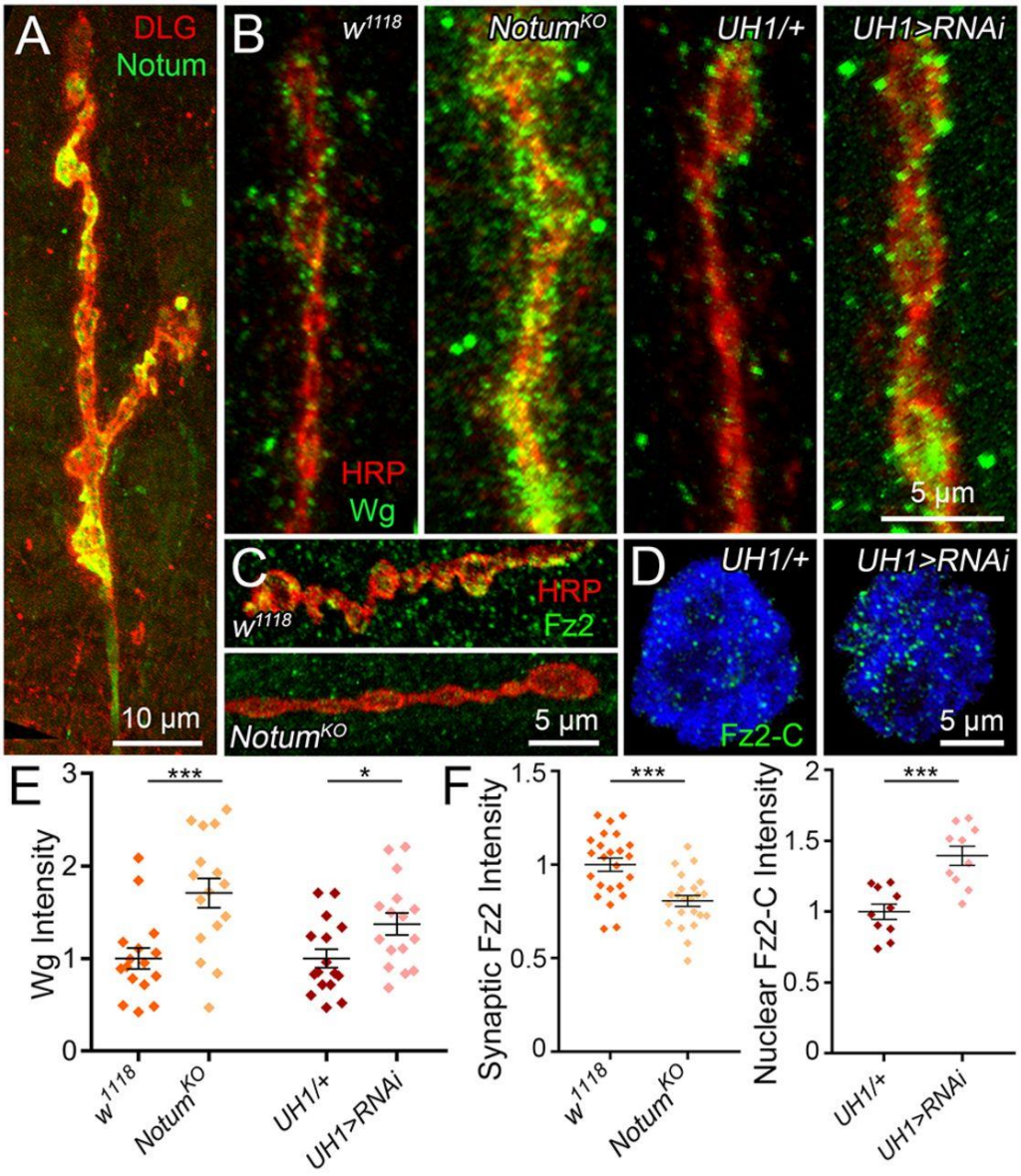

Fig. 7: Extracellular Notum reduces Wg ligand levels and trans-synaptic signaling. (A) Representative image of muscle 4 NMJ co-labeled for CRISPR-generated Notum:HA (Notum, green) and synaptic label anti-Discs Large (DLG, red). (B) Representative NMJ bouton images of extracellular anti-Wingless labeling (Wg, green) co-labeled with synaptic marker anti-horseradish peroxidase (HRP, red) in *w*^{1118} background control versus *Notum*^{KO} null mutant and *UH1-Gal4/+* transgenic control versus *UH1>Notum:RNAi*. (C) Representative synaptic bouton images of anti- Fz2-C (green) at the NMJ (HRP, red) in *w*^{1118} and *Notum*^{KO}. (D) Representative images of postsynaptic nuclei co-labeled with anti-Fz2-C (green) and nuclear label DRAQ5 (blue) in *UH1/+* control versus *UH1>Notum:RNAi*. (E) Quantified Wg fluorescent intensities in all four genotypes normalized to control. (F) Quantified Fz2 fluorescent intensities at the NMJ synaptic terminal (left) and postsynaptic nuclei (right) in *Notum*^{KO} and *UH1>Notum:RNAi* normalized to controls (*w*^{1118} *and UH1/+*). **P*≤0.05, ****P*≤0.001.

Notum secreted from muscle and glia regulates presynaptic NMJ architecture

Wg trans-synaptic signaling regulates NMJ growth, synaptic bouton formation and ultrastructural assembly (Packard et al., 2002). We therefore hypothesized that loss of Notum control of Wg trans-synaptic signaling should perturb synaptic architecture. Each NMJ terminal consists of a relatively stereotypical muscle innervation pattern, with consistent axon branching and synaptic bouton formation (Menon et al., 2013). Wg signaling bidirectionally regulates synaptic morphogenesis, with Wg knockdown causing a decrease in synaptic bouton number and Wg overexpression causing an increase in synaptic bouton number (Packard et al., 2002). To test the requirement for Notum in synaptic architectural development, we used immunocytochemistry to co-label the wandering third instar larval NMJ with both presynaptic anti-HRP and postsynaptic anti-DLG markers (Dear et al., 2016; Jumbo-Lucioni et al., 2016). We used characterized *Notum* RNAi transgenic lines (Perkins et al., 2015) for ubiquitous (*UH1*-Gal4), neuronal (*elav*-Gal4), glial (*repo*-Gal4) and muscle (*24B*-Gal4) cell-targeted knockdown studies (Fig. 8; Fig. S4A,B). We used the characterized *Notum*^{KO} null mutant to completely eliminate Notum (Kakugawa et al., 2015), with side-by-side comparisons with presynaptic Wg overexpression (Fig. 9). Transmission electron microscopy (TEM) studies were used in parallel to examine synaptic bouton ultrastructure (Dear et al., 2016; Parkinson et al., 2013) in direct comparison with the confocal analyses (Fig. 9).

We find that Notum negatively regulates NMJ structural development, with roles limiting growth and synaptic bouton formation (Fig. 8A). When Notum is knocked down ubiquitously (*UH1*-Gal4>*Notum:RNAi*), there is a clear increase in NMJ size, branching and bouton number (Fig. 8 Fig. 8A). In quantified measurements, global Notum loss causes significant increases in synaptic area (*UH1*-Gal4/+, 211.6±8.49 μm^2 versus *UH1>Notum:RNAi*, 277.6±11.09; $n \geq 14$, $P<0.0001$), branching (*UH1*/+, 2.8±0.2 versus *UH1>Notum:RNAi*, 3.69±0.2; $P=0.003$) and bouton number (*UH1*/+, 24.67±0.88 versus *UH1>Notum:RNAi*, 35.38±1.08; $P<0.0001$; Fig. 8B). To test cell-specific requirements, Notum was knocked down in neurons (*elav*-Gal4), muscle (*24B*-Gal4) or

glia (*repo*-Gal4). Qualitatively, NMJ terminals with muscle-targeted Notum RNAi are expanded indistinguishably from global knockdown, whereas neuron-targeted Notum loss has little discernable effect (Fig. 8A). In quantified measurements, muscle-specific Notum knockdown causes a significant expansion of synaptic area (*24B*-Gal4/+, 203.7±6.73 μm^2 versus *24B>Notum:RNAi*, 232.1±10.03; $n \geq 15$, $P=0.027$), branching (*24B*/+, 2.73±0.18 versus *24B>Notum:RNAi*, 3.69±0.25; $P=0.005$) and bouton number (*24B*/+, 21.33±0.8 versus *24B>Notum:RNAi*, 33.5±1.26; $P<0.0001$; Fig. 8B). Glial-specific RNAi increases synaptic bouton number more weakly (*repo*-Gal4/+, 32.19±1.14 versus *repo>Notum*:*RNAi*, 39.38±1.88; $n=16$, $P=0.0027$; Fig. S4A,B), but does not affect branching. In contrast, neuron-specific Notum knockdown causes no significant change in any synaptic parameter (Fig. 8B). These results show that Notum secreted from muscle and glia both limit presynaptic structure, with muscle-derived Notum having the greater role.

Null *Notum*^{KO} NMJs show phenotypes similar to ubiquitous Notum knockdown, with striking increases in synapse size, branching and bouton formation (Fig. 9A). In quantified measurements, mutants display highly significant increases in area (w^{1118}, 165.9±5.48 μm^2 versus *Notum*^{KO}, 235.4±9.60; $n=16$, $P<0.0001$), branching (w^{1118}, 2.5±0.16 versus *Notum*^{KO}, 4.19±0.28; $P<0.0001$) and bouton number (w^{1118}, 23.31±0.90 versus *Notum*^{KO}, 37.69±1.2; $P<0.0001$; Fig. 9B). Importantly, Wg overexpression (*elav*-Gal4>UAS-Wg) causes a very similar synaptic expansion (Fig. 9A), consistent with previous reports (Packard et al., 2002). Neuronal overexpression increasing synaptic Wg ligand levels by 33% (data not shown) causes an obvious expansion of synaptic size, branching and bouton formation (Fig. 9A). In quantified measurements, Wg overexpression increases synaptic area (*elav*-Gal4/+, 234.3±15.36 μm^2 versus *elav>wg*, 284.9±10.51; $n=16$, $P=0.01$), branching (*elav*/+, 2.44±0.16 versus *elav>wg*, 3.19±0.23; $P=0.01$) and bouton number (*elav*/+, 29.13±1.50 versus *elav>wg*, 40.56±1.42; $P<0.0001$; Fig. 9B). Bouton diameter quantification shows a non-significant trend towards small boutons in both comparisons (w^{1118} versus *Notum*^{KO}, *elav*-Gal4/+ versus *elav>wg*), with boutons

closely packed and harder to delineate in both *Notum*^{KO} and Wg overexpression conditions (Fig. 9A, insets). At the ultrastructural level, control NMJs typically show a single bouton embedded in the SSR, whereas mutants usually have several boutons sharing a single SSR (Fig. 9C). Quantification shows a significant increase in boutons per SSR (*w*^{1118}, 1.19±0.10 versus *Notum*^{KO}, 2.44±0.39; *P*=0.0075; Fig. 9D). These results show that Notum coordinates synapse development by negatively regulating Wg signaling.

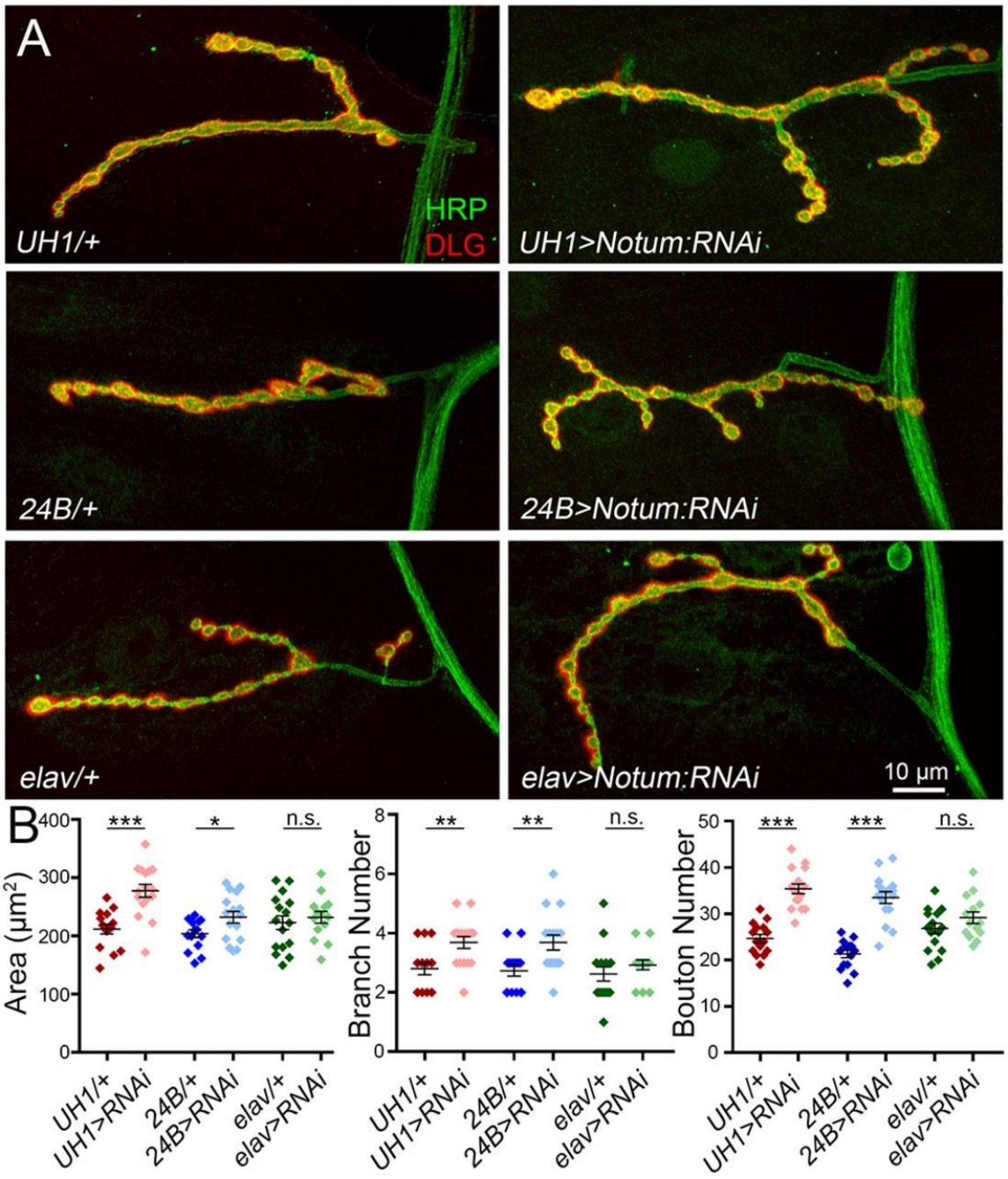

Fig. 8: Postsynaptic Notum secretion limits presynaptic structural development. (A) Representative confocal images of muscle 4 NMJs co-labeled for presynaptic HRP (green) and postsynaptic DLG (red) with cell-targeted *Notum* RNAi knockdown (top, ubiquitous *UH1-Gal4/+* versus *UH1>Notum:RNAi*; middle, postsynaptic muscle *24B-Gal4/+* versus *24B>Notum:RNAi*; bottom, presynaptic neuron *elav-Gal4/+* versus *elav>Notum:RNAi*). (B) Quantified NMJ area, branch number and synaptic bouton number for the six genotypes. *$P \leq 0.05$, **$P \leq 0.01$, ***$P \leq 0.001$; n.s., not significant.

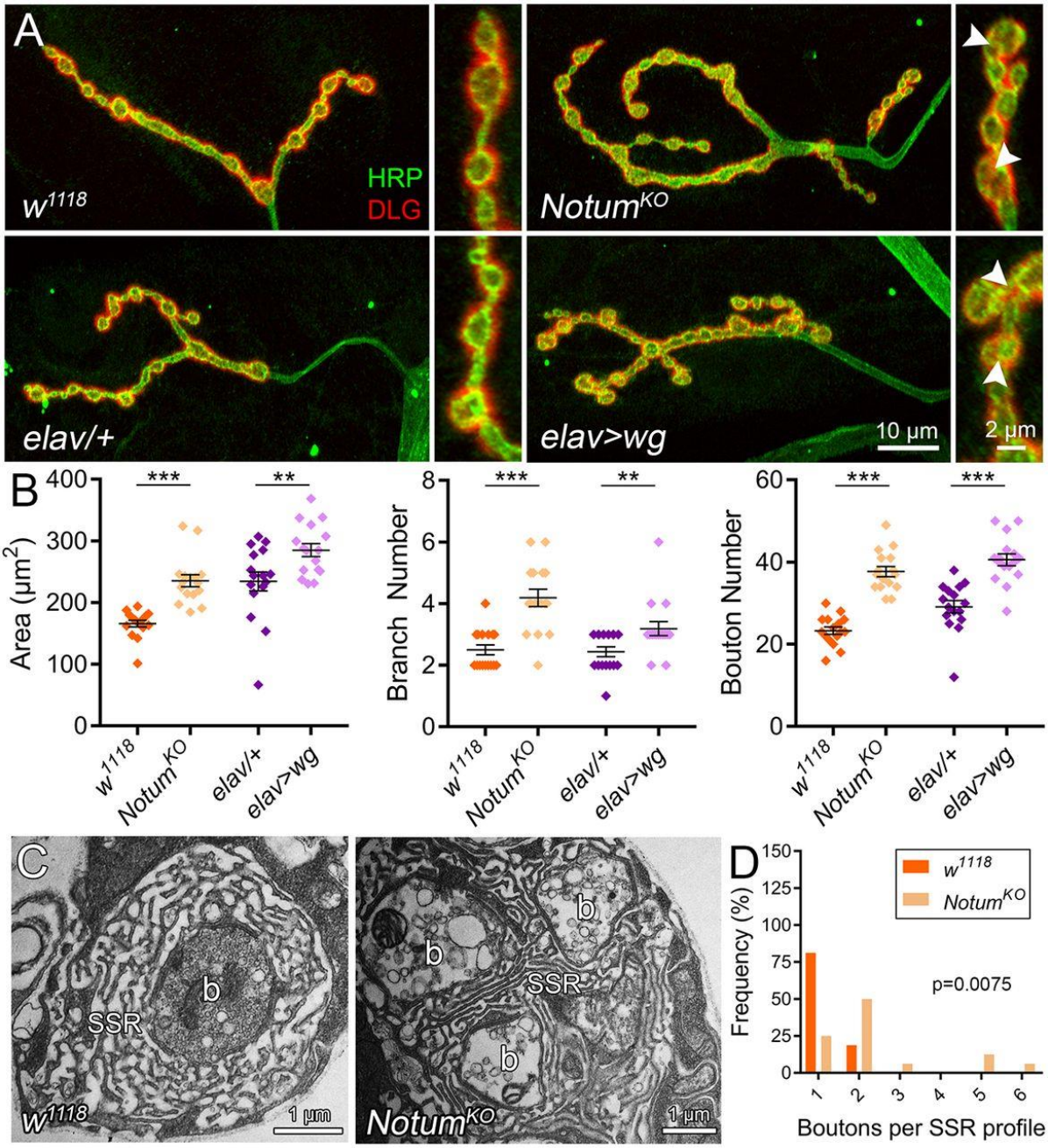

Fig. 9: Elevated Wg signaling phenocopies Notum null mutant synaptic defects. (A) Representative images of muscle 4 NMJs co-labeled for HRP (green) and DLG (red) with Notum null mutant (top row: w^{1118} background control versus $Notum^{KO}$) and Wg overexpression (bottom row: elav-Gal4/+ control versus elav>wg). Insets show higher magnification boutons in all four conditions, with clustered boutons in mutants (arrowheads). (B) Quantified NMJ area, branch number and synaptic bouton number for the four genotypes. **P≤0.01 and ***P≤0.001. (C) Representative TEM images of w^{1118} and $Notum^{KO}$ synaptic boutons. b, bouton; SSR, subsynaptic reticulum. (D) Quantification of bouton number per SSR profile shown in a frequency histogram.

Notum limits NMJ synaptic functional differentiation and movement output

Structural and functional development occur simultaneously, but are regulated by distinct molecular mechanisms (Menon et al., 2013). Wg trans-synaptic signaling also regulates synaptic functional differentiation, including both neurotransmission strength and activity-dependent processes that modulate total synaptic output (Ataman et al., 2008; Packard et al., 2002). To test whether secreted Notum contributes to NMJ functional development, spontaneous miniature EJC (mEJC) and nerve stimulation-evoked excitatory junction current (EJC) recordings were made using two-electrode voltage-clamp (TEVC) configuration to obtain linear measurements of synaptic function (Dear et al., 2016; Parkinson et al., 2016). To test consequences on behavioral motor output, coordinated movement was assayed in parallel. We used a well-established roll-over test that measures a precisely orchestrated sequence of bilateral muscle contractions mediated by NMJ function (Bodily et al., 2001; Jumbo-Lucioni et al., 2016). To dissect functional mechanisms, activity-dependent live dye imaging was carried out as a measure of synaptic vesicle (SV) cycling. We used physiological motor nerve stimulation to drive FM1-43 lipophilic dye incorporation, as a measure of both SV endocytosis and pool size, and repeat depolarization in the absence of dye to drive release, as a measure of SV exocytosis within boutons and across the synaptic terminal (Parkinson et al., 2013; Vijayakrishnan et al., 2010). Results of these functional studies are displayed in Figs. 10 and 11, and described below.

Notum negatively regulates NMJ functional differentiation, resulting in elevated neurotransmission strength in *Notum*^{KO} mutants (Fig. 10A). In quantified measurements, EJC amplitudes are significantly elevated in nulls compared with matched genetic controls (*w*^{1118}, 1.0±0.06 versus *Notum*^{KO}, 1.30±0.06; $n \geq 16$, $P=0.0009$; Fig. 10B), with a corresponding increase in mEJC frequency but no change in amplitude (Fig. S5A,B). Elevated function is maintained with high frequency stimulation, with higher quantal content (Fig. S5C,D). Glial *repo>Notum:RNAi* knockdown causes no changes (Fig. S4C-E), indicating that the requirement is entirely from postsynaptic Notum. As with structure, *Notum* null functional defects are phenocopied by Wg

overexpression (Fig. 10A). In quantified measurements, EJC amplitudes are significantly elevated with Wg overexpression compared with control (*elav*-Gal4/+, 1.0±0.08 versus *elav>wg*, 1.36±0.11; $n \geq 7$, $P=0.024$; Fig. 10B). Consequences of elevated NMJ function were tested using the roll-over assay (Movies 1 and 2). Ubiquitous Notum knockdown results in faster movement (*UH1*-Gal4/+, 19.31±1.57 s versus *UH1>Notum:RNAi*, 11.87±1.59; $n=15$, $P=0.002$), as does muscle-targeted RNAi (*24B*-Gal4/+, 16.47±2.4 s versus *24B>Notum:RNAi*, 8.48±1.17; $P=0.007$), but no change occurs with neuronal knockdown ($P=0.5$; Fig. 10C). The glial knockdown is also faster (*repo*-Gal4/+, 17.83±1.53 s versus *repo>Notum:RNAi*, 12.93±1.33; $P=0.022$; Fig. S4F). Notum knockout increases speed (w^{1118}, 19.24±1.63 s versus $Notum^{KO}$, 12.02±1.82; $P=0.006$), again phenocopied by Wg overexpression (*wg*-Gal4/+, 15.69±1.61 s versus *wg*-Gal4>*wg,* 8.73±1.32; $P=0.002$; Fig. 10C). These results show that Notum loss of function (LOF) and Wg GOF similarly augment functional synaptic differentiation and motor output.

Loss of Notum increases both NMJ morphogenesis and functional differentiation (compare Figs. 9 and 10), making it difficult to disassociate the structural and functional contributions. Therefore, to independently test functional development on the level of individual synaptic boutons, lipophilic FM1-43 live dye imaging was performed using physiological nerve stimulation to induce SV cycling (Fig. 11). Each synaptic bouton harbors functionally discrete SV pools that participate in active endocytosis-exocytosis turnover cycling. Upon neuronal stimulation, $Notum^{KO}$ mutants clearly and reproducibly load less dye compared with matched controls (Fig. 11A). In quantified measurements, loaded FM1-43 dye intensities per bouton reveal a very highly significant decrease in *Notum* null boutons relative to matched controls (normalized w^{1118}, 1.0±0.02 versus $Notum^{KO}$, 0.83±0.06; $n \geq 127$ boutons, $P=<0.0001$; Fig. 11B,C). To study SV release exocytosis, NMJ terminals were depolarized with nerve stimulation a second time in the absence of FM1-43 to drive dye release (Fig. 11A). Both controls and mutants appear comparable in the level of synaptic FM-143 exocytosis. Null *Notum* boutons load significantly less dye and therefore have less dye to release; however, the unload/load dye ratio in mutants is unchanged

compared with matched controls (*P*=0.55; Fig. 11C, right). These results reveal defects in presynaptic function in the absence of Notum that predict impairments in presynaptic SV organization.

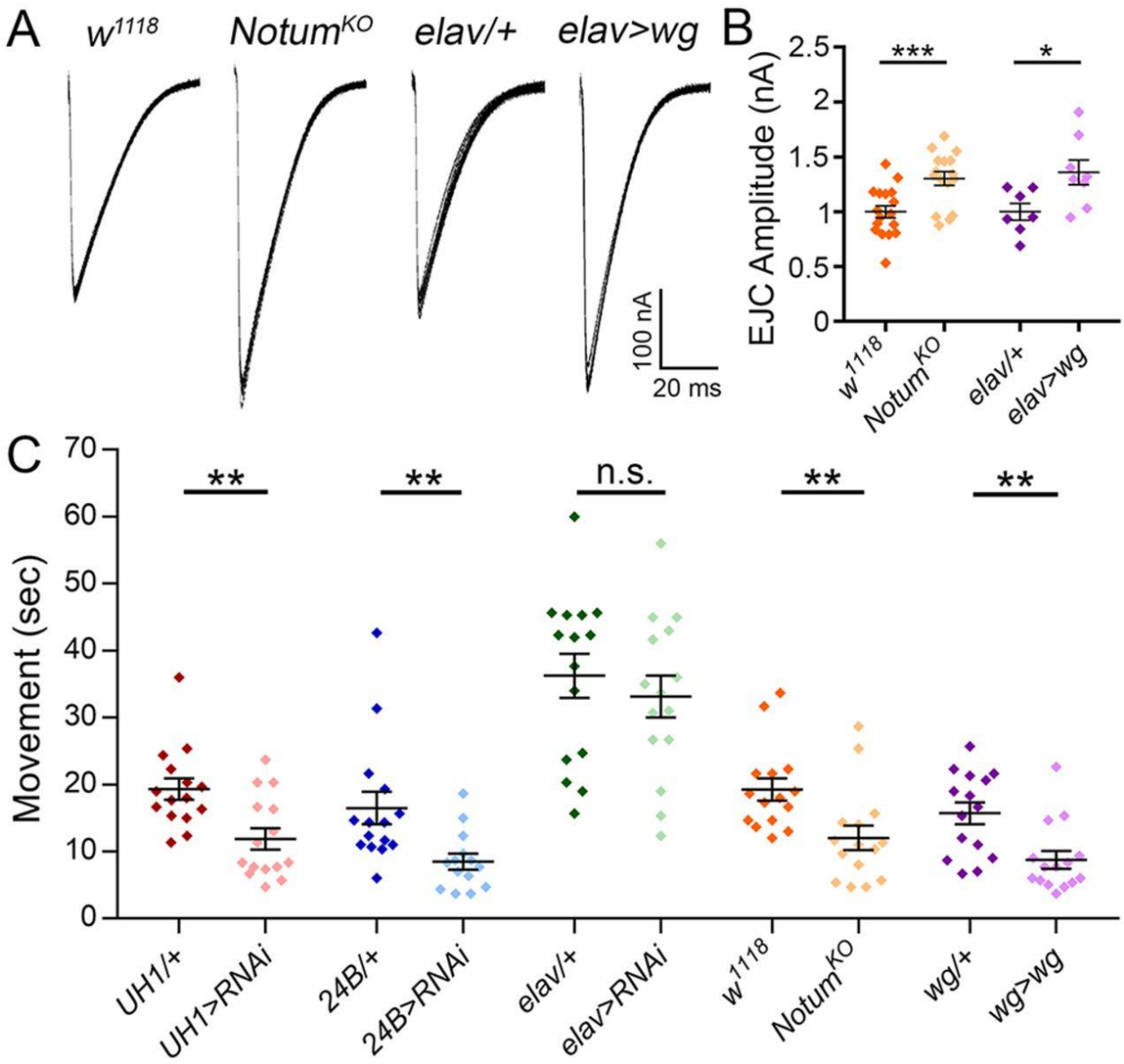

Fig. 10: Notum loss strengthens synapse function and improves reaction rate. (A) Representative nerve stimulation-evoked EJC traces (1.0 mM Ca^{2+}) from *w*^{1118} background control versus *Notum*^{KO} null mutant and *elav-Gal4/+* transgenic control versus *elav>wg* overexpression. (B) Quantification of EJC amplitudes in all four genotypes. (C) Coordinated movement rollover reaction time quantification for the denoted ten genotypes. *$P \leq 0.05$, **$P \leq 0.01$, ***$P \leq 0.001$; n.s., not significant.

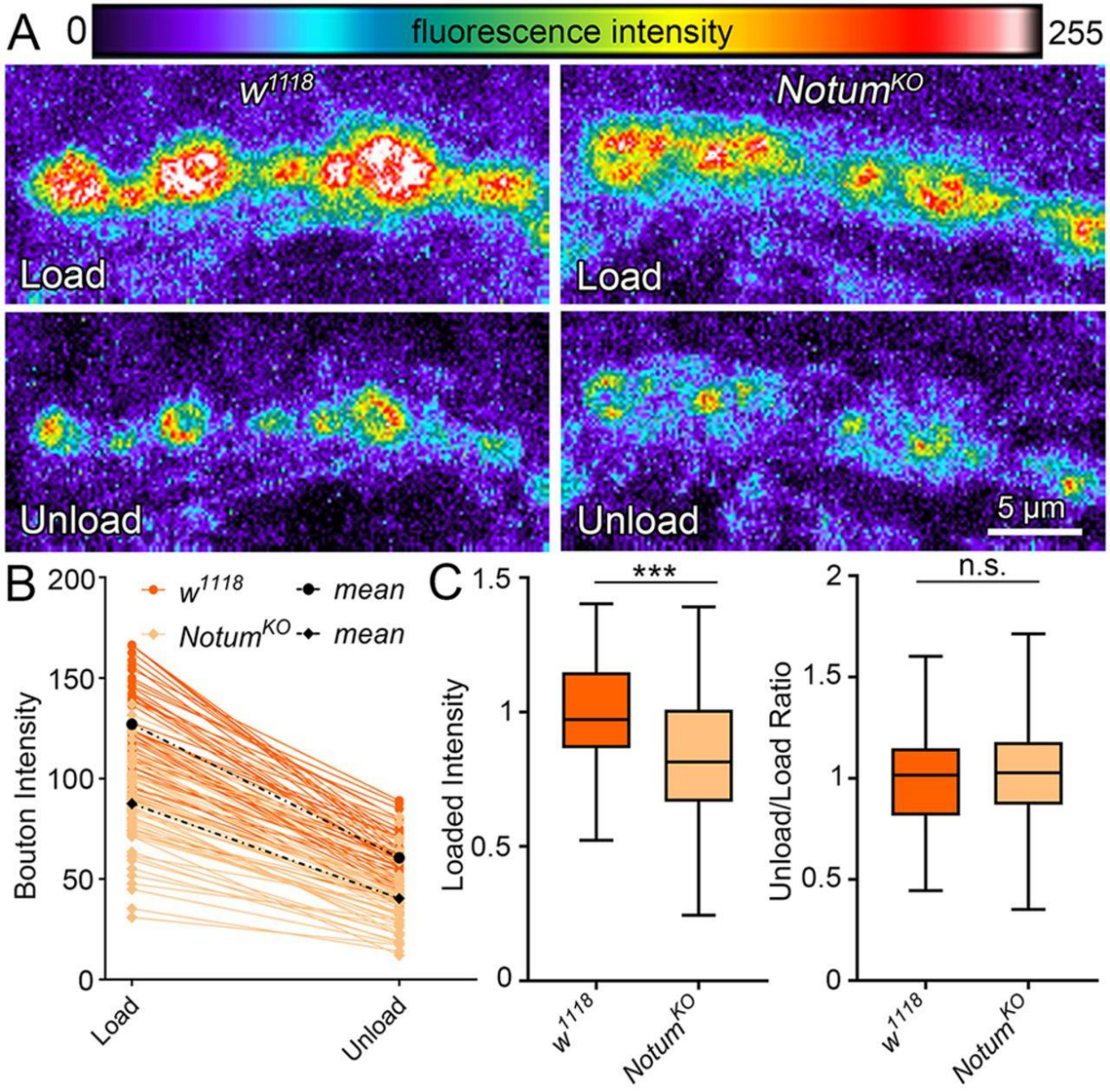

Fig. 11: Notum loss alters presynaptic differentiation via vesicle trafficking. (A) Representative synaptic bouton images of FM 1-43 dye imaging with depolarization-induced loading (top) and unloading (bottom) in *w*^{1118} control (left) and *Notum*^{KO} (right). Fluorescent intensity is represented as a heat map. (B) Sample quantification of FM1-43 dye loaded and unloaded bouton fluorescence for all boutons from a single NMJ of each genotype. (C) Box-and-whisker plot quantification of the loaded bouton fluorescence (left) and unload/load ratio (right) for all boutons. ***$P \leq 0.001$; n.s. not significant.

Notum regulates ultrastructural and molecular synaptic assembly

The requirement for Notum for functional synaptogenesis may reflect pre- or postsynaptic roles, or a combination of both. We next tested these mechanistic possibilities with a combination of confocal imaging for synaptic components (Jumbo-Lucioni et al., 2016) and TEM ultrastructure studies (Dear et al., 2016). At the *Drosophila* NMJ, presynaptic boutons are embedded in an elaborate postsynaptic SSR (Fig. 12A). In *Notum* mutants, the multiple boutons in a single SSR field are on average reduced in cross-sectional area per bouton (w^{1118}, 5.93±1.23 µm^2 versus *Notum*^{KO}, 3.35±0.51; n≥19 boutons, P=0.028), but if the total bouton areas per SSR are combined, mutants are indistinguishable from controls (w^{1118}, 7.04±1.41 µm^2 versus *Notum*^{KO}, 7.37±1.24; P=0.862). Furthermore, SSR area is obviously reduced in *Notum* null mutants (Fig. 12A), with the quantified SSR/bouton ratio significantly decreased compared with controls (w^{1118}, 3.91±0.34 versus *Notum*^{KO}, 2.66±0.28; n≥15 boutons, P=0.009; Fig. 12B). This phenotype is also observed at the confocal level, with a very significant decrease in postsynaptic DLG area (normalized w^{1118}, 1.0±0.08 versus *Notum*^{KO}, 0.65±0.08; n=16, P=0.005). Within boutons, uniform (40-50 nm) SVs are interspersed with larger vacuoles (>75 nm; Fig. 12A). In *Notum* null boutons, SVs are very obviously reduced in abundance and more numerous vacuoles are expanded in size (Fig. 12A, right). In quantified measurements, the SV density per synaptic bouton area is greatly decreased in *Notum* mutants compared with matched controls (w^{1118}, 40.39±3.98 versus *Notum*^{KO}, 20.87±2.36), a highly significant 50% reduction (n≥15 boutons, P<0.0001; Fig. 12C). Quantification of enlarged vacuole diameter (>75 nm) shows highly significant increases in *Notum* null mutants (w^{1118}, 113.52±3.15 nm versus *Notum*^{KO}, 175.10±8.64; P<0.0001; Fig. 12D). These results reveal severely impaired presynaptic and postsynaptic ultrastructural development in the absence of Notum.

NMJ function depends on the number and composition of postsynaptic glutamate receptors (GluRs) juxtaposing presynaptic Bruchpilot (Brp) active zone release sites (Kittel et al., 2006; Qin et al., 2005; Rasse et al., 2005; Wagh et al., 2006). Brp-positive synapses are elevated

in the absence of Notum (Fig. 13A). In quantified measurements, Brp punctae number is very significantly increased in *Notum* nulls compared with controls (normalized w^{1118}, 1.0±0.05 versus $Notum^{KO}$, 1.35±0.06; n=16, P=0.0002; Fig. 13C). There are two GluR classes defined by inclusion of either IIA or IIB subunits (Featherstone et al., 2005; Qin et al., 2005). There is a striking increase of both glutamate receptor classes in *Notum* nulls (Fig. 13B). In quantified measurements, Notum loss results in a highly significant increase in GluRIIA clusters in mutants compared with controls (w^{1118}, 1.0±0.08 versus $Notum^{KO}$, 1.41±0.09; n≥15, P=0.002; Fig. 13D, left), with a strong increase in overall GluRIIA levels measured by fluorescence intensity (w^{1118}, 1.0±0.05 versus $Notum^{KO}$, 1.58±0.20; n≥15, P=0.009). Similarly, GluRIIB clusters are increased in *Notum* nulls (w^{1118}, 1.0±0.06 versus $Notum^{KO}$, 1.39±0.08; P=0.0006; Fig. 13D, right), although the overall GluRIIB fluorescence intensity is not significantly different (w^{1118}, 1.0±0.06 versus $Notum^{KO}$, 0.88±0.08; n≥15, P=0.238). Synaptic density (synapse number/bouton) is not changed by loss of Notum (Brp: w^{1118}, 1.0±0.04 versus $Notum^{KO}$, 0.97±0.05; n≥15, P=0.529; GluRIIA: w^{1118}, 1.0±0.05 versus $Notum^{KO}$, 0.99±0.04; n≥15, P=0.855; GluRIIB: w^{1118}, 1.0±0.03 versus $Notum^{KO}$, 0.97±0.04; n≥15, P=0.532). Wg GOF phenocopies pre- and postsynaptic changes (Fig. 13A,B). In quantified measurements, Brp punctae are significantly increased with Wg GOF compared with controls (*elav*-Gal4/+, 1.0±0.05 versus *elav>wg*, 1.50±0.09; n≥15, P<0.0001; Fig. 13C). Similarly, both GluR classes are elevated by Wg overexpression, including GluRIIA clusters (*elav*-Gal4/+, 1.0±0.05 versus *elav>wg*, 1.29±0.08; n=16, P=0.0041) and GluRIIB clusters (*elav*-Gal4/+, 1.0±0.05 versus *elav>wg*, 1.34±0.07; P=0.0004; Fig. 13D). These results indicate Notum restricts synaptic molecular development by limiting Wg trans-synaptic signaling.

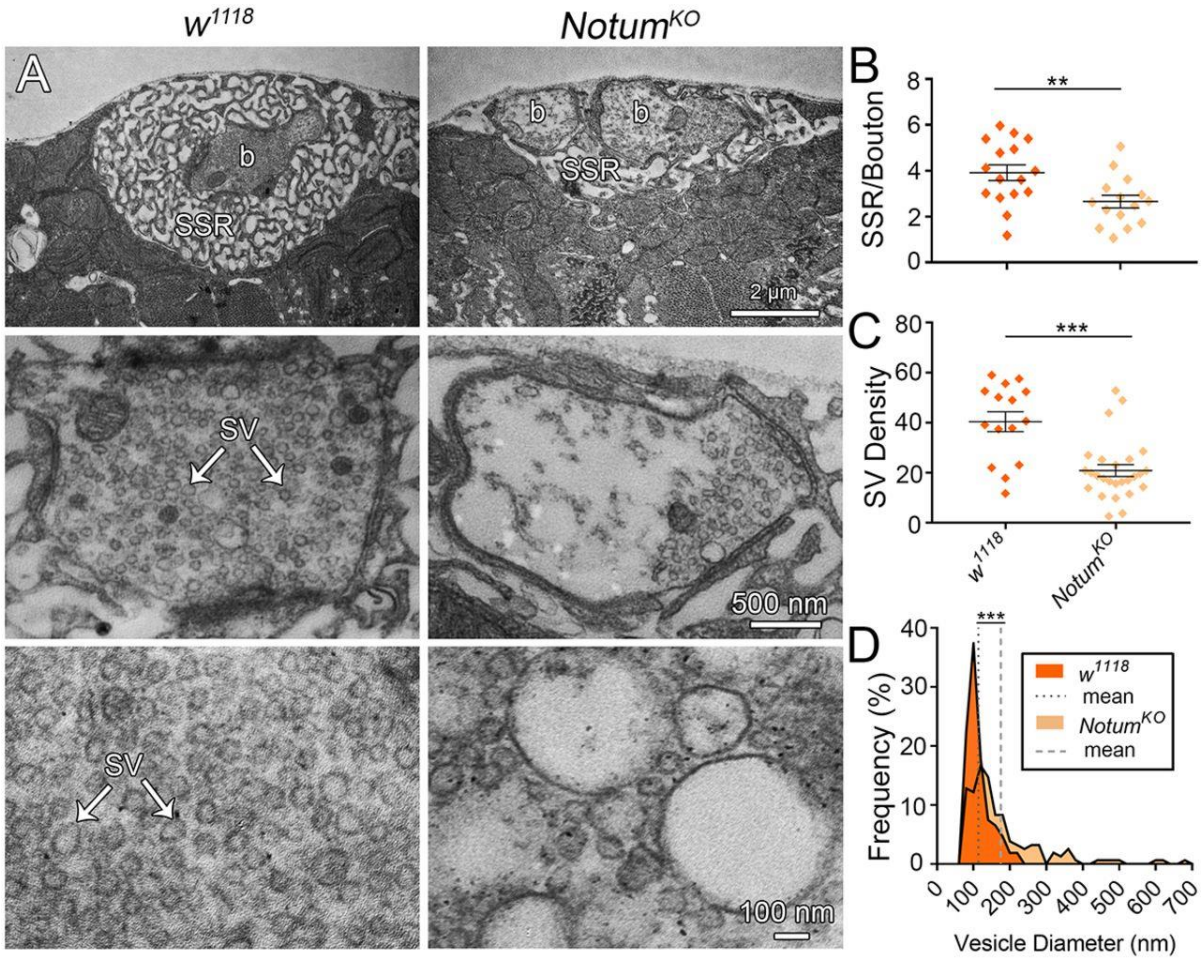

Fig. 12: Ultrastructural synaptic development depends on Notum function. (A) Representative TEM images of *w*^{1118} and *Notum*^{KO} synaptic boutons, with different examples shown at three magnifications; low to include the entire SSR surrounding a bouton (b, top), medium for a presynaptic bouton (middle) and high for better visualization of the synaptic vesicles (SV, bottom). (B) Quantification of SSR/bouton area ratio. (C) Quantification of SV density in NMJ boutons. (D) Frequency distribution of vesicle diameters for both genotypes, with mean diameter indicated by a dotted/dashed line. ***P*≤0.01, ****P*≤0.001.

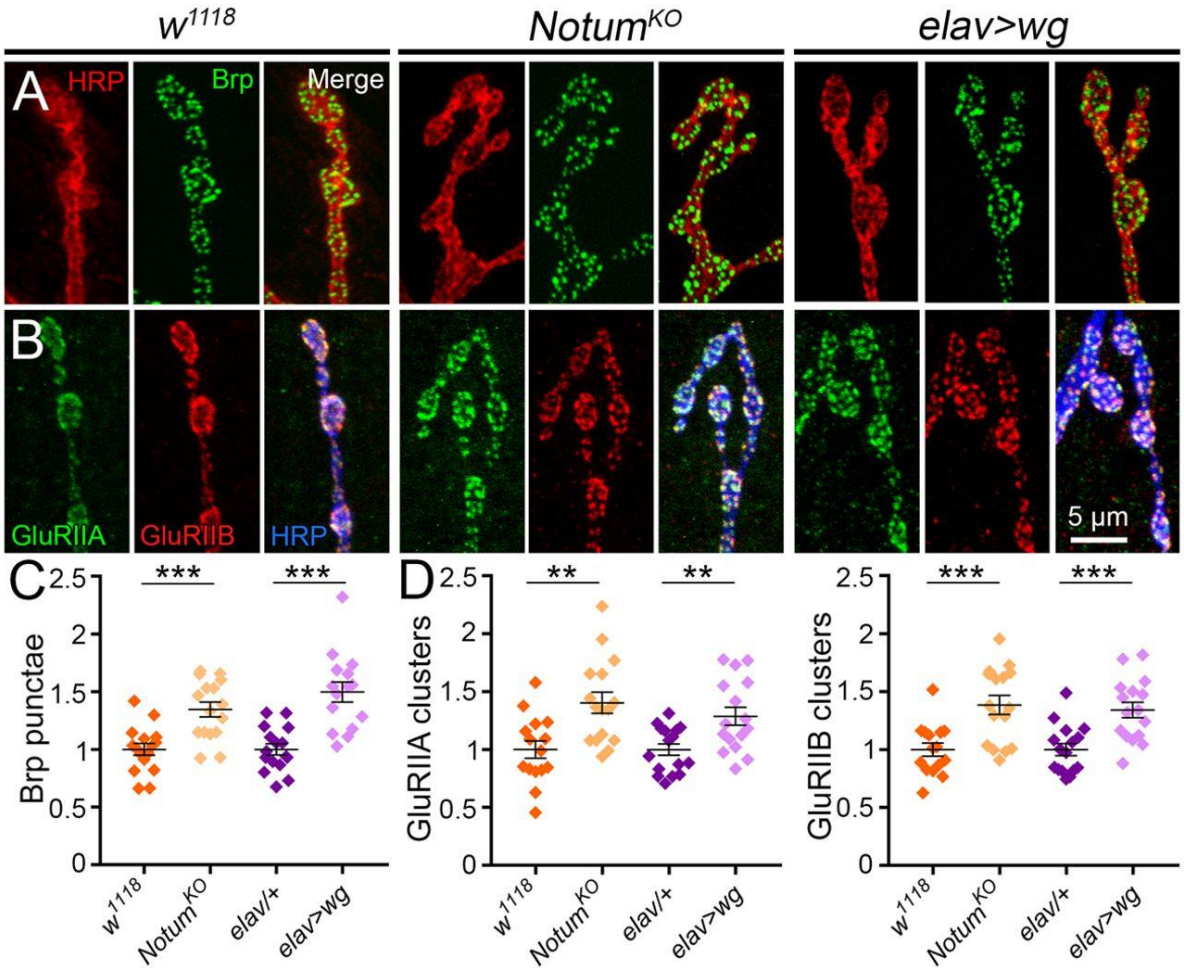

Fig. 13: Notum limits both pre- and postsynaptic molecular assembly. (A) Representative NMJ images co-labeled for HRP (red) and presynaptic anti-Bruchpilot (Brp, green) in *w*^{1118}, *Notum*^{KO} and *elav>wg*. (B) Synaptic boutons co-labeled for HRP (blue), GluRIIA (green) and GluRIIB (red) receptor classes in *w*^{1118}, *Notum*^{KO} and *elav>wg*. (C) Quantification of presynaptic Brp punctae in the genotypes shown, with inclusion of the *elav/+* control. (D) Quantification of postsynaptic GluRIIA/GluRIIB in the genotypes shown. ***P*≤0.01, ****P*≤0.001.

Restoring Wg levels in Notum mutants suppresses synaptogenic phenotypes

Based on all the studies described above, our working hypothesis is that the *Notum* mutant synaptogenic phenotypes arise from a lack of extracellular Wg inhibition, allowing for run-away Wg trans-synaptic signaling in the absence of Notum function. The prediction of this hypothesis is that reducing Wg levels towards normal in the *Notum* background should suppress the synaptogenic phenotypes. To test this prediction, we combined a heterozygous *wg* null ($wg^{1\text{-}17}$/+; also called wg^{CX4}; Baker, 1987) with the homozygous *Notum* null to generate the final genotype of $wg^{1\text{-}17}$/+; $Notum^{KO}$/$Notum^{KO}$ (Fig. 14). We first tested whether this double mutant genetically restores Wg expression. At the NMJ, Wg is normally expressed in a dynamic manner, with highly elevated extracellular ligand levels at a subset of synaptic boutons (Fig. 14A). Null *Notum* mutants show clearly elevated Wg expression, with a higher intensity and expanded spatial distribution of the secreted signal. In contrast, $wg^{1\text{-}17}$/+; $Notum^{KO}$/$Notum^{KO}$ synapses exhibit Wg levels that are indistinguishable from controls, with a similar level and pattern of extracellular release (Fig. 14A). In quantified measurements, *Notum* nulls show significantly elevated synaptic Wg intensity compared with matched controls (normalized w^{1118}, 1.0±0.08 versus $Notum^{KO}$, 1.4±0.08; n=16, P=0.0069), and removing one copy of *wg* significantly decreases Wg levels ($wg^{1\text{-}17}$/+; $Notum^{KO}$/$Notum^{KO}$, 1.1±0.10; P=0.0474 compared with $Notum^{KO}$; Fig. 14C). In the double mutants, there is no significant difference remaining in Wg levels at the synapse compared with w^{1118} (P=0.7325).

We hypothesized that correcting Wg trans-synaptic signaling in *Notum* mutants should alleviate defects in synaptic terminal development. To test this hypothesis, we compared NMJ architecture between the genetic controls, *Notum* nulls and null mutants with restored normal Wg levels (Fig. 14B). Control NMJs display few branches and a highly consistent number of evenly spaced synaptic boutons, whereas *Notum* mutants are characterized by rampant synaptogenesis with larger terminals, more branching and elevated, more variable synaptic bouton formation (Fig. 14B). In sharp contrast to the null condition, the $wg^{1\text{-}17}$/+; $Notum^{KO}$/$Notum^{KO}$ synapses exhibit

synaptic growth and architecture that is indistinguishable from normal, with a reduction in the terminal area, loss of the excess branching and correction of the supernumerary bouton levels that characterize the *Notum* mutants (Fig. 14B). In quantified measurements, the *Notum* nulls show highly significantly elevated synaptic bouton number compared with their matched controls (w^{1118}, 24.31±1.22 versus $Notum^{KO}$, 33.25±1.74; n=16, P<0.0001), whereas removing one copy of *wg* significantly decreases bouton number completely back to the control levels (wg^{1-17}/+; $Notum^{KO}$/$Notum^{KO}$, 27.13±1.07; P=0.0078 compared with $Notum^{KO}$; Fig. 14D). In the double mutants with corrected synaptic Wg levels, there is no significant difference remaining in NMJ synaptogenesis compared with genetic controls (P=0.324 compared with w^{1118} background control). This genetic correction demonstrates that Notum defects in synaptogenesis are due to elevated Wg signaling.

We hypothesized that correcting Wg trans-synaptic signaling in *Notum* mutants should alleviate the strengthening of neuromuscular function driving faster coordinated movement response times. To test this hypothesis, we tested motor function using the behavioral roll-over assay (Bodily et al., 2001; Jumbo-Lucioni et al., 2016). Control animals exhibit an orchestrated series of bilateral muscle contractions that enable rapid righting behavior, but *Notum* null mutants are remarkably proficient in this response and show an obvious improvement in coordinated movement time (Fig. 14E). In contrast, deletion of one *wg* copy from these mutants clearly impairs performance. In quantified measurements, *Notum* mutants show significantly faster roll-over times compared with matched controls (w^{1118}, 19.0±1.02 s versus $Notum^{KO}$, 6.49±0.46; n=23, P<0.0001), and correcting Wg levels significantly impairs this response time back towards control levels (wg^{1-17}/+; $Notum^{KO}$/$Notum^{KO}$, 9.91±1.18; P=0.032 compared with $Notum^{KO}$; Fig. 14E). This correction is significant albeit only partial, and a significant difference remains compared with genetic controls (P<0.0001 compared with w^{1118}). This likely reflects the possibility that Notum-Wg interactions happen throughout the nervous system to modulate behavioral output, and may well involve other Wnt signaling interactions in addition to Wg. Taken together, the results of this

study strongly support the conclusion that secreted Notum functions to restrict Wg ligand levels in the extracellular synaptomatrix and limit Wg trans-synaptic signaling, and that this function in turn puts a brake on structural and functional synaptogenesis to impede coordinated movement response times.

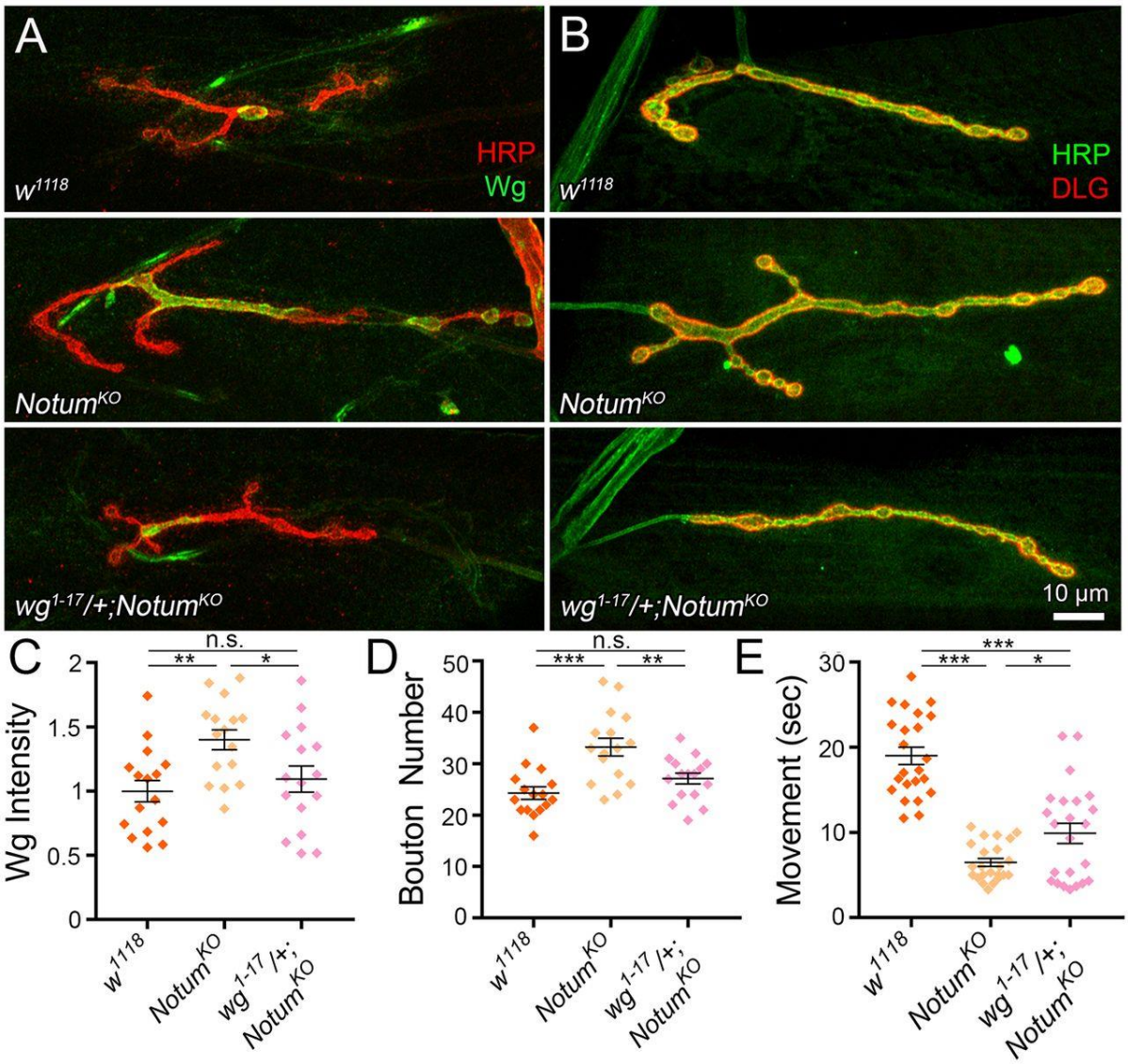

Fig. 14: Restoring normal synaptic Wg levels alleviates *Notum* null phenotypes. (A) Representative NMJ images co-labeled for HRP (red) and Wg (green) in w^{1118}, $Notum^{KO}$ and the mutant with removal of one copy of *wg* (wg^{1-17}/+; $Notum^{KO}/Notum^{KO}$). (B) The same genotypes co-labeled for HRP (green) and DLG (red). (C) Quantification of extracellular Wg ligand level (C) and bouton number (D) in above three genotypes. (E) Coordinated movement rollover reaction time quantification for the three genotypes. *P≤0.05, **P≤0.01, ***P≤0.001; n.s., not significant.

Discussion

Tightly coordinated trans-synaptic signals are required for proper development of the pre- and postsynaptic apparatus to ensure efficient communication at the synapse. This signaling is both coordinated and controlled in the extracellular space through the actions of secreted and transmembrane glycans, HSPG co-receptors and secreted enzymes, such as matrix metalloproteinase classes (Dear et al., 2016; Jumbo-Lucioni et al., 2016; Parkinson et al., 2016). Wg (Wnt-1) mediates a crucial trans-synaptic signaling pathway regulated by these extracellular synaptic mechanisms, with key roles in both structural and functional synaptogenesis (Ataman et al., 2008; Mathew et al., 2005; Miech et al., 2008; Packard et al., 2002; Speese et al., 2012). Here, we propose Notum as a novel extracellular regulator limiting Wg trans-synaptic signaling to control NMJ synaptogenesis. Wg is post-translationally modified by addition of palmitoleate on a conserved serine (S239) by membrane-bound *O*-acyltransferase (MBOAT) Porcupine (Kadowaki et al., 1996; Zhai et al., 2004). This lipidation event is required for Fz2 receptor binding and is essential for signaling (Janda et al., 2012). At the synaptic interface, the glycosylphosphatidylinositol (GPI)-anchored glypican Dally-like Protein (Dlp) regulates Wg trans-synaptic signaling (Lin and Perrimon, 1999; Kreuger et al., 2004; Yan et al., 2009; Dani and Broadie, 2012), and Notum was initially described as cleaving such GPI-anchored glypicans from the cell surface (Traister et al., 2008), affecting their ability to interact with the Wg ligand. However, Notum was recently re-defined as a secreted carboxylesterase, not a phospholipase, with structural studies showing a hydrophobic pocket that binds and then cleaves palmitoleate (Kakugawa et al., 2015).

Notum is consistently reported to act primarily as an extracellular Wg feedback inhibitor (Giráldez et al., 2002; Kakugawa et al., 2015). Our studies support this function within the synaptomatrix during synaptogenesis. At the *Drosophila* NMJ, Wg is secreted from both presynaptic neurons (Packard et al., 2002) and associated peripheral glia (Kerr et al., 2014), with the glial function specifically regulating synaptic transmission strength and postsynaptic glutamate

receptor clustering. Our analyses suggest that Notum is secreted from both postsynaptic muscle and peripheral glia, establishing a dynamic, Wg-like expression pattern surrounding synaptic boutons (Dani et al., 2012). In *Notum* null mutants, Wg signaling is increased at the developing NMJ, revealed by both decreased Fz2 receptor in the synaptic membrane (Wg-driven endocytosis) and an increase in nuclear Fz2-C punctae (FNI pathway). These findings are consistent with Notum function limiting Wg signaling, as established in other developmental contexts (Kakugawa et al., 2015). Notum appears to provide a fascinating directional regulation of Wg trans-synaptic signaling, affecting the anterograde FNI signaling pathway in muscles (Mathew et al., 2005), but not the autocrine divergent canonical pathway in neurons (Miech et al., 2008). Despite the strong elevation in synaptic Wg ligand levels in *Notum* null mutants, we see no evidence of altered presynaptic Futsch or changes in the microtubule cytoskeleton. However, Notum strongly limits Fz2 C-terminus nuclear import into the postsynaptic nuclei, which is known to drive RNP translational regulation of synaptic mRNAs to control synapse structural and functional differentiation (Speese et al., 2012).

Synaptic morphogenesis and architectural development is strongly perturbed in *Notum* null mutants, including increased NMJ area, branching and bouton formation, consistent with Notum function inhibiting Wg trans-synaptic signaling (Packard et al., 2002). Elevating presynaptic Wg closely phenocopies *Notum* synaptic defects, including expanded innervation area, more branching and supernumerary synaptic boutons. Our results show that Notum secreted from muscle and peripheral glia controls Wg in the extracellular space, with targeted *Notum* RNAi resulting in a similar NMJ expansion to *Notum* nulls, whereas neuronal *Notum* knockdown produces no effects. Interestingly, the glial-targeted RNAi increases boutons with no change in branching, whereas muscle knockdown has a stronger impact also affecting branching. Presynaptic Futsch/Map1B microtubule loops have been proposed to mediate Wg-dependent branching and bouton formation (Nahm et al., 2013; Roos et al., 2000; Wang et al., 2007). However, neuronal Wg overexpression has no discernable effect on Futsch-positive microtubule

loops. Consistently, Notum LOF also does not impact this pathway, with *Notum* mutants displaying no change in Futsch-labeled looped, bundled, punctate or splayed microtubules (Jumbo-Lucioni et al., 2016; Packard et al., 2002). Wg binding to the presynaptic Fz2 receptor might activate another divergent Wnt pathway that does not involve Futsch (Menon et al., 2013). Alternatively, Wg signaling via muscle Fz2 may produce a retrograde signal back to the neuron to alter presynaptic development. To test these two possibilities, future studies will employ cell-targeted Fz2 knockdown in *Notum* nulls to assay for suppression of the synaptic overgrowth phenotypes.

Measures of functional synaptic differentiation reveal elevated neurotransmission and faster motor output function with both *Notum* knockout and Wg overexpression. These results are consistent with Notum function inhibiting Wg trans-synaptic signaling, and consistent with previously characterized roles of Wg in NMJ functional development (Packard et al., 2002). Notum LOF increases presynaptic function selectively with an elevated mEJC frequency, greater EJC quantal content and heightened synaptic vesicle release during maintained high-frequency stimulation. Some of these effects might be related to to the increased synaptic bouton numbers. Both Notum LOF and Wg GOF also cause NMJ boutons to clump together, with ultrastructural studies showing multiple boutons sharing one SSR profile. These are not satellite boutons (Ashley et al., 2005), but rather aberrantly developing boutons that could result in functional defects. Notum knockdown in glia does not cause detectable mEJC/EJC changes, although Wg from glia regulates NMJ functional properties (Kerr et al., 2014). Interestingly, loss of Notum appears to improve motor performance, and *repo*-targeted *Notum* RNAi shows that glial Notum contributes to this function. This is an unusual outcome in a mutant condition, and we assume there must be a counter-balancing cost for the increased neuromuscular function. Live FM dye imaging reveals that *Notum* mutants load less dye into synaptic boutons upon nerve stimulation, indicating a role in synaptic vesicle endocytosis and/or the developmental regulation of synaptic vesicle pool size (Verstreken et al., 2008). These results show that Notum function limits Wg trans-synaptic

signaling to control presynaptic differentiation that is crucial for synapse function and motor output. As with Wg (Kerr et al., 2014), the source of Notum (muscle versus glia) appears to be important for distinct synaptogenic functions. Notum from peripheral glia regulates only bouton formation, whereas Notum from muscle regulates both NMJ growth and function.

Electron microscopy reveals a very strong decrease in synaptic vesicle density in *Notum* null boutons, providing an explanation for the live FM1-43 dye imaging defects. One of the most striking ultrastructural phenotypes is numerous, enlarged synaptic vesicular bodies. These organelles are highly reminiscent of bulk endosomes, in which a large area of presynaptic membrane is internalized, and will subsequently bud off synaptic vesicles (Clayton and Cousin, 2009). This pathway is usually driven by intense stimulation during activity-dependent bulk endocytosis (ADBE), as first observed at the frog NMJ (Miller and Heuser, 1984). This pathway is induced by high frequency trains of stimulation (Clayton et al., 2008), and several proteins have been identified that affect the formation of bulk endosomes, including Syndapin (Clayton et al., 2009) and Rolling Blackout (RBO; also known as Stambha A) (Vijayakrishnan et al., 2009). At the *Drosophila* NMJ, conditional *rbo*^{ts} mutants block ADBE, reducing the number and size of bulk endosomes (Vijayakrishnan et al., 2009). It will be interesting to test Wg GOF for enlarged endosomal structures, and study their involvement in Wg-dependent synaptic maturation. On the postsynaptic side, Notum also drives proper differentiation. Notum LOF reduces the postsynaptic DLG scaffold and postsynaptic SSR layering. The reduced SSR area in *Notum* mutants is surprising, given that a reduction in postsynaptic Wg signaling also results in fewer SSR layers (Packard et al., 2002; Kamimura et al., 2013). However, to our knowledge, SSR architecture has not been studied following Wg overexpression. Postsynaptic SSR formation might be sensitive to bidirectional Wg changes, and may be reduced if Wg is tipped in either direction.

Mechanistically, Notum controls both pre- and postsynaptic molecular assembly, with LOF defects phenocopied by Wg overexpression. The results are consistent with Notum function inhibiting Wg trans-synaptic signaling, and consistent with previously characterized roles for Wg

in synaptic molecular development (Packard et al., 2002). We analyzed both the presynaptic active zone protein Bruchpilot (Wagh et al., 2006; Menon et al., 2013) and the two postsynaptic GluR classes (Featherstone et al., 2005; Qin et al., 2005). Both presynaptic Brp and postsynaptic GluRs are misregulated in *Notum* nulls, with an increase in synapse number but not density. Importantly, both Notum LOF and Wg GOF elevate synapse number. Consistently, Wnt7a overexpression in mouse cerebellar cells also increases the number of synaptic sites and causes accumulation of presynaptic proteins required for synaptic vesicle function (Hall et al., 2000). The increased synapse density per NMJ might compensate for reduced neurotransmission per bouton, leading to a net stronger overall NMJ function. In *Notum* mutants, this could reconcile the elevated synaptic strength measured by electrophysiology compared with compromised single bouton function measured by FM dye imaging and impaired TEM ultrastructure. In any case, synaptic assembly during development is regulated by Notum function limiting Wg trans-synaptic signaling.

Genetically reducing Wg by combining a heterozygous *wg* null mutation into the homozygous *Notum* null background reduces extracellular synaptic Wg back to control levels. Wg reduction suppresses synaptogenic defects, restoring increased NMJ area, branching and bouton numbers completely back to normal. Both $Notum^{KO}$ and Wg GOF cause hyperactive movement, with roll-over speeds supporting synaptogenic defects of larger, stronger NMJs in both mutant conditions. However, $Notum^{KO}$ motor function is only partially restored by correcting Wg levels. One explanation for incomplete rescue is that multiple Wnts may contribute to motor behavior. Serine lipidation is conserved for all Wnts, and we know at least two other Wnts act at the *Drosophila* NMJ (Wnt2, Wnt5; Liebl et al., 2010; Liebl et al., 2008). Wnts are the only secreted ligands suggested to be *O*-palmitoleated on a serine to function as Notum substrates (Kakugawa et al., 2015). In future studies, we will test contributions of other Wnts. There is growing evidence that Wnts function in activity-dependent mechanisms at both mammalian and *Drosophila* synapses (Ataman et al., 2008; Gogolla et al., 2009). Our future studies will investigate these

mechanisms, exploring both muscle and peripheral glial-derived Notum. We will also study how Notum interacts with other extracellular Wg regulators at the synaptic interface. Secreted and membrane-tethered HSPGs play key roles in Wg regulation at the *Drosophila* NMJ (Kamimura et al., 2013; Dear et al., 2016), and Notum deacylates Wg in a HSPG-assisted mechanism (Kakugawa et al., 2015). For example, both Wg and Notum bind HSPG Dlp, which could serve as a signaling platform to colocalize them in the synaptic cleft. Our future work will dissect spatial and contextual functions of Notum regulation of Wg signaling at the developing synapse.

Materials and Methods

Drosophila stocks

All *Drosophila* stocks were reared on standard cornmeal/agar/molasses food at 25°C. The genetic background control for all studies was w^{1118}. Null mutant w^{1118}*; Notum*^{KO} *(4)(w+)/TM6b* animals, *Notum-HA(23)/TM6* and *UAS-Notum-V5/Cyo* lines were obtained from Jean-Paul Vincent (Francis Crick Institute, London, UK) (Kakugawa et al., 2015). Transgenic studies were performed with neuronal *elav*-Gal4, glial *repo*-Gal4, muscle-specific *24B*-Gal4 and ubiquitous *UH1*-Gal4 driver lines (Bloomington *Drosophila* Stock Center, Indiana University, Bloomington, IN, USA) crossed to characterized *UAS-Notum-RNAi* lines (#35650 and #55379 from the Harvard Transgenic RNAi Project; TRiP) (Perkins et al., 2015). For Wg studies, overexpression experiments were performed with *UAS-wg*::GFP (Pfeiffer et al., 2002), and suppression experiments were performed with wg^{1-17} null mutant (aka wg^{CX4} (Baker, 1987)) comparing wg^{1-17}/+ with wg^{1-17}/+*; Notum*^{KO}/*Notum*^{KO}*.*

Generation of Notum-HA line

A C-terminal HA-tagged knock-in version of Notum was generated by CRISPR/Cas9 genome editing as described (Gokcezade et al., 2014). The gRNA target (overlapping with the *Notum* stop

codon) was cloned into the pDCC6 vector. This vector was then co-injected into w^{1118} embryos with the following ssODN:

CACACGCTCAACAACATGGAGCGCACCGAGTTGGTCAACATGCTCACCCAGCAGGCTAAC *TACCCATACGACGTCCCTGACTATGCG*ggg*TATCCGTATGATGTGCCAGATTACGCC***TAG***G CTCACCAAATACCCTGTACCCTTTTGGGGGGATCCGAAAGTGGGCATGGAAATCGT. The two HA epitope tags are indicated in italics and the stop codon is indicated in bold.

Behavioral assays

Coordinated movement assays were conducted using the 'rollover assay' as previously reported (Bodily et al., 2001; Jumbo-Lucioni et al., 2016). Using forceps, an individual wandering third instar was placed on a 100×15 mm plate coated with 1% agarose and allowed 30 s to acclimate at 20°C. Using a fine paintbrush, the larva was rolled over so that the ventral midline was exactly upwards (t=0). A stopwatch was used to record righting time, when the dorsal midline was exactly upwards. The assay was repeated three times on the same animal, and the three times were averaged for a single data point.

Immunocytochemistry

Wandering third instars were dissected in physiological solution, fixed and permeabilized with 0.2% Triton X-100 (three times for 10 min each), except for extracellular labeling. Primary antibodies used included: rabbit anti-HRP, mouse anti-DLG, rabbit anti-HA, mouse anti-Wg, rabbit anti-Fz2-C, mouse anti-GluRIIA, rabbit anti-GluRIIB, mouse anti-Brp, mouse anti-Futsch, goat anti-GFP, Cy3-conjugated goat anti-HRP, and Cy5-conjugated goat anti-HRP. Further antibody details are included in Table S1. The fluorescent probe DRAQ5 was used for nuclear staining (1:1000; Invitrogen, 62254). The lectin Vicia Villosa (VVA-TRITC) was used as an NMJ marker (1:200; EY Laboratories, R-4601-2). HA immunoreactivity was visualized using a tyramide signal

amplification kit (TSA, Sigma T20911) using HRP-conjugated goat anti-rabbit (1:200; Invitrogen, 31460), biotinylated tyramide and streptavidin-488 (1:200, Invitrogen, S-11223) (Bogdanik et al., 2004). Preparations were processed with primary antibodies overnight at 4°C and secondary antibodies for 2 h at room temperature (RT), washed three times for 10 min each, and mounted in Fluoromount G (Electron Microscopy Sciences).

Confocal imaging

All imaging was performed on a Zeiss LSM 510 META laser-scanning confocal microscope, with images projected in Zen (Zeiss) and analyzed using ImageJ (NIH open source). NMJ area and intensity measurements were made with HRP signal delineated *z*-stack areas of maximum projection using the threshold and wand-tracing tools within ImageJ. Synaptic boutons were defined as HRP- and DLG-positive varicosities >2 µm. Branches were defined as axonal processes with at least two boutons. Brp and GluR punctae were counted using the multi-point tool within ImageJ. Fz2-C intensity measurements were made with DRAQ5 signal delineated *z*-stack nuclei with maximum projections.

Western blotting

Western blots from wandering third instars were performed with standard procedures (Gagliardi et al., 2014). Eight larvae were dissected in ice-cold PBS, with the ventral nerve cord (VNC) separated from the body musculature. Both tissues were transferred independently to RIPA buffer [10 mM Tris-HCl (pH 8.0), 1 mM EDTA, 1% Triton X-100, 0.1% sodium deoxycholate, 0.1% SDS, 140 mM NaCl, 1 mM PMSF]. The equivalent of two VNCs and two body musculatures were loaded separately onto the same 4-12% gel and probed with anti-HA.11 (1:2000, Covance).

Electrophysiology

Wandering third instars were dissected longitudinally along the dorsal midline, internal organs removed, and the body walls glued down (Vetbond by 3 M). Peripheral motor nerves were cut at the base of the VNC. Dissections and recordings were carried out at 18°C in physiological saline (in mM): 128 NaCl, 2 KCl, 4 $MgCl_2$, 1.0 $CaCl_2$, 70 sucrose and 5 HEPES {2-[4-(2-hydroxyethyl)piperazin-1-yl]ethanesulfonic acid; pH 7.2}. Preparations were imaged with a Zeiss Axioskop microscope using 40× water-immersion objectives. Muscle 6 in abdominal segments 2/3 was impaled with two intracellular microelectrodes (1-mm outer diameter borosilicate capillaries; World Precision Instruments) of ~15 MΩ resistance filled with 3 M KCl. Muscles were clamped at −60 mV using an Axoclamp-2B amplifier. Spontaneous mEJC recordings were made in 2 min sessions and low-pass filtered. For EJC records, motor nerves were sucked into a fire-polished suction electrode and stimulated using 0.5 ms suprathreshold voltage stimuli at 0.2 Hz from a Grass S88 stimulator. Nerve stimulation-evoked EJC recordings were filtered at 2 kHz. To quantify EJCs, ten consecutive traces were averaged and the average peak value recorded. Clampex 9.0 was used for data acquisition and Clampfit 9 was used for data analysis.

FM imaging

FM1-43 (4 μM; Invitrogen) was added in 1 mM Ca^{2+} physiological saline (see above). The motor nerve was stimulated with a suction electrode (20 Hz, 1 min), and then the bath saline was replaced several times in quick succession with Ca^{2+}-free saline to halt SV cycling. *z*-stacks of stimulated (loaded) NMJs were taken with the Zeiss LSM 510 confocal microscope using 40× water immersion objectives. Ca^{2+}-free saline was replaced with 1 mM Ca^{2+} saline (without FM1-43), and the same motor nerve stimulated (20 Hz, 20 s) for SV exocytosis and dye release. The saline was replaced several times in quick succession with Ca^{2+}-free saline to halt SV cycling. *z*-stacks of unloaded NMJs were then taken. Images were quantified by outlining individual boutons

using the ImageJ elliptical selections tool and measuring fluorescence values in loaded and unloaded conditions. The ratio of unloaded/loaded intensities was calculated in Microsoft Excel (2013). Images for display were exported to Adobe Photoshop.

Electron microscopy

Wandering third instars were dissected and fixed overnight at 4°C in 2.5% glutaraldehyde, followed by secondary fixation in 1% osmium tetroxide for 1 h at RT. Preparations were washed in 0.1 M sodium cacodylate buffer three times (10 min each), followed by ddH_2O three times (15 min each). *En bloc* uranyl acetate staining was carried out using 2% uranyl acetate (2 h at RT, dark). Preparations were rinsed in ddH_2O three times (15 min each), followed by an ethanol dehydration series (30, 50, 70, 90, 95, 100, 100%), propylene oxide infiltration and resin embedding (Embed-812). Body wall muscles 6/7 from abdominal segments 2/3 were dissected free and embedded into a semi-hardened resin block. The muscles from four animals were put in each block, with three blocks made per genotype. Blocks were polymerized at 60°C for 48 h. Thick (1 µm) sections were cut using a glass knife, stained with Toluidine Blue for 1 min on a Thermostat slide warmer (45°C) and imaged on a compound microscope at 100× for bouton identification. Once a bouton was found, ultrathin (50 nm) sections were cut using a DiATOME diamond knife on a Leica Ultracut UCT ultramicrotome and then collected on uncoated 200 mesh copper grids. All TEM imaging was performed on a Philips CM10 transmission electron microscope operating at 80 kV, with images collected using a 4-megapixel AMT CCD camera. Bouton area, SSR area, SV number and SV size were measured in ImageJ. Single bouton profiles that were ≤2 μm^2 were not considered in the quantification.

Statistical measurements

Statistical comparisons were performed using GraphPad Prism software (Version 7.0 for Windows). Student's *t*-tests were used for pair-wise comparisons and one-way ANOVAs for data

sets of three or more comparisons, followed by a post hoc Tukey's multiple comparisons test. Fisher's exact tests were used with discrete data using R statistical software (Version 3.2.5). Graphs show mean±s.e.m. made with Prism, with significance displayed as *$P \leq 0.05$, **$P \leq 0.01$, ***$P \leq 0.001$ and $P > 0.05$ (not significant, n.s.). Sample sizes reported in the text (n) indicate the number of NMJs, unless otherwise stated.

References

Ashley J, Packard M, Ataman B, Budnik V (2005) Fasciclin II signals new synapse formation through amyloid precursor protein and the scaffolding protein dX11/mint. J Neurosci 25:5943-55.

Ataman B, Ashley J, Gorczyca M, Ramachandran P, Fouquet W, Sigrist SJ, Budnik V (2008) Rapid activity-dependent modifications in synaptic structure and function require bidirectional Wnt signaling. Neuron 57:705-18.

Baker N (1987) Molecular cloning of sequences from *wingless*, a segment polarity gene in *Drosophila*: the spatial distribution of a transcript in embryos. EMBO J 6:1765-73.

Bodily KD, Morrison CM, Renden RB, Broadie K (2001) A novel member of the Ig superfamily, *turtle*, is a CNS-specific protein required for coordinated motor control. J Neurosci 21:3113-25.

Bogdanik L, Mohrmann R, Ramaekers A, Bockaert J, Grau Y, Broadie K, Parmentier ML (2004) The *Drosophila* metabotropic glutamate receptor DmGluRA regulates activity-dependent synaptic facilitation and fine synaptic morphology. J Neurosci 24: 9105-16.

Clayton EL, Cousin MA (2009) The molecular physiology of activity-dependent bulk endocytosis of synaptic vesicles. J Neurochem 111:901-14.

Clayton EL, Evans GJO, Cousin MA (2008) Bulk synaptic vesicle endocytosis is rapidly triggered during strong stimulation. J Neurosci 28:6627-32.

Clayton EL, Anggono V, Smillie KJ, Chau N, Robinson PJ, Cousin MA (2009) The phospho-dependent dynamin-syndapin interaction triggers activity-dependent bulk endocytosis of synaptic vesicles. J Neurosci 29:7706-17.

Dani N, Broadie K (2012) Glycosylated synaptomatrix regulation of trans-synaptic signaling. Dev Neurobiol 72:2-21.

Dani N, Nahm M, Lee S, Broadie K (2012) A targeted glycan-related gene screen reveals heparan sulfate proteoglycan sulfation regulates WNT and BMP trans-synaptic signaling. PLoS Genet 8:e1003031.

Dear ML, Dani N, Parkinson W, Zhou S, Broadie K (2016) Two classes of matrix metalloproteinases reciprocally regulate synaptogenesis. Development 143:75-87.

Featherstone DE, Rohrbough J, Liebl F, Karr J, Sheng Q, Rodesch CK, Broadie K (2005) An essential Drosophila glutamate receptor subunit that functions in both neuropil and neuromuscular junction. J Neurosci 25:3199-208.

Friedman SH, Dani N, Rushton E, Broadie K (2013) Fragile X mental retardation protein regulates trans-synaptic signaling in *Drosophila*. Dis Model Mech 6:1400-13.

Gagliardi M, Hernandez A, McGough IJ, Vincent JP (2014) Inhibitors of endocytosis prevent Wnt/Wingless signalling by reducing the level of basal β-catenin/Armadillo. J Cell Sci 127:4918-26.

Gerlitz O, Basler K (2002) Wingful, an extracellular feedback inhibitor of Wingless. Genes Dev 16:1055-59.

Giráldez AJ, Copley RR, Cohen SM (2002) HSPG modification by the secreted enzyme notum shapes the wingless morphogen gradient. Dev Cell 2:667-76.

Gogolla N, Galimberti I, Deguchi Y, Caroni P (2009) Wnt signaling mediates experience-related regulation of synapse numbers and mossy fiber connectivites in the adult hippocampus. Neuron 62: 510-25.

Gokcezade J, Sienski G, Duchek P (2014) Efficient CRISPR/Cas9 plasmids for rapid and versatile genome editing in Drosophila. G3 (Bethesda) 4:2279-82.

Hall AC, Lucas FR, Salinas PC (2000) Axonal remodeling and synaptic differentiation in the cerebellum is regulated by WNT-7a signaling. Cell 100:525-35.

Harris KP, Littleton JT (2015) Transmission, development, and plasticity of synapses. Genetics 201:345-75.

Jan LY, Jan YN (1976) L-Glutamate as an excitatory transmitter at the *Drosophila* larval neuromuscular junction. J Physiol 262:215-36.

Janda CY, Waghray D, Levin AM, Thomas C, Garcia KC (2012) Structural basis of Wnt recognition by frizzled. Science 337:59-64.

Jumbo-Lucioni P, Parkinson W, Broadie K (2014) Overelaborated synaptic architecture and reduced synaptomatrix glycosylation in a *Drosophila* classic galactosemia disease model. Dis Model Mech 7:1365-78.

Jumbo-Lucioni PP, Parkinson WM, Kopke DL, Broadie K (2016) Coordinated movement, neuromuscular synaptogenesis and trans-synaptic signaling defects in *Drosophila* galactosemia models. Hum Molec Genet 25:3699-714.

Kadowaki T, Wilder E, Klingensmith J, Zachary K, Perrimon N (1996) The segment polarity gene *porcupine* encodes a putative multitransmembrane protein involved in Wingless processing. Genes Dev 10:3116-28.

Kakugawa S, Langton PF, Zebisch M, Howell SA, Chang TH, Liu Y, Feizi T, Bineva G, O'Reilly N, Snijders AP, Jones EY, Vicent JP (2015) Notum deacylates Wnt proteins to suppress signalling activity. Nature 519:187-92.

Kamimura K, Ueno K, Nakagawa J, Hamada R, Saitoe M, Maeda N (2013) Perlecan regulates bidirectional Wnt signaling at the *Drosophila* neuromuscular junction. J Cell Biol 200:219-33.

Kerr KS, Fuentes-Medel Y, Brewer C, Barria R, Ashley J, Abruzzi KC, Sheehan A, Tasdemir-Yilmaz OE, Freeman MR, Budnik V (2014) Glial Wingless/Wnt regulates glutamate receptor clustering and synaptic physiology at the *Drosophila* neuromuscular junction. J Neurosci 34:2910-20.

Keshishian H, Broadie K, Chiba A, Bate M (1996) The *Drosophila* neuromuscular junction: a model system for studying synaptic development and function. Annu Rev Neurosci 19:545-75.

Kittel RJ, Wichmann C, Rasse TM, Fouquet W, Schmidt M, Schmid A, Wagh DA, Pawlu C, Kellner RR, Willig KI, Hell SW, Buchner E, Heckmann M, Sigrist SJ (2006) Bruchpilot promotes active zone assembly, Ca^{2+} channel clustering, and vesicle release. Science 312:1051-4.

Kreuger J, Perez L, Giraldez AJ, Cohen SM (2004) Opposing activities of dally-like glypican at high and low levels of wingless morphogen activity. Dev Cell 7:503-12.

Langton PF, Kakugawa S, Vincent JP (2016) Making, exporting, and modulating Wnts. Trends Cell Biol 26;756-65.

Liebl FLW, Wu Y, Featherstone DE, Noordermeer JN, Fradkin L, Hing H (2008) Derailed regulates development of the Drosophila neuromuscular junction. Dev Neurobiol 68:152-65.

Liebl FLW, McKeown C, Yao Y, Hing HK (2010) Mutations in Wnt2 alter presynaptic motor neuron morphology and presynaptic protein localization at the Drosophila neuromuscular junction. PLoS ONE 5:e12778.

Lin X, Perrimon N (1999) Dally cooperates with *Drosophila* Frizzled 2 to transduce Wingless signalling. Nature 400:281-4.

Mata J, Curado S, Ephrussi A, Rørth P (2000) Tribbles coordinates mitosis and morphogenesis in *Drosophila*by regulating string/CDC25 proteolysis. Cell 101:511-22.

Mathew D, Ataman B, Chen J, Zhang Y, Cumberledge S, Budnik V (2005) Wingless signaling at synapses is through cleavage and nuclear import of receptor DFrizzled2. Science 310:1344-47.

Menon KP, Carrillo RA, Zinn K (2013) Development and plasticity of the *Drosophila* larval neuromuscular junction. Wiley Interdiscip Rev Dev Biol 2:647-70.

Miech C, Pauer HU, He X, Schwarz TL (2008) Presynaptic local signaling by a canonical wingless pathway regulates development of the *Drosophila* neuromuscular junction. J Neurosci 28:10875-84.

Miller TM, Heuser JE (1984) Endocytosis of synaptic vesicle membrane at the frog neuromuscular junction. J Cell Biol 98:685-98.

Nahm M, Lee MJ, Parkinson W, Lee M, Kim H, Kim YJ, Kim S, Cho YS, Min BM, Bae YC, Broadie K, Lee S (2013) Spartin regulates synaptic growth and neuronal survival by inhibiting BMP-mediated microtubule stabilization. Neuron 77:680-95.

Packard M, Koo ES, Gorczyca M, Sharpe J, Cumberledge S, Budnik V (2002) The *Drosophila* Wnt, Wingless, provides an essential signal for pre- and postsynaptic differentiation. Cell 111:319-30.

Parkinson W, Dear ML, Rushton E, Broadie K (2013) N-glycosylation requirements in neuromuscular synaptogenesis. Development 140:4970-81.

Parkinson WM, Dookwah M, Dear ML, Gatto CL, Aoki K, Tiemeyer M, Broadie K (2016) Synaptic roles for phosphomannomutase type 2 in a new *Drosophila* congenital disorder of glycosylation disease model. Dis Model Mech 9:513-27.

Perkins LA, Holderbaum L, Tao R, Hu Y, Sopko R, McCall K, Yang-Zhou D, Flockhart I, Binari R, Shim HS, Miller A, Housden A, Foos M, Randkelv S, Kelley C, Namgyal P, Villalta C, Liu LP, Jiang X, Huan-Huan Q, Wang X, Fujiyama A, Toyoda A, Ayers K, Blum A, Czech B, Neumuller R, Yan D, Cavallaro A, Hibbard K, Hall D, Cooley L, Hannon GJ, Lehmann R, Parks A, Mohr SE, Ueda R, Kondo S, Ni JQ, Perrimon N (2015) The Transgenic RNAi Project at Harvard Medical School: Resources and Validation. Genetics 201:843-52.

Pfeiffer S, Ricardo S, Manneville JB, Alexandre C, Vincent JP (2002) Producing cells retain and recycle Wingless in *Drosophila* embryos. Curr Biol 12:957-62.

Qin G, Schwarz T, Kittel RJ, Schmid A, Rasse TM, Kappei D, Ponimaskin E, Heckmann M, Sigrist SJ (2005) Four different subunits are essential for expressing the synaptic glutamate receptor at neuromuscular junctions of *Drosophila*. J Neurosci 25:3209-18.

Rasse TM, Fouquet W, Schmid A, Kittel RJ, Mertel S, Sigrist CB, Schmidt M, Guzman A, Merino C, Qin G, Quentin C, Madeo FF, Heckmann M, Sigrist SJ (2005) Glutamate receptor dynamics organizing synapse formation in vivo. Nat. Neurosci. 8:898-905.

Roos J, Hummel T, Ng N, Klämbt C, Davis GW (2000) *Drosophila* Futsch regulates synaptic microtubule organization and is necessary for synaptic growth. Neuron 26:371-82.

Speese SD, Ashley J, Jokhi V, Nunnari J, Barria R, Li Y, Ataman B, Koon A, Chang YT, Li Q, Moore MJ, Budnik V (2012) Nuclear envelope budding enables large ribonucleoprotein particle export during synaptic Wnt signaling. Cell 149:832-46.

Traister A, Shi W, Filmus J (2008) Mammalian Notum induces the release of glypicans and other GPI-anchored proteins from the cell surface. Biochem J 410:503-11.

Verstreken P, Ohyama T, Bellen HJ (2008) FM 1-43 labeling of synaptic vesicle pools at the *Drosophila*neuromuscular junction. Methods Mol Biol 440:349-69.

Vijayakrishnan N, Woodruff, EA III, Broadie K (2009) Rolling blackout is required for bulk endocytosis in non-neuronal cells and neuronal synapses. J Cell Sci 122:114-25.

Vijayakrishnan N, Phillips SE, Broadie K (2010) *Drosophila* rolling blackout displays lipase domain-dependent and -independent endocytic functions downstream of dynamin. Traffic 11:1567-78.

Wagh DA, Rasse TM, Asan E, Hofbauer A, Schwenkert I, Durrbeck H, Buchner S, Dabauvalle MC, Schmidt M, Qin G, Wichmann C, Kittel R, Sigrist SJ, Buchner E (2006) Bruchpilot, a protein with homology to ELKS/CAST, is required for structural integrity and function of synaptic active zones in *Drosophila*. Neuron 49:833-44.

Wang X, Shaw WR, Tsang HTH, Reid E, O'Kane CJ (2007) *Drosophila* spichthyin inhibits BMP signaling and regulates synaptic growth and axonal microtubules. Nat Neurosci 10:177-85.

Yan D, Wu Y, Feng Y, Lin S-C, Lin X (2009) The core protein of glypican Dally-like determines its biphasic activity in wingless morphogen signaling. Dev Cell 17:470-81.

Zhai L, Chaturvedi D, Cumberledge S (2004) Drosophila Wnt-1 undergoes a hydrophobic modification and is targeted to lipid rafts; a process that requires Porcupine. J Biol Chem 279: 33220-7.

Chapter III

FM Dye Cycling at the Synapse: Comparing High Potassium Depolarization, Electrical and Channelrhodopsin Stimulation

Danielle L. Kopke[1], Kendal Broadie[2]

[1]Department of Biological Sciences, Vanderbilt University

[2]Departments of Biological Sciences, Pharmacology, Cell and Developmental Biology, Kennedy Center for Research on Human Development, Vanderbilt University and Medical Center

This paper is published under the same title in the Journal of Visualized Experiments, 2018.

- **Disclosures**

  The authors declare no competing interests.

- **Acknowledgements**

  We thank Broadie Lab members for contributions to this article. This work was supported by NIH R01s MH096832 and MH084989 to K.B., and NIH predoctoral fellowship F31 MH111144 to D.L.K.

Summary

Synaptic vesicle (SV) cycling is the core mechanism of intercellular communication at neuronal synapses. FM dye uptake and release are the primary means of quantitatively assaying SV endo- and exocytosis. Here, we compare all the stimulation methods to drive FM1-43 cycling at the *Drosophila* neuromuscular junction (NMJ) model synapse.

Abstract

FM dyes are used to study the synaptic vesicle (SV) cycle. These amphipathic probes have a hydrophilic head and hydrophobic tail, making them water-soluble with the ability to reversibly enter and exit membrane lipid bilayers. These styryl dyes are relatively non-fluorescent in aqueous medium, but insertion into the outer leaflet of the plasma membrane causes a >40X increase in fluorescence. In neuronal synapses, FM dyes are internalized during SV endocytosis, trafficked both within and between SV pools, and released with SV exocytosis, providing a powerful tool to visualize presynaptic stages of neurotransmission. A primary genetic model of glutamatergic synapse development and function is the *Drosophila* neuromuscular junction (NMJ), where FM dye imaging has been used extensively to quantify SV dynamics in a wide range of mutant conditions. The NMJ synaptic terminal is easily accessible, with a beautiful array of large synaptic boutons ideal for imaging applications. Here, we compare and contrast the three ways to stimulate the *Drosophila* NMJ to drive activity-dependent FM1-43 dye uptake/release: 1) bath application of high [K^+] to depolarize neuromuscular tissues, 2) suction electrode motor nerve stimulation to depolarize the presynaptic nerve terminal, and 3) targeted transgenic expression of channelrhodopsin variants for light-stimulated, spatial control of depolarization. Each of these methods has benefits and disadvantages for the study of genetic mutation effects on the SV cycle at the *Drosophila* NMJ. We will discuss these advantages and disadvantages to assist the selection of the stimulation approach, together with the methodologies specific to each strategy.

In addition to fluorescent imaging, FM dyes can be photoconverted to electron-dense signals visualized using transmission electron microscopy (TEM) to study SV cycle mechanisms at an ultrastructural level. We provide the comparisons of confocal and electron microscopy imaging from the different methods of *Drosophila* NMJ stimulation, to help guide the selection of future experimental paradigms.

Introduction

The beautifully-characterized *Drosophila* larval neuromuscular junction (NMJ) glutamatergic synapse model has been used to study synapse formation and function with a vast spectrum of genetic perturbations[1]. The motor neuron terminal consists of multiple axon branches, each with many enlarged synaptic boutons. These capacious varicosities (up to 5 µm in diameter) contain all of the neurotransmission machinery, including uniform glutamatergic synaptic vesicles (SVs; ~40 nm in diameter) in cytosolic reserve and readily-releasable pools[2]. These vesicles dock at the presynaptic plasma membrane fusion site active zones (AZs), where exocytosis mediates the glutamate neurotransmitter release for *trans*-synaptic communication. Subsequently, the SVs are retrieved from the plasma membrane via kiss-and-run recycling or clathrin-mediated endocytosis (CME) for repeated exo/endocytosis cycles. The *Drosophila* NMJ is easily accessible and well-suited for both isolating and characterizing SV cycle mutants. Using forward genetic screens, novel mutations have led to the identification of new genes critical for the SV cycle[3]. Moreover, reverse genetic approaches starting with already known genes have led to the elucidation of new SV cycle mechanisms through the careful description of mutant cycling phenotypes[4]. The *Drosophila* NMJ is nearly ideal as an experimental synaptic preparation for dissecting SV endocytosis and exocytosis mechanisms via methods to optically track vesicle cycling during neurotransmission.

A range of fluorescent markers allow visual tracking of vesicles during cycling dynamics, but the most versatile are FM dye analogs which is first synthesized by Mao, F., *et al*.[5].

Structurally, FM dyes contain a hydrophilic head and a lipophilic tail connected through an aromatic ring, with a central region conferring spectral properties. These styryl dyes partition reversibly in membranes, do not 'flip-flop' between membrane leaflets and so are never free in the cytosol, and are far more fluorescent in membranes than water[5]. Reversible insertion into a lipid bilayer causes a 40-fold increase in fluorescence[6]. At neuronal synapses, classic FM dye labeling experiments consist of bathing the synaptic preparation with the dye during depolarizing stimulation to load dye via SV endocytosis. External dye is then washed away and the SV cycle is arrested in a calcium-free ringer solution to image loaded synapses[7]. A second round of stimulation in a dye-free bath triggers FM release through exocytosis, a process that can be followed by measuring the fluorescence intensity decrease. SV populations from a single vesicle to pools containing hundreds of vesicles can be quantitatively monitored[6,7]. FM dyes have been used to dissect activity-dependent mobilization of functionally distinct SV pools, and to compare kiss-and-run vs. CME cycling[8,9]. The method has been modified to separately assay evoked, spontaneous and miniature synaptic cycle activities (with highly sensitive equipment to detect very small fluorescence changes and reduce photobleaching)[10]. Assays can be extended to the ultrastructural level by photoconverting the fluorescent FM signal into an electron-dense label for transmission electron microscopy[11,12,13,14].

Historically, bathing synaptic preparations in a high concentration of potassium (hereafter referred to as "high [K^+]") has been the method of choice for depolarizing stimulation to induce SV cycling; ranging from the frog cholinergic NMJ[5], to cultured rodent brain hippocampal neurons[15], to the *Drosophila* glutamatergic NMJ model[16,17]. This high [K^+] approach is simple, requires no specialized equipment, and is therefore accessible to most labs, but has limitations for both application and data interpretation. A much more physiologically appropriate method is to use suction electrode electrical stimulation of the nerve[4,5,12]. This approach drives action potential propagation for direct stimulation of the presynaptic nerve terminal, and results can be directly compared to electrophysiological assays of neurotransmission function[13,14,15], but requires

specialized equipment and is technically much more challenging. With the advent of optogenetics, the use of channelrhodopsin neuronal stimulation has additional advantages, including tight spatiotemporal control of channel expression using the binary Gal4/UAS system[20]. This approach is technically much easier than suction electrode stimulation and requires nothing more than a very cheap LED light source. Here, we employ imaging of FM1-43 (*N*-(3-triethylammoniumpropyl)-4-(4-(dibutylamino)styryl) pyridinium dibromide) to both compare and contrast these three different stimulation methods at the *Drosophila* NMJ: simple high [K^+], challenging electrical and new channelrhodopsin approaches.

Protocol

1. Larval Glue Dissection

1. Thoroughly mix 10 parts of silicone elastomer base with 1 part of silicone elastomer curing agent from the elastomer kit (**Table 2**).
2. Coat 22 x 22 mm glass coverslips with the elastomer and cure on a hot plate at 75 ˚C for several hours (until no longer sticky to the touch).
3. Place a single elastomer-coated glass coverslip into the custom-made plexi glass dissection chamber (**Figure 15**, bottom) in preparation for the larval dissection.
4. Prepare the glue pipettes from borosilicate glass capillary using a standard microelectrode puller to obtain the desired taper and tip size.
5. Gently break off the micropipette tip, and to the other end, attach 2 ft of flexible plastic tube (1/32" interior diameter, ID; 3/32" outside diameter, OD; 1/32" wall; **Table 2**) with mouth fitting (P2 pipette tip).
6. Fill a small container (0.6 mL Eppendorf tube cap) with a small volume (~20 µL) of glue (**Table 2**) in preparation for the larval dissection.
7. Fill the chamber with saline (in mM): 128 NaCl, 2 KCl, 4 $MgCl_2$, 1 $CaCl_2$, 70 sucrose, and 5 2-[4-(2-hydroxyethyl)piperazin-1-yl]ethanesulfonic acid (HEPES) pH 7.2.

8. Add anti-horse radish peroxidase (HRP) antibody conjugated to Alexa Fluor 647 (anti-HRP:647; dilute 1:10 from a 1 mg/mL stock) for labeling the NMJ presynaptic terminal during dissection[21,22].
9. Using a fine paintbrush (size 2), remove a wandering third instar from the food vial and place onto the elastomer-coated cover glass.
10. Fill the glass micropipette tip with a small volume of glue using negative air pressure generated by mouth with attachment (step 1.5).
11. Position larva dorsal side up with forceps and glue the head to the elastomer-coated coverslip with a small drop of glue using positive air pressure by mouth.
12. Repeat this procedure with the posterior end of the larva, making sure that the animal is stretched taut between the two glue attachments.
13. Using scissors (blades 3 mm; **Table 2**), make a horizontal cut (~1 mm) at posterior and a vertical cut all along the dorsal midline.
14. Using fine forceps (#5, **Table 2**), gently remove dorsal trachea, gut, fat body and other internal organs covering the musculature.
15. Repeat the gluing procedure for the four body wall flaps, making sure to gently stretch the body wall both horizontally and vertically.
16. Lift the ventral nerve cord (VNC) using forceps, carefully cut the motor nerves with the scissors, and then completely remove the VNC.
17. Replace the dissection saline with Ca^{2+}-free saline (same as the above dissection saline without the $CaCl_2$) to stop SV cycling.

2. Option 1: High [K^+] FM Dye Loading

1. From a FM1-43 stock solution (4 mM), add 1 µL to 1 mL of 90 mM KCl solution (high [K^+] in dissection saline) for a final concentration of 4 µM.
2. Using a pipette, replace the Ca^{2+}-free saline in the imaging chamber with the high [K^+] FM dye solution to stimulate SV endocytosis dye uptake.

3. Immediately start a digital timer for the pre-determined duration of the high [K^+] depolarizing stimulation period (*e.g.*, 5 min; **Figure 16**).
4. To confirm a healthy larval preparation, note the strong contractions of the musculature for the duration of the high [K^+] depolarization period.
5. When the timer period ends, quickly remove the high [K^+] FM dye solution and replace with Ca^{2+}-free saline to stop SV cycling.
6. Wash in quick succession with the Ca^{2+}-free saline (5x for 1 min) to ensure the high [K^+] FM dye solution is completely removed.
7. Maintain the larval preparation in fresh Ca^{2+}-free saline for immediate imaging with the confocal microscope.

3. Imaging: Confocal Microscopy

1. Use an upright confocal microscope with a 40X water immersion objective to image NMJ dye fluorescence (other microscopes can be used).
2. Image muscle 4 NMJ of abdominal segments 2-4 (other NMJs can be imaged) and collect images using appropriate software (**Table 2**).
3. Use a HeNe 633 nm laser to excite HRP:647 (with long-pass filter > 635 nm) and an Argon 488 nm laser to excite FM1-43 (with bandpass filter 530-600 nm).
4. Operationally determine optimal gain and offset for both channels.
   NOTE: These settings will remain constant throughout the rest of the experiment.
5. Take a confocal Z-stack through the entire selected NMJ from the HRP-marked top to bottom of the synaptic terminal.
6. Take careful note of the NMJ imaged (segment, side and muscle) to ensure excess to the exact same NMJ after FM dye unloading.

4. High [K^+] Stimulation: FM Dye Unloading

1. Replace Ca^{2+}-free saline with the high [K^+] saline (without FM1-43 dye) to drive depolarization, SV exocytosis and dye release.

2. Immediately start a digital timer for the pre-determined duration of the high [K^+] stimulation period (*e.g.*, 2 min; **Figure 16**).
3. When the timer period ends, immediately remove the high [K^+] saline and replace with Ca^{2+}-free saline to stop SV cycling.
4. Wash in quick succession with Ca^{2+}-free saline (5x for 1 min) to ensure the high [K^+] saline is completely removed.
5. Maintain the larval preparation in fresh Ca^{2+}-free saline for immediate imaging with the confocal microscope.
6. Be certain to image the FM1-43 dye fluorescence at the same NMJ noted above using the same confocal settings.

5. Option 2: Electrical Stimulation FM Dye Loading

1. Prepare a suction pipette using the microelectrode puller (**Table 2**) to obtain the required taper and tip size.
2. Fire-polish the microelectrode tip with a micro-forge until a single motor nerve can be sucked up with a tight fit.
3. Slide suction pipette onto the electrode holder on a micromanipulator and attach to the long flexible plastic tube and a syringe.
4. Set stimulator parameters (*e.g.*, 15 V, 20 Hz frequency, 20 ms duration and time of 5 min (**Figure 16**) or 1 min (**Figure 17**)).
5. Replace the Ca^{2+}-free saline on the larval preparation with above FM1-43 saline (4 µM; 1 mM $CaCl_2$) on the electrophysiology rig.
6. Put the preparation on the microscope stage and raise the stage until the larva and suction pipette are in focus (40X water-immersion objective).
7. Suck up a loop of cut motor nerve innervating the selected hemisegment with negative air pressure generated by the syringe into the suction electrode.

8. Test the suction electrode function with a short burst of stimulation while visually monitoring for the muscle contraction in the selected hemisegment.
9. Stimulate the motor nerve using selected parameters (step 5.4) to drive SV endocytosis and FM1-43 dye uptake (**Figure 16**).
10. Wash in quick succession with Ca^{2+}-free saline (5x for 1 min) to ensure the FM1-43 dye solution is completely removed.
11. Maintain the larval preparation in fresh Ca^{2+}-free saline for immediate imaging using the confocal imaging protocol from above.
12. Take careful note of the NMJ imaged (segment, side and muscle) to ensure access to the exact same NMJ after FM dye unloading.

6. Electrical Stimulation: FM Dye Unloading

1. Replace the Ca^{2+}-free saline with regular saline (without FM1-43 dye)and place the preparation back on the electrophysiology rig stage.
2. Set the stimulator parameters for unloading (*e.g.*, 15 V, 20 Hz frequency, 20 ms duration and time of 2 min (**Figure 16**) or 20 s (**Figure 17**)).
3. Suck the same motor nerve into the same electrode as above, and then stimulate to activate SV exocytosis and FM1-43 dye release.
4. Wash in quick succession with Ca^{2+}-free saline (5x for 1 min) to ensure the external dye is completely removed.
5. Maintain the larval preparation in fresh Ca^{2+}-free saline for immediate imaging with the confocal microscope.
6. Ensure to image the FM1-43 dye fluorescence at the same NMJ noted above using the same confocal settings.

7. Option 3: Channelrhodopsin Stimulation FM Dye Loading

1. Raise ChR2-expressing larvae on food containing the ChR2 co-factor all-trans retinal (dissolved in ethanol; 100 µM final concentration).

2. Place the larval preparation in the plexiglass chamber on a dissection microscope stage equipped with a camera port.
3. Attach a blue LED (470 nm; **Table 2**) to a programmable stimulator using a coaxial cable and place the LED into the camera port.
4. Focus the blue LED light beam onto the dissected larval function using the microscope zoom function.
5. Replace the Ca^{2+}-free saline on the larval preparation with above FM1-43 saline (4 µM; 1 mM $CaCl_2$) on the optogenetic stage.
6. Set the LED parameters using the stimulator (*e.g.*, 15 V, 20 Hz frequency, 20 ms duration and time of 5 min (**Figure 16**)).
7. Start the light stimulation and track with a timer for the pre-determined duration of the optogenetic stimulation period (*e.g.*, 5 min; **Figure 16**).
8. When the timer stops, quickly remove the FM dye solution and replace with Ca^{2+}-free saline to stop the SV cycling.
9. Wash in quick succession with the Ca^{2+}-free saline (5x for 1 min) to ensure the FM dye solution is completely removed.
10. Maintain the larval preparation in fresh Ca^{2+}-free saline for immediate imaging with the confocal microscope using imaging protocol from above.
11. Take careful note of the NMJ imaged (segment, side and muscle) to ensure access to the exact same NMJ after FM dye unloading.

8. Channelrhodopsin Stimulation: FM Dye Unloading

1. Replace Ca^{2+}-free saline with regular saline (without FM1-43 dye)on the dissection microscope stage with camera port LED focused on the larva.
2. Set the stimulator parameters for unloading (*e.g.,* 15 V, 20 Hz frequency, 20 ms duration and time of 2 min (**Figure 16**)).

3. Start the light stimulation and track with a timer for the pre-determined duration of the optogenetic stimulation period (*e.g.,* 2 min; **Figure 16**).
4. When the timer period ends, quickly remove the FM dye solution and replace with Ca^{2+}-free saline to stop the SV cycling.
5. Wash in quick succession with Ca^{2+}-free saline (5x for 1 min) to ensure the external dye is completely removed.
6. Maintain the larval preparation in fresh Ca^{2+}-free saline for immediate imaging with the confocal microscope.
7. Ensure to image the FM1-43 dye fluorescence at the same NMJ noted above using the same confocal settings.

9. Fluorescence Quantification

1. Load the image in Image J (NIH open source) and create a maximum intensity projection by clicking Image | Stacks | Z Project.
2. Using the anti-HRP:647 channel, go to Image | Adjust | Threshold and slide the top tool bar until just the NMJ is highlighted.
3. Using the wand tool, click on the NMJ. If the NMJ is discontinuous, hold the Shift button and select all parts.
4. Change the image to the FM1-43 dye channel and go to Analyze | Measure to obtain the fluorescence measurement.
5. Repeat steps 9.1-9.4 for the "unloaded" image from the same NMJ (identified segment, side and muscle).
6. To obtain the percentage of dye that was unloaded, take the ratio of the unloaded/loaded fluorescence intensities.

   NOTE: This procedure can be modified to analyze fluorescence on a bouton-per-bouton basis using either the "oval" or "freehand" selection tools. Background fluorescence can be subtracted by sampling the muscle fluorescence. Agents can also be added to reduce this background.

Representative Results

Figure 15 shows the work-flow for the activity-dependent FM dye imaging protocol. The experiment always begins with the same larval glue dissection, regardless of the stimulation method subsequently used. **Figure 15a** is a schematic of a dissected larva, showing the ventral nerve cord (VNC), radiating nerves and repeated hemisegmental muscle pattern. The VNC is removed and the preparation bathed in a 4 µM solution of FM1-43 (**Figure 15b**, pink). The preparation is then stimulated in the presence of FM dye using one of the three possible options to load the dye via activity-dependent SV endocytosis (**Figure 15cI-III**). Next, FM dye cycling is arrested using Ca^{2+}-free saline and a specific NMJ terminal that has been loaded with FM dye is imaged using a confocal microscope ("loaded image"; **Figure 15d**). In this case, the muscle 4 NMJ is selected with the schematic showing placement of the nerve, NMJ terminal branching and FM loaded synaptic boutons. The synaptic preparation is stimulated for a second time using the same method selected above, but in the absence of FM dye to drive SV exocytosis and FM1-43 release (**Figure 15e**). The same identified NMJ (muscle 4 NMJ in this example) is then re-imaged using the HRP:647 synaptic label and residual FM1-43 vesicle signal ("unloaded image"; **Figure 15f**). The experimenter determines the strength and duration of loading and unloading phases to optimize the measurements for a specific assay or mutant condition. Fluorescence intensity is quantified after loading and unloading (**Figure 15d, 1f**), to obtain the measurements of synaptic dye endocytosis, exocytosis and the percentage of loaded FM dye released. Analyses can be done for the entire NMJ or single boutons.

FM dye cycling can be stimulated in three ways: 1) high [K^+] saline depolarization of the entire preparation, 2) suction electrode stimulation of the motor nerve, or 3) light driven activation of targeted channelrhodopsin (ChR2; **Figure 16**). For a direct side-by-side comparison of all three methods, we stimulated with each approach for 5 min in the presence of FM1-43 (loading) and then for 2 min in the absence of FM1-43 (unloading), and imaged HRP-labeled NMJs using identical confocal settings (**Figure 16**). The high [K^+] saline depolarization method follows the

widely-used FM1-43 protocol for the *Drosophila* larval NMJ[23], except we use glue instead of pins for the larval dissection. The glue avoids the interference with the microscope objectives and enables more precise determination of body wall tension, but does require a moderate learning curve. All three methods produce strong and consistent fluorescent signals throughout the NMJ synaptic bouton arbor and within individual synaptic boutons (insets). The high [K^+] saline depolarization method causes all NMJs to be FM-loaded throughout the larva as it depolarizes every neuron in the animal (**Figure 16A**, middle). The nerve suction electrode electrical stimulation method drives only in a single hemisegment of the larvae for which the corresponding innervating motor nerve has been stimulated (**Figure 16B**, middle). Unstimulated segments in the same animal are distinguishable using the HRP label but contain no observable fluorescent dye loading, and serve as excellent internal controls. The optogenetic ChR2 method produces targeted depolarization dependent on the transgenic Gal4 driver employed (**Figure 16C**). Here, the driver was a vesicular glutamate transporter (vglut) Gal4, so all glutamatergic neurons are depolarized with blue light stimulation, including all of the glutamatergic motor neurons. As a result, all NMJs are loaded with FM1-43 dye in this example (**Figure 16C**, middle). Cell-specific drivers can be used to label specific NMJs and leave others unlabeled for an internal control.

FM dye unloading was achieved via the same method that was used to load dye. In the first method, the larval preparation was simply bathed in high [K^+] saline in the absence of FM1-43 to depolarize cells, drive SV exocytosis, and unload the synaptic terminals (**Figure 16A**, right). We typically select a shorter unloading period (2 min), so unloading is partial and terminals remain visible in the FM channel. Suction electrode electrical stimulation unloading is considerably more challenging, because it involves returning to the same hemisegment, identifying the same nerve, and re-stimulating that nerve in the absence of FM1-43 to drive dye unloading (**Figure 16B**, right). Note that the dye unloading was again partial. The ChR2 unloading entails a second period of blue LED illumination of the larval preparation in the absence of FM1-43 to activate the channels, depolarize the motor neurons and stimulate SV exocytosis dye release (**Figure 16C**, right). With

this timescale of unloading (2 min), each of these depolarization methods unloaded only a percentage of the loaded FM1-43 dye, with the high [K^+] strongest and ChR2 weakest in driving dye release (**Figure 16**). We measured the LED light intensity used (140 μW/mm^2), which was in the published range (20-1000 μW/mm^2)[24,25,26]. ChR2 is maximally activated by ~1 mW illumination from 50-200 mW light sources, with ChR2 effectiveness also dependent on the ATR concentration fed to larva[27,28]. Thus, ChR2 stimulation strength can be manipulated. Moreover, the relationship may not remain true with other stimulation strengths, timescales or genotypes. If the experimenter is working with a mutant that has diminished SV endocytosis or unusually fast exocytosis, the stimulation parameters may need to be altered to maintain an observable signal after unloading. The anti-HRP label allows one to identify the NMJ even in the complete absence of the FM signal, but this is not ideal for quantification. In principle, the unloading stimulation could also be of a different type from the loading stimulation.

We recently studied the loss of the secreted synaptic deacylase Notum effects on the SV cycle using electrical stimulation[4]. Here, we extend this analysis to compare 1) high [K^+] depolarization and 2) suction electrode motor nerve stimulation methods (**Figure 17**). We find that both methods give a similar result, showing reduced FM1-43 dye loading in a *Notum* null mutant; however, the degree of the phenotype is distinct between the two methods. After the depolarization with high [K^+] saline for five min, there is a large decrease in loaded fluorescence intensity between genetic background control (w^{1118}) with high levels and *Notum* null mutants ($Notum^{KO}$) with low levels (**Figure 17A**, top). In quantified measurements, normalized FM fluorescence intensity within HRP-outlined NMJ terminals is significantly reduced in the absence of Notum (w^{1118} 1.0 ± 0.05 vs. $Notum^{KO}$ 0.57 ± 0.07; n≥13, p<0.0001; **Figure 17B**). After electrical stimulation at 20 Hz for 1 min, we find an insignificant decrease in loaded FM1-43 intensity between controls and *Notum* nulls when quantifying whole NMJ fluorescence (w^{1118} 1.0 ± 0.05 vs. $Notum^{KO}$ 0.86 ± 0.06; n = 8, p = 0.10; **Figure 17A**, B). When measuring dye incorporation on a bouton-per-bouton basis, we find a significant decrease in dye loaded with both of the methods.

In quantified measurements after stimulation with high [K^+] saline, normalized FM fluorescence intensity per bouton is significantly decreased (w^{1118} 1.0 ± 0.02 vs. $Notum^{KO}$ 0.52 ± 0.02; n≥241, p<0.0001; **Figure 17C**). After electrical stimulation, normalized fluorescence intensity per bouton is also significantly decreased, albeit to a lower degree (w^{1118} 1.0 ± 0.02 vs. $Notum^{KO}$ 0.83 ± 0.02; n≥127, p<0.0001; **Figure 17C**).

The result differences between the two stimulation paradigms could be due to a number of factors. First, the stimulation strength is presumed to be greater with high [K^+] compared to electrical motor nerve stimulation. Electrophysiology recordings cannot be done in the presence of the high [K^+] saline, but the larval neuromusculature is clearly being robustly stimulated, as muscle contractions are strong and continual throughout the 5 min bathing period. However, we do not know the strength or frequency of the stimulation. In contrast, the electrical stimulation is much more controlled with the user choosing the exact voltage strength and frequency of stimulation. Second, the stimulation duration was longer with high [K^+] compared to electrical nerve stimulation (**Figure 17**). We chose 1 min of 20 Hz electrical stimulation after repeated trials. After 1 min of dye loading, there was a strong and reliable FM1-43 signal, so we chose that paradigm for our study[4], although 5 min of stimulation gave an even stronger fluorescent signal (**Figure 16**). Thus, the length of the stimulation paradigm is likely contributing to the magnitude variability in FM1-43 loading between high [K^+] and electrical stimulation (**Figure 17B, C**). Although the high [K^+] method showed a more robust phenotype for *Notum* mutants, we still used the electrical method because of the greater control[4]. There are many parameters to control such as strength, frequency and duration of stimulation, and those settings must be decided based on the mutant and the question. For example, the stimulation method choice may depend on the SV pool interrogated[7] and the activity-dependent mechanism investigated[10].

After FM1-43 loading into the NMJ terminal, one can employ fluorescence dye photoconversion to produce the electron-dense signal for electron microscopy (**Figure 18**). In this method, the dye-loaded preparation is exposed to intense fluorescent light in the presence of

diaminobenzidine (DAB), with the reactive oxygen species from the FM dye oxidizing the DAB to create a dark precipitate (**Figure 18A**)[11]. Please see the JoVE article on photoconversion of styryl dyes for complete details[12]. The benefit of this method is that SVs are clearly revealed at an ultrastructural level, although the SV cycle is of course arrested with static electron microscope imaging. In the absence of stimulation, synaptic boutons at the *Drosophila* NMJ are densely loaded with vesicles (~40 nm in diameter; **Figure 18B**), with the rare occurrence of enlarged organelles (**>**100 nm in diameter) presumed to be cycling endosomes. High [K^+] saline depolarizing stimulation strongly changes this profile, with a partial depletion of the SV population and the rapid accumulation of numerous enlarged organelles (**>**100 nm in diameter) thought to derive from bulk endocytosis of the plasma membrane (**Figure 18C**, left). Although similar compartments exist in unstimulated controls, the high density of these organelles after high [K^+] saline depolarization raises the concern that this may be a non-physiological response. Suction electrode electrical stimulation of the motor nerve is relatively more efficient in depleting the SV population and does not produce more of the enlarged endosomal vesicles (**Figure 18D**, left). This suggests that the bulk endocytosis driven by high [K^+] depolarization helps maintain the SV population during more intense demand.

FM1-43 photoconversion can be accomplished using either high [K^+] saline depolarization or suction electrode electrical stimulation of the motor nerve, to compare synaptic ultrastructure relative to a resting bouton (**Figure 18**). With high [K^+] depolarizing stimulation, both individual SVs and enlarged vesicles (**>**100 nm in diameter) can be labeled with the electron-dense DAB precipitate following light-driven photoconversion (**Figure 18C**, right). For unknown reasons, the enlarged vesicle membrane is typically less densely labeled than the smaller SV membrane. Moreover, SVs often appear filled with the DAB precipitate, rather than just the membrane, but this does make them much easier to distinguish from the unlabeled vesicles. With suction electrode stimulation of the motor nerve, the cycling SV population can also be marked relative to unlabeled SVs (**Figure 18D**, right). With electrical stimulation, enlarged vesicles (**>**100 nm in

diameter) are not detectably formed in boutons and, consistently, the membranes of the presumed endosomes are not labeled by FM1-43 photoconversion. As above, cycling SVs are typically filled with the DAB precipitate in a somewhat all-or-none fashion, and therefore more easily distinguishable from SVs that have not been formed during the stimulation (**Figure 18D**, right). We have not yet attempted photoconversion following ChR2 stimulation. With different time courses of stimulation, FM1-43 dye photoconversion allows one to determine where SVs are formed, how SVs are trafficked, and the timing of movement between different spatial pools within the synaptic bouton. The comparison of high $[K^+]$ and nerve stimulation allows the dissection of bulk and single SV endocytosis mechanisms.

Name	Company	Catalog Number	Comments
SylGard 184 Silicone Elastomer Kit	Fisher Scientific	NC9644388	To put on cover glass for dissections
Microscope Cover Glass 22x22-1	Fisherbrand	12-542-B	To put SylGard on for dissections
Aluminum Top Hot Plate Type 2200	Thermolyne	HPA2235M	To cure the SylGard
Plexi glass dissection chamber	N/A	N/A	Handmade
Borosilicate Glass Capillaries	WPI	1B100F-4	To make suction and glue micropipettes
Laser-Based Micropipette Puller	Sutter Instrument	P-2000	To make suction and glue micropipettes
Tygon E-3603 Laboratory Tubing	Component Supply Co.	TET-031A	For mouth and suction pipette
P2 pipette tip	USA Scientific	1111-3700	For mouth pipette
0.6-mL Eppendorf tube cap	Fisher Scientific	05-408-120	Used to put glue in for dissection
Vetbond 3M	WPI	vetbond	Glue used for dissections
Potassium Chloride	Fisher Scientific	P-217	Forsaline
Sodium Chloride	Millipore Sigma	S5886	For saline
Magnesium Chloride	Fisher Scientific	M35-500	For saline
Calcium Chloride Dihydrate	Millipore Sigma	C7902	For saline
Sucrose	Fisher Scientific	S5-3	For saline
HEPES	Millipore Sigma	H3375	For saline
HRP:Alexa Fluor 647	Jackson ImmunoResearch	123-605-021	To label neuronal membranes
Paintbrush	Winsor & Newton	94376864793	To manipulate the larvae
Dumont Dumostar Tweezers #5	WPI	500233	Used during dissection
7 cm McPherson-Vannas Microscissors (blades 3 mm)	WPI	14177	Used during dissection
FM1-43	Fisher Scientific	T35356	Fluorescent styryl dye
Digital Timer	VWR	62344-641	For timing FM dye load/unload
LSM 510 META laser-scanning confocal microscope	Zeiss		For imaging the fluorescent markers
Zen 2009 SP2 version 6.0	Zeiss		Software for imaging on confocal
HeNe 633nm laser	Lasos		To excite HRP:647 during imaging
Argon 488nm laser	Lasos		To excite the FM dye during imaging
Micro-Forge	WPI	MF200	To fire polish glass micropipettes
20mL Syringe Slip Tip	BD	301625	To suck up the axon for electrical stimulation.
Micro Manipulator (magnetic base)	Narishige	MMN-9	To control the suction electrode for electrical stimulation
Stimulator	Grass	S48	To control the LED and electrical stimulation
Zeiss Axioskop Microscope	Zeiss		Used during electrical stimulation.
40X Achroplan Water Immersion Objective	Zeiss		Used during electrical stimulation and confocal imaging
All-trans Retinal	Millipore Sigma	R2500	Essential co-factor for ChR2
Zeiss Stemi Microscope with camera port	Zeiss	2000-C	Used during channelrhodopsin stimulation
LED 470nm	ThorLabs	M470L2	Used for ChR activation
T-Cube LED Driver	ThorLabs	LEDD1B	To control the LED
LED Power Supply	Cincon Electronics Co.	TR15RA150	To power the LED
Optical Power and Energy Meter	ThorLabs	PM100D	To measure LED intensity

Table 2: List of materials for FM dye loading/unloading at NMJ.

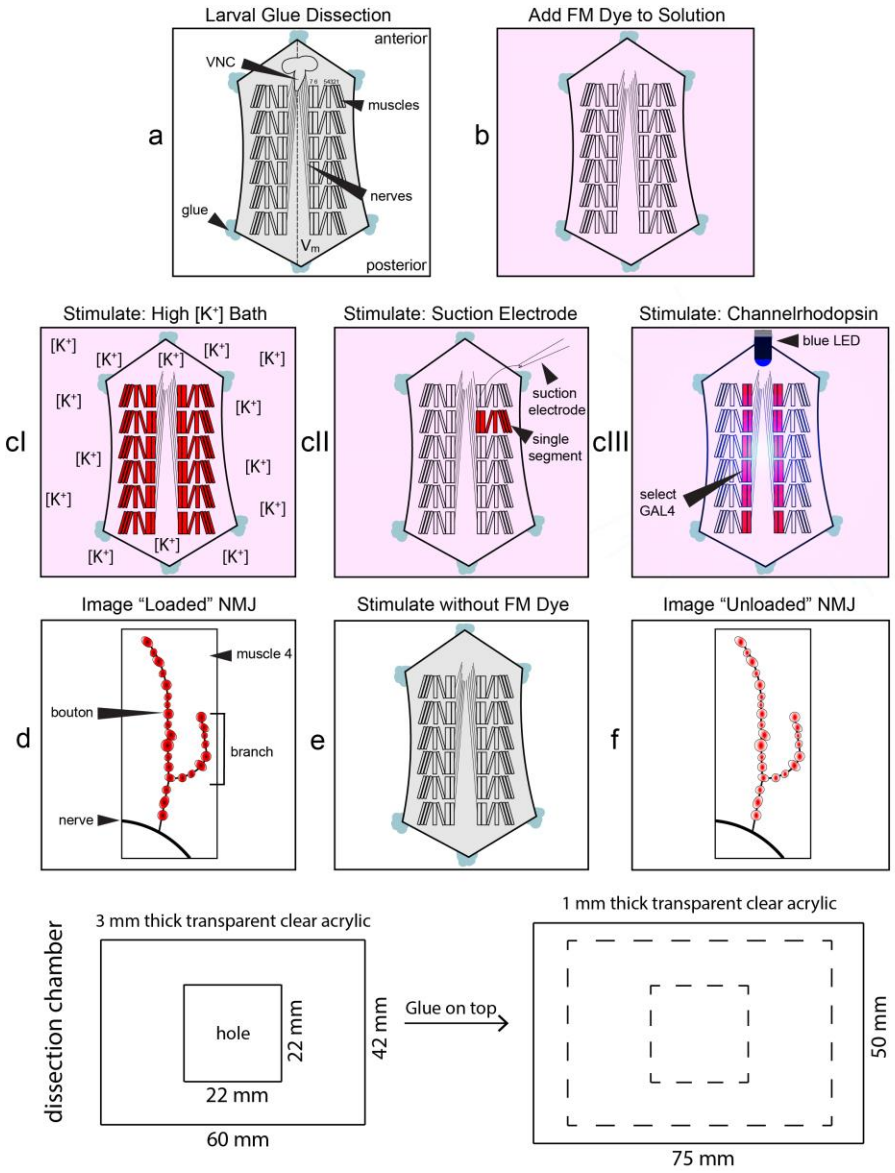

Figure 15: Flowchart of FM1-43 dye loading protocol at the *Drosophila* NMJ. The larval glue dissection produces a flattened neuromusculature preparation, with the ventral nerve cord (VNC) projecting segmental nerves from the ventral midline (Vm) to the hemisegmentally repeated body wall muscle arrays (step a). The VNC is cut free, and the entire larval dissection is then incubated in the pink FM1-43 solution (4 µM) in preparation for stimulation (step b). FM1-43 is then loaded with a selected stimulation paradigm (step 3); with the options of high $[K^+]$ depolarization of the entire larva (cI), suction electrode stimulation of a single motor nerve (cII), or light-driven activation of highly targeted channelrhodopsin (cIII). FM1-43 incorporation is arrested using Ca^{2+}-free saline and the dye-loaded NMJ imaged (step d). A second stimulation is then done without FM1-43 in the bath to drive dye synaptic vesicle exocytosis (step e). The same NMJ is then re-imaged to assay the unloaded synaptic terminal (step f). Fluorescent intensity is measured from both loaded and unloaded NMJs to quantify SV endocytosis and SV exocytosis levels. The bottom panel shows the construction parameters and dimensions for the transparent acrylic chamber used for these studies.

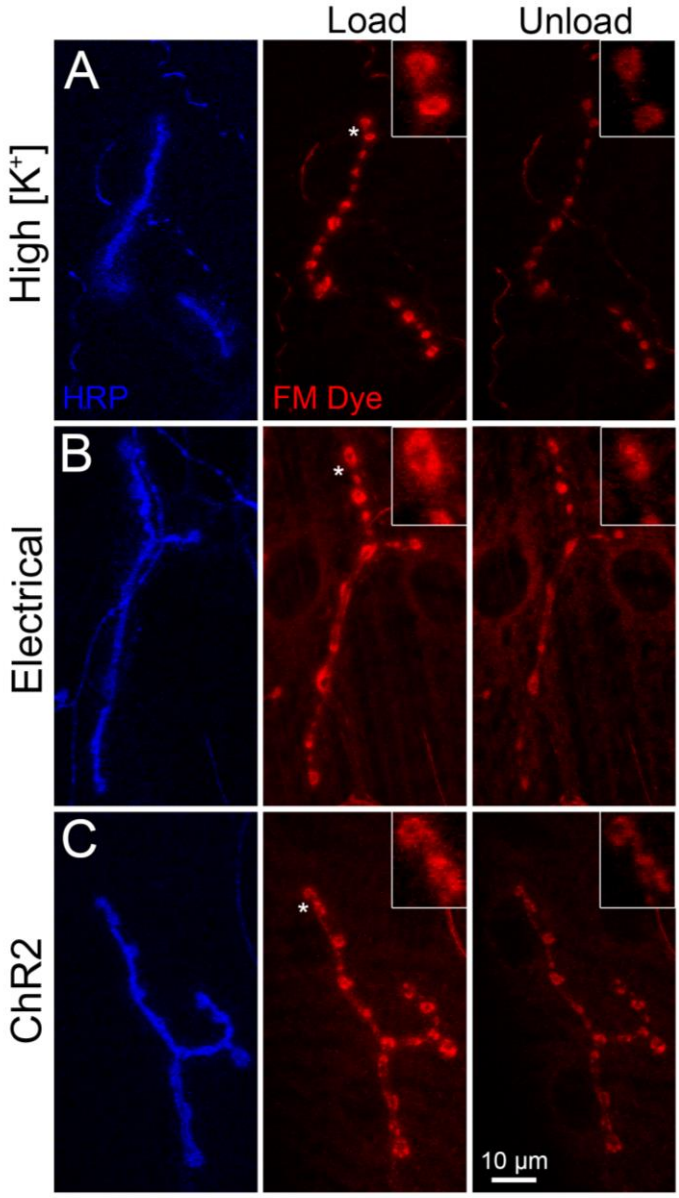

Figure 16: FM dye loading and unloading comparison of all stimulation methods. Comparison of FM1-43 dye loading and unloading in the wandering third instar NMJ with 1) high [K^+] depolarization of the entire larval preparation (top), 2) suction electrode electrical stimulation of the motor nerve (middle) and 3) light-driven activation of the targeted channelrhodopsin (ChR2) only in motor neurons (bottom). (**A**) The larval NMJ labeled with the anti-HRP:647 presynaptic membrane marker (blue, left), loaded with FM1-43 via high [K^+] depolarization for 5 min (middle) and then unloaded via high [K^+] depolarization for 2 min. (**B**) Comparison with suction electrode electrical nerve stimulation with the same stimuli periods for both FM1-43 dye loading and unloading. (**C**) Targeted *vglut*-Gal4**>**UAS-ChR2-H134R expression in motor neurons activated with blue (470 nm) light for the same stimuli periods of FM1-43 dye loading and unloading. Asterisks refer to insets displaying higher magnification boutons. The scale bar is 10 µm, with inset synaptic boutons enlarged 3.5X from main panels.

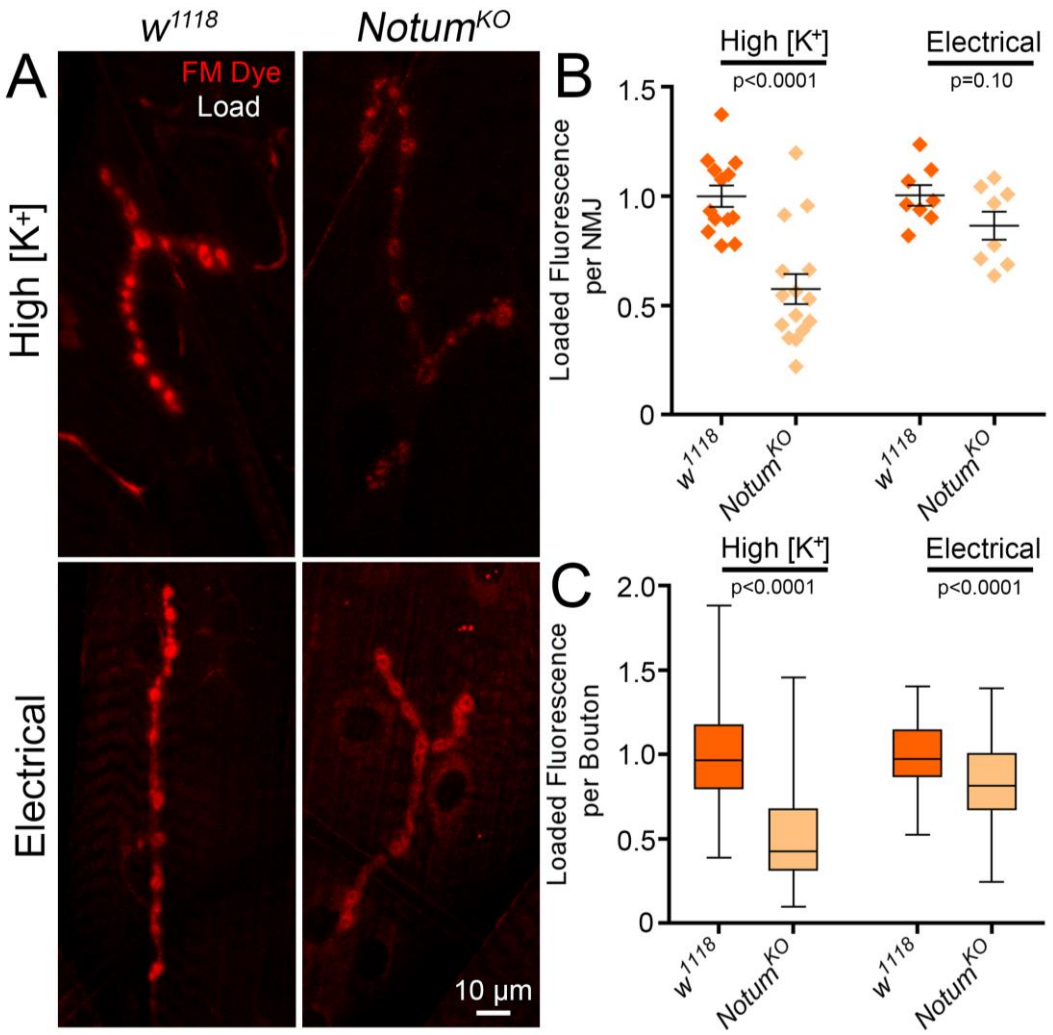

Figure 17: *Notum* null mutants show reduced FM dye loading in synaptic boutons. FM1-43 loaded into synaptic terminals of the wandering third instar NMJ comparing the genetic control (w^{1118}) to *Notum* null mutants ($Notum^{KO}$). (**A**) NMJ boutons labeled with high [K^+] depolarization of entire larval preparation (top) or suction electrode stimulation of one motor nerve (bottom) in w^{1118} (left) and $Notum^{KO}$ (right). (**B**) Quantified loaded FM1-43 fluorescence per NMJ as a scatter plot comparing the high [K^+] depolarization and suction electrode stimulation in w^{1118} controls vs. $Notum^{KO}$ mutants. (**C**) Quantified loaded fluorescence on a bouton-per-bouton basis as a box-and-whisker plot comparing high [K^+] depolarization and suction electrode stimulation in w^{1118} controls vs. $Notum^{KO}$. Student's two-tailed t-tests were performed for each comparison with p-values displayed on the graphs. Bars show mean ± SEM made with Prism (Version 7.0 for Windows). The electrical stimulation data has been adapted with permission from Kopke *et al*., Development 144(19):3499-510, 2017.

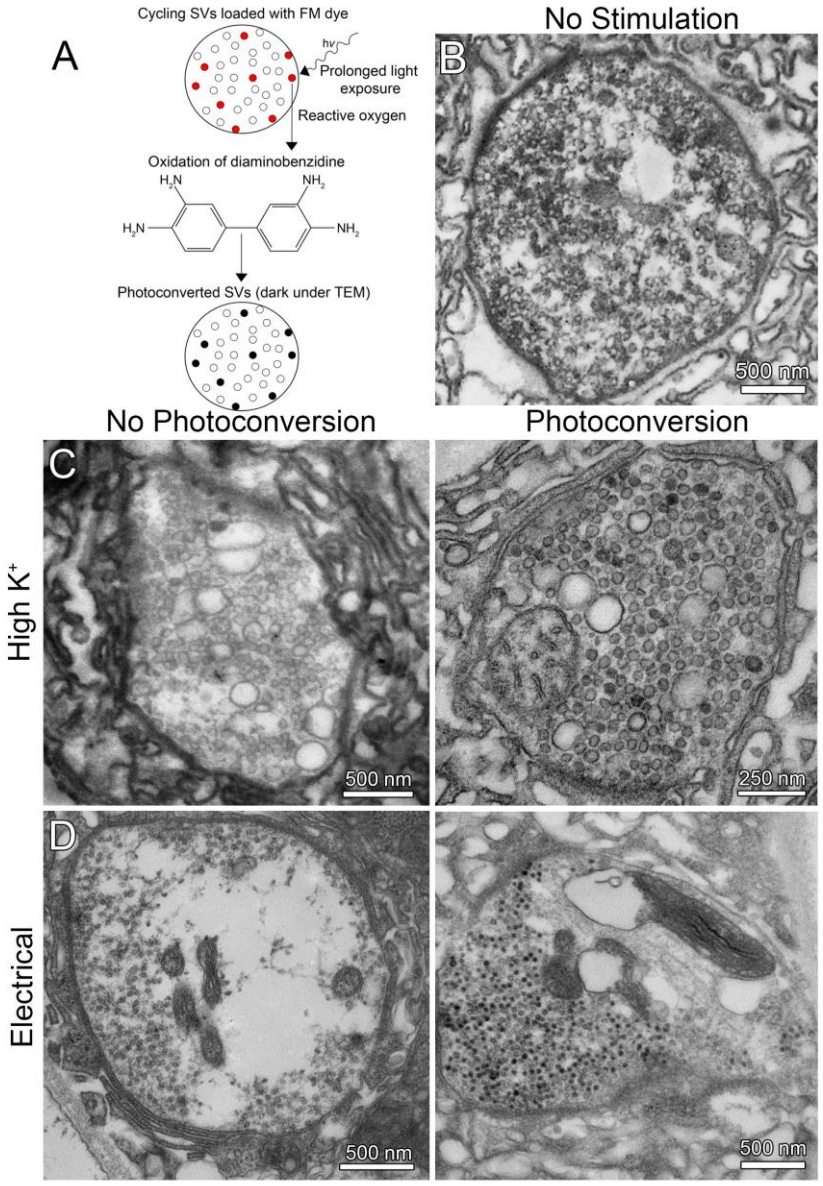

Figure 18: Synaptic ultrastructure with FM dye photoconversion to mark vesicles. Fluorescent FM1-43 can be photoconverted to an oxidized diaminobenzidine (DAB) electron-dense precipitate for visualization via transmission electron microscopy (TEM). (**A**) A schematic diagram of the photoconversion method to label the *Drosophila* NMJ following activity-dependent FM1-43 dye loading. (**B**) Representative TEM image of a wildtype synaptic bouton at rest (unstimulated). Note dense population of uniform-sized SVs. (**C**) Synaptic boutons that have been stimulated with high [K^+] saline depolarization for 5 min, without photoconversion (left) or with FM1-43 photoconversion (right). Note the presence of bulk endosomal structures, labeled and unlabeled. (**D**) Synaptic boutons that have been electrically stimulated with a nerve suction electrode at 20 Hz for 5 min with no photoconversion (left) or with FM1-43 photoconversion (right). Note that the dye-loaded vesicles appear much darker than adjacent unloaded vesicles.

Discussion

High [K^+] saline depolarizing stimulation is by far the easiest of the three options for activity-dependent FM dye cycling, but likely the least physiological[29]. This simple method depolarizes every accessible cell in the entire animal, and so does not allow directed studies. It may be possible to locally apply high [K^+] saline with a micropipette, but this will still depolarize pre/postsynaptic cells and likely synapse-associated glia[1]. Another major concern is that high [K^+] depolarization drives rapid formation of bulk endosomes that are only rarely seen in unstimulated boutons. However, bulk endosome formation is an active mechanism blocked by mutations[29], indicating a real physiological process. Thus, FM1-43 imaging with high [K^+] depolarization can be used to selectively study bulk endocytosis at synapses. Suction electrode electrical stimulation of the motor nerve is a much more controlled method. It has the advantage that only a single axon bundle is stimulated, and only the presynaptic termini is directly depolarized (of course, the muscle fiber is then depolarized by transmitter action). It therefore provides a great internal control of NMJs in the same animal that are not stimulated. This method allows one to tightly control the stimulation parameters, unlike the high [K^+] stimulation method, enabling direct comparison with electrophysiology recordings[4]. However, this technique requires specialized equipment and a fairly high level of technical skill, and is therefore less accessible. Light-driven activation of targeted channelrhodopsin (ChR2) has the advantage of targeting select neurons[30]. This method requires no familiarity with electrophysiology methods, and can be done with very cheap equipment in any lab, but this approach does require basic familiarity with *Drosophila* genetics.

The choice of stimulation parameters is critically important for testing SV cycle dynamics queried within a range of genetic conditions with highly variable phenotypes[1]. For all methods, the external [Ca^{2+}] used is a key parameter controlling the driving force of SV cycling. With the high [K^+] stimulation method, an important choice is [K^+] used, which determines the degree of depolarization strength. Measurements of *Drosophila* haemolymph indicate a [K^+] of 5 mM, and 90 mM is typically the concentration most often selected for activity stimulation[3,7,15,17,31]. However,

a [K^+] range from 30-90 mM has been employed to vary the stimulation strength[5,16,32]. Another critical parameter decision is the length of the high [K^+] stimulation for both FM1-43 loading and unloading. The period for loading determines whether the entire cycling SV population is effectively loaded, or only a subset of active vesicles[7]. The period for unloading similarly dictates the percentage of SVs undergoing exocytosis in the stimulation period, which can either reveal or obscure mutant phenotypes dependent on rate changes in the SV cycling frequency[2]. With suction electrode electrical motor nerve stimulation, parameter choices include also stimulation voltage, frequency, duration and pulse interval. Temporally patterned activity is a key determinant of SV cycling dynamics[7], and different stimulation patterns can selectively mobilize distinct SV pools. With targeted light-driven ChR2 activation, the choices include all of the above (with light intensity variables) and additional transgenic options discussed in the next section. With these parameter choices comes more experimental control, but also increased technical complexity.

Channelrhodopsin-2 (ChR2) is a light-gated membrane channel permeable to mono- and divalent cations[33]. If ChR2 stimulation is selected, there are many choices to be made including the Gal4 driver, UAS-ChR2 construct and light source variables for channel activation. Gal4 drivers range from ubiquitous to highly specific. For example, ubiquitous UH1-Gal4 (*daughterless*) would express ChR2 in every cell, whereas CcapR-Gal4 (Janelia) drives ChR2 in the muscle 6/7 NMJ but not the muscle 4 NMJ[31,34]. This selectivity can be used as a powerful internal control. There are likewise many UAS-ChR2 variants, including ChR2-H134R (used here; the mutated residue causes increased photocurrents)[35], VChR1, ChIEF and many more[36]. Each of these channel variants has distinct properties of light gating, conductance, ion selectivity, kinetics and desensitization. Note some constructs contain a fluorescent tag that could interfere with FM imaging. For example, the UAS-ChR2-H134R used here is tagged with mCherry (ex: 587 nm, em: 610 nm), but does not produce detectible emission with the FM1-43 (ex: 479 nm, em: 598 nm) imaging filters. Technical parameter choices include the light source, wavelength and intensity for channel activation. An option used here is a cheap blue-emitting LED, with stimulation

visually confirmed by assaying muscle contractions. We were also successful in activating ChR2 using epifluorescence, although a scanning confocal laser was not sufficient. Epifluorescence could be used in targeted stimulation (specific segments instead of the whole animal), but stimulation parameters are difficult to control, whereas the LED connected up to a simple stimulator easily alters both the duration and frequency of light pulses. Focusing the LED light through the dissection microscope camera port allows more controlled, intense light stimulation.

It is up to the experimenter to decide whether or not to leave the ventral nerve cord/brain intact during the stimulation paradigm. We chose to remove the entire central nervous system for the comparison of the three methods used here, but sometimes the upstream wiring is left intact[15]. A complication is that endogenous neural activity occurs whenever the nervous system is left whole. The degree of this activity is highly variable from animal to animal, dependent in large degree on the dissection expertise of the experimenter. This variable activity can contribute to the amount of FM1-43 dye that is loaded and unloaded, which is therefore not solely due to the exogenous stimulation employed[15]. A related technical complication is that intact dissected larvae contract the musculature in fictive movement, and this displacement greatly interferes with NMJ imaging. This movement is alleviated if the central nervous system is removed, and also through the application of Ca^{2+}-free saline during imaging[4]. These approaches used here are sufficient to enable excellent FM1-43 dye imaging in the NMJ preparation. However, some experimenters choose to add drugs to inhibit muscle contraction (*e.g.,* ryanodine, philanthotoxin-433), or use action potential blockers (*e.g.,* tetrodotoxin)[37,38]. A range of drugs can be used to selectively manipulate the SV cycle, in order to highlight certain steps, or accentuate mutant phenotypes to examine neurotransmission mechanisms. For example, some experimenters have employed Veratridine (activates voltage-gated Na^+ channels[39]) to increase SV loading in the reserve pool, Cyclosporin A (inhibits Calcineurin activity[40]) to enhance SV endocytosis, and Forskolin (activates adenylyl cyclase[41], which enhances synaptic transmission[42]) to increase the exo/endo cycling pool[7,43,44]. Such pharmacological manipulations can provide additional insights. Lastly, FM1-43

background can occur to varying degrees based on quality of dissection, washing effectiveness and stimulation protocol. Some add a sulfobutylated derivative of β-cyclodextrin Advasep-7[45], or the aqueous fluorophore sulforhodamine[46], to quench nonspecific fluorescence and improve signal-to-background ratio.

There are numerous techniques that can accompany FM fluorescent imaging to further understanding of the SV cycle (*e.g.,* electrophysiology, synaptopHluorin, electron microscopy). An example shown here is FM fluorescence photoconversion that is used to investigate the SV cycle in ultrastructural detail. SVs are organized into several pools that are spatially and functionally distinct[2]. The readily releasable pool (RRP) contains vesicles immediately released upon acute stimulation. A larger recycling pool maintains SV release under conditions of moderate activity. An internal reserve pool (RP) is only recruited with strong (seemingly near non-physiological) stimulation[2]. The SV pools that are activated depend on the type of stimulation used[47], and reports from the *Drosophila* NMJ using FM photoconversion have revealed key insights into spatial and functional properties of these different SV pools[48]. FM photoconversion can be used to study SV pools activated under different stimulation paradigms, and query questions such as the long-debated trafficking interaction between endosomes and SVs[49]. If the experimenter is interested in FM imaging in combination with other activity-dependent changes at the synapse, there is a reportedly fixable analog of the FM1-43 dye (FM1-43FX). This probe should allow one to fix the *Drosophila* NMJ after activity-dependent dye loading, and then follow up with antibody labeling to test for correlations between bouton activity level (FM dye fluorescence) and activity-dependent expression of a protein of interest. In the future, it will be extremely rewarding to explore additional methods that could enable the combination of FM dye imaging with other imaging approaches at the beautiful *Drosophila* NMJ model synapse.

References

1. **Menon KP, Carrillo RA, Zinn K** (2013) Development and plasticity of the *Drosophila* larval neuromuscular junction. Wiley Interdiscip Rev Dev Biol 2(5): 647-70.

2. **Rizzoli SO, Betz WJ** (2005) Synaptic vesicle pools. Nat Rev Neurosci 6(1):57-69.

3. **Long AA, Kim E, Leung HT, Woodruff E 3rd, An L, Doerge RW, Pak WL, Broadie K** (2008) Presynaptic calcium channel localization and calcium-dependent synaptic vesicle exocytosis regulated by the Fuseless protein. J Neurosci 28(14): 3668-82.

4. **Kopke DL, Lima SC, Alexandre C, Broadie K** (2017) Notum coordinates synapse development via extracellular regulation of Wingless trans-synaptic signaling. Development 144(19):3499-510.

5. **Betz WJ, Mao F, Bewick GS** (1992) Activity-dependent fluorescent staining and destaining of living vertebrate motor nerve terminals. J Neurosci 12(2):363-75.

6. **Richards DA, Bai J, Chapman ER** (2005) Two modes of exocytosis at hippocampal synapses revealed by rate of FM1-43 efflux from individual vesicles. J Cell Biol. 168(6):929-39.

7. **Verstreken P, Ohyama T, Bellen HJ** (2008) FM 1-43 labeling of synaptic vesicle pools at the drosophila neuromuscular junction. Methods Mol Biol 440:349-69.

8. **Dickman DK, Horne JA, Meinertzhagen IA, Schwarz TL** (2005) A Slowed Classical Pathway Rather Than Kiss-and-Run Mediates Endocytosis at Synapses Lacking Synaptojanin and Endophilin. Cell 123(3):521-33.

9. **Verstreken P, Kjaerulff O, Lloyd TE, Atkinson R, Zhou Y, Meinertzhagen IA, Bellen HJ** (2002) Endophilin Mutations Block Clathrin-Mediated Endocytosis but Not Neurotransmitter Release. Cell 109(1):101-12.

10. **Iwabuchi S, Kakazu Y, Koh JY, Goodman KM, Harata NC** (2014) Examination of synaptic vesicle recycling using FM dyes during evoked, spontaneous, and miniature synaptic activities. J Vis Exp (85):e50557.

11. **Sandell JH, Masland RH** (1988) Photoconversion of some fluorescent markers to a diaminobenzidine product. J Histochem Cytochem 36(5):555-9.

12. **Opazo F, Rizzoli SO** (2010) Studying Synaptic Vesicle Pools using Photoconversion of Styryl Dyes. J Vis Exp (36):e1790.

13. **Sabeva NS, Bykhovskaia M** (2017) FM1-43 Photoconversion and Electron Microscopy Analysis at the Drosophila Neuromuscular Junction. Bio-protocol 7(17).

14. **Sabeva N, Cho RW, Vasin A, Gonzalez A, Littleton JT, Bykhovskaia M** (2017) Complexin Mutants Reveal Partial Segregation between Recycling Pathways That Drive Evoked and Spontaneous Neurotransmission. J Neurosci 37(2):383-96.

15. **Ryan TA, Reuter H, Wendland B, Schweizer FE, Tsien RW, Smith SJ** (1993) The kinetics of synaptic vesicle recycling measured at single presynaptic boutons. Neuron 11(4):713-24.

16. **Ramaswami M, Krishnan KS, Kelly RB** (1994) Intermediates in synaptic vesicle recycling revealed by optical imaging of Drosophila neuromuscular junctions. Neuron 13(2):363-75.

17. **Trotta N, Rodesch CK, Fergestad T, Broadie K** (2004) Cellular bases of activity-dependent paralysis in Drosophila stress-sensitive mutants. J Neurobiol 60(3):328-47.

18. **Long AA, Mahapatra CT, Woodruff EA 3rd, Rohrbough J, Leung HT, Shino S, An L, Doerge RW, Metzstein MM, Pak WL, Broadie K** (2010) The nonsense-mediated decay pathway maintains synapse architecture and synaptic vesicle cycle efficacy. J Cell Sci 123(19):3303-15.

19. **Parkinson W, Dear ML, Rushton E, Broadie K** (2013) N-glycosylation requirements in neuromuscular synaptogenesis. Development 140(24):4970-81.

20. **Brand AH, Perrimon N** (1993) Targeted gene expression as a means of altering cell fates and generating dominant phenotypes. Development **118**(2):401-15.

21. **Jan LY, Jan YN** (1982) Antibodies to horseradish peroxidase as specific neuronal markers in Drosophila and in grasshopper embryos. Proc Natl Acad Sci 79(8):2700-4.

22. **Paschinger K, Rendić D, Wilson IBH** (2009) Revealing the anti-HRP epitope in Drosophila and Caenorhabditis. Glycoconj J 26(3):385-95.

23. **Ramachandran P, Budnik V** (2010) FM1-43 labeling of Drosophila larval neuromuscular junctions. Cold Spring Harb Protoc (8):prot5471.

24. **Yawo H, Kandori H, Koizumi A** (2015) Optogenetics: light-sensing proteins and their applications.

25. **Pulver SR, Pashkovski SL, Hornstein NJ, Garrity PA, Griffith LC** (2009) Temporal dynamics of neuronal activation by Channelrhodopsin-2 and TRPA1 determine behavioral output in Drosophila larvae. J Neurophysiol 101(6):3075-88.

26. **Hornstein NJ, Pulver SR, Griffith LC** (2009) Channelrhodopsin2 Mediated Stimulation of Synaptic Potentials at Drosophila Neuromuscular Junctions. J Vis Exp (25):e1133.

27. **Britt JP, McDevitt RA, Bonci A** (2012) Use of channelrhodopsin for activation of CNS neurons. Curr Protoc Neurosci Chapter 2, Unit 2.16.

28. **Lin JY** (2011) A user's guide to channelrhodopsin variants: features, limitations and future developments. Exp Physiol 96(1):19-25.

29. **Vijayakrishnan N, Woodruff EA, Broadie K** (2009) Rolling blackout is required for bulk endocytosis in non-neuronal cells and neuronal synapses. J Cell Sci 122:114-25.

30. **Honjo K, Hwang RY, Tracey WD** (2012) Optogenetic manipulation of neural circuits and behavior in Drosophila larvae. Nat Protoc 7(8)1470-78.

31. **Dear ML, Shilts J, Broadie K** (2017) Neuronal activity drives FMRP- and HSPG-dependent matrix metalloproteinase function required for rapid synaptogenesis. Sci Signal 10(504).

32. **Baldwin ML, Rostas JAP, Sim ATR** (2003) Two modes of exocytosis from synaptosomes are differentially regulated by protein phosphatase types 2A and 2B. J Neurochem **8**5(5):1190-9.

33. **Nagel G, Szellas T, Huhn W, Kateriya S, Adeishvili N, Berthold P, Ollig D, Hegemann P, Bamberg E** (2003). Channelrhodopsin-2, a directly light-gated cation-selective membrane channel. Proc Natl Acad Sci 100(24):13940-5.

34. **Pfeiffer BD, Jenett A, Hammonds AS, Ngo TT, Misra S, Murphy C, Scully A, Carlson JW, Wan KH, Laverty TR, Mungall C, Svirskas R, Kadonaga JT, Doe CQ, Eisen MB, Celniker SE, Rubin GM** (2008) Tools for neuroanatomy and neurogenetics in Drosophila. Proc Natl Acad Sci 105(28):9715-20.

35. **Nagel G, Brauner M, Liewald JF, Adeishvili N, Bamberg E, Gottschalk A** (2005) Light Activation of Channelrhodopsin-2 in Excitable Cells of Caenorhabditis elegans Triggers Rapid Behavioral Responses. Curr Biol 15(24):2279-84.

36. **Lin JY** (2011) A user's guide to channelrhodopsin variants: features, limitations and future developments. Exp Physiol 96(1):19-25.

37. **Sullivan KM, Scott K, Zuker CS, Rubin GM** (2000) The ryanodine receptor is essential for larval development in Drosophila melanogaster. Proc Natl Acad Sci 97(11):5942-7.

38. **Narahashi T, Moore JW, Scott WR** (1964) Tetrodotoxin Blockage of Sodium Conductance Increase in Lobster Giant Axons. J Gen Physiol 47(5):965-74.

39. **Narahashi T** (1974) Chemicals as tools in the study of excitable membranes. Physiol Rev 54(4):813-89.

40. **Kuromi H, Yoshihara M, Kidokoro Y** (1997) An inhibitory role of calcineurin in endocytosis of synaptic vesicles at nerve terminals of Drosophila larvae. Neurosci Res 27(2):101-13.

41. **Seamon KB, Daly JW** (1983) Forskolin, cyclic AMP and cellular physiology. Trends Pharmacol Sci 4:120-3.

42. **Zhang D, Kuromi H, Kidokoro Y** (2000) Synaptic Transmission at the Drosophila Neuromuscular Junction: Effects of Metabotropic Glutamate Receptor Activation. Slow Synaptic Responses Modul 260-5.

43. **Kuromi H, Kidokoro Y** (1999) The optically determined size of exo/endo cycling vesicle pool correlates with the quantal content at the neuromuscular junction of Drosophila larvae. J Neurosci 19(5):1557-65.

44. **Kuromi H, Kidokoro Y** (2002) Selective Replenishment of Two Vesicle Pools Depends on the Source of Ca2+ at the Drosophila Synapse. Neuron 35(2):333-43.

45. **Kay AR, Alfonso A, Alford S, Cline HT, Holgado AM, Sakmann B, Snitsarev VA, Stricker TP, Takahashi M, Wu LG** (1999) Imaging Synaptic Activity in Intact Brain and Slices with FM1-43 in C. elegans, Lamprey, and Rat. Neuron 24(4):809-17.

46. **Pyle JL, Kavalali ET, Choi S, Tsien RW** (1999) Visualization of Synaptic Activity in Hippocampal Slices with FM1-43 Enabled by Fluorescence Quenching. Neuron 24(4):803-08.

47. **Denker A, Rizzoli SO** (2010) Synaptic vesicle pools: an update. Front Synaptic Neurosci 2:135.

48. **Denker A, Kröhnert K, Rizzoli SO** (2009) Revisiting synaptic vesicle pool localization in the Drosophila neuromuscular junction. J Physiol 587(12):2919-26.

49. **Wucherpfennig T, Wilsch-Bräuninger M, González-Gaitán M** (2003) Role of Drosophila Rab5 during endosomal trafficking at the synapse and evoked neurotransmitter release. J Cell Biol 161(3):609-24.

Chapter IV

Carrier of Wingless (Cow) Regulation of *Drosophila* Neuromuscular Junction Development

This paper is published under the same title in the journal *eNeuro*, 2020.

Author Names and Affiliations:

Danielle L. Kopke[1], Shannon N. Leahy[1], Dominic J. Vita[1], Sofia C. Lima[1],

Zachary L. Newman[2] and Kendal Broadie[1]

[1]Department of Biological Sciences, Kennedy Center for Research on Human Development, Vanderbilt University, Nashville, TN 37235, USA

[2]Department of Molecular and Cell Biology, University of California, Berkeley, Berkeley, CA 94720, USA

Author Contributions:

D.L.K., S.C.L. and K.B. designed the research program; D.L.K., S.N.L., S.C.L. and D.J.V. performed the research; D.L.K., S.N.L., S.C.L., Z.L.N. and D.J.V. analyzed data. D.L.K. and K.B. wrote the manuscript, and all authors edited the manuscript.

Correspondence: kendal.broadie@vanderbilt.edu

Conflict of Interest: The authors report no conflict of interest.

Funding Sources: This work was supported by National Institutes of Health grant MH096832 to K.B. and F31MH111144 to D.L.K.

Abstract

The first Wnt signaling ligand discovered, *Drosophila* Wingless (Wg; Wnt1 in mammals), plays critical roles in neuromuscular junction (NMJ) development, regulating synaptic architecture and function. Heparan sulfate proteoglycans (HSPGs), consisting of a core protein with heparan sulfate (HS) glycosaminoglycan (GAG) chains, bind to Wg ligands to control both extracellular distribution and intercellular signaling function. *Drosophila* HSPGs previously shown to regulate Wg *trans*-synaptic signaling at the NMJ include the glypican Dally-like Protein (Dlp) and perlecan Terribly Reduced Optic Lobes (Trol). Here, we investigate synaptogenic functions of the most recently described *Drosophila* HSPG, secreted Carrier of Wingless (Cow), which directly binds Wg in the extracellular space. At the glutamatergic NMJ, we find that Cow secreted from the presynaptic motor neuron acts to limit synaptic architecture and neurotransmission strength. In c*ow* null mutants, we find increased synaptic bouton number and elevated excitatory current amplitudes, phenocopying presynaptic Wg overexpression. We show *cow* null mutants exhibit an increased number of glutamatergic synapses and increased synaptic vesicle (SV) fusion frequency based both on GCaMP imaging and electrophysiology recording. We find that membrane-tethered Wg prevents *cow* null defects in NMJ development, indicating that Cow mediates secreted Wg signaling. It was shown previously that the secreted Wg deacylase Notum restricts Wg signaling at the NMJ, and we show here that Cow and Notum work through the same pathway to limit synaptic development. We conclude Cow acts cooperatively with Notum to coordinate neuromuscular synapse structural and functional differentiation via negative regulation of Wg *trans*-synaptic signaling within the extracellular synaptomatrix.

Significance Statement

Wnt intercellular signaling is disrupted in numerous devastating neurological disorders, including Alzheimer's disease. Therefore, an understanding of Wnt signaling regulation is important for the design and implementation of targeted treatments. As a disease model, the *Drosophila* glutamatergic NMJ system is large, accessible and genetically malleable, and thus well suited for discovering the molecular and cellular mechanisms of Wnt signaling regulation. Extracellular HSPGs are important players as regulators of Wnt intercellular signaling. Here, we show secreted HSPG Carrier of Wingless (Cow), which directly binds to the founding Wnt-1 ligand, regulates NMJ structure and function. The mammalian homolog of Cow, Testican-2, is highly expressed in the brain. Studying this HSPG in *Drosophila* should inform mechanisms of Wnt regulation in human brain.

Introduction

The developing nervous system requires the coordinated action of many signaling molecules to ensure proper synapse formation and function. One key class of signals is the Wnt ligands. The first discovered Wnt, *Drosophila* Wingless (Wg), is secreted from presynaptic neurons (Packard et al., 2002) and glia (Kerr et al., 2014) at the developing glutamatergic neuromuscular junction (NMJ) to bind to the Frizzled-2 (Fz2) receptor (Bhanot et al., 1996) in both anterograde and autocrine signaling. In the postsynaptic muscle, Wg binding to Fz2 activates the non-canonical Frizzled Nuclear Import (FNI) pathway, which leads to Fz2 endocytosis and cleavage of the Fz2 C-terminus (Mathew et al., 2005). The Fz2-C fragment is trafficked to the nucleus to control translation of synaptic mRNAs and glutamate receptors (GluRs; Speese et al., 2012). In presynaptic neurons, Wg binding to Fz2 activates a divergent canonical pathway inhibiting glycogen synthase kinase 3β (GSK3β) homolog Shaggy (Sgg) to control microtubule cytoskeletal dynamics via the microtubule-associated protein 1B (MAP1B) homolog Futsch

(Miech et al., 2008), resulting in synaptic bouton growth (Franco et al., 2004; Ataman et al., 2008). The Wg signaling ligand must be tightly regulated in the synaptic extracellular space (synaptomatrix) to ensure proper NMJ development.

One critical category of proteins regulating Wg ligand in the synaptomatrix is heparan sulfate proteoglycans (HSPGs; Kamimura and Maeda, 2017). HSPGs consist of a core protein to which heparan sulfate (HS) glycosaminoglycan (GAG) chains are covalently attached. HS GAG chains are composed of repeating disaccharide subunits expressing variable sulfation patterns (the “sulfation code”; Masu, 2016). These GAG chains bind secreted extracellular ligands to regulate intercellular signaling. There are 3 HSPG families: transmembrane, GPI-anchored and secreted. The *Drosophila* genome encodes only 5 HSPGs, with 3 known to affect NMJ development; transmembrane Syndecan (Johnson et al., 2006), GPI-anchored Dally-like Protein (Dlp; Johnson et al., 2006; Dani et al., 2012), and secreted Perlecan (Kamimura et al., 2013). A second secreted HSPG recently characterized in *Drosophila* was named Carrier of Wingless (Cow; Chang and Sun, 2014). In the developing wing disc, Cow directly binds secreted Wg and promotes its extracellular transport in an HS-dependent manner. Cow shows a biphasic effect on Wg target genes. Removing Cow results in a Wg overexpression phenotype for short-range targets, and a loss-of-function phenotype for long-range targets (Chang and Sun, 2014).

The mammalian homolog of Cow, Testican-2, is highly expressed within the developing mouse brain (Vannahme et al., 1999), and inhibits neurite extension in cultured neurons (Schnepp et al., 2005), although the mechanism of action is not known. We therefore set out to characterize Cow functions at the developing *Drosophila* NMJ. We use the larval NMJ model because it is large, accessible and particularly well characterized for HSPG-dependent Wg *trans*-synaptic signaling (Sears and Broadie, 2018). Each NMJ terminal consists of a relatively stereotypical innervation pattern, with consistent axonal branching and synaptic bouton formation (Menon et al., 2013). Boutons are the functional unit of the NMJ, containing presynaptic components required for neurotransmission including glutamate-containing synaptic vesicle (SV) pools and

specialized active zone (AZ) sites for SV fusion. AZs contain Bruchpilot (Brp) scaffolds, which both cluster Ca^{2+} channels (Kittel et al., 2006) and tether SVs (Hallermann et al., 2010). AZs are directly apposed to glutamate receptor (GluR) clusters in the postsynaptic muscle membrane (Schuster et al., 1991). This spatially precise juxtaposition is critical for high-speed and efficient synaptic communication between neuron and muscle.

In this study, we sought to test Cow functions at the NMJ, with the hypothesis that Cow should facilitate extracellular Wg transport across the synapse. Structurally, *cow* null mutants display overelaborated NMJs with more boutons and more synapses, phenocopying Wg overexpression. This phenotype is replicated with targeted neuronal Cow knockdown, but not muscle Cow knockdown, consistent with Cow secretion from the presynaptic terminal. Functionally, *cow* null mutants display increased synaptic transmission strength. Both electrophysiology recording and postsynaptically targeted GCaMP imaging show increased SV fusion, indicating elevated presynaptic function. Replacing native Wg with a membrane-tethered Wg blocks secretion (Alexandre et al., 2014). Tethered Wg has little effect on NMJ development, but when combined with the *cow* null suppresses the synaptic bouton increase, indicating that Cow mediates only secreted Wg signaling. It was recently shown that Notum, a secreted Wg deacylase, also restricts Wg signaling at the NMJ (Kopke et al., 2017). We show here that combining null *cow* and *notum* heterozygous mutants causes a synergistic increase in NMJ development, indicating nonallelic noncomplementation. Moreover, combining null *cow* and *notum* homozygous mutants did not cause an increase in NMJ development compared to the single nulls, indicating an interaction within the same pathway. We conclude that Cow functions via negative regulation of Wg *trans*-synaptic signaling.

Materials & Methods

Drosophila genetics

All *Drosophila* stocks were reared on standard cornmeal/agar/molasses food at 25°C in a 12-hour light/dark cycling incubator. Mixed sexes were used for all experiments except the SynapGCaMP imaging (females only). The genetic background control was w^{1118}. The $cow^{5\Delta}$ mutant, *UAS-cow-miRNA-1* (referred to as *UAS-cow-RNAi*) *and UAS-SP-eGFP-cow* (referred to as *UAS-Cow::eGFP*) lines (Chang and Sun, 2014) were obtained from Yi Henry Sun (Institute of Molecular Biology, Academia Sinica, Taipei, Taiwan). The cow^{GDP} #03259 (y[1] w[*]; Mi{y[+mDint2]=MIC}Cow[MI03259]/TM3, Sb[1] Ser[1]) and cow^{GDP} #12802 (y[1] w[*]; Mi{y[+mDint2]=MIC}Cow[MI12802]) mutants, and the *cow* Df #6193 (w[1118]; Df(3R)Exel6193, P{w[+mC]=XP-U}Exel6193/TM6B, Tb[1]) and *cow* Df #619 (w[1118]; Df(3R)BSC619/TM6C, cu[1] Sb[1]) deficiencies were all obtained from the Bloomington *Drosophila* Stock Center (stock numbers 40757, 58669, 7672 and 25694, respectively; Indiana University, Bloomington, IN, USA). Cow-Gal4 was obtained from the Vienna Tile (VT) collection of the Vienna *Drosophila* Resource Center (VT046086). Neuronal *vesicular glutamate transporter* (*vglut)-Gal4* and muscle-specific *24B-Gal4* driver lines were obtained from the Bloomington *Drosophila* Stock Center. The *MHC-CD8-GCaMP6f-Sh* Ca^{2+} reporter (SynapGCaMP6f; Newman et al., 2017) was obtained from Ehud Isacoff (University of California, Berkeley, CA, USA). Control *wg{KO; FRT Wg FRT QF; pax-Cherry}* and membrane-tethered *wg{KO; FRT NRT-Wg FRT QF; pax-Cherry}* (Alexandre et al., 2014) were obtained with permission from Andrea Page-McCaw (Department of Cell and Developmental Biology, Vanderbilt University, TN, USA). Null $notum^{KO}$ *(4)(w+)* (Kakugawa et al., 2015) was obtained from Jean-Paul Vincent (Francis Crick Institute, London, UK).

PCR/RT-PCR studies

Staged *Drosophila* eggs were dechorionated using bleach for 30 secs, washed with dH_20 3X, and embryos genotyped by GFP marker with an epifluorescent microscope. 5 embryos per genotype were homogenized in 10µl Gloor and Engels DNA extraction buffer (10 mM Tris HCL pH 8.2, 1 mM EDTA pH 8.0, 25 mM NaCl and 200 µg/mL Proteinase K) with a glass rod in an Eppendorf tube, and the homogenate incubated at 37°C for 30 mins, and then 95°C for 2 mins. For each PCR reaction, ~10ng of DNA was used with the following primers: forward 5'-GCAACATTCTGGCTTCGTGTCATGC-3' and reverse 5'-CTCTCGACTTGCAAATAGCAGACGATGATC-3' for the *cow* gene (product size 1927); forward 5'-GTGGAAAAGCGGTTGAAATAGGG-3' and reverse 5'-GTCCACATCCACAAAGATGCC-3' for the *dfmr1* gene control (product size 3850). For the RT-PCR studies, 1 embryo per genotype was used with The RNeasy Micro Kit (Qiagen, 74004) to extract RNA. The OneStep RT-PCR Kit (Qiagen, 210212) was used. For each reaction, ~7ng of RNA was used with the following primers: forward 5'-AGAACAGCAACTTGAATGCCTATC-3' and reverse 5'-CGAAGCATCTGCACCATTCC-3' for the *cow* gene (product size 348); forward 5'-TAAACTGCGAGAGGTTTTCC-3' and reverse 5'- ATTCGATGAGTGTACGCTG-3' for the *dmgalectin* gene control (product size 321). Products were loaded on a 0.8% agarose gel in TAE buffer with purple gel loading dye (NEB, B7025S) and SYBR safe DNA gel stain (ThermoFisher, S33102), and run at 100V for 30 mins.

Cow antibodies

We used a well-characterized, published anti-Cow antibody (Chang and Sun, 2014). New rabbit anti-Cow antibodies were also made by ABclonal (Woburn, MA) against amino acids 36-236. Three antiserums were recovered and affinity purified (29, 30, 31). Cow antibody 31 was pre-

absorbed against *cow* nulls (*cow*^{GDP}) for imaging studies. Cow antibody 31 was used for Figures 1, 2 and 4.

Western blotting

Staged *Drosophila* eggs (18-24 hour post-fertilization (hpf) for maximum expression; www.fruitfly.org) were dechorionated using bleach for 30 secs, washed with dH_20 3X, and embryos genotyped by GFP marker with an epifluorescent microscope. 25 embryos were placed into an Eppendorf tube with 24µl RIPA buffer (150 mM sodium chloride, 1% Triton X-100, 0.5% sodium deoxycholate, 0.1% sodium dodecyl sulfate, 50 mM Tris) and protease inhibitor cocktail (Sigma, P8340), then immediately snap-frozen in a dry ice ethanol bath. Samples were sonicated (Branson Sonifier 250, settings: 90% duty, output 2) for 20 secs, vortexed (Standard Mini Vortexer, VMR Scientific Products, speed 4) for 5 secs, and then centrifuged at 14000 RPM for 10 mins. The supernatant was then transferred to new tubes with 1X NuPage LDS buffer (Invitrogen, NP007) and 5% 2-mercaptoethanol (Sigma, M7154), then vortexed as above. Samples were incubated at RT for 20 mins, heated at 100°C for 10 mins, then centrifuged as above. Equal volumes of lysate were loaded into precast NuPage 4-12% Bis-Tris gels (Invitrogen, NP0336) with NuPage running buffer (Life Technologies, NP002) and NuPage antioxidant (Invitrogen, NP0005). Electrophoresis was done at 150 V for 2 hrs. Protein was then transferred overnight at 4°C with constant 30 mA current to nitrocellulose membranes (PROTRAN, NBA085C001EA) in the NuPage transfer buffer (Life Technologies, NP0006-1) supplemented with 20% methanol (Honeywell, AH230-4). Following transfer, membranes were rinsed with dH_20, air dried at RT for 1 hr, and then blocked with 2% non-fat powdered milk in TBS-T (0.1% Tween-20, 150 mM sodium chloride, 5mM potassium chloride, 25 mM Tris, pH 7.6) at RT for 1 hr with rotation. Primary antibodies were incubated overnight in 2% milk in TBST. Membranes were then washed in TBST (5x6 mins), followed by incubation in secondary antibody at RT in 2% milk in

TBST for 1 hr with rotation, and washed again as before. Imaging was performed on a LI-COR Odyssey Imager with analysis on Image Studio Lite (LI-COR Biosciences). Total protein was assessed via the REVERT total protein stain (LI-COR, 926-11011). Primary antibodies: rabbit anti-Cow (this study, Ab 31) and goat anti-GFP (Abcam, ab6662), both at 1:1,000. Secondary antibodies: IRDye 680 donkey anti-rabbit (LI-COR, 926-68073) and IRDye 800 donkey anti-goat (LI-COR, 926-32214), both at 1:10,000.

Confocal imaging

Wandering third instars were dissected in physiological solution containing (in mM): 128 NaCl, 2 KCl, 0.2 $CaCl_2$, 4 $MgCl_2$, 70 sucrose, 5 HEPES {2-[4-(2-hydroxyethyl)piperazin-1-yl]ethanesulfonic acid} at pH 7.2. The samples were fixed with 4% paraformaldehyde (EMS; 15714) diluted in PBS (Corning; 46-013-CM). For intracellular labeling, samples were permeabilized with 0.2% Triton X-100 (Fisher Scientific; BP151-100) 3X for 10 mins each). Embryos were bleached for de-chorionation, fixed with heptane and paraformaldehyde, and de-vitillinized with methanol. Primary antibodies: mouse anti-DLG (4F3; 1:250), mouse anti-Wg (4D4; 1:1) and mouse anti-Brp (nc82; 1:200), all from the Developmental Studies Hybridoma Bank (DSHB); Alexa Fluor 488-conjugated goat anti-HRP (123-545-021; 1:250), Cy3-conjugated goat anti-HRP (123-165-021; 1:250), and Alexa Fluor 647-conjugated goat anti-HRP (123-605-021; 1:250), all from Jackson ImmunoResearch; rabbit anti-GluRIIC (Marrus et al., 2004; 1:5,000) and rabbit anti-GFP (abcam, ab290; 1:1,500). Preparations were incubated with primary antibodies overnight at 4°C and secondary antibodies at RT for 2 hrs, washed 3X for 10 mins each, and then mounted in Fluoromount-G (EMS, 17984-25) onto 25x75x1mm slides (Fisher Scientific, 12-544-2) with a 22x22-1 coverslip (Fisher Scientific, 12-542-B) and sealed with clear nail polish (Sally Hansen). Imaging was performed on a Zeiss LSM 510 META laser-scanning confocal microscope, with images projected in Zen (Zeiss) and analyzed using ImageJ (NIH). NMJ intensity

measurements were made with HRP signal delineated Z-stack areas of maximum projection using ImageJ threshold and wand-tracing tools.

TEVC electrophysiology

Wandering third instars were dissected longitudinally along the dorsal midline, internal organs removed, and body walls glued down (Vetbond, 3M). Peripheral motor nerves were cut at the base of the ventral nerve cord (VNC). Dissections and two-electrode voltage-clamp (TEVC) recordings were both carried out at 18°C in physiological saline (in mM): 128 NaCl, 2 KCl, 4 MgCl2, 1.5 CaCl2, 70 sucrose and 5 HEPES; pH 7.2. Preparations were imaged employing a Zeiss Axioskop microscope with a Zeiss 40X water-immersion objective. Muscle 6 in abdominal segments 3-4 was impaled with two intracellular electrodes (1-mm outer diameter borosilicate capillaries; World Precision Instruments, 1B100F-4) of ~15 MΩ resistance filled with 3 M KCl. The muscles were clamped at −60 mV using an Axoclamp-2B amplifier (Axon Instruments). Spontaneous mEJC recordings were made in continuous 2 min sessions and low-pass filtered. For EJC records, the motor nerve was stimulated with a fire-polished suction electrode using 0.5 ms suprathreshold voltage stimuli at 0.2 Hz from a Grass S88 stimulator. Nerve stimulation-evoked EJC recordings were filtered at 2 kHz. To quantify EJC amplitude, 10 consecutive traces were averaged and the average peak value recorded. Clampex 9.0 was used for data acquisition, and Clampfit 9 was used for data analysis (Axon Instruments).

SynapGCaMP imaging

For SynapGCaMP quantal imaging experiments, wandering third instars were dissected and type 1b NMJs imaged in physiological saline (in mM): 70 NaCl, 5 KCl, 1.5 $CaCl_2$, 25 $MgCl_2$, 10 $NaHCO_3$, 5 trehalose, 115 sucrose, 5 HEPES; pH 7.2. Fluorescence images were acquired with a Vivo Spinning Disk Confocal microscope (3i Intelligent Imaging Innovations, Denver, CO), with

a 63X 1.0NA water immersion objective (Zeiss), LaserStack 488nm (50 mW) laser, Yokogawa CSU-X1 A1 spinning disk (Tokyo, Japan), and EMCCD camera (Photometrics Evolve, Tucson, AZ). Image capture and analysis was performed as reported previously (Newman et al., 2017). Briefly, spontaneous events were imaged at 20 Hz (50 ms exposures; streaming capture mode) for 30 secs. Movies were then filtered, registered, and bleach-corrected prior to ΔF conversion. Using the Delta ΔF data, a XYT local maxima algorithm was applied to the thresholded ΔF data to identify where and when quantal release events occur (Newman et al., 2017). Quantal coordinates were used to calculate ΔF/F amplitudes and frequencies (normalized to the baseline SynapGCaMP6f 2D area).

Structured illumination microscopy

Dissected wandering third instar preparations were imaged using a Nikon N-SIM in 3D SIM mode, configured with a 100x EX V-R diffraction grating, automated TiE inverted fluorescence microscope stand, 100x SR Apo 1.49 NA objective, Andor DU-897 EM-CCD, and 488/561nm lasers. Image acquisition was managed through NIS-Elements (Nikon Instruments, Inc.), and stacks were acquired with a 0.12um step size. Stack reconstruction of the raw data was used prior to rendering and analysis. To acquire larger fields-of-view and capture whole NMJs, SIM images were stitched together using the automated tiling method within NIS-Elements software.

LSM image analysis

We used Imaris Version 9.3.0 to quantify LSM images using the “surfaces” function to identify the number and volume of Brp punctae:

1. Open image file and click “add new surfaces” to start the wizard.
2. Algorithm settings click “segment only a region of interest”.
3. Select region of interest (ROI) in X, Y and Z.
4. Select “source channel” and thresholding conditions.

5. Adjust threshold until all spots are selected.
6. Enable “split touching objects” with seed points diameter (0.4 µm).
7. Use “quality filter” to adjust selections with minimal background.
8. Click “finish” to execute all creation steps and exit the wizard.
9. Click “edit” tab and delete extraneous spots by hand.
10. Click “statistics” tab and export values to Microsoft Excel.

SIM image analysis

We used Imaris Version 9.3.0 to quantify SIM images using the “spots” function to identify the number of Brp punctae and GluR clusters:

1. Open image file and click “add new spots” to start the wizard.
2. Algorithm settings click “segment only a region of interest” with “different spot sizes (region growing)”.
3. Select region of Interest (ROI) in X, Y and Z.
4. Select “source channel” and click “background subtraction”.
5. Classify spots with a “quality” filter type and adjust by eye.
6. Spot regions click “local contrast”.
7. Region threshold with diameter from “region volume”.
8. Click “finish” to execute all creation steps and exit the wizard.
9. Click “edit” tab and delete extraneous spots by hand.
10. Click “statistics” tab and export values to Microsoft Excel.

Statistical analyses

All statistical measurements were performed within GraphPad Prism (Version 7.04 for Windows). The D’Agostino-Pearson K-squared normality test was done on all datasets to check for normality.

For comparisons of 2 genotypes, a t-test (normally distributed) or Mann-Whitney test (not normally distributed) was done. For all other comparisons of >2 genotypes, an ordinary one-way ANOVA (normally distributed) or Kruskal-Wallis test (not normally distributed) was done. All graphs were made in Prism and the data are represented in scatter plots with the mean ± standard error of the mean (SEM).

Results

Carrier of Wingless (Cow) genetic locus, mutants and expression profiles

The *cow* gene encodes 3 transcripts (*cow*-RC, -RD, -RE), with *cow*-RD containing a long 3'-UTR (Fig. 19A). We acquired a reported *cow* null mutant ($cow^{5\Delta}$; Chang and Sun, 2014), two mutations from the Gene Disruption Project (cow^{GDP} 03259 and 12802; Bellen et al., 2004; Nagarkar-Jaiswal et al., 2015) and two *cow* deficiencies from the Bloomington *Drosophila* Stock Center (Df[619] and Df[6193]). The $cow^{5\Delta}$ mutant has a 9,119 bp deletion starting in the 3' UTR that does not remove *cow* coding sequence, but published as a well-characterized protein null (Chang and Sun, 2014). The cow^{GDP} lines are minos mediated integration cassette (Mi{MIC}) insertions; 03259 in *cow* intron 1, and 12802 in *cow* intron 4. Df[619] completely removes *cow* and 31 other genes, while *cow* Df[6193] removes *cow* and 41 other genes. PCR tests were done using primers in the $cow^{5\Delta}$ deletion region (Fig. 19A). As expected, there are no PCR products from $cow^{5\Delta}$ or either *cow* Df (Fig.19B). Next, RT-PCR tests were done using primers spanning an exon-exon junction to ensure mRNA amplification (Fig. 19A). The RNA extraction was confirmed using primers for a control gene (*dfmr1*; Fig. 19C). The *cow* transcript in the genetic background control w^{1118} is present at similar levels in the $cow^{5\Delta}$ line (Fig. 19D). There is no detectable *cow* transcript in either of the *cow* Dfs, or in one of the cow^{gdp} lines (03259), and only a very faint product in the other cow^{gdp} line (12802; Fig. 19D). Thus, cow^{gdp} 03259 is an RNA null allele.

The published *cow*$^{5\Delta}$ mutation has been reported to have similar transcript levels to wildtype, but to have no detectable Cow protein expression (Chang and Sun, 2014). We therefore next examined protein levels via Western blotting using the published, well characterized Cow antibody (Chang and Sun, 2014), as well as 3 new antibodies made for this study (see Methods). Cow protein has a predicted molecular weight of ~75 kDa (without HS chains) and ~100 kDA (with HS chains). The 2 Cow protein bands are clearly present in the *w*^{1118} controls and absent in both *cow* deficiency lines (Fig. 19E). Cow protein is also undetectable in the *cow*^{gdp} lines, even at heightened levels of protein loading (Fig. 19E). In stark contrast to previously published work (Chang and Sun, 2014), both Cow protein bands are present at normal levels in *cow*$^{5\Delta}$ mutants (Fig. 19E, arrows). In our studies, *cow*$^{5\Delta}$ mutants typically die as early stage larvae, and the few escapers can be raised to the third instar only with constant care. In contrast, both *cow*^{gdp} protein nulls are fully adult viable, both as homozygotes and as heterozygotes over Df[619]. Thus, our evidence indicates *cow*$^{5\Delta}$ does not affect Cow expression, but has a second site larval lethal mutation. Further, the Cow protein is not required for full adult viability. For the remainder of experiments, *cow*^{gdp} 03259 and *cow* Df[619] were used, as both show complete removal of Cow RNA and protein.

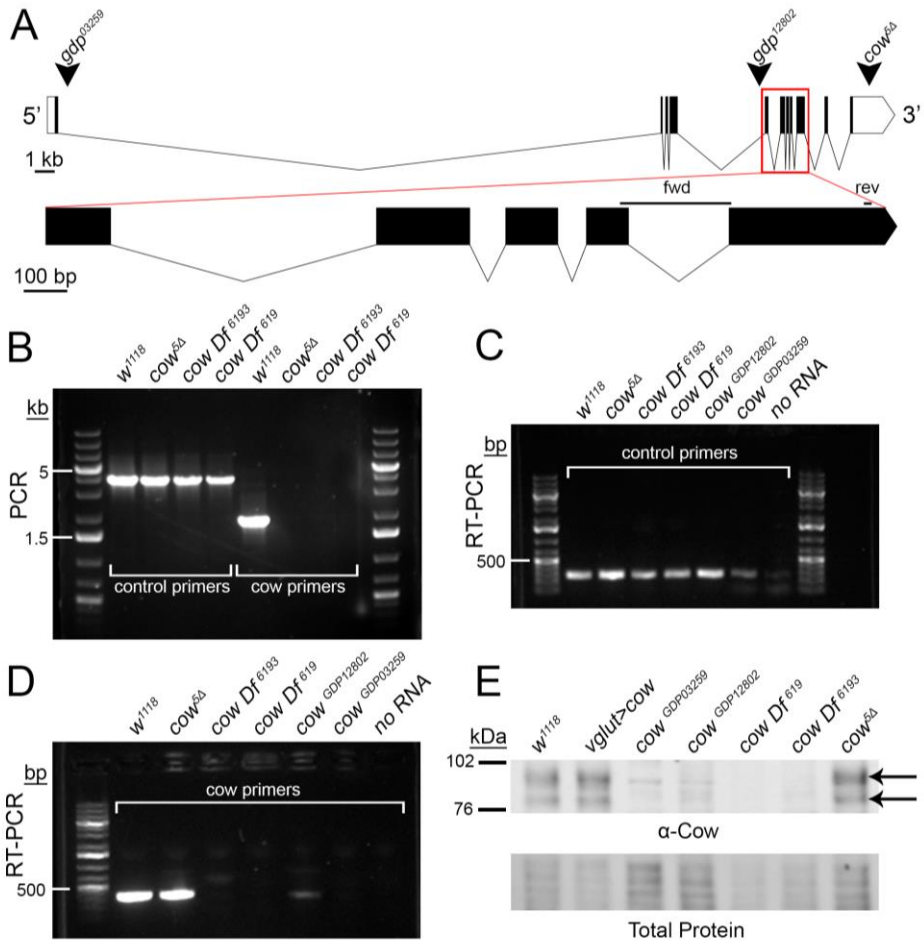

Fig. 19: Carrier of Wingless (Cow) genetic locus and mutant characterization

(A) Intron/exon structure of the *cow* gene (transcript *cow-RD*; flybase.org). Arrowheads indicate gene disruption project (gdp) inserts in two different lines (03259 and 12802). The third arrowhead indicates where the published *cow*$^{5\Delta}$ deletion begins in the 3' UTR and runs 9,119 bp downstream (Chang and Sun, 2014). Below, the expanded region outlined with the red box is labeled "fwd" and "rev" to depict the RT-PCR primer pair. (B) PCR products from the genotypes listed. Control (*dfmr1* gene) and *cow* primers from the region of the *cow*$^{5\Delta}$ deletion. (C,D) RT-PCR products from the genotypes listed using both control (*dmgalectin* gene) and *cow* primers. (E) Western blot of the indicated genotypes using an anti-Cow antibody, with the total protein stain shown below. The two arrows indicate Cow protein with and without GAG chains.

To assess Cow protein expression in controls and null mutants, we performed anti-Cow labeling and Cow-Gal4 to drive UAS-Cow::eGFP (Fig. 20). In control embryos, Cow is widely expressed, including localization in the ventral nerve cord (VNC; Fig. 20A). In *cow* null mutants (cow^{GDP}/cow^{GDP}), antibody labeling is undetectable (Fig. 20A, right). Since Cow has a signal peptide, and has been previously established to be secreted (Chang and Sun, 2014), we tested Cow expression at the NMJ using antibody labeling with non-permeabilizing conditions. In the w^{1118} control wandering third instar NMJ, Cow appears secreted from a dynamic subset of type 1b synaptic boutons (Fig. 20B, arrows). Cow is also present in a punctate pattern along the peripheral nerve bundle (arrowhead). In *cow* nulls, neuronal and synaptic antibody labeling is lost (Fig. 20B, right). Within NMJ synaptic boutons co-labeled for both Cow and Wingless (Wg) antibody, the two secreted proteins have overlapping expression patterns, colocalizing in the extracellular synaptomatrix surrounding the same boutons (Fig. 20C). Using Cow-Gal4 to drive a UAS-Cow::eGFP, GFP is present throughout the wandering third instar wing imaginal disc, including punctae surrounding the wing pouch (Fig. 20D, left). Cow::eGFP is also present at the NMJ, in punctae within and surrounding the synaptic boutons within a single confocal slice (Fig. 20D, right). Overall, Cow is expressed in both neuronal and non-neuronal tissue in embryos, larvae and imaginal discs, and co-localizes with Wg in the NMJ.

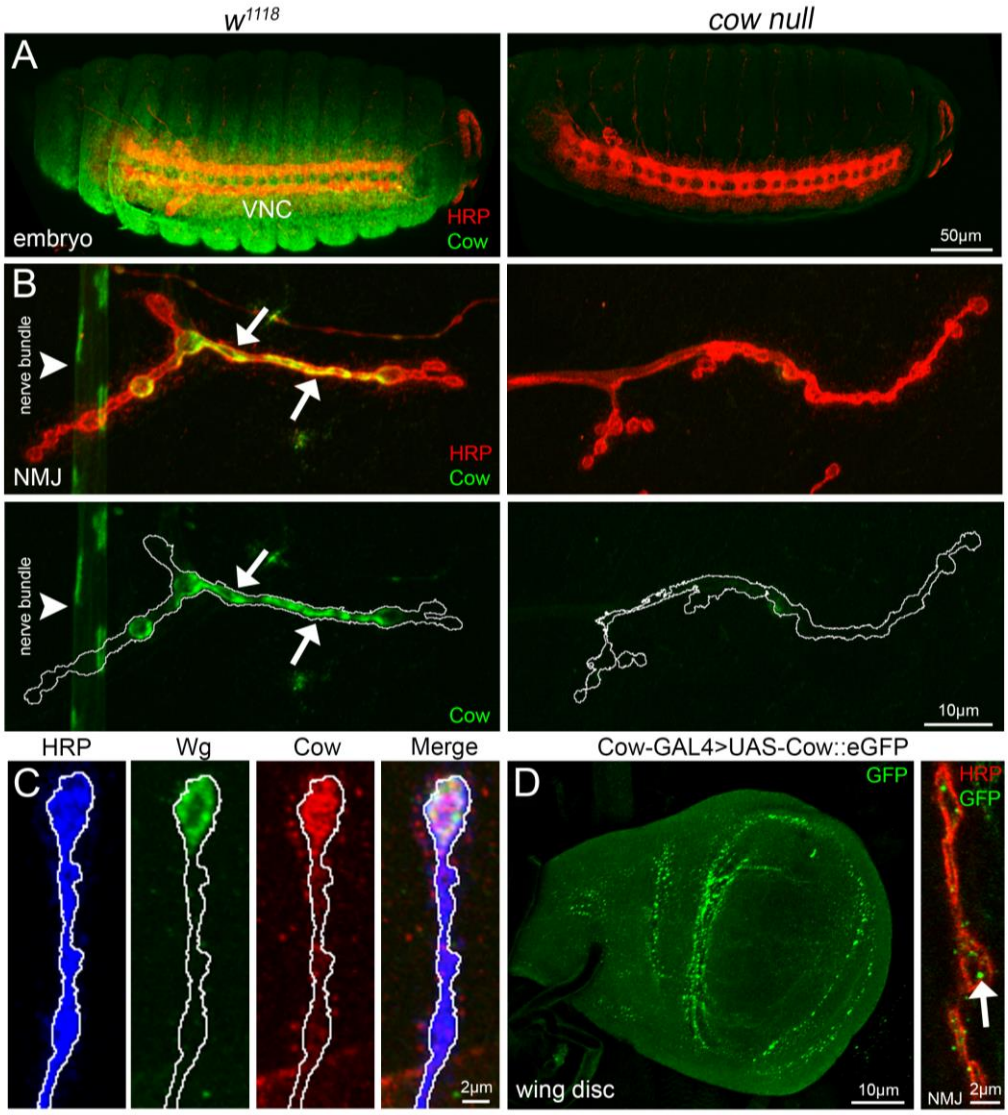

Fig. 20: Cow expression in embryos, larval NMJ synaptic terminal and wing disc

(A) Confocal images of stage 16 embryos co-labeled with anti-horseradish peroxidase (HRP, red) to mark neuronal membranes and anti-Cow (green) in genetic background control (w^{1118}, left) and *cow* null (cow^{GDP}/cow^{GDP}, right). The ventral nerve cord (VNC) is labeled. (B) Confocal images of third instar NMJ co-labeled with anti-HRP (red) and anti-Cow (green) in control (w^{1118}, left) and *cow* null (cow^{GDP}/cow^{GDP}, right). From non-permeabilized labeling, Cow appears secreted from a dynamic subset of synaptic boutons (arrows) and also present in the nerve bundle (arrowhead). Cow is shown without HRP in below images. White line marks the NMJ terminal HRP domain. (C) Higher magnification images of w^{1118} NMJ synaptic boutons co-labeled with anti-HRP (blue), anti-Wingless (Wg, green) and anti-Cow (red), with merged image on right. White line marks the NMJ terminal HRP domain. (D) Cow-GAL4 driving UAS-Cow::eGFP in wandering third instar wing imaginal disc (left) and NMJ co-labeled with anti-HRP (red) and anti-GFP (green, right). For the NMJ, a single confocal section (0.5 µm) shows Cow punctae (arrow) within and surrounding synaptic boutons.

Presynaptic Cow restricts NMJ growth and synaptic bouton formation

Wg *trans*-synaptic signaling regulates NMJ growth and synaptic bouton formation (Packard et al., 2002), thus we hypothesized that if Cow regulates Wg at the NMJ, Cow loss should affect the NMJ architecture. Each NMJ terminal consists of a relatively stereotypical muscle innervation pattern, with a consistent number of axon branches and large synaptic boutons (Menon et al., 2013). Wg signaling bidirectionally regulates synaptic development, with *Wg* knockdown decreasing NMJ synaptic bouton number and *Wg* overexpression (OE) increasing boutons (Packard et al., 2002; Kopke et al., 2017), including an increase in satellite boutons (small boutons connected to the mature (parent) bouton or adjacent axon; Torroja et al., 1999; Gatto and Broadie, 2008). To test Cow requirements in synaptic architectural development, we labeled the wandering third instar NMJ. Anti-horseradish peroxidase (HRP) was used to label the NMJ terminal by binding to extracellular fucosylated N-glycans associated with the presynaptic neural membrane (Jan and Jan, 1982; Parkinson et al., 2013). Anti-Discs Large (DLG) was used to label the postsynaptic scaffold in the subsynaptic reticulum (Lahey et al., 1994; Parnas et al., 2001). We used cow^{GDP}/Df (referred to as *cow* null) to eliminate *cow* globally, and characterized *cow* RNAi lines (Chang and Sun, 2014) for both motor neuron (*vglut*-Gal4) and muscle (*24B*-Gal4) cell-targeted knockdown studies. Sample images and the summary of results are shown in Figure 21.

Cow restrains NMJ development, specifically restricting synaptic bouton formation. When Cow is knocked out completely, there is a clear increase in boutons (Fig. 21A, left). In quantified measurements, *cow* nulls show a very significant increase in synaptic bouton number (w^{1118} 25.53±1.37 vs. cow^{GDP}/Df 41.13±1.6*;* $p<0.0001$; Fig. 21A, right). With targeted *cow* knockdown in presynaptic motor neurons (*vglut*-Gal4>*cow-RNAi)*, there is the same increase in NMJ bouton formation (Fig. 21B), indicating Cow originates from the neuron. Interestingly, presynaptic Cow knockdown also increases the number of satellite boutons; (Fig. 21B; inset). Presynaptic *cow* knockdown causes very significantly elevated mature bouton numbers (*vglut*-Gal4/+ 26.69±1.49

vs. *vglut>cow-RNAi* 37.38±1.75; p=0.0002) as well as an increased percentage of satellite boutons (*vglut*-Gal4/+ 2.9±0.89% vs. *vglut>cow-RNAi* 5.77±1.86; p=0.061; Fig. 21B, right). Conversely, postsynaptic *cow* knockdown (*24B*-Gal4>*cow-RNAi*) causes no discernable differences from the controls (Fig. 21C, right). Mature and satellite bouton quantifications demonstrate no effect of removing Cow from the muscle (mature; *24B/+* 30.63±1.73 vs. *24B>cow-RNAi* 28.06±1.04; p>0.9999; Fig. 21C, right). Taken together, these results show Cow originating from the presynaptic motor neuron restricts the formation of NMJ synaptic boutons.

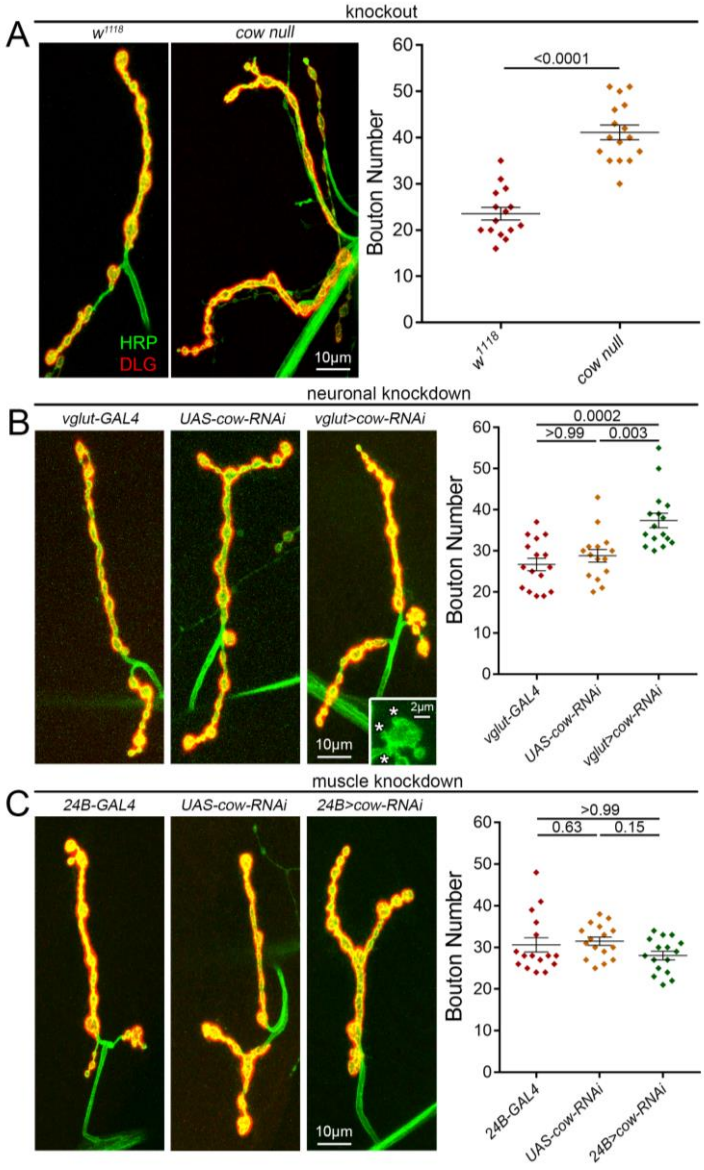

Fig. 21: Presynaptically secreted Cow limits NMJ synaptic bouton number

(A) Confocal images of the muscle 4 NMJ co-labeled with anti-horseradish peroxidase (HRP, green) to mark the presynaptic membrane and anti-Discs Large (DLG, red) to mark the postsynaptic domain in the genetic background control (w^{1118}, left) and the *cow* null mutant (cow^{GDP}/Df, right). Synaptic bouton number is shown in a scatter plot, with mean ± SEM. (B) Representative confocal NMJ images of motor neuron-targeted Gal4 driver control (*vglut*-Gal4/+, left), UAS-RNAi transgene control (UAS-*cow*-RNAi/+, middle) and *cow* RNAi knockdown (vglut>*cow*-RNAi, right). Satellite boutons (asterisks) are shown in the inset. Right: synaptic bouton number is shown in a scatter plot, with mean ± SEM. (C) Representative confocal NMJ images of muscle-targeted Gal4 driver control (24B-Gal4/+, left), UAS-RNAi transgene control (UAS-*cow*-RNAi/+, middle) and *cow* RNAi knockdown (24B>*cow*-RNAi, right). Synaptic bouton number is quantified to the right. P-values are shown for each statistical comparison.

When Cow is overexpressed (OE) in motor neurons (*vglut*-Gal4>*UAS-Cow*), Cow is elevated at the NMJ with a concomitant decrease in extracellular Wg ligand (Fig. 22A). The NMJs have a typical number of mature boutons, but an increase in satellite boutons (Fig. 22B). Interestingly, *cow* neuronal OE causes HRP redistribution with distinct spots of accumulation (Fig. 22B, heatmap on right). Quantification shows a significant increase in Cow levels secreted at the NMJ terminal (normalized *vglut*-Gal4/+ 1.0±0.06 vs. *vglut>cow* 3.04±0.06*;* p<0.0001), with a significant decrease in extracellular Wg levels (*vglut*-Gal4/+ 1.0±0.08 vs. *vglut>cow* 0.67+0.06*;* p=0.001; Fig. 22C). Quantification shows no change in bouton number (*vglut*-Gal4/+ 25.25±0.81 vs. *vglut>Cow* 27.06±1.4; P=0.27), but a significant increase in satellite boutons (*vglut*-Gal4/+ 2.33±0.94% vs. *vglut>cow* 7.12±0.67; p=0.0003; Fig. 22D). Whereas neuronal *cow* OE elevates normal Cow expression at the NMJ, muscle *cow* OE causes aberrant, ectopic expression (normalized *24B*-Gal4/+ 1.0±0.03 vs. *24B>cow* 3.91±0.23; p<0.0001), which increases Wg ligand (*24B*-Gal4/+ 1.0±0.07 vs. *24B>Cow* 1.52±0.14*;* p=0.003). Muscle targeted *cow* OE causes no change in mature boutons (*24B*-Gal4/+ 30.38±1.94 vs. *24B>cow* 29.81±1.46*;* P=0.82) or the percentage of satellite boutons (*24B*-Gal4/+ 3.16±1.16% vs. *24B>cow* 5.48±1.58; P=0.2486). We next assayed synaptic functional differentiation to test if these structural changes have functional consequences.

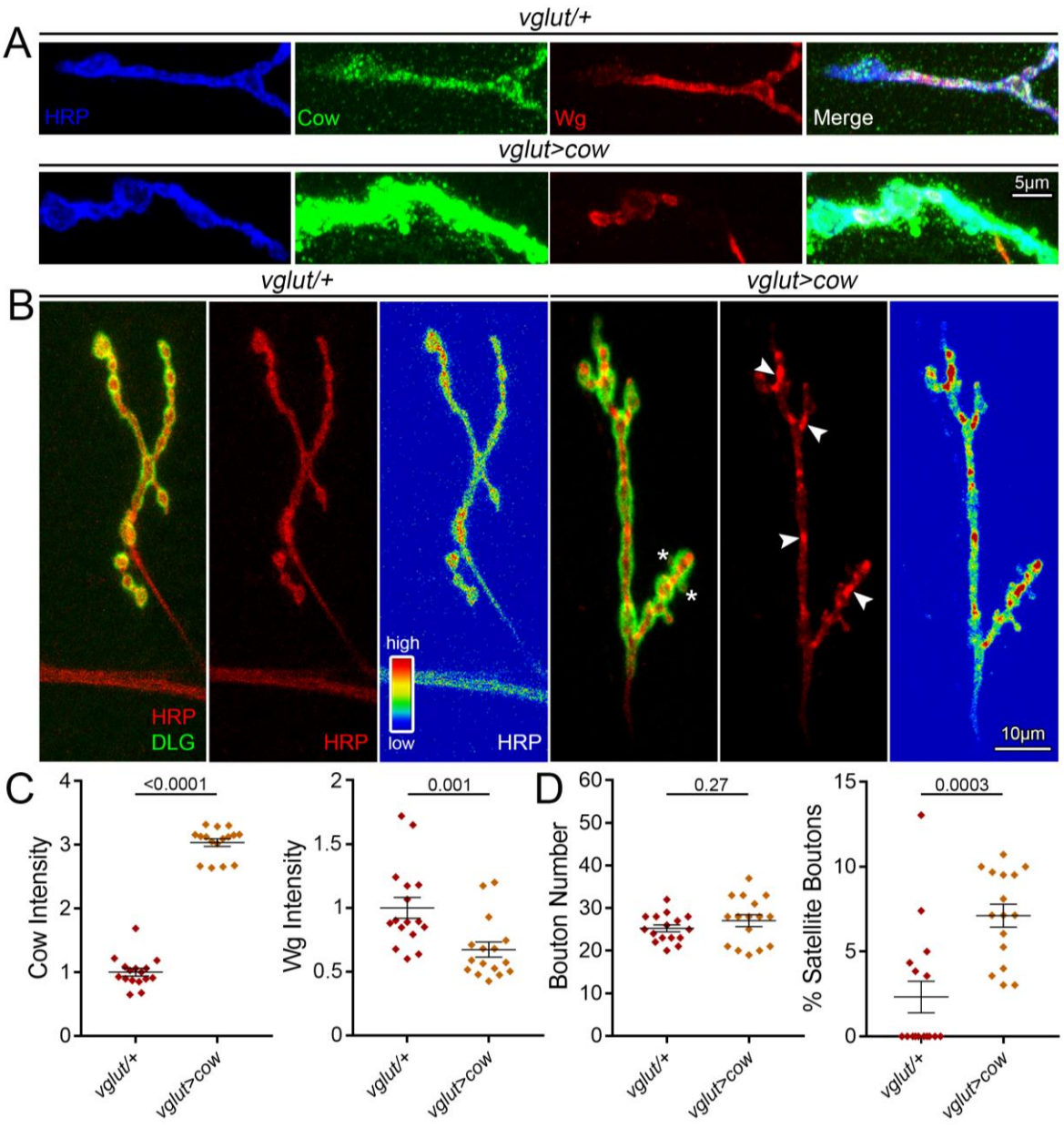

Fig. 22: Presynaptic Cow elevation decreases Wg and increases satellite boutons

(A) Confocal images of NMJ boutons triple-labeled with anti-HRP (blue), -Cow (green) and -Wg (red), and merged (far right) comparing transgenic controls (*vglut-Gal4*/+) to motor neuron Cow overexpression condition (*vglut>cow*). Labeling done in the absence of detergent to reveal only secreted Cow and Wg. (B) Representative muscle 4 NMJ images co-labeled for presynaptic HRP (red) and postsynaptic DLG (green) comparing controls (*vglut-Gal4*/+) to neuronal Cow overexpression (*vglut>cow*). Asterisks indicate satellite boutons. The second panel shows HRP alone with arrows indicating distinct spots of HRP accumulation and the third panel shows HRP expression heatmap. (C) Quantification of confocal fluorescence intensity for Cow (left) and Wg (right) in the two conditions. (D) Quantification of synaptic bouton number (left) and the percentage of satellite boutons (right) in transgenic controls vs. *cow* neuronal overexpression. P-values are shown for each statistical comparison.

Cow restricts presynaptic vesicle fusion and neurotransmission strength

We utilized two methods to assay NMJ synaptic functional differentiation and neurotransmission strength: 1) two-electrode voltage-clamp (TEVC) electrophysiology (Dani et al., 2012; Parkinson et al., 2013; Kopke et al., 2017), and 2) imaging genetically encoded calcium reporter SynapGCaMP6f (Newman et al., 2017). For assaying evoked transmission, muscle 6 was clamped (-60 mV) while the motor nerve was stimulated with a suction electrode (1.5 mM [Ca^{2+}]). Excitatory junction current (EJC) traces were recorded (0.2 Hz, 10 consecutive stimuli) to measure the average amplitude. For assaying miniature EJC (mEJC) events, spontaneous synaptic vesicle fusions were recorded, measuring frequency and amplitude. The mEJC frequency indicates presynaptic vesicular release (number of active synapses, fusion probability), and mEJC amplitude indicates number of activated postsynaptic receptors. For quantal imaging, the SynapGCaMP reporter (*MHC-CD8-GCaMP6f-Sh*) contains a myosin heavy chain (MHC) promoter for muscle targeting, CD8 transmembrane domain for membrane targeting, and Shaker (Sh) K^+ channel C-terminal tail for postsynaptic targeting (Newman et al., 2017). By imaging transmission, we are able to specifically determine the changes in quantal activity at the convergent motor neuron inputs separately. Live imaging recordings were made of the SynapGCaMP reporter at muscle 4, with spontaneous event frequency divided by the NMJ synaptic area, and event amplitude measured as the change in the fluorescence signal over the baseline NMJ fluorescence ($\Delta F/F_0$). Representative recordings and summarized data are shown in Figure 23.

With nerve stimulation, evoked transmission is clearly and consistently increased in *cow* nulls compared to w^{1118} controls (Fig. 23A). Quantified measurements show EJC amplitude significantly elevated (w^{1118} 175.4 ±9.93 nA vs. cow^{GDP} 214.6±12.24; p=0.023; w^{1118} 175.4±9.93 vs. cow^{GDP}/Df 254.2±14.99; p=0.012; Fig. 23B). Although the cow^{GDP}/Df mutants show a slight increase in mEJC frequency, no change was observed in the cow^{GDP} nulls. We found no change

in amplitude (Fig. 23C). In quantified measurements, mEJC frequency is slightly increased in homozygous mutants and more increased in the cow^{GDP}/Df (w^{1118} 1.396±0.19 Hz vs. cow^{GDP}/cow^{GDP} 1.764±0.23; p=0.58; w^{1118} 1.396±0.19 vs. cow^{GDP}/Df 2.41±0.49; p=0.05; Fig. 23D, left). There is no significant change in mEJC amplitude (w^{1118} 0.75±0.03 nA vs. cow^{GDP}/cow^{GDP} 0.87±0.06; p=0.189; w^{1118} 0.75±0.03 nA vs. cow^{GDP}/Df 0.72±0.05; p=0.886; Fig. 23D, right). Neuronally-targeted *cow*-RNAi causes an increase in mEJC frequency (*vglut*-Gal4/+ 1.5±0.33 Hz vs. *vglut>Cow-RNAi* 2.45±0.3; p=0.045), but not amplitude (*vglut*-Gal4/+ 0.8±0.03 nA vs. *vglut>Cow-RNAi* 0.85±0.42; p=0.4325). SynapGCaMP imaging also shows increased fusion frequency in type Ib boutons (Fig. 23E). In quantal imaging measurements, spontaneous fusion frequency increases (*vglut*-Gal4/+ 1.62±0.47 Hz/µm^2 vs. *vglut>cow-RNAi* 2.98±0.36; p=0.051; Fig. 23F, left). Interestingly, event magnitude also significantly increases (*vglut*-Gal4/+ 0.79±0.04 $\Delta F/F_0$ vs. *vglut>cow-RNAi* 1.06±0.09; p=0.012; Fig. 23F, right). These results demonstrate that Cow limits evoked neurotransmission strength and suggest that neuronally secreted Cow regulates synaptic vesicle fusion at the presynaptic active zone.

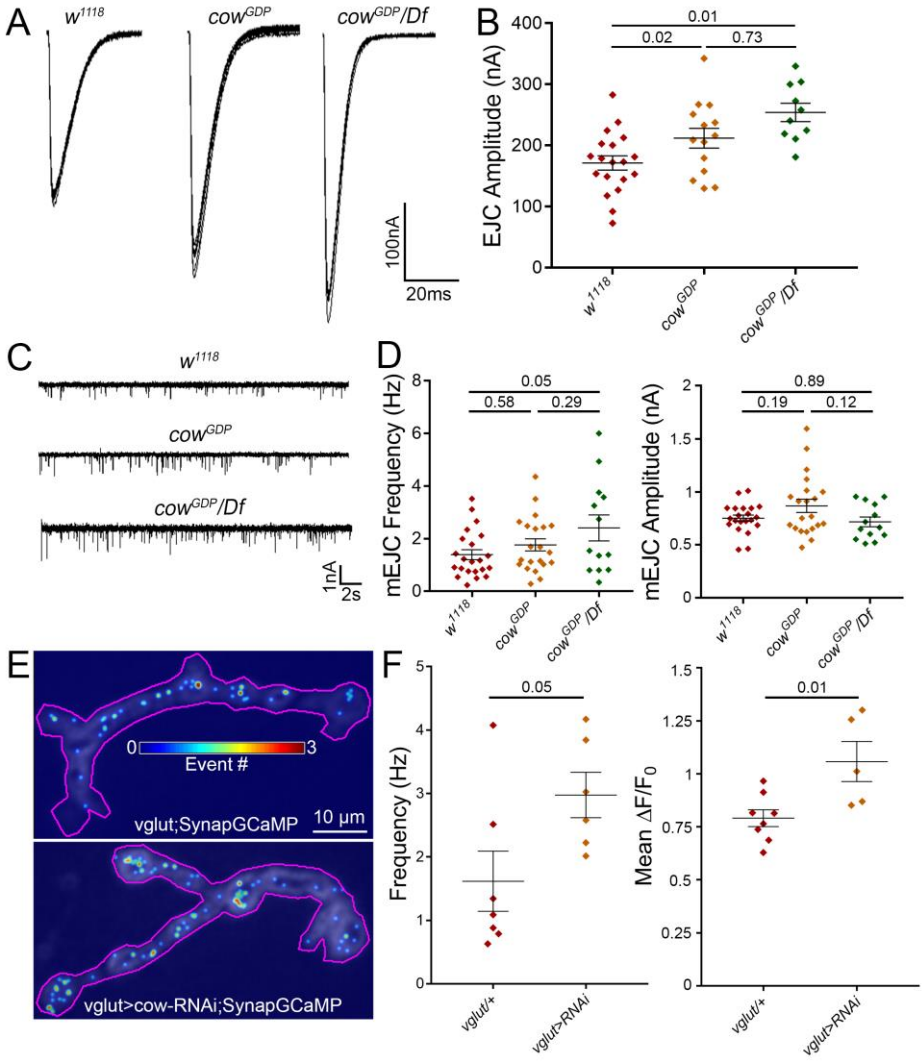

Fig. 23: Presynaptic Cow limits synaptic vesicle fusion for NMJ neurotransmission

(A) Representative motor nerve stimulation-evoked EJC traces (1.5 mM [Ca^{2+}]) from the *w*^{1118} genetic background control, *cow*^{GDP} homozygous mutant and *cow*^{GDP}*/Df* mutant. (B) Quantification of EJC amplitudes in the three genotypes shown in a scatter plot, with mean ± SEM. (C) Representative miniature EJC (mEJC) recording traces from the same genotypes. (D) Quantification of mEJC frequency (left) and amplitude (right) from the three genotypes. (E) Representative probability maps (30 sec) of SynapGCaMP imaging of mEJC events in motor neuron-targeted Gal4 driver control (*vglut*-Gal4/+, top) and *cow* RNAi knockdown (*vglut>cow*-RNAi, bottom) indicating mEJC location (dot) and frequency (color; see scale inset). (F) Quantification of SynapGCaMP event frequency (Hz/µm^2; left) and fluorescence intensity ($\Delta F/F_0$; right) shown in scatter plots, with mean ± SEM. P-values are shown for each statistical comparison.

Cow restricts presynaptic active zone and glutamatergic synapse formation

We next used imaging to assay pre- and postsynaptic molecular components of the synapse to test the hypothesis of increased NMJ synapse number in *cow* mutants. The presynaptic active zone (AZ) is the specialized site of synaptic vesicle (SV) fusion that mediates release of the glutamate neurotransmitter. Bruchpilot (Brp) tethers both the voltage-gated Ca^{2+} channels and SVs to the AZ, and is the best AZ marker (Hallermann et al., 2010). Each AZ directly apposes a postsynaptic glutamate receptor (GluR) cluster to mediate fast neurotransmission (Schuster et al., 1991). We used co-labeling with both anti-Brp (Wagh et al., 2006) and anti-GluRIIC (aka GluRIII; Marrus et al., 2004) to compare *cow* null mutants to w^{1118} genetic background controls (Fig. 24). Brp AZ punctae occur much more often in *cow* null NMJs (Fig. 24A), but are consistently smaller in volume (Fig. 24B). In quantified measurements, the number of Brp AZ punctae per NMJ is significantly increased in the *cow* null mutants compared to matched controls (w^{1118} 193.1±10.55 vs. cow^{GDP} 284.8±10.54; $p<0.0001$; Fig. 24A, right), but the average volume of the Brp AZ synaptic punctae is significantly decreased in the mutants (w^{1118} 0.86±0.033 μm^3 vs. cow^{GDP} 0.72±0.025; $p=0.0019$; Fig. 24B, right). This is consistent with a previous report also showing a reciprocal relationship between Brp AZ punctae number and volume (Graf et al., 2009).

Brp AZ punctae are precisely juxtaposed to GluR clusters in a functional synapse (Menon et al., 2013). For better resolution to image postsynaptic GluR clusters and quantify the synaptic apposition, structured illumination microscopy (SIM) was employed (Gustafsson, 2000). To compare to previous laser-scanning confocal imaging (LSM), Brp AZs were first measured to find a consistent increase in the *cow* null mutants, but with larger punctae numbers presumably due to increased resolution (w^{1118} 298.6±17.2 vs. cow^{GDP} 387.9±17.86; $p=0.0019$; Fig. 24C). There is also a similar increase in GluR clusters (w^{1118} 382±23.21 vs. cow^{GDP} 542.8±29.41; $p=0.0004$; Fig. 24D). Brp punctae and GluR clusters almost always partner, with rare exceptions seen at a similar

frequency in controls and mutants (Fig. 24D). There are more GluR clusters than Brp punctae in both genotypes. The GluR/Brp ratio was measured to test for defects in synaptic apposition. If there is a larger ratio in the mutants compared to controls, this would indicate more GluR clusters without a Brp AZ. Conversely, a smaller ratio would indicate more GluR clusters paired with a presynaptic partner. Quantified measurements show no difference in the GluR/Brp ratio between controls and the *cow* null mutants (w^{1118} 1.29±0.04 vs. cow^{GDP} 1.36±0.05; p=0.272). Taken together, these results demonstrate that Cow limits NMJ synapse formation, consistent with strengthened neurotransmission.

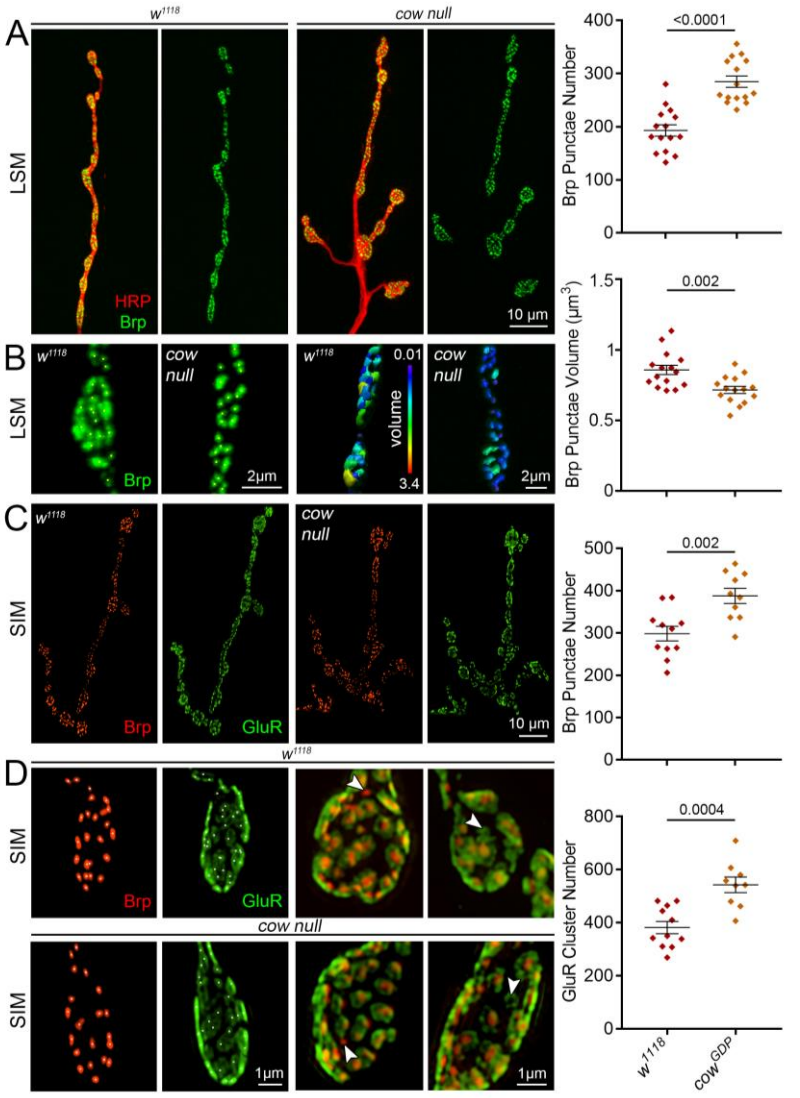

Fig. 24: Cow limits presynaptic active zones and glutamatergic synapse number

(A) Representative muscle 4 NMJ images from a confocal laser-scanning microscope (LSM) of genetic background controls (w^{1118}, left) and cow null mutants (cow^{GDP}, right) co-labeled for presynaptic membrane marker (HRP, red) and the active zone scaffold Bruchpilot (Brp, green). Brp alone is shown in right panels and quantified Brp punctae number is shown to the right. (B) High magnification synaptic bouton images with Brp puncate identified using Imaris software (asterisks, left) and volume indicated in a heatmap (scale 0.01-3.4 μm^3, right). Quantified Brp punctae volume shown to the right. (C) Representative NMJ images from a structured illumination microscope (SIM) of controls (w^{1118}) and *cow* nulls (cow^{GDP}) co-labeled for both presynaptic active zones (Brp, red) and postsynaptic glutamate receptors (GluRIIC, green). The quantified Brp punctae number is shown to the right. (D) High magnification SIM images of juxtaposed Brp punctae and GluR clusters at synapses. Arrowheads indicate Brp or GluR domains without a partner, which are observed at equal frequency in both genotypes. Quantified GluR cluster number is shown to the right. P-values are shown for each statistical comparison.

Membrane-tethering Wg prevents cow null defects in NMJ development

Our starting hypothesis was that Cow regulates Wg by binding the ligand in the extracellular space and carrying it across the synaptic cleft (from neuron to muscle). This hypothesis is based on published work demonstrating that Cow is secreted, directly binds secreted Wg, and acts to mediate intercellular transport (Chang and Sun, 2014). To test this hypothesis, we obtained transgenic lines with the *wg* gene cut from its native locus via FRT sites and then replaced either without (*FRT-wg*; transgenic control) or with (*NRT-wg*) a membrane tether. Importantly, HA-tagged *NRT-wg* is not secreted from Wg-expressing cells, and fails to maintain expression of long-range Wg targets (Alexandre et al., 2014). We tested whether tethering Wg to the membrane affects NMJ development. Comparing *FRT-wg* to *NRT-wg*, there is increased expression of the Wg ligand around presynaptic boutons (data not shown). To determine if tethered Wg can bind Fz2 receptors, NMJ bouton number was measured to assess presynaptic Wg signaling. Next, *NRT-wg* was combined with the *cow* null mutant (*NRT-wg; cow^{GDP}*) to test the hypothesis that Cow normally acts to regulate secreted Wg function. If Wg needs to be secreted and transported dependent on Cow function, then *NRT-wg* and *NRT-wg; cow^{GDP}* would be predicted to have the same phenotype. Representative images and summarized data are shown in Figure 25.

In comparing the control *FRT-wg* and tethered *NRT-wg*, there is no change in mature NMJ bouton number, but there is a clear increase in the number of immature satellite boutons when Wg is tethered (Fig. 25A). In quantified measurements, *NRT-wg* has the same number of NMJ synaptic boutons as the control (*FRT-wg* 26.71±1.04 vs. *NRT-wg* 27.04±1.72; p=0.999; Fig. 25A,B), but a 4-fold increase in the percentage of satellite boutons (*FRT-wg* 2.04±0.77% vs. *NRT-wg* 8.3±1.62; p=0.0019; Fig. 25C). When membrane-tethered Wg is placed in the *cow* null background (*NRT-wg; cow^{GDP}*), both the mature synaptic bouton number and the percentage of satellite boutons are similar to the *FRT-wg* control levels (Fig. 25A). In quantified measurements, the mature bouton number is no longer different between the two genotypes (*FRT-wg* 26.71±1.04

vs. *NRT-wg; cow*^{GDP} 26.78±0.97; p=0.999; Fig. 25B), and the satellite boutons are also restored to near normal levels (*FRT-wg* 2.04±0.77% vs. *NRT-wg; cow*^{GDP} 3.60±1.1; p=0.999; Fig. 25C). Taken together, these results suggest Cow facilitates Wg-dependent satellite bouton formation, and that Wg has to be secreted for Cow to act on it. However, in contrast to the original hypothesis, Cow acts as a negative regulator of secreted Wg signaling at the NMJ, suggesting that it should interact with other Wg negative regulators in the extracellular synaptomatrix.

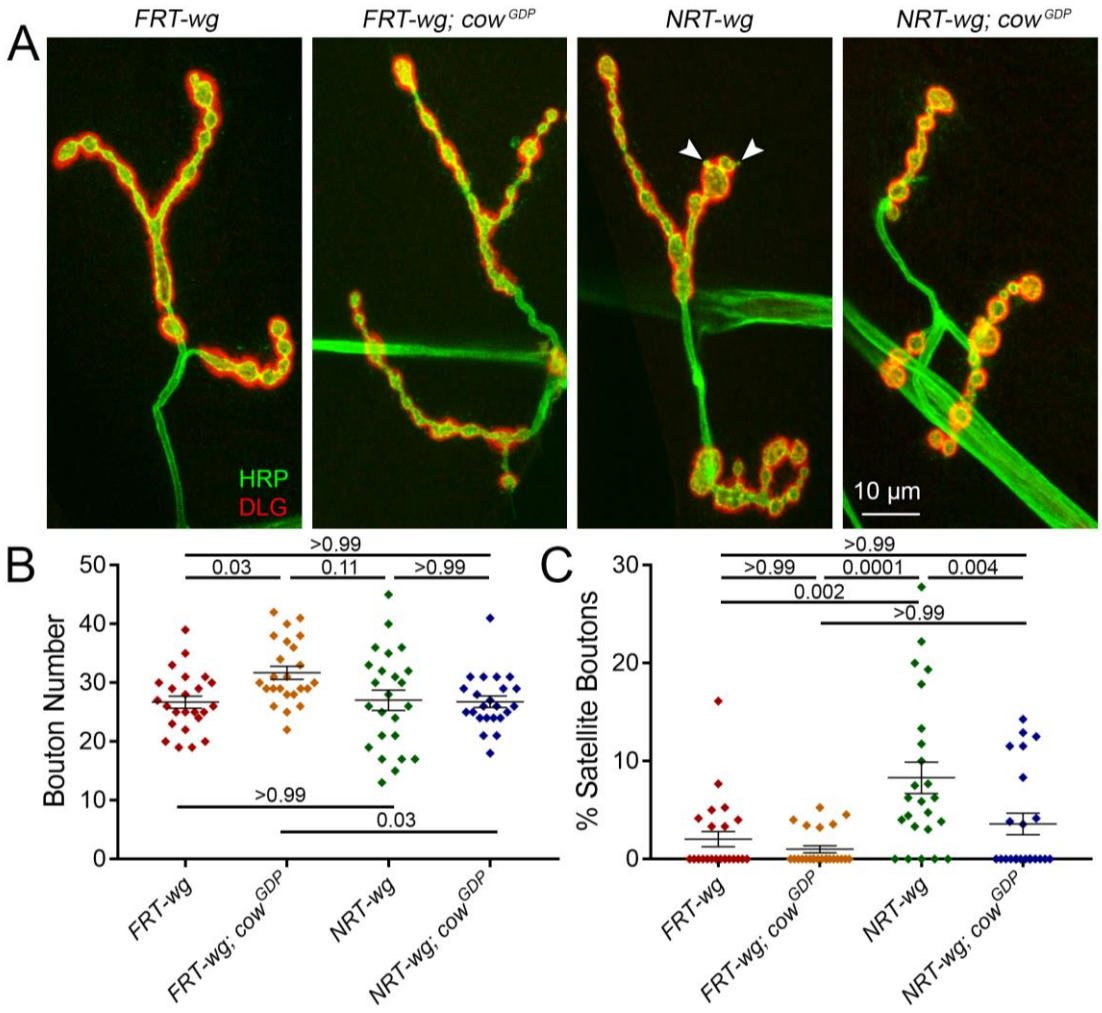

Fig. 25: Membrane-tethered Wg prevents *cow* null defects in bouton formation

(A) Representative confocal images of muscle 4 NMJs co-labeled with presynaptic HRP marker (green) and postsynaptic DLG marker (red) in Wg control (*FRT-wg*), cow null (*FRT-wg*; *cow*^{GDP}), tethered Wg (*NRT-wg*), and tethered Wg in *cow* null background (*NRT-wg; cow*^{GDP}). (B,C) Quantification of total NMJ synaptic bouton number (B) and the percentage of satellite boutons (C) in the four genotypes shown in a scatter plot, with mean ± SEM. P-values are shown for each statistical comparison.

Cow and Notum function together to restrict NMJ growth and bouton formation

The secreted deacylase Notum has also been recently shown to regulate NMJ synaptic bouton formation via the negative regulation of Wg *trans*-synaptic signaling (Kopke et al., 2017). Notum restricts Wnt signaling by cleaving the Wg palmitoyl group that binds to Fz2 receptors (Kakugawa et al., 2015). In *notum* null mutants, NMJ Wg signaling is elevated both pre- and postsynaptically, resulting in increased synaptic bouton number, synapse number and neurotransmission strength (Kopke et al., 2017). To test the hypothesis that the increased NMJ development in *cow* null mutants is similarly caused by an increase in Wg *trans*-synaptic signaling, we performed the genetic test of combining *cow* and *notum* null heterozygotes to assay effects on NMJ synaptic bouton development. The failure of mutant alleles at two different loci to complement one another is one method to test for an *in vivo* interaction of the gene products in a common signaling mechanism (nonallelic noncomplementation; Yook et al., 2001; Hawley and Gilliland, 2006). In this case, the interaction tests the hypothesis that Cow and Notum have closely associated functions in the regulation of Wg synaptic signaling via direct interaction with the Wg ligand in the extracellular synaptomatrix. We compared bouton formation in genetic background control (w^{1118}); *cow* null (cow^{GDP}) and *notum* null ($notum^{KO}$) homo- and heterozygotes; *cow/notum* *trans*-heterozygotes; and *cow/notum* double null mutant ($cow^{GDP},notum^{KO}/cow^{GDP},notum^{KO}$). Representative images and summarized data are shown in Figure 26.

The *trans*-heterozygote has a clearly expanded NMJ with more synaptic boutons compared to controls, as well as other *wg* mutant phenotypes such as the appearance of ghost boutons (Fig. 26A; inset). Ghost boutons are immature boutons that contain the HRP marker, but do not yet contain the postsynaptic DLG protein (Ataman et al., 2006). The *cow* ($cow^{GDP}/+$) and *notum* ($notum^{KO}/+$) heterozygotes alone are no different from w^{1118} controls, and lack synaptic features of impaired Wg signaling (Fig. 26A). In quantified measurements, *trans*-heterozygotes have strongly increased bouton numbers (w^{1118} 28.33±1.46 vs. $cow^{GDP}/notum^{KO}$ 46.13±1.08; $p<0.0001$; Fig. 26A, right). Extracellular Wg labeling without cellular permeabilization in all these

genotypes indicates no difference in the Wg fluorescence intensity (Fig. 26B). In quantified measurements, there is no detectable change in Wg ligand levels between controls and *cow/notum trans*-heterozygotes (normalized w^{1118} 1.0±0.09 vs. cow^{GDP}/+; $notum^{KO}$/+ 0.9±0.09; p=0.852; Fig. 26B, right). The double null mutants have significantly increased bouton numbers compared to controls but no increase compared to each null alone (w^{1118} 22.94±1.05 vs. cow^{GDP}, $notum^{KO}/cow^{GDP},notum^{KO}$ 29.13±0.97; p=0.0005; Fig. 26C, right). Interestingly, *trans*-heterozygotes show no change in nerve-stimulation evoked EJC recordings. These results indicate Cow and Notum act in the same pathway to restrict Wg signaling in structural development, and that the level of extracellular Wg ligand alone is not predictive of signaling activity.

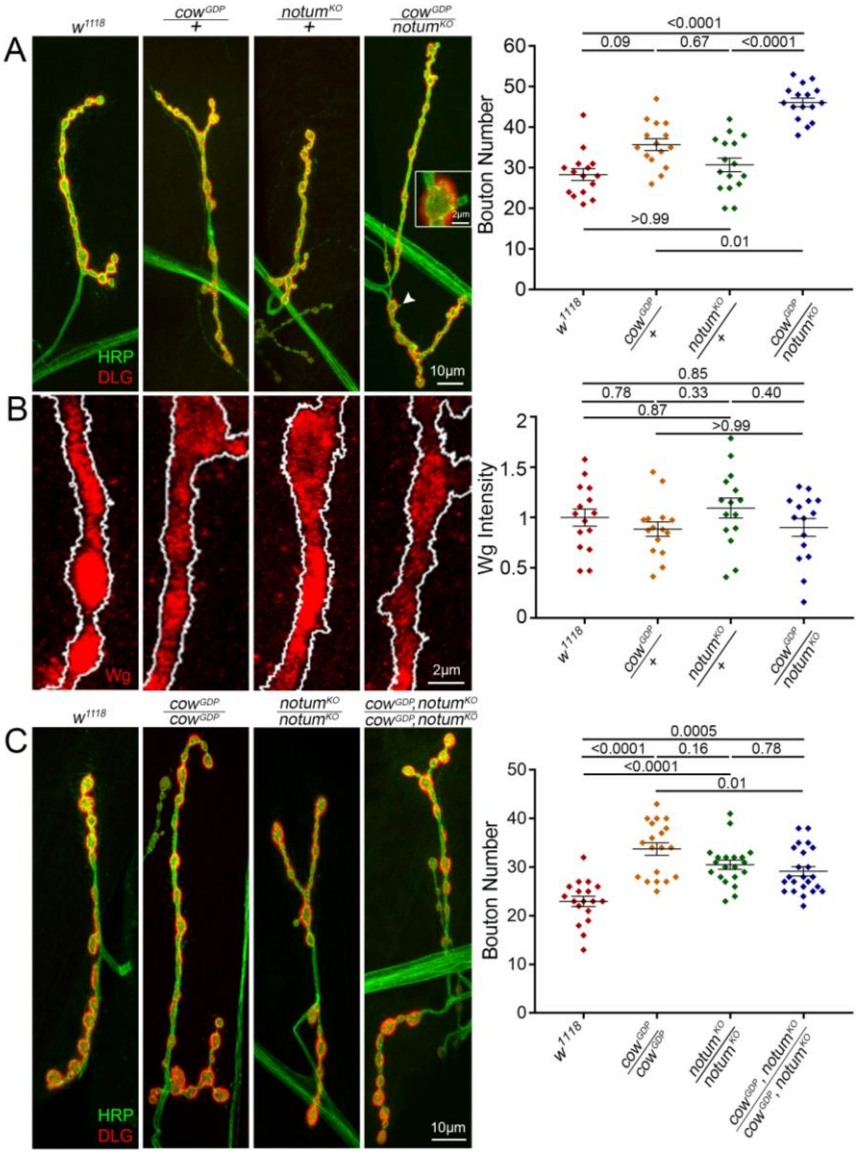

Fig. 26: Cow and Notum act in the same Wg pathway to limit NMJ bouton number

(A) Confocal images of the muscle 4 NMJ co-labeled with presynaptic HRP marker (green) and postsynaptic DLG marker (red) in the genetic background control (w^{1118}), *cow* null heterozygote (cow^{GDP}/+), *notum* null heterozygote ($notum^{KO}$/+) and *cow/notum* transheterozygote ($cow^{GDP}/notum^{KO}$). Quantified bouton number is shown to the right. (B) High magnification NMJ confocal images of anti-Wg labeling at synaptic boutons of the same indicated genotypes. The presynaptic HRP marker boundary is outlined in white. Quantified Wg fluorescence intensity is shown to the right, normalized to the background control (w^{1118}). (C) Confocal images of the muscle 4 NMJ co-labeled with presynaptic HRP marker (green) and postsynaptic DLG marker (red) in the genetic background control (w^{1118}), *cow* null (cow^{GDP}/cow^{GDP}), *notum* null ($notum^{KO}/notum^{KO}$) and *cow/notum* double null ($cow^{GDP},notum^{KO}/cow^{GDP},notum^{KO}$). Quantified bouton number is shown to the right. P-values are shown for each statistical comparison.

Discussion

The function of signaling ligands in the extracellular space is tightly regulated to ensure coordinated intercellular development, often via glycan-dependent mechanisms (Dani and Broadie, 2012; Parkinson et al., 2013; Shilts and Broadie, 2017). The most recently discovered *Drosophila* HSPG, secreted Cow, was characterized with this role (Chang and Sun, 2014). In the developing wing disc, the Wnt Wg is produced in a stripe of cells at the dorsal/ventral margin boundary, and acts as an intercellular morphogen through Fz2 receptor signaling (Zecca et al., 1996; Bhanot et al., 1996; Neumann and Cohen, 1997). The glypican HSPGs Dally and Dally-like (Dlp), bound to outer plasma membrane leaflets via GPI anchors, bind Wg to regulate both ligand distribution and intercellular signaling (Tsuda et al., 1999; Baeg et al., 2001; Dani et al., 2012; Dear et al., 2017). It has been proposed that Dally/Dlp HSPGs are involved in the movement of extracellular Wg to form a morphogen gradient (Han et al., 2005). However, in *dally dlp* double mutant clones, extracellular Wg is detected far away from Wg-secreting cells, suggesting another extracellular factor can transport Wg. Cow was shown to fill this role by binding extracellular Wg to increase stability and rate of movement from producing to receiving cells (Chang and Sun, 2014). Supporting this model, *cow* mutants manifest Wg ligand gain-of-function (GOF)/overexpression phenotypes for short-range targets, and loss-of-function (LOF) phenotypes for long-range targets.

At the NMJ, such a long-range Wg morphogen transport function is not seemingly required, except perhaps as a clearance mechanism, but Wg extracellular regulation and short-range Wg transport to cross the synaptic cleft is critical for NMJ development (Packard et al., 2002; Friedman et al., 2013; Dear et al., 2016; Parkinson et al., 2016). At the forming NMJ, Wg from neurons and glia signals both presynaptically (neuronal) and postsynaptically (muscle) via Fz2 receptors (Packard et al., 2002; Kerr et al., 2014). In the motor neuron, Wg signaling inhibits the glycogen synthase kinase 3β (GSK3β) homolog Shaggy (Sgg) to regulate the microtubule-associated protein 1B (MAP1B) homolog Futsch to modulate microtubule dynamics controlling

NMJ bouton formation (Miech et al., 2008). However, Futsch distribution and microtubule dynamics do not change with elevated Wg signaling (Kopke et al., 2017), so this pathway alone does not explain the increased bouton formation with increased Wg signaling. In the postsynaptic muscle, Wg signaling drives Fz2 endocytosis and C-terminus cleavage, with transport to the nucleus regulating mRNAs involved in synaptogenesis, including postsynaptic GluR distribution (Speese et al., 2012). In *wg* mutants, GluRs are more diffuse; with clusters irregular in size/shape, increased receptor numbers and a larger postsynaptic volume (Packard et al., 2002; Speese et al., 2012; Kerr et al., 2014). Thus, Wg *trans*-synaptic signaling controls both NMJ structure and function.

Based on the findings from Chang and Sun (2014), we hypothesized that Cow binds Wg to facilitate the transport across the synapse to Fz2 receptors on the muscle. If this is correct, we would expect a presynaptic Wg overexpression (OE) phenotype in the absence of Cow (Wg buildup at the source), and a postsynaptic Wg decrease/loss phenotype (failure of Wg transport). Presynaptically, we find increased synaptic bouton number in *cow* null mutants phenocopying the Wg OE condition (Kopke et al., 2017), consistent with this hypothesis. These results indicate that Cow normally inhibits NMJ bouton formation, consistent with the effects of inhibiting presynaptic Wg signaling (Packard et al., 2002). Postsynaptically, we find an increased number of GluR clusters due to elevated synapse formation in *cow* null mutants, but no evidence of diffuse GluR clusters of irregular size/shape and larger volume as has been reported in *wg* mutants (Packard et al., 2002; Speese et al., 2012; Kerr et al., 2014). Therefore, we do not find strong support for the second prediction of the hypothesis. GluR changes within single postsynaptic domains are challenging to see even with enhanced resolution microscopy (such as the structured illumination microscopy (SIM) used here; Gustafsson, 2000), but future studies could focus more on GluRIIA cluster size/shape/intensity in *cow* mutants. If GluR defects are detected in *cow* nulls, it would be interesting to test the Frizzled Nuclear Import (FNI) pathway (Mathew et al., 2005).

Wg signaling regulates multiple steps of NMJ development including branching, satellite bouton budding and synaptic bouton maturation (Koles and Budnik, 2012). None of the *cow* manipulations cause changes in branching, indicating Cow does not regulate this Wg signaling, likely working in concert with other Wg regulators. Wg loss (wg^{ts}) decreases bouton formation (Packard et al., 2002), while neural Wg OE increases branching, satellite and total bouton numbers (Packard et al., 2002; Miech et al., 2008; Kopke et al., 2017). Satellite boutons represent an immature stage of development, with small boutons connected to the mature (parent) bouton or adjacent axon (Torroja et al., 1999; Gatto and Broadie, 2008). Neuronal Cow OE does not change mature bouton number, but increases satellite bouton budding. Neuronal Cow RNAi also increases satellite boutons. Thus, changing neural Cow levels in either direction elevates satellite bouton numbers, suggesting different consequences on budding versus developmental arrest. It also appears that the cellular source of secreted Cow, or the balance between sources, may be important for proper Wg regulation. Importantly, glia-secreted Wg regulates distinct aspects of synaptic development (Kerr et al., 2014), with loss of glial-derived Wg accounting for some, but not all, of *wg* mutant phenotypes. Similarly, cell-targeted *cow* manipulations cause different NMJ phenotypes. There is no evidence for normal Cow function in postsynaptic muscle, but it remains possible that Cow secreted from glia could regulate Wg *trans*-synaptic signaling.

Increasing Wg signaling elevates evoked transmission strength and functional synapse number (Kopke et al., 2017), which is phenocopied in *cow* null mutants. Block of postsynaptic Wg signaling causes increased SV fusion frequency and amplitude of miniature excitatory junctional potentials (Speese et al., 2012). With neuronal *cow* RNAi, there is a similar increase in event frequency and amplitude. These results suggest a decrease in postsynaptic Wg signaling when *cow* is lost, supporting the Wg transport hypothesis. Blocking Wg secreted from neurons or glia increases muscle GluR cluster size, albeit with differential effects on neurotransmission efficacy (Kerr et al., 2014). Reducing neuronal Wg has no effect on mEJC frequency, but reducing glial-derived Wg increases SV fusion frequency (Kerr et al., 2014). Both nerve-evoked and

spontaneous neurotransmission are increased in *cow* null mutants, together with increased Brp active zones and postsynaptic GluR clusters forming supernumerary synapses. SynapGCaMP is an exciting new tool to test function at individual synapses (Newman et al., 2017). With targeted neuronal *cow* RNAi, there is an increase in both the number of SV fusion events and the postsynaptic Ca^{2+} signal amplitude, consistent with both presynaptic and postsynaptic regulation of Wg signaling (Packard et al., 2002; Speese et al., 2012; Kerr et al., 2014). These functional phenotypes, combined with coordinated changes in pre- and postsynaptic formation suggest Cow regulates *trans*-synaptic Wg transport.

There were differences between spontaneous synaptic vesicle fusion findings between TEVC electrophysiological recordings and SynapGCaMP reporter (*MHC-CD8-GCaMP6f-Sh*) Ca^{2+} imaging (Newman et al., 2017). Motor neuron presynaptically targeted *cow* RNAi showed stronger impacts on SV fusion frequency with imaging in contrast to recordings, comparable to effects in the cow^{GDP} null mutants. Moreover, SynapGCaMP imaging revealed significantly larger SV fusion event magnitudes in contrast to the lack of change found with TEVC recording. While the basis of these differences in unknown, we speculate that it is due to the differential nature or sensitivity of these two methods. The Ca^{2+} imaging is based on measuring the change in the fluorescence signal over the baseline NMJ fluorescence ($\Delta F/F_0$; Newman et al., 2017), and it may be that glutamate receptor Ca^{2+} permeability or intracellular Ca^{2+} signaling dynamics is changed in a way not directly related to detectable membrane current changes in the *cow* mutants. TEVC recordings capture whole NMJ activity, whereas with imaging we only captured type 1b bouton activity normalized to area. In future studies, SynapGCaMP imaging can be used to map spatial changes in synapse function by assaying quantal activity separately in convergent type 1s and 1b motor neuron inputs and within discrete synaptic boutons (Newman et al., 2017). Moreover, differences between cow^{GDP} and cow^{GDP}/Df conditions could be influenced by second-site enhancing mutations on the Df chromosome. Overall, it should be noted that the changes in

spontaneous SV fusion frequency and amplitude in *cow* mutants are subtle and variable, and need to be further studied in the future.

Wg is lipid-modified via palmitoylation to become strongly membrane associated (Zhai et al., 2004). The hydrophobic moiety is located at the interface of Wg and Fz2 binding, shielded from the aqueous environment by multiple extracellular transporters until signaling interaction with the receptor (Takada et al., 2017). There have been many modes of extracellular Wg transport demonstrated, primarily from work in the wing disc, including microvesicles, lipoproteins, exosomes and cytoneme membrane extensions (Greco et al., 2001; Panáková et al., 2005; Gross et al., 2012; Huang and Kornberg, 2015). These multiple mechanisms of transport are much less studied at the synapse; however, exosome-like vesicles containing the Wg-binding protein Evenness Interrupted (Evi) have been demonstrated at the *Drosophila* NMJ (Korkut et al., 2009). Cow could be considered an alternative extracellular Wg transport method (Chang and Sun, 2014), acting to shield Wg while facilitating transport through the extracellular synaptomatrix (Dani and Broadie, 2012; Dear et al., 2016). In addition, HSPGs have been shown to regulate ligands by stabilizing, degrading or sequestering the ligand, or as bifunctional co-receptors, or facilitators of transcytosis (Lin, 2004; Dani et al., 2012; Dear et al., 2017). Results presented here are consistent with the hypothesis that Cow is mediating Wg transport across the NMJ synapse (Chang and Sun, 2014), but also that Cow has an additional role in the negative regulation of Wg synaptic signaling.

The need for secreted Wg has been recently challenged, with Wg tethering to the membrane (*NRT-wg*) showing Wg secretion to be largely dispensable for development (Alexandre et al., 2014). In contrast, other recent studies suggest that Wg release and spreading is necessary (Beaven and Denholm, 2018; Pani and Goldstein, 2018; Stewart et al., 2019). We find tethering Wg at the NMJ synapse increases extracellular Wg ligand levels, with no change in mature bouton numbers. This Wg accumulation shows *NRT-wg* is more stable at the synaptic signaling interface, consistent with other studies (Morata and Struhl, 2014; Chaudhary and

Boutros, 2018). However, even though Wg levels increase, Wg signaling is less effective. With *NRT-wg*, only the budding of new satellite bouton is increased, with no increase in mature bouton formation. Reducing Wg function causes Fz2 upregulation (Cadigan et al., 1998; Chaudhary and Boutros, 2018), so we hypothesize Wg signaling could be maintained by increased presynaptic Fz2 receptors. When Wg is tethered, Cow cannot mediate intercellular transport, so the hypothesis predicts similar phenotype with (*NRT-wg*) or without Cow (*NRT-wg; cow*^{GDP}). Indeed, Cow removal in the *NRT-wg* condition does not impact synaptic bouton number, although it does block the increase in satellite boutons, consistent with a Cow role in greater Wg stability (Chang and Sun, 2014). These results show that Wg secretion is required for the elevated NMJ development characterizing *cow* mutant animals.

To further test how Cow is working through the Wg pathway to negatively regulate NMJ development, we turned to genetic interaction tests with the Wg negative regulator Notum (Gerlitz and Basler, 2002; Giráldez et al., 2002; Kakugawa et al., 2015). At the NMJ, Wg *trans*-synaptic signaling is elevated in the absence of Notum, and null *notum* mutants display larger NMJs with more synaptic boutons, increased synapse number and elevated neurotransmission (Kopke et al., 2017). All these defects are phenocopied by neuronal Wg OE, showing that the positive synaptogenic phenotypes arise from lack of Wg signaling inhibition. Consistently, genetically correcting Wg levels at the synapse in *notum* nulls alleviates synaptogenic phenotypes (Kopke et al., 2017). We show here that *cow* null mutants have the same phenotypes of expanded NMJs, supernumerary synaptic boutons, greater synapse number/function and strengthened transmission, suggesting Cow acts like Notum in regulating Wg signaling. We performed a genetic test to ask whether Cow and Notum work in this same pathway. While *cow* and *notum* null heterozygotes do not exhibit NMJ defects, *cow/notum trans*-heterozygotes display grossly expanded NMJs with excess boutons. This combined haplo-insufficiency (type 3 SSNC) of nonallelic noncomplementation suggests Cow and Notum share related roles (Yook et al., 2001; Hawley and Gilliland, 2006). When we tested full double mutants, there is no additive effect,

showing that Cow and Notum restrict Wg signaling in the same pathway. However, this pathway convergence appears restricted only to the control of structural synaptogenesis but not functional neurotransmission, although the control neurotransmission amplitude was elevated in these studies.

Cow now joins the list of synaptic HSPGs with key roles in NMJ development. HSPGs have been implicated in vertebrate NMJ synapse formation for >3 decades (Kamimura and Maeda, 2017; Condomitti and Wit, 2018). The Agrin HSPG is secreted from presynaptic terminals to maintain postsynaptic acetylcholine receptor clustering (Godfrey et al., 1984; Hubbard et al., 2013). Another secreted HSPG, Perlecan, regulates acetylcholinesterase localization (Peng et al., 1999; Arikawa-Hirasawa et al., 2002). *Drosophila* NMJ analyses have begun to more systematically elucidate HSPG roles in NMJ formation and function (Ren et al., 2009; Kamimura and Maeda, 2017). In particular, the glypican HSPG Dlp regulates Wg signaling to modulate both NMJ structure and function, including the regulation of active zone formation and SV release (Johnson et al., 2006; Dani et al., 2012; Friedman et al., 2013; Dear et al., 2017). Wg binds the core Dlp protein, with HS chains enhancing this binding, to retain Wg on the cell surface, where it can both compete with Fz2 receptors and facilitate Wg-Fz2 binding (Yan et al., 2009). This biphasic activity depends on the ratio of Wg, Fz2 and Dlp HSPG as expounded in 'exchange factor model' (Yan et al., 2009; Dear et al., 2016). Cow may impact this exchange factor mechanism as a fourth player, acting with Dlp to modulate Wg transport and Wg-Fz2 binding at the synaptic interface. It will be important to test Dlp levels and distribution in *cow* nulls to see how Cow fits into this model.

In addition to Cow, Perlecan (Trol) is another secreted HSPG reported to regulate bidirectional Wg signaling at the *Drosophila* NMJ (Kamimura et al., 2013). Trol has been localized near the muscle membrane, where it promotes postsynaptic Wg accumulation. In the absence of Trol, Wg builds up presynaptically, causing excess satellite bouton formation (Kamimura et al., 2013). It is interesting to note that *cow* mutants enhance Wg signaling without increasing satellite

boutons. In *trol* mutants, ghost boutons increase due to decreased postsynaptic Wg signaling (Kamimura et al., 2013). Note that cow mutants do not exhibit ghost boutons, which fails to support decreased postsynaptic Wg signaling. Other postsynaptic defects in *trol* mutants (e.g. reduced subsynaptic reticulum (SSR), increased postsynaptic pockets; Kamimura et al., 2013) are NMJ ultrastructural features that could be a future focus using electron microscopy studies. Similar to *cow* mutants, extracellular Wg levels are decreased in the absence of Trol, speculated due to increased Wg proteolysis, since HS protects HS-binding proteins from degradation (Saksela et al., 1988). In *cow* mutants, it is not yet known whether Wg is decreased due to elevated signaling (ligand/receptor endocytosis), or increased degradation due to Cow no longer protecting/stabilizing the ligand. Given synaptic Fz2 is internalized with Wg binding (Mathew et al., 2005), future experiments could test internalized Fz2 levels in *cow* mutants as a proxy of Wg signaling.

In summary, we have confirmed here new tools to study Cow HSPG function, and discovered Cow from presynaptic motor neurons restricts NMJ bouton formation, glutamatergic synapse number and NMJ functional differentiation. Cow acts within the same Wg *trans*-synaptic signaling pathway as Notum by regulating the Wg ligand in the extracellular synaptomatrix. Secreted Cow modulates extracellular Wg ligand levels, with additional functions controlling Wg signaling efficacy, which may be independent or dependent of Wg transport. It will be interesting to determine whether Cow core protein and/or its HS chains are important for the synaptic structural and functional phenotypes. Wg must be secreted for Cow to act on it, as shown by the membrane-tethered interaction studies, showing secreted Cow must work on the freely-diffusible Wg ligand. Perhaps most informative for our future studies will be dissection of the interactions, coordination or redundancy of the multiple synaptic HSPGs at the NMJ, to further the understanding of extracellular Wg *trans*-synaptic signaling regulation during synaptic development. *Drosophila* is particularly well-suited model to study HSPGs owing to the relatively reduced complexity in this system (17 HSPGs in mammals vs. 5 in *Drosophila*; Sarrazin et al.,

2011). We look forward to expanding future studies to examine multiple synaptic HSPGs in parallel, with the goal of elucidating the surprisingly complex control of *trans*-synaptic signaling occurring within the extracellular synaptomatrix.

References

Alexandre C, Baena-Lopez A, Vincent JP (2014) Patterning and growth control by membrane-tethered Wingless. Nature 505(7482):180-5.

Arikawa-Hirasawa E, Rossi SG, Rotundo RL, Yamada Y (2002) Absence of acetylcholinesterase at the neuromuscular junctions of perlecan-null mice. Nat Neurosci 5:119-23.

Ataman B, Ashley J, Gorczyca D, Gorczyca M, Mathew D, Wichmann C, Sigrist SJ, Budnik V (2006) Nuclear trafficking of *Drosophila* Frizzled-2 during synapse development requires the PDZ protein dGRIP. PNAS 103(20):7841-46.

Ataman B, Ashley J, Gorczyca M, Ramachandran P, Fouquet W, Sigrist SJ, Budnik V (2008) Rapid Activity-Dependent Modifications in Synaptic Structure and Function Require Bidirectional Wnt Signaling. Neuron 57(5):705-18.

Baeg GH, Lin X, Khare N, Baumgartner S, Perrimon N (2001) Heparan sulfate proteoglycans are critical for the organization of the extracellular distribution of Wingless. Development 128:87-94.

Beaven R, Denholm B (2018) Release and spread of Wingless is required to pattern the proximo-distal axis of *Drosophila* renal tubules. eLIFE 7:e35373.

Bellen HJ, Levis RW, Liao G, He Y, Carlson JW, Tsang G, Evans-Holm M, Hiesinger PR, Schulze KL, Rubin GM, Hoskins RA, Spralding AC (2004) The BDGP Gene Disruption Project: Single Transposon Insertions Associated With 40% of Drosophila Genes. Genetics 167:761-81.

Bhanot P, Brink M, Samos CH, Hsieh J-C, Wang Y, Macke JP, Andrew D, Nathans J, Nusse R (1996) A new member of the *frizzled* family from *Drosophila* functions as a Wingless receptor. Nature 382:225-30.

Cadigan KM, Fish MP, Rulifson EJ, Nusse R (1998) Wingless Repression of *Drosophila* frizzled 2 Expression Shapes the Wingless Morphogen Gradient in the Wing. Cell 93(5):767-77.

Chang Y-H, Sun YH (2014) Carrier of Wingless (Cow), a Secreted Heparan Sulfate Proteoglycan, Promotes Extracellular Transport of Wingless. PLoS ONE 9(10):e111573.

Chaudhary V, Hingole S, Frei J, Port F, Strutt D, Boutros M (2019) Robust Wnt signaling is maintained by a Wg protein gradient and Fz2 receptor activity in the developing *Drosophila* wing. Development 146(15):dev174789.

Condomitti G, de Wit J (2018) Heparan Sulfate Proteoglycans as Emerging Players in Synaptic Specificity. Front Mol Neurosci 11:14.

Dani N, Broadie K (2012) Glycosylated synaptomatrix regulation of trans-synaptic signaling. Dev Neurobiol 72(1):2-21.

Dani N, Nahm M, Lee S, Braodie K (2012) A Targeted Glycan-Related Gene Screen Reveals Heparan Sulfate Proteoglycan Sulfation Regulates WNT and BMP Trans-Synaptic Signaling. PloS Genetics 8(11):e1003031.

Dear ML, Dani N, Parkinson W, Zhou S, Broadie K (2016) Two classes of matrix metalloproteinases reciprocally regulate synaptogenesis. Development 143(1):75-87.

Dear ML, Shilts J, Broadie K (2017) Neuronal activity drives FMRP- and HSPG-dependent matrix metalloproteinase function required for rapid synaptogenesis. Sci Signal 10(504):eaan3181.

Franco B, Bogdanik L, Bobinnec Y, Debec A, Bockaert J, Parmentier M-L, Grau Y (2004) Shaggy, the Homolog of Glycogen Synthase Kinase 3, Controls Neuromuscular Junction Growth in *Drosophila*. J Neurosci 24(29):6573-7.

Friedman S, Dani N, Rushton E, Broadie K (2013) Fragile X mental retardation protein regulates trans-syanptic signaling in *Drosophila*. Dis Model Mech 6(6):1400-13.

Gatto CL, Broadie K (2008) Temporal requirements of the fragile X mental retardation protein in the regulation of synaptic structure. Development 135:2637-48.

Gerlitz O, Basler K (2002) Wingful, an extracellular feedback inhibitor of Wingless. Genes Dev 16(9):1055-9

Giráldez AJ, Copley RR, Cohen SM (2002) HSPG Modification by the Secreted Enzyme Notum Shapes the Wingless Morphogen Gradient. Cell 2(5):667-76.

Godfrey EW, Nitkin RM, Wallace BG, Rubin LL, McMahan UJ (1984) Components of Torpedo electric organ and muscle that cause aggregation of acetylcholine receptors on cultured muscle cells. JCB 99(2):615-27.

Graf ER, Daniels RW, Burgess RW, Schwarz TL, DiAntonio A (2009) Rab3 Dynamically Controls Protein Composition at Active Zones. Neuron 64(5):663-77.

Greco V, Hannus M, Eaton S (2001) Argosomes: A Potential Vehicle for the Spread of Morphogens through Epithelia. Cell 106(5):633-45.

Gross JC, Chaudhary V, Bartscherer K, Boutros M (2012) Active Wnt proteins are secreted on exosomes. Nat Cell Biol 435(7038):58-65.

Gustafsson MGL (2000) Surpassing the lateral resolution limit by a factor of two using structured illumination microscopy. J Microsc 198(2):82-7.

Hallermann S, Kittel RJ, Wichmann C, Weyhersmüller A, Fouquet W, Mertel S, Owald D, Eimer S, Depner H, Schwärzel M, Sigrist SJ, Heckmann M (2010) Naked Dense Bodies Provoke Depression. J Neurosci 30(43):14340-45.

Han C, Yan D, Belenkaya TY, Lin X (2005) Drosophila glypicans Dally and Dally-like shape the extracellular Wingless morphogen gradient in the wing disc. Development 132(4):667-79.

Hawley RS, Gilliland WD (2006) Sometimes the result is not the answer: the truths and the lies that come from using the complementation test. Genetics 174(1):5-15.

Huang H, Kornberg TB (2015) Myoblast cytonemes mediate Wg signaling from the wing imaginal disc and Delta-Notch signaling to the air sac primordium. eLIFE 4:e06114.

Hubbard SR, Gnanasambandan K (2013) Structure and activation of MuSK, a receptor tyrosine kinase central to neuromuscular junction formation. Biochim Biophys Acta 1834(10):2166-2169.

Jan LY, Jan YN (1982) Antibodies to horseradish peroxidase as specific neuronal markers in Drosophila and in grasshopper embryos. PNAS 79(8):2700-4.

Johnson KG, Tenney AP, Ghose A, Duckworth AM, Higashi ME, Parfitt K, Marcu O, Heslip TR, Marsh JL, Schwarz TL, Flanagan JG, Van Vactor D (2006) The HSPGs Syndecan and Dallylike Bind the Receptor Phosphatase LAR and Exert Distinct Effects on Synaptic Development. Neuron 49(4):517-31.

Kakugawa S, Langton PF, Zebisch M, Howell SA, Chang T-H, Liu Y, Feizi T, Bineva G, O'Reilly N, Snijders AP, Jones EY, Vincent JP (2015) Notum deacylates Wnt proteins to suppress signalling activity. Nature 519(7542):187-92.

Kamimura K and Maeda N (2017) Heparan sulfate proteoglycans in *Drosophila* neuromuscular development. Biochim Biophys Acta 1861(10):2442-6.

Kamimura K, Ueno K, Nakagawa J, Hamada R, Saitoe M, Maeda N (2013) Perlecan regulates bidirectional Wnt signaling at the *Drosophila* neuromuscular junction. JCB 200(2):219.

Kerr KS, Fuentes-Medel Y, Brewer C, Barria R, Ashley J, Abruzzi KC, Sheehan A, Tasdemir-Yilmaz OE, Freeman MR, Budnik V (2014) Glial Wingless/Wnt Regulates Glutamate Receptor Clustering and Synaptic Physiology at the *Drosophila* Neuromuscular Junction. J Neuorsci 34(8):2910-20.

Koles K, Budnik V (2012) Wnt Signaling in Neuromuscular Junction Development. Cold Spring Harb Perspect Biol 4:a008045.

Kopke DL, Lima SC, Alexandre C, Broadie K (2017) Notum coordinates synapse development via extracellular regulation of Wingless trans-synaptic signaling. Development 144(19):3499-510.

Korkut C, Ataman B, Ramachandran P, Ashley J, Barria R, Cherbesi N, Budnik V (2009) Trans-Synaptic Transmission of Vesicular Wnt Signals through Evi/Wntless. Cell 139(2):393-404.

Kittel RJ, Wichmann C, Rasse TM, Fouquet W, Schmidt M, Schmid A, Wagh DA, Pawlu C, Kellner RR, Willig KI, Hell SW, Buchner E, Heckmann M, Sigrist SJ (2006) Bruchpilot Promotes Active Zones Assembly, Ca^{2+} Channel Clustering, and Vesicle Release. Science 312(5776):1051-4.

Lahey T, Gorczyca M, Jia X-X, Budnik V (1994) The drosophila tumor suppressor gene *dlg* is required for normal synaptic bouton structure. Neuron 13(4):823-35.

Lin X (2004) Functions of heparan sulfate proteoglycans in cell signaling during development. Development 131(24):6009-21.

Marrus SB, Portman SL, Allen MJ, Moffat KG, DiAntonio A (2004) Differential Localization of Glutamate Receptor Subunits at the *Drosophila* Neuromuscular Junction. J Neurosci 24(6):1406-15.

Masu M (2016) Proteoglycans and axon guidance: a new relationship between old partners. J Neurochem 139(2):58-75.

Mathew D, Ataman B, Chen J, Zhang Y, Cumberledge S, Budnik V (2005) Wingless signaling at synapses is through cleavage and nuclear import of receptor DFrizzled2. Science 310(5752):1344-7.

Menon KP, Carrillo RA, Zinn K (2013) Development and plasticity of the *Drosophila* larval neuromuscular junction. WIREs Dev Biol 2:647-70.

Miech C, Pauer H-U, He X, Schwarz TL (2008) Presynaptic Local Signaling by a Canonical Wingless Pathway Regulates Development of the *Drosophila* Neuromuscular Junction. J Neurosci 28(43):10875-84.

Morata G and Struhl G (2014) Tethered wings. Nature 505:162-3.

Nagarkar-Jaiswal S, Lee P-T, Campbell ME, Chen K, Anguiano-Zarate S, Gutierrez MC, Busby T, Lin W-W, He Y (2015) A library of MiMICs allows tagging of genes and reversible, spatial and temporal knockdown of proteins in Drosophila. eLIFE 4:e05338.

Neumann CJ, Cohen SM (1997) Long-range action of Wingless organizes the dorsal-ventral axis of the *Drosophila* wing. Development 124:871-80.

Newman ZL, Hoagland A, Aghi K, Worden K, Levy SL, Son JH, Lee LP, Isacoff EY (2017) Input-Specific Plasticity and Homeostasis at the *Drosophila* Larval Neuromuscular Junction. Neuron 93(6):1388-404.

Packard M, Koo ES, Gorczyca, Sharpe J, Cumberledge S, Budnik V (2002) The Drosophila Wnt, wingless, provides an essential signal for pre- and postsynaptic differentiation. Cell 111(3):319-30.

Panáková D, Sprong H, Marois E, Thiele C, Eaton S (2005) Lipoprotein particles are required for Hedgehog and Wingless signaling. Nature 435(7038):58-65.

Pani AM, Goldstein B (2018) Direct visualization of a native Wnt in vivo reveals that a long-range Wnt gradient forms by extracellular dispersal. eLIFE 7:e38325.

Parkinson W, Dear ML, Rushton E, Broadie K (2013) N-glycosylation requirements in neuromuscular synaptogenesis. Development 140(24):4970-81.

Parkinson WM, Dookwah M, Dear ML, Gatto CL, Aoki K, Tiemeyer M, Broadie K (2016) Synaptic roles for phosphomannomutase type 2 in a new Drosophila congenital disorder of glycosylation disease model. Dis Model Mech 9:513-27.

Parnas D, Haghighi AP, Fetter RD, Kim SW, Goodman CS (2001) Regulation of Postsynaptic Structure and Protein Localization by the Rho-Type Guanine Nucleotide Exchange Factor dPix. Neuron 32(3):415-24.

Peng HB, Xie H, Rossi SG, Rotundo RL (1999) Acetylcholinesterase Clustering at the Neuromuscular Junction Involves Perlecan and Dystroglycan. JCB 145(4):911.

Ren Y, Kirkpatrick CA, Rawson JM, Sun M, Selleck SB (2009) Cell Type-Specific Requirements for Heparan Sulfate Biosynthesis at the Drosophila Neuromuscular Junction:

Effects on Synapse Function, Membrane Trafficking, and Mitochondondrial Localization. J Neurosci 29(26):8539-50.

Saksela O, Moscatelli D, Sommer A, Rifkin DB (1988) Endothelial cell-derived heparan sulfate binds basic fibroblast growth factor and protects it from proteolytic degradation. J Cell Biol 107(2):743-51.

Sarrazin S, Lamanna WC, Esko JD (2011) Heparan Sulfate Proteoglycans. Cold Spring Harb Perspect Biol 3(7):a004952.

Schnepp A, Lindgren PK, Hülsmann H, Kröger S, Paulsson M, Hartmann U (2005) Mouse Testican-2 Expression, Glyocosylation and Effects on Neurite Outgrowth. J Biol Chem 280(12):11274-80.

Schuster CM, Ultsch A, Schloss P, Cox JA, Schmitt B, Betz H (1991) Molecular cloning of an invertebrate glutamate receptor subunit expressed in *Drosophila* muscle. Science 254(5028)112-4.

Sears JC, Broadie K (2018) Fraile X Mental Retardation Protein regulates activity-dependent membrane trafficking and trans-synaptic signaling mediated synaptic remodeling. Front Mol Neurosci 10:440.

Shilts J, Broadie K (2017) Secreted tissue inhibitor of matrix metalloproteinase restricts *trans*-synaptic signaling to coordinate synaptogenesis. J Cell Sci 130(14):2344-58.

Speese SD, Ashley J, Jokhi V, Nunnari J, Barria R, Li Y, Ataman B, Koon A, Chang Y-T, Li Q, Moore MJ, Budnik V (2012) Nuclear Envelope Budding Enables Large Ribonucleoprotein Particle Export during Synaptic Wnt Signaling. Cell 149(4):832-46.

Stewart RA, Ramakrishnan A-B, Cadigan KM (2019) Diffusion and function of Wnt ligands. PLoS Genet 15(6):e1008154.

Takada S, Fijumori S, Shinozuka T, Takada R, Mii Y (2017) Differences in the secretion and transport of Wnt proteins. J Biochem 161(1):1-7.

Torroja L, Packard M, Gorczyca M, White K, Budnik V (1999) The *Drosophila* ß-Amyloid Precursor Protein Homolog Promotes Synapse Differentiation at the Neuromuscular Junction. J Neurosci 19(18):7793-803.

Tsuda M, Kamimura K, Nakato H, Archer M, Staatz W, Fox B, Humphrey M, Olson S, Futch T, Kaluza V, Siegfried E, Stam L, Selleck SB (1999) The cell-surface proteoglycan Dally regulates Wingless signalling in *Drosophila*. Nature 400:276-80.

Vannahme C, Schübel S, Herud M, Gösling S, Hülsmann H, Paulsson M, Hartmann U, Maurer P (1999) Molecular Cloning of Testican-2: Defining a Novel Calcium-Binding Proteoglycan Family Expressed in Brain. J Neurochem 73(1):12-20.

Wagh DA, Rasse TM, Asan E, Hofbauer A, Schwenkert I, Dürrbeck H, Buchner S, Dabauvalle M-C, Schmidt M, Qin G, Wichmann C, Kittel R, Sigrist S, Buchner E (2006) Bruchpilot, a Protein with Homology to ELKS/CAST, Is Required for Structural Integrity and Function of Synaptic Active Zones in *Drosophila*. Neuron 49(6):833-44.

Yan D, Wu Y, Feng Y, Lin S-C, Lin X (2009) The Core Protein of Glypican Dally-Like Determines Its Biphasic Activity in Wingless Morphogen Signaling. Dev Cell 17:470-81.

Yook KJ, Proulx SR, Jorgensen EM (2001) Rules of Nonallelic Noncomplementation at the Synapse in *Caenorhabditis elegans.* Genetics 158(1):209-20.

Zecca M, Basler K, Struhl G (1996) Direct and Long-Range Action of a Wingless Morphogen Gradient. Cell 87(5):833-44.

Zhai L, Chaturvedi D, Cumberledge S (2004) *Drosophila* Wnt-1 Undergoes a Hydrophobic Modification and Is Targeted to Lipid Rafts, a Process That Requires Porcupine. JBC 279(32):33220-7

CHAPTER V

Conclusions and Future Directions

The characterization of extracellular regulators of Wg signaling formed the foundation of this dissertation work. In mammals, a wide range of secreted Wnt antagonists exist, including the Dickkopf proteins (Dkk; Glinka et al., 1998; Niehrs, 2006), Wise/sclerostin domain-containing 1 (SOSTDC1; Itasaki et al., 2003), insulin-like growth-factor binding protein 4 (IGFBP-4; Cruciat and Niehrs, 2013), secreted Frizzled-related proteins (sFRPs; Leyns et al., 1997; Wang et al., 1997), Wnt-inhibitory factor 1 (WIF-1; Hsieh et al., 1999) and Cerberus (Bouwmeester et al., 1996; Piccolo et al., 1999). Dkk, SOSTDC1 and IGFBP inhibit Wnt signaling by binding to LRP5/6 to disrupt Fz-LRP dimerization, therefore specifically reducing canonical signaling. sFRPs, WIF and Cerberus bind Wnt directly, and therefore inhibit both canonical and noncanonical signaling. The Wnt agonists R-spondin (RSPO) and Norrin promote signaling by binding to Wnt receptors or releasing a Wnt-inhibitory step (de Lau et al., 2011; Ke et al., 2013). Surprisingly, no *Drosophila* homologs have been found for any of these Wnt regulators, despite strong conservation of intracellular mechanism. I therefore focused my work on two *Drosophila* Wg-binding extracellular regulators with mammalian homologs; Notum and Carrier of Wingless (Cow), specifically in a neuronal context where two non-canonical Wnt pathways modulate the proper structure and function of NMJ synapses.

Overall, my data strongly supports that Cow and Notum work through Wg to affect the structure and function of the neuromuscular junction (NMJ). I've shown here that Notum is secreted from muscle and glia, while Cow is secreted from neurons, and that both serve to downregulate Wg signaling. Most synaptic phenotypes of *notum* and *cow* mutants recapitulate

Wg overexpression including overabundance of type 1b boutons/synapses and elevated neurotransmission. I have also discovered new phenotypes in *notum* nulls not previously described to be linked to Wg signaling, such as defects in the presynaptic synaptic vesicle (SV) cycle and bulk endocytosis. This body of work characterizes two extracellular Wg regulators with previously unknown neuronal functions. The mechanistic details whereby Cow and Notum reduce Wg signaling at the NMJ remain to be further explored.

Mechanisms of Notum Function

My work established Notum as a negative extracellular Wg regulator at the NMJ suggesting a similar function to other tissues and models. I found that removing Notum caused an increase in Wg ligand in the NMJ synaptomatrix and expanded terminals comprised of more synaptic boutons and synapses. To directly test if synaptic phenotypes were due to an increase in Wg signaling, I genetically reduced Wg in the $Notum^{KO}$ mutant to test for the suppression of selected defects. I tested extracellular Wg levels and found that removing a copy of *wg* (*wg*/+ heterozygote) in the $Notum^{KO}$ background reduced the levels of Wg back to control. Furthermore, the increase in synaptic boutons characterizing $Notum^{KO}$ animals was suppressed by removing a copy of *wg*. These *notum* null NMJ phenotypes are accompanied by alterations in components of the Wg signaling pathway that may point toward a specific mechanism of Notum in Wg signaling. Follow-up experiments are needed to solidify the enzymatic activity of Notum and its specific position within the Wg signaling pathway at the NMJ.

Postsynaptically, Wg signaling results in cleavage of the Fz2 C-terminus and translocation into muscle nuclei (Mathew et al., 2005). Using a Fz2-C antibody, I found a decrease of the Fz2 receptor at the postsynaptic membrane and concomitant increase of Fz2-C in postsynaptic nuclei. These experiments show that loss of Notum causes a build-up and/or stabilization of Wg in the extracellular synaptomatrix at the NMJ. This allows a larger portion of Wg to bind Fz2 receptors, mediating an increase in receptor internalization (less receptor at the

membrane) and more Fz2-C traveling to the nucleus (increase in Fz2C nuclear punctae). Notum molecular function was first described in the wing disc as a lipase cleaving the GPI anchor of glypican HSPGs (Kreuger et al., 2004) and to release glypicans from the surface of mammalian cells (Traister et al., 2008). However, this role would affect signaling by many ligand classes, and Notum appeared to specifically affects Wg signaling (Flowers et al., 2012; Giráldez et al., 2002; Gerlitz and Basler, 2002; Petersen and Reddien, 2011; Torisu et al., 2008). This discrepancy was recently explained when the Notum crystal structure was resolved (Kakugawa et al., 2015). A hydrophobic pocket was characterized near the catalytic triad that can fit a 16-carbon lipid. The palmotoleic acid appended to Wg fits into this pocket precisely, and is cleaved by the adjacent enzymatic active site (Kakugawa et al., 2015). Importantly, it was found that Notum has an HSPG-binding motif and can bind to the synaptic glypican Dally-like protein (Dlp), but does not cleave this co-receptor (Kakugawa et al., 2015). In summary, Notum has been shown to cleave the Wg palmotoleic acid group in an HSPG-assisted mechanism.

The enzymatic activity of Notum on Wg gives insight into its ability to control Wg signaling. The lipid moiety on Wg interacts with the receptor Fz2, so cleaving it renders Wg less able to bind Fz2 and therefore decreases Wg signaling (Janda et al., 2012). At the NMJ, it is important to determine whether this is the mechanism of action for Notum. One way to test the enzymatic role of Notum (a carboxylesterase) is by adding a known carboxylesterase to a larval preparation and testing if Wg is downregulated. A complementary strategy would be to add in the lipid that is attached to Wg (palmitoleic acid) to a larval preparation dissolved in a solvent such as DMSO (compared to a DMSO control). If it competes with Notum, we would expect an increase in Wg signaling. Alternatively, a more directed genetic approach could be used. Palmitoleic acid is attached to Wg at a serine residue at position 239 (Zhai et al., 2004). Previously, co-immunoprecipitation (co-IP) was used to examine complex formation between WgS239A (an amino acid substitution that results in Wg lacking palmitoleic acid) and Fz2, to reveal a 90% reduction in receptor binding (Tang et al., 2012). Importantly, WgS239A is still secreted normally,

so the results are not due to a decrease in Wg exocytosis. Using WgS239A as the genetic background, increasing or decreasing Notum should not modulate the Wg phenotypes observed at the NMJ in WgS239A alone because it no longer has a substrate to act on. Overall, these experiments would address if Notum acts enzymatically as a carboxylesterase on Wg at the NMJ.

In addition to understanding how Notum acts to regulate Wg, it is important to know what induces Notum expression at the NMJ. Published studies suggest that Notum is a negative feedback inhibitor; if Wg signaling is high, it induces Notum expression, which then turns off Wg signaling (Gerlitz and Basler, 2002; Giráldez et al., 2002). We have not yet tested this idea at the NMJ, but recalling the FNI pathway, there is a plausible method by which this could be done. In the FNI pathway, Wg binding to the Fz2 causes the ligand-receptor complex to get endocytosed (Mathew et al., 2005). The Fz2 C-terminus then gets proteolytically cleaved and translocates to the nucleus. Nuclear Fz2-C binds to mRNAs to form RNPs, which can travel towards postsynaptic sites (Speese et al., 2012). Here, the mRNAs are thought to undergo local translation to assist with the formation and plasticity of NMJ synaptic connections. Could these nuclear RNPs contain *notum* mRNA? This idea could be tested using the Fz2-C antibody, doing an IP pulldown, and performing reverse transcription PCR with probes specific to *notum* RNA. This method has already been employed to identify the mRNAs present in Fz2-C foci (Speese et al., 2012), although a complete list was not published. If *notum* RNA is present, this mechanism would allow the postsynaptic cell to respond to increased Wg signaling by upregulating translation of Notum, thus achieving negative feedback inhibition of Wg signaling.

The poor quality and sparse quantity of the Fz2-C antibody limits the study of Fz2C/RNA interactions. With the development of increasingly sophisticated genetic tools such as the clustered regularly interspaced short palindromic repeats (CRISPR)/Cas9 system, a better tool could be produced to study Fz2-C/RNA foci. Specifically, the new native and tissue-specific fluorescence (NATF) strategy could be employed, combining CRISPR/Cas9 with split-GFP reconstitution to yield bright, cell-specific protein labeling (Siwei et al., 2019). The larger part

of GFP containing the first 10 β-strands (GFP1-10) and the smaller part containing the last β-strand (GFP11) can spontaneously interact to form a highly stable GFP. GFP11 is only 16 amino acids, so many copies can be added to a protein and not interfere with the protein function (Siwei et al., 2019). The multiple GFP copies result in a much brighter fluorescent signal. Several copies of GFP11 could be inserted in tandem at the genomic locus of Fz2 at the C-terminus using CRISPR/Cas9, and GFP1-10 could be expressed with a nuclear localization signal (NLS). Only when Fz2-C enters the nucleus will the split-GFP combine to form a fully functional (fluorescent) GFP. To perform immunoprecipitation experiments, an antibody that recognizes only the complete GFP molecule could be used (Doll et al., 2017). The advantages of this new tool are higher signal/noise ratio, signal amplification so it can be used with live imaging, and avoiding continuous reliance on a quickly depleting Fz2-C antibody reserve.

Notum and HSPG Dlp

Another important question that arose from this work is whether Notum functions cooperatively with other Wg regulators at the NMJ. Early Notum reports suggested that Notum works as a phospholipase to release GPI-anchored proteins from the cell surface to affect Wg signaling (Kreuger et al., 2004; Traister et al., 2008). However, a more recent report could not replicate those results and suggested that instead, Notum works in concert with the GPI-anchored HSPG Dlp to suppress Wg signaling (Kakugawa et al., 2015). To test whether Notum acts by cleaving the GPI anchor of Dlp, supporting early published reports, we could add phosphatidylinositol-specific phospholipase C (PI-PLC; cleaves GPI anchors) to a larval preparation and test whether NMJ structure and function phenocopies Notum OE. However, this cleaves all GPI anchors and is not specific to Dlp. Furthermore, it might affect Dlp localization. We could take a genetic approach and generate a transgenic line in which the Dlp GPI anchor is replaced with a transmembrane domain (*Dlp*$^{-GPI}$) and test whether NMJ structure and function

phenocopies *Notum*^{KO}. Moreover, overexpressing Notum in the *Dlp*$^{-GPI}$ genetic background would not be expected to have any additional effect compared to *Dlp*$^{-GPI}$ alone.

Another possibility is that Dlp is acting as a scaffold to co-localize Notum and Wg in the extracellular synaptomatrix. Notum binds to the glycosaminoglycan (GAG) chains on the Dlp co-receptor and Wg binds directly to Dlp (Yan et al., 2009). Therefore, Dlp may be required to localize Notum near Wg to perform its enzymatic function. To test whether Dlp is needed for co-localization of Notum and Wg, we could utilize the proximity ligation assay (PLA; Gustafsdottir et al., 2005). This technique is used to detect *in situ* protein-protein interactions, with two primary antibodies recognizing specific proteins of interest that are predicted to interact. Secondary antibodies coupled with oligonucleotides (PLA probes) bind to the primary antibodies. If the PLA probes are in close enough proximity (40nm), connector oligos join the PLA probes and ligate. The resulting circular DNA template gets amplified via DNA polymerase and complementary detection oligos coupled to fluorophores hybridize to the amplicon. Since Notum binds Dlp heparan sulfate (HS) chains (Kakugawa et al., 2015), and the Dlp core protein contributes to the main activity of Dlp in Wg signaling (Yan et al., 2009), we could use a Dlp genetically modified without HS chains (*Dlp*$^{-HS}$; Yan et al., 2009) to test PLA with antibodies against Notum and Wg. We would expect for controls to produce a PLA signal if Dlp is working as a scaffold to co-localize Notum and Wg. *Dlp*$^{-HS}$ would not be expected to interrupt Wg localization much on its own, so if the PLA signal is lost, we would conclude that Dlp HS chains are needed to localize Notum near Wg.

Notum specificity for Wg at the NMJ

The interaction of Dlp, Wg and Notum may serve to give Notum specificity to Wg instead of other Wnt proteins at the NMJ. Notum cleaves palmitoleic acid, and all known Wnts (except Wnt8) undergo palmitoylation (Ching et al., 2008). Thus, in theory, Notum should act on most Wnt ligands. Supporting this promiscuity, the coordinated movement defect seen in *Notum*^{KO} was only partially rescued by removal of one copy of *wg*; the animals were still faster than matched controls,

but significantly slower than *Notum*^{KO} alone. All other tested *Notum*^{KO} phenotypes were recapitulated with Wg OE. Therefore, we propose that Notum acts specifically on Wg at the NMJ, but on multiple Wnts throughout the body to influence whole-animal behavior such as movement speed. The *Drosophila* NMJ is a good model to test this hypothesis because Wg, Wnt2 and Wnt5 have separable synaptic roles (Packard et al., 2002; Liebl et al., 2010; Liebl et al., 2008). If Notum acted on all Wnts in a similar manner, then all Wnt signaling should be enhanced with the loss of Notum. My results showed Wg ligand increases in the absence of Notum. Future experiments could address whether this is true for Wnt2 and Wnt5.

The literature suggests that Notum may not act on all Wnts at the NMJ. For example, Wnt2 negatively regulates branch number (Liebl et al., 2010). The expected phenotype in a *Notum* mutant would be more Wnt2 signaling and therefore less branches, which is the opposite of what we observe. If Notum acted equally on Wg and Wnt2 in this context, we might expect no change in branch number in a *Notum* mutant. Even if Notum is capable of cleaving each Wnt palmitoylation, perhaps Notum specifically cleaves only Wg at the NMJ, and this might be accomplished by the timing of expression, concentrations of each ligand, differing affinities for each Wnt, or localization. Supporting the localization hypothesis, as discussed above, Dlp binds both Wg and Notum (Yan et al., 2009; Kakugawa et al., 2015), so it is conceivable that Dlp acts as a scaffold to keep Notum localized near Wg and away from other Wnts in the NMJ synaptomatrix. Alternatively, Notum may not affect Wnt2/5 signaling because it's unknown whether the lipid appended to Wnt2/5 is required for signaling. The palmitoylation has only been implicated as crucial for the Wnt/Fz2 complex, and the receptor for Wnt2 is currently unidentified (but doesn't appear to be Fz, Fz2 or Fz3), and the receptor for Wnt5 is Derailed (Drl; Liebl et al., 2008; Liebl et al., 2010; Koles and Budnik, 2012).

Notum Regulation of Bouton Segregation

Further supporting the specificity of Notum for Wg, both *Notum*^{KO} and Wg OE shared a novel "bouton cluster" phenotype (Chapter II) that hasn't been described for other NMJ Wnts. Normally, boutons are arranged as easily discernable "beads on a string". In contrast, mutant boutons were no longer easily distinguishable. When visualized at the electron microscopy (EM) level, each bouton is seen surrounded by subsynaptic reticulum (SSR) membrane folds, with ~75% of SSR profiles containing 1 bouton. In contrast, with *Notum* loss only ~25% or SSR profiles contain 1 bouton and up to 6 boutons were present in a single SSR profile. Interestingly, the multiple boutons per SSR profile were reduced in cross-sectional area per bouton, but when total bouton areas per SSR were combined, mutants were indistinguishable from controls. These results suggest Notum has a role in synaptic bouton segregation. This phenotype may be caused by cytoskeletal dysregulation. Wg has been shown to regulate the cytoskeleton through the microtubule associated protein 1b (MAP1B) homolog Futsch (Miech et al., 2008). Typically, Futsch phenotypes are measured using a Futsch antibody to label the NMJ and then the boutons are classified into categories based on the morphology of Futsch (bundled, splayed, punctate, or looped). In *wg* mutants, there was a decrease in NMJ boutons containing a loop (Packard et al., 2002). Based on this phenotype, we tested Futsch loop morphology in *notum* mutants and Wg OE, but saw no differences in loops (Fig. S3). It would be worthwhile to follow up on whether the bouton segregation phenotype is due to presynaptic cytoskeletal changes, perhaps regulated by a protein other than Futsch.

One protein that might be involved in cytoskeletal reorganization contributing to bouton separation is the actin-associated protein Cortactin (Cttn). Cttn has been recently implicated in morphological modifications associated with synaptic plasticity (Alicea et al., 2017). Cortactin promotes actin polymerization and stabilizes branched actin structures (Urono et al., 2001). Rapid, activity-dependent bouton formation has been visualized at the *Drosophila* NMJ using an acute activity paradigm, and this is dependent on Wg signaling (Ataman et al., 2008). Wg and

Cttn levels significantly increase following this activity paradigm in control animals, but not in *wg* mutant animals. In summary, Wg signaling is required for the increase of synaptic Cttn provoked by stimulation, which in turn promotes bouton growth by the regulation of actin dynamics. We could test for suppression of the bouton separation phenotype in *cttn, notum* double mutants. Further studies are crucial to address precise Notum functions in bouton formation and separation both during development and during activity-dependent synaptic plasticity modifications.

Notum Regulation of SV Cycle and Bulk Endocytosis

Accompanying the structural defects in bouton morphology, I found several functional defects related to the SVs in Notum mutants. First, I used the FM dye technique to explore SV cycling. FM dye is a lipophilic dye that is highly fluorescent when incorporated into membranes and gets trapped inside newly-formed SVs (Betz et al., 1992). I induced activity in control and *Notum* mutant animals to activate SV cycling, including SV fusion (exocytosis) and the reuptake of adjacent membrane to replenish the SV pool (endocytosis). I found that *Notum* mutants load less dye after stimulation. Since this defect is only a snapshot in time, it could indicate that either fewer SVs formed (i.e. cycle is slower) or more SVs released (i.e. cycle is faster). To test these possibilities, I re-stimulated the same NMJs in the absence of dye. This causes exocytosis (dye release) and a resulting decrease in fluorescence. Both controls and *Notum* mutants appeared comparable in the level of synaptic FM-143 exocytosis. Null *Notum* boutons had less dye to release, so I measured the unload/load dye ratio and found it was unchanged, indicating that the SV cycling rate is slower in the absence of Notum and/or the endocytosis part of the SV cycle is defective.

I turned to the high resolution of electron microscopy (EM) in order to gain more insight into the SVs and potential endocytosis defects in Notum mutants. In EM studies, SVs were much less abundant in $Notum^{KO}$, with a significant decrease in SV density. Typically, control synaptic boutons are full of uniform SVs (~50nm in diameter), with occasional enlarged vacuoles (>70nm). These vacuoles were much larger in the absence of Notum. The large presynaptic membrane

vacuoles observed in *Notum* mutants are almost certainly not SVs, but are rather reminiscent of bulk endosomes (Clayton and Cousin, 2009). Bulk endocytosis is activated specifically during intense stimulation, i.e. high-frequency trains of action potentials (Clayton et al., 2008). During this activity-dependent process, a large area of presynaptic plasma membrane is internalized to compensate for the rapid loss of membrane that just occurred due to high-frequency SV fusion. Many SVs can subsequently bud off from bulk endosomes to be added back to cycling or reserve SV pools (Clayton and Cousin, 2009).

The Rolling Blackout (Rbo) protein is absolutely required for bulk endocytosis at the *Drosophila* NMJ (Vijayakrishnan et al., 2009). To test whether the vacuoles are indeed bulk endosomes, double mutants with the conditional temperature-sensitive mutant rbo^{ts} could be studied (*Notum,* rbo^{ts}). If indeed the vacuoles observed in *Notum* mutants are bulk endosomes, then removing Rbo should suppress their appearance. Since this is a temperature-sensitive mutant, conditional studies with tight temporal control can be conducted. *Notum* mutants are certainly faster in a coordinated movement rollover assay, which implies their NMJs are more active, and this may explain the increased bulk endosome formation. Movement assays could also be conducted in the *Notum,* rbo^{ts} double mutants. Finally, to link the SV cycling alterations in Notum mutants to SV density and enlarged vacuole phenotypes seen with EM, I could employ a live time-course of FM dye loading with parallel diaminobenzidine photoconversion to visualize dye-loaded SVs with the resolution of EM (Fig. 18; Long et al., 2010; Parkinson et al., 2013).

Mechanisms of Cow Function

How hydrophobic Wg is transported from its presynaptic release sites to receptors on either side of the synaptic cleft is not clear. To understand extracellular Wg movement regulation at the NMJ we investigated Cow, a secreted HSPG previously characterized in Wg transportation in the developing wing disc (Chang and Sun, 2014). Cow was named “carrier of wingless” because of its role in binding and transporting Wg through the extracellular space. Cow was

shown to enhance the rate of extracellular movement of Wg, dependent on the presence of Cow HS chains (Chang and Sun, 2014). Loss of Cow affected Wg-dependent target gene expression in a biphasic pattern. For a short-range target (Neur), *cow* had the opposite effect of Wg signaling, while for a long-range target (Dll), *cow* had the same effect as Wg signaling (Zecca et al., 1996; Chang and Sun, 2014). This was reconciled with a model that Cow serves to carry Wg away from source cells (Wg-producing) to distant target cells (Wg-receiving). In the absence of Cow, Wg builds up at the source to cause an increase in short-range signaling and since it can no longer travel, a decrease in long-range signaling. We addressed here whether Cow similarly acts on Wg transport at the *Drosophila* NMJ.

Our original hypothesis was that Cow may function to carry the Wg ligand across the synapse cleft, consistent with the published molecular function (Chang and Sun, 2014). More specifically, we hypothesized that Cow and Wg are both secreted from the neuronal presynaptic terminal, Cow binds to Wg at the membrane, the complex traverses the synaptomatrix, and Cow then hands off Wg to Fz2 receptors on postsynaptic muscle cells. If this were the case, we would expect an increase in presynaptic Wg signaling and a decrease in postsynaptic Wg signaling in *cow* mutants. We indeed observed the predicted increase in presynaptic Wg signaling (assayed by presynaptic bouton growth). Extracellular Wg ligand itself doesn't change much, but the slight decrease could be a result of more Wg signaling occurring (more intracellular, less extracellular; Fig. S6). The only postsynaptic read-out we measured was GluR clustering, with an increase in clustering, suggesting that perhaps postsynaptic Wg was not decreased as hypothesized (Kerr et al., 2014). However, in the future it will be interesting to assay postsynaptic signaling directly, with either the Fz2C antibody (Mathew et al., 2005) or the split-GFP genetic assay (Siwei et al., 2019) mentioned in a previous section to test nuclear signaling via the FNI pathway. Alternatively, Cow may serve to negatively regulate both pre- and postsynaptic Wg signaling by carrying Wg away from the synapse (e.g. to a perisynaptic space to be endocytosed or degraded).

We hypothesized that since Wg traversing the synaptic cleft is short-range, in the absence of Cow, Wg would build up at the neuronal source to cause an increase in signaling in the presynaptic cells (Wg-producing). I utilized a *cow* null mutant (cow^{GDP}) to test for NMJ defects in the complete absence of Cow. I began by testing for Wg phenotypes in NMJ presynaptic structure. Loss of *wg* causes a decrease in synaptic bouton formation, while Wg OE causes an opposite increase in bouton numbers (Packard et al., 2002; Kopke et al., 2017). With the loss of Cow, I observed an increase in the number of synaptic boutons at individual NMJs compared to matched controls, a phenocopy of Wg OE. How is Cow negatively regulating Wg? In published work, Cow is proposed to bind Wg to regulate its extracellular distribution (Chang and Sun, 2014). To test if Wg has to be freely diffusible for Cow to act on it at the NMJ, we took advantage of a genetic tool "NRT-Wg", in which the transmembrane domain of neurotactin (NRT) is fused to Wg to tether the ligand to the membrane (Alexandre et al., 2014). Wg was excised from its genetic locus and this construct put in its place, so all of the encoded Wg is membrane-tethered and expressed at endogenous levels under native control. We tested what happens to secreted, extracellular Wg at the synapse when this construct is expressed, and we found a significant increase in Wg levels. Surprisingly, this did not have any effect on bouton number, suggesting that although more Wg is present, it is less efficient at signaling. When this tethered Wg was recombined with a *cow* null, we no longer observed an increase in bouton number that characterizes the *cow* mutant. This result indicates that Wg has to be secreted into the synaptomatrix for Cow to act on it, and supports the evidence from other tissue contexts that Cow normally physically carries Wg away (Chang and Sun, 2014), rather than other possible negative regulation mechanisms, such as masking or sequestering.

Our results indicate that extracellular Wg increases when Wg is tethered to the membrane, yet there is no increase in presynaptic Wg signaling, which leads us to believe that tethered Wg is less efficient at signaling (Chaudhary et al., 2019). Tethering Wg to neurons should eliminate all postsynaptic Wg signaling. However, we do not know if tethered Wg can reach across the

synaptic cleft to initiate signaling. In addition, it has been shown that active Wnt proteins can be secreted on exosomes (Gross et al., 2012). Exosomes containing Wg are secreted from neurons to facilitate *trans*-synaptic signaling at the *Drosophila* NMJ, presumably via fusion of multivesicular bodies with the plasma membrane (Korkut and Ataman et al., 2009). Finally, filopodia are thin, actin-based extensions of the plasma membrane, and cytonemes are filopodia specialized for exchange of signaling proteins, which have been observed at *Drosophila* NMJs (Ramírez-Weber and Kornberg, 1999; Ritzenthaler et al., 2000). If any of these mechanisms are at play in the Wg signaling context, then tethering Wg to the neuronal membrane may not block postsynaptic Wg signaling. Nevertheless, tethering Wg to the membrane prevents the *cow* mutant phenotype.

Cow Protein Domains

Despite work characterizing the role of Cow controlling Wg movement through the extracellular space, nothing is known about other possible functions of Cow that may be mediated by interactions between Cow and other proteins. Characterized Cow protein domains include Kazal and thyroglobulin type-1 (www.flybase.org), which are both predicted proteinase inhibitor domains (Laskowski and Kato, 1980). According to the MEROPS database, the Cow protein most likely inhibits peptidases from the papain-like cysteine peptidase superfamily (Rawlings et al., 2018). Interestingly, soluble wingless-interacting molecule (Swim) is another member of this same family (www.flybase.org). However, the lack of a conserved residue in the active site of Swim probably renders it enzymatically inactive as a peptidase (Mulligan et al., 2012). Like Cow, Swim is secreted and extracellular, and expressed at high levels in the *Drosophila* larval nervous system (www.flybase.org). Swim was named for its ability to bind the Wg ligand with nanomolar affinity. Wg itself is insoluble, but remains in solution when increasing amounts of Swim are added (Mulligan et al., 2012). Swim is a putative member of the lipocalin family that facilitate transport of hydrophobic proteins.

Wg has two attached hydrophobic lipids, so it needs to be shielded from the aqueous extracellular environment to move away from the membrane (Takada et al., 2017). Swim is proposed to shield the palmitate moiety at C93, to maintain Wg solubility and promote long-range Wg signaling. Similar to Cow, reduction of Swim in larval wing discs decreased the range of extracellular Wg diffusion and lead to Wg LOF phenotypes (Mulligan et al., 2012; Chang and Sun, 2014). One issue with this model is that Swim did not affect short-range Wg signaling, and therefore would not be predicted to affect signaling across the narrow synaptic cleft (~20nm). Another possibility is that Cow interacts with Cathepsin B1; a paralog of Swim that is also extracellular and involved in lysosomal protein degradation, but with an unknown relationship to Wg (Burleigh et al., 1974; www.flybase.org). However, interestingly, it has been shown that Wg is degraded in lysosomal compartments (Piddini et al., 2005). In summary, Cow may negatively regulate Wg signaling indirectly; through inhibiting a promoter of Wg signaling (e.g. Swim) or by promoting a lysosomal Wg-degradation enhancer protein (e.g. Cathepsin B1). Physical interactions between and Cow and the above proteins can be tested using co-IP in WT and transgenic flies in which different Cow domains have been mutated. Genetic interaction tests between Cow and verified interactors can be performed to test for NMJ Wg phenotypes.

In addition to its protease inhibitor domains, Cow contains EF-hand calcium (Ca^{2+}) binding domains. Our cell-specific GAL4/UAS RNAi knockdown studies suggest that Cow is secreted from the neuronal side of the NMJ, which makes the Ca^{2+} binding domain of Cow particularly intriguing. Synapses are tightly reliant on Ca^{2+} signaling for all of their functions. Neurons express multiple classes voltage-dependent, calcium-selective ion channels that are important for synaptic transmission through the release of neurotransmitters into the synaptic cleft via SV fusion (Simons, 1988). The local depletion in calcium concentrations initiated by synaptic activity could be detected by Cow in the extracellular synaptomatrix and affect either its localization or function. Indeed, it has been shown that Ca^{2+} induces a large conformational change in Testican-2, the mammalian homolog of Cow (Vannahme et al., 1999). Activity reportedly stimulates the secretion

of Wg in a Ca^{2+}-dependent manner (Ataman et al., 2008). The conformational changes of Cow during differing Ca^{2+} concentrations might instruct binding to Wg in an activity-dependent manner. This could be tested by altering extracellular calcium levels and performing PLA with Cow and Wg to test for changes in co-localization. To test activity-dependence, the CcapR-GAL4 driver could be used (Jenett et al., 2014), which drives in only a subset of motor neurons, to drive expression of a UAS-channelrhodopsin (ChR). ChRs are a light-gated ion channels that can be used to activate neurons (Nagel et al., 2002). The light-exposed larvae could be analyzed for a PLA signal between Cow and Wg, and the degree of signal co-localization compared between the activated motor neurons versus the internal control motor neurons.

A final piece of insight about Cow interactors comes from the Cow homolog mammalian Testican-2 (gene name: SPOCK2), a member of the secreted protein acidic and rich in cysteine (SPARC) protein family. When SPARC was added to cultured cells, metalloproteinases (MMPs) were upregulated (Tremble, 1993). MMPs cleave secreted and membrane-associated targets to sculpt the extracellular environment and modulate intercellular signaling (Dear et al., 2016). Testican-1 and -3 inhibit MMPs, but, uniquely, Testican-2 abolishes this inhibition (Nakada et al., 2001; Nakada et al., 2003). Testican-2 inhibits MMP inhibitors to activate MMPs. Interestingly, secreted and membrane-anchored *Drosophila* MMPs are both expressed at the NMJ and their functions are required for proper structural and functional synaptic development (Dear et al., 2016). Removal of either MMP results in increased NMJ structure and function, indicating MMPs normally function to restrict bouton formation and neurotransmission strength. Furthermore, the mechanism of restriction is accomplished through the *trans*-synaptic Wg pathway (Dear et al., 2016). Fz2 receptor cleavage and Fz2C intracellular trafficking to the muscle nuclei are increased in both MMP mutants, indicating an increase in Wg signaling (Dear et al., 2016). We propose that Cow may function by promoting MMPs, which in turn restrict Wg *trans*-synaptic signaling. We could test this by overexpressing Cow and performing an in situ zymography assay measuring proteolytic activity. DQ gelatin is a fluorogenic substrate and upon

proteolytic digestion, the fluorescence is revealed as a readout of net enzymatic activity. This assay has been used to measure MMP activity (Dear et al., 2017). If Cow promotes MMP activity, we would predict an increase in gelatinase fluorescence and a decrease in Wg signaling.

Cow Interaction with Other HSPGs

The role of Cow's domains might be further complicated by the interactions of its HS chains. There are now 4 HSPGs known to be expressed at the NMJ: Cow, Dlp, Sdc, and Trol (Chang and Sun, 2014; Johnson et al., 2006; Kamimura et al., 2013). Do they interact? Are their functions overlapping, redundant or antagonistic? To study this question, mutants or RNAi lines for each gene could be used and then the expression levels of the others tested. I tested Sdc levels in a *cow* null and didn't find a change in abundance of signal coinciding with the neuron, however the distribution of the signal surrounding the boutons does appear to be increased (Fig. S7). Synaptic phenotypes could be measured using *trans*-heterozygotes to test genetic interactions. The failure of mutant alleles at two different loci to complement one another is the best evidence of *in vivo* interaction of the proteins in a common mechanism (nonallelic noncomplementation; Hawley and Gilliland, 2006; Yook et al., 2001). We have tested the interaction of Cow and Dlp in this way and found evidence for such nonallelic noncomplementation (Fig. S8). Bouton number is significantly increased in the *cow,dlp* double heterozygote in comparison to each single heterozygote alone. This result is somewhat surprising given that *dlp* mutants reportedly display no change in bouton number (Johnson et al., 2006). However, in the same study, it was found that Dlp OE was sufficient to decrease bouton number. My results indicate that Dlp and Cow negatively regulate bouton number through the same mechanistic pathway. The common mechanism is likely through Wg signaling, as our lab and others have shown that Dlp regulates Wg signaling (Dani et al., 2012; Yan et al., 2009).

Another example that indicates the interaction of HSPGs is the result that elevation of Dlp enhanced the Sdc bouton number phenotype, suggesting that there might be an antagonistic

relationship between the two HSPGs (Johnson et al., 2006). Both bind to the receptor LAR, with Dlp showing a greater affinity. Dlp was found to restrict active zone number while Sdc was found to promote synaptic bouton formation (Johnson et al., 2006). Due to its increased affinity, Dlp has a competitive advantage over Sdc for binding to LAR. Perhaps a pre-bound complex of Sdc and LAR could stimulate NMJ growth before inhibition by Dlp-LAR binding. This mechanism could provide a time- and/or HSPG concentration- dependent switch from bouton formation to active zone formation (Johnson et al., 2006). The Dlp glypican is expressed mostly in postsynaptic muscles, the transmembrane Sdc is expressed in presynaptic neurons, the secreted HSPG Trol is released from postsynaptic muscles, and the secreted Cow HSPG is released from presynaptic neurons. Clearly, the HSPG type and cellular source may both be vitally important, but there is much work to be done to elucidate the relevance of these characteristics and how several HSPGs interact in space and time at the developing NMJ synapse.

In addition to the HSPG timing of expression, concentration, distribution and extracellular presentation, the composition of the HSPG glycosaminoglycan (GAG) chains may be important determinants of their synaptic function. The nascent precursor heparan sulfate (HS) chain consists of glucuronic acid (GlcA) and *N*-acetylglucosamine (GlcNAc), which can then be substantially modified (Grobe, 2014). In the final HS chain, highly modified IdoA/GlcNS domains (*N*-sulfated; NS) alternate with largely unmodified GlcA/GlcNAc domains (*N*-acetylated; NA; Maccarana et al., 1996; Esko and Selleck, 2002). A recent study discovered that a member of the Wnt family, Wnt8, preferentially associates with NS domains in *Xenopus* (Mii et al., 2017). Wnt8 immunohistochemistry combined with live imaging of a fluorescently-tagged Wnt8 revealed a punctate distribution of Wnt at the cell boundary. Injection of heparitinase (cleaves HS) greatly reduced the punctate signals, suggesting that HS chains are responsible for the punctate distribution of Wnt (Mii et al., 2017). A similar heparitinase treatment has been employed at the NMJ and it also reduces Wg signal (Kamimura et al., 2013).

The organization of HS chains can be visualized by creating antibodies that specifically recognize one type (NA) or the other (NS). Surprisingly, NA and NS HS chains form distinct clusters, and Wnt8 co-localized only with the NS clusters (Mii et al., 2017). These findings suggest that NS HS clusters serve as pre-existing cores to accumulate Wnt ligand, recruit the Frizzled receptor, and then internalize and phosphorylate LRP6 to form signalosomes (Mii et al., 2017). In contrast, NA HS clusters accumulate Frzb, a member of the secreted Frizzled-related protein (sFRP) family of Wnt antagonists (Leyns et al., 1997; Wang et al., 1997). Fzb shifts Wnt association from NS HS to NA HS, preventing the internalization of Wnt8, and therefore preventing signaling (Mii et al., 2017). Overall, these N-acetyl-rich HS and N-sulfo-rich HS clusters constitute a cellular platform for the regulation of Wnt distribution and signaling together with Frzb. So far, no sFRPs have been identified in the *Drosophila* genome (Mii and Taira, 2011), but this could be a generalizable mechanism of HS modifications instructing the proper distribution of ligands and inhibitors along the plasma membrane. We could use these NA/NS antibodies at the NMJ to test if Wg is preferentially co-localized with either type, while co-labeling with Cow and/or Notum to test for any overlap.

Importance of Cellular Source

Through genetic interaction tests, we found that Cow and Notum act at the synapse on functionally related processes. Specifically, to test the Wg signaling mechanism, we combined a cow^{GDP} heterozygote with a $Notum^{KO}$ heterozygote, since we know Notum negatively regulates Wg signaling at the NMJ. If the double heterozygote (cow^{GDP}/+; $Notum^{KO}$/+) showed an enhanced phenotype, it would suggest that both proteins function together through Wg to cause the NMJ phenotypes (Hawley and Gilliland, 2006; Hays et al., 1989; Rancourt et al., 1994; Yook et al., 2001). We found that the single heterozygotes alone were both indistinguishable from the control, whereas the double heterozygote exhibited a large increase in NMJ synaptic bouton number, including additional phenotypes associated with aberrant Wg signaling (e.g. ghost boutons;

Ataman et al., 2006). These findings show a classic nonallelic noncomplementation interaction, strongly suggesting that Cow and Notum both work though the negative regulation of Wg signaling to control NMJ synaptic development. Taken together, these data suggest that Cow and Notum both serve to negatively regulate Wg signaling to control synaptic structure, function and molecular synapse composition at the *Drosophila* NMJ. Why does the NMJ need two negative Wg regulators? One reason could be separable functions of Wg regulation based on cell source (e.g. neuron vs. muscle vs. glia). We did see a lot of similarities; i.e. Cow and Notum both negatively regulate bouton number and neurotransmission strength. However, we also saw differences; i.e. Notum regulates bouton separation (clusters seen in mutants) while Cow regulates bouton growth (satellites seen in mutants), with both phenotypes observed upon Wg OE (Table 3).

Although it may be counterintuitive, published evidence suggests that ligand source is important for signaling function, and the same could be true for secreted ligand regulators. First, neural- vs. glial-derived Wg regulate distinct aspects of NMJ development (Packard et al., 2002; Kerr et al., 2014). For example, blocking neuronal Wg decreased synaptic bouton number but did not change SV fusion frequency, whereas blocking glial Wg had no effect on bouton number and increased fusion frequency. In contrast, both pools of Wg were needed to promote normal evoked neurotransmission amplitudes and organization of GluRIIA clusters (Kerr et al., 2014). Second, the glass bottom boat (Gbb) ligand secreted from both neurons and muscles is “tagged” based on source (James et al., 2014). Neural-derived Gbb regulates neurotransmission strength, while muscle-derived Gbb regulates NMJ growth. We have identified two Wg regulators, with my data suggesting that one is secreted from muscle and glia (Notum) and the other being secreted only from neurons (Cow). Interestingly, a muscle-specific Notum KD causes a change in bouton number and neurotransmission properties, while a glial-specific Notum KD causes the same structural phenotype, but does not change neurotransmission. Additionally, a neuronal-specific

Cow KD caused a change in bouton number, while a glial-specific Cow KD did not (Fig S9), however it will be important to test this genotype with functional assays in the future.

Final Conclusions

Taken together, this thesis work has shown Notum and Cow negatively regulate Wg signaling in a neuronal context during synaptogenesis at the *Drosophila* NMJ. In the absence of Notum or Cow, we observe defects in synaptic architecture and neurotransmission function that phenocopy the overexpression of Wg in neurons. We provide evidence that Wg can be locally inhibited in the synaptomatrix. For Notum, this is likely by reducing the ability of Wg ligand to interact with the Fz2 receptor. For Cow, this is likely by carrying Wg away from the neuronal secretion source to reduce signaling at the synapse. There is still much to be elucidated about the mechanism of Notum and Cow action in this synaptic context. For example, testing whether Wg signaling induces the expression of Notum to create a negative feedback loop, or if Cow interacts with other HSPGs to establish the correct distribution of the Wg ligand both basally and in response to neuronal activity. In Notum mutants, we identified phenotypes not previously linked to Wg signaling such as aberrant SV cycling and bulk endocytosis. In the future, it will be important to test if these functional and ultrastructural phenotypes can be induced by Wg OE and suppressed by reducing Wg in the *Notum* mutant background. Overall, this work identifies two new molecular players important for Wg regulation in the synaptomatrix.

A fascinating discovery has been the importance of secreted regulators within the NMJ extracellular synaptomatrix to control the signaling that drives synaptogenesis. This is very counter-intuitive, both based on the tiny width of the synaptic cleft (~20nm at *Drosophila* NMJ) and the need to “second guess” the tight regulative controls on both ligand secretion and receptor presentation. Why have this extensive ligand regulation in the extracellular space? The reason remains unclear. As a glutamatergic synapse, the *Drosophila* NMJ is arguably more similar to excitatory synapses of mammalian CNS than to mammalian NMJs (e.g. narrow cleft lacking a

basal lamina). In the mammalian brain, Wnt signaling dysregulation has severe pathological consequences, including neurodegenerative disease states (Libro et al., 2016). As an extracellular enzyme with a well-defined active site, Notum may be a target for chemical inhibition to ease conditions associated with deficient Wnt signaling (Kakugawa et al., 2015). Likewise, for the secreted HSPG Cow, it may be possible to target Wnt-HSPG binding interactions by developing drugs that would specifically affect the regulation of Wnt signaling. This could involve pharmaceutically targeting HSPG-modifying enzymes, rather than the HSPG itself. In summary, we hope that this work will shed light on possible treatments for patients with devastating neurological disorders in which Wnt signaling goes awry (Libro et al., 2016).

References

Alexandre C, Baena-Lopez A, Vincent J-P (2014) Patterning and growth control by membrane-tethered Wingless. Nature 505(7482):180-5.

Alicea D, Perez M, Moldonado C, Dominicci-Cotto C, Marie B (2017) Cortactin Is a Regulator of Activity-Dependent Synaptic Plasticity Controlled by Wingless. J Neurosci 37(8):2203-15.

Ataman B, Ashley J, Gorczyca D, Gorczyca M, Mathew D, Wichmann C, Sigrist SJ, Budnik V (2006) Nuclear trafficking of Drosophila Frizzled-2 during synapse development requires the PDZ protein dGRIP. PNAS 103(20):7841-46.

Ataman B, Ashley J, Gorczyca M, Ramachandran P, Fouquet W, Sigrist SJ, Budnik V (2008) Rapid Activity-Dependent Modifications in Synaptic Structure and Function Require Bidirectional Wnt Signaling. Neuron 57(5):705-18.

Betz WJ, Mao F, Bewick GS (1992) Activity-dependent fluorescent staining and destaining of living vertebrate motor nerve terminals. J Neurosci 12(2):363-75.

Bouwmeester T, Kim S, Sasai Y, Lu B, De Robertis EM (1996) Cerberus is a head-inducing secreted factor expressed in the anterior endoderm of Spemann's organizer. Nature 382(6592):595-601.

Burleigh MC, Barrett AJ, Lazarus GS (1974) Cathepsin B1: A Lysosomal Enzyme that Degrades Native Collagen. Biochem J 137:387-98.

Chang Y-H, Sun YH (2014) Carrier of Wingless (Cow), a Secreted Heparan Sulfate Proteoglycan, Promotes Extracellular Transport of Wingless. PLoS ONE 9(10):e111573.

Chaudhary V, hingole S, Frei J, Port F, Strutt D, Boutros M (2019) Robust Wnt signaling is maintained by a Wg protein gradient and Fz2 receptor activity in the developing *Drosophila* wing. Development 146(15):dev174789.

Ching W, Hang HC, Nusse R (2008) Lipid-independent Secretion of a *Drosophila* Wnt Protein. J Biol Chem 283(25):17092-8.

Clayton EL, Cousin MA (2009) The molecular physiology of activity-dependent bulk endocytosis of synaptic vesicles. J Neurochem 111:901-14.

Clayton EL, Evans GJO, Cousin MA (2008) Bulk synaptic vesicle endocytosis is rapidly triggered during strong stimulation. J Neurosci 28:6627-32.

Cruciat CM, Niehrs C (2013) Secreted and transmembrane wnt inhibitors and activators. Cold Spring Harb Perspect Biol 5(3):a015081.

Dani N, Nahm M, Lee S, Broadie K (2012) A targeted glycan-related gene screen reveals heparan sulfate proteoglycan sulfation regulates WNT and BMP trans-synaptic signaling. PLoS Genet 8:e1003031.

De Lau W, Barker N, Low TY, Koo BK, Li VS, Teunissen H, Kujala P, Haegebarth A, Peters PJ, van de Wetering M, Stange DE, van Es JE, Guardavaccaro D, Schasfoort RB, Mohri Y, Nishimori K, Mohammed S, Heck AJ, Clevers H (2011) Lgr5 homologues associated with Wnt receptors and mediate R-spondin signalling. Nature 476(7360):293-7.

Dear ML, Dani N, Parkinson W, Zhou S, Broadie K (2016) Two classes of matrix metalloproteinases reciprocally regulate synaptogenesis. Development 143:75-87.

Dear ML, Shilts J, Broadie K (2017) Neuronal activity drives FMRP- and HSPG-dependent matrix metalloproteinase function required for rapid synaptogenesis. Sci Signal 10(504).

Doll CA, Vita DJ, Broadie K (2017) Fragile X Mental Retardation Protein Requirements in Activity-Dependent Critical Period Neural Cicruit Refinement. Curr Biol 27(15):2318-30.

Esko JD, Selleck SB (2002) Order Out of Chaos: Assembly of Ligand Binding Sites in Heparan Sulfate. Annu Rev Biochem 71:435-71.

Flowers GP, Topczewska JM, Topczewski J (2012) A zebrafish Notum homolog specifically blocks the Wnt/β-catening signaling pathway. Development 139:2416-25.

Gerlitz O, Basler K (2002) Wingful, an extracellular feedback inhibitor of Wingless. Genes Dev 16:1055-59.

Giráldez AJ, Copley RR, Cohen SM (2002) HSPG modification by the secreted enzyme notum shapes the wingless morphogen gradient. Dev Cell 2:667-76.

Glinka A, Wu W, Delius H, Monaghan AP, Blumenstock C, Niehrs C (1998) Dickkopf-1 is a member of a new family of secreted proteins and functions in head induction. Nature 391(6665):357-62.

Grobe K (2014) N-Deacetylase/N-Sulfotransferase (Heparan Glucosaminyl) 1 (NDST1). Handbook of Glycosyltransferases and Related Genes 2:1091-103.

Gross JC, Chaudhary V, Bartscherer K, Boutros M (2012) Active Wnt proteins are secreted on exosomes. Nat Cell Biol 435(7038):58-65.

Gustafsdottir SM, Schallmeiner E, Fredriksson S, Gullberg M, Söderberg O, Jarvius M, Jarvius J, Howell M, Landegren U (2005) Proximity ligation assays for sensitive and specific protein analyses. Anal Biochem 345(1):2-9.

Hawley RS, Gilliland WD (2006) Sometimes the Result is Not the Answer: The Truths and the Lies That Come From Using the Complementation Test. Genetics 174(1):5-15.

Hays TS, Deuring R, Robertson B, Prout M, Fuller MT (1989) Interacting proteins identified by genetic interactions: a missense mutation in alpha-tubulin fails to complement alleles of the testis-specific beta-tubulin gene of Drosophila melanogaster. Mol Cell Biol 9(3):875-84.

Hsieh JC, Kodjabachian L, Rebbert ML, Rattner A, Smallwood PM, Samos CH, Nusse R, Dawid IB, Nathans J (1999) A new secreted protein that binds to Wnt proteins and inhibits their activities. Nature 398(6726):431-6.

Itasaki N, Jones CM, Mercurio S, Rowe A, Domingos PM, Smith JC, Krumlauf R (2003) Wise, a context-dependent activator and inhibitor of Wnt signaling. Development 130(18):4295-305.

James RE, Hoover KM, Bulgari D, McLaughlin CN, Wilson CG, Wharton KA, Levitan ES, Broihier HT (2014) Crimpy enables discrimination of presynaptic and postsynaptic pools of a BMP at the Drosophila neuromuscular junction. Dev Cell 31(5):586-98.

Janda CY, Waghray D, Levin AM, Thomas C, Garcia KC (2012) Structural basis of Wnt recognition by frizzled. Science 337:59-64.

Jenett A, Rubin GM, Ngo TTB, Shepherd D, Murphy C, Dionne H, Pfeiffer BD, Cavallaro A, Hall D, Jeter J, Iyer N, Fetter D, Hausenfluck JH, Peng H, Trautman ET, Svirskas RR, Myers EW, Iwinski ZR, Aso Y, DePasquale Gm, Enos A, Hulamm P, L SCB, Li HH, Laverty TR, Long F, Qu L, Murphy SD, Rokicki K, Safford T, Shaw K, Simpson JH, Sowell A, Tae S, Yu Y, Zugates CT (2012) A GAL4-Driver Line Resource for *Drosophila* neurobiology. Cell Rep 2(4):991-1001.

Johnson KG, Tenney AP, Ghose A, Duckworth AM, Higashi ME, Parfitt K, Marcu O, Heslip TR, Marsh JL, Schwarz TL, Flanagan JG, Van Vactor D (2006) The HSPGs Syndecan and Dallylike bind the receptor phosphatase LAR and exert distinct effects on synaptic development. Neuron 49(4):517-31.

Kakugawa S, Langton PF, Zebisch M, Howell SA, Chang TH, Liu Y, Feizi T, Bineva G, O'Reilly N, Snijders AP, Jones EY, Vicent JP (2015) Notum deacylates Wnt proteins to suppress signalling activity. Nature 519:187-92.

Kamimura K, Ueno K, Nakagawa J, Hamada R, Saitoe M, Maeda N (2013) Perlecan regulates bidirectional Wnt signaling at the Drosophila neuromuscular junction. JCB 200(2):219.

Ke J, Karikumar KG, Erice C, Chen C, Gu X, Wang L, Parker N, Cheng Z, Xu W, Williams BO, Melcher K, Miller LJ, Xu HE (2013) Structure and function of Norrin in assembly and activation of a Frizzled 4-LRP5/6 complex. Genes and Dev 27:2305-19.

Kerr KS, Fuentes-Medel Y, Brewer C, Barria R, Ashley J, Abruzzi KC, Sheehan A, Tasdemir-Yilmaz OE, Freeman MR, Budnik V (2014) Glial Wingless/Wnt regulates glutamate receptor clustering and synaptic physiology at the *Drosophila* neuromuscular junction. J Neurosci 34:2910-20.

Koles K, Budnik V (2012) Wnt Signaling in Neuromuscular Junction Development. Cold Spring Harb Perspect Biol 4:a008045.

Korkut C, Ataman B, Ramachandran P, Ashley J, Barria R, Cherbesi N, Budnik V (2009) Trans-Synaptic Transmission of Vesicular Wnt Signals through Evi/Wntless. Cell 139(2):393-404.

Kreuger J, Perez L, Giraldez AJ, Cohen SM (2004) Opposing activities of Dally-like glypican at high and low levels of Wingless morphogen activity. Dev Cell 7(4):503-12.

Laskowski M, Kato I (1980) Protein inhibitors of proteinases. Annu Rev Biochem 49:593-626.

Leyns L, Bouwmeester T, Kim SH, Piccolo S, De Robertis EM (1997) Frzb-1 is a secreted antagonist of Wnt signaling expressed in the Spemann organizer. Cell 88(6):747-56.

Libro R, Bramanti P, Mazzon E (2016) The role of the Wnt canonical signaling in neurodegenerative diseases. Life Sci 158:78-88.

Liebl FLW, Wu Y, Featherstone DE, Noordermeer JN, Fradkin L, Hing H (2008) Derailed regulates development of the Drosophila neuromuscular junction. Dev Neurobiol 68:152-65.

Liebl FLW, McKeown C, Yao Y, Hing HK (2010) Mutations in Wnt2 alter presynaptic motor neuron morphology and presynaptic protein localization at the Drosophila neuromuscular junction. PLoS ONE 5:e12778.

Long AA, Mahapatra CT, Woodruff EA 3rd, Rohrbough J, Leung HT, Shino S, An L, Doerge RW, Metzstein MM, Pak WL, Broadie K (2010) The nonsense-mediated decay pathway maintains synapse architecture and synaptic vesicle cycle efficacy. J Cell Sci 123(19):3303-15.

Maccarana M, Sakura Y, Tawada A, Yoshida K, Lindahl U (1996) Domain structure of heparan sulfates from bovine organs. J Biol Chem 271(30):17804-10.

Mathew D, Ataman B, Chen J, Zhang Y, Cumberledge S, Budnik V (2005) Wingless signaling at synapses is through cleavage and nuclear import of receptor DFrizzled2. Science 310:1344-47.

Miech C, Pauer HU, He X, Schwarz TL (2008) Presynaptic local signaling by a canonical wingless pathway regulates development of the *Drosophila* neuromuscular junction. J Neurosci 28:10875-84.

Mii Y, Taira M (2011) Secreted Wnt "inhibitors" are not just inhibitors: regulation of extracellular Wnt by secreted Frizzled-related proteins. Dev Growth Differ 53(8):911-23.

Mii Y, Yamamoto T, Takada R, Mizumoto S, Matsuyama M, Yamada S, Takada S, Taira M (2017) Roles of two types of heparan sulfate clusters in Wnt distribution and signaling in Xenopus. Nat Commun 8(1):1973.

Mulligan KA, Fuerer C, Ching W, Fish M, Willert K, Nusse R (2012) Secreted Wingless-interacting molecule (Swim) produces long-range signaling by maintaining Wingless solubility. Proc Natl Acad Sci USA 109(2):370-7.

Nagel G, Ollig D, Fuhrmann M, Kateriya S, Musti AM, Bamberg E, Hegemann P (2002) Channelrhodopsin-1: a light-gated proton channel in green algae. 296(5577):2395-8.

Nakada M, Yamada A, Takino T, Miyamori H, Takahashi T, Yamashita J, Sato H (2001) Suppression of membrane-type 1 matrix metalloproteinase (MMP)-mediated MMP-2 activation and tumor invasion by testican 3 and its splicing variant gene product, N-Tes. Cancer Res 61(24):8896-902.

Nakada M, Miyamori H, Yamashita J, Sato H (2003) Testican 2 abrogates inhibition of membrane-type matrix metalloproteinases by other testican family proteins. Cancer Res 63(12):3364-9.

Newman ZL, Hoagland A, Aghi K, Worden K, Levy SL, Son JH, Lee LP, Isacoff EY (2017) Input-Specific Plasticity and Homeostasis at the Drosophila Larval Neuromuscular Junction. Neuron 93(6):1388-404.

Niehrs C (2006) Function and biological roles of the Dickkopf family of Wnt modulators. Oncogene 25(57):7469-81.

Packard M, Koo ES, Gorczyca M, Sharpe J, Cumberledge S, Budnik V (2002) The *Drosophila* Wnt, Wingless, provides an essential signal for pre- and postsynaptic differentiation. Cell 111:319-30.

Parkinson W, Dear ML, Rushton E, Broadie K (2013) N-glycosylation requirements in neuromuscular synaptogenesis. Development 140:4970-81.

Petersen CP, Reddien PW (2011) Polarized notum activation at wounds inhibits Wnt function to promote planarian head regeneration. Science 332(6031):852-5.

Piccolo S, Agius E, Leyns L, Bhattacharyya S, Grunz H, Bouwmeester T, De Robertis EM (1999) The head inducer Cerberus is a multifunctional antagonist of Nodal, BMP and Wnt signals. Nature 397(6721):707-10.

Piddini E, Marshall F, Dubois L, Hirst E, Vincent JP (2005) Arrow (LRP6) and Frizzled2 cooperate to degrade Wingless in Drosophila imaginal discs. Development 132(24):5479-89.

Ramírez-Weber FA, Kornberg TB (1999) Cytonemes: cellular processes that project to the principal signaling center in Drosophila imaginal discs. Cell 97(5):599-607.

Rancourt DE, Tsuzuki T, Capecchi MR (1995) Genetic interaction between hoxb-5 and hoxb-6 revealed by nonallelic noncomplementation. Genes and Dev 9:108-22.

Rawlings ND, Barrett AJ, Thomas PD, Huang X, Bateman A, Finn RD (2018) The MEROPS database of proteolytic enzymes, their substrates and inhibitors in 2017 and a comparison with peptidases in the PANTHER database. Nucleic Acids Res 46(D1):D624-32.

Ritzenthaler S, Suzuki E, Chiba A (2000) Postsynaptic filopodia in muscle cells interact with innervating motoneuron axons. Nat Neurosci 3(10):1012-7.

Simons TJB (1988) Calcium and neuronal function. Neurosurg Rev 11:119-29.

Siwei H, Cuentas-Condori A, Miller DM (2019) NATF (Native and Tissue-Specific Fluorescence): A Strategy for Bright, Tissue-Specific GFP Labeling of Native Proteins in *Caenorhabditis elegans*. Genetics 212(2):387-95.

Speese SD, Ashley J, Jokhi V, Nunnari J, Barria R, Li Y, Ataman B, Koon A, Chang YT, Li Q, Moore MJ, Budnik V (2012) Nuclear envelope budding enables large ribonucleoprotein particle export during synaptic Wnt signaling. Cell 149:832-46.

Takada S, Fijumori S, Shinozuka T, Takada R, Mii Y (2017) Differences in the secretion and transport of Wnt proteins. J Biochem 161(1):1-7.

Tang X, Wu Y, Belenkaya TY, Huang Q, Ray L, Qu J, Lin X (2012) Roles of N-glycosylation and lipidation in Wg secretion and signaling. Dev Biol 364(1):32-41.

Torisu Y, Watanabe A, Nonaka A, Midorikawa Y, Makuuchi M, Shimamura T, Sugimura H, Niida A, Akiyama T, Iwanari H, Kodama T, Zeniya M, Aburatani H (2008) Human homolog of NOTUM, overexpressed in hepatocellular carcinoma, is regulated transcriptionally by beta-catenin/TCF. Cancer Sci 99(6):1139-46.

Traister A, Shi W, Filmus J (2008) Mammalian Notum induces the release of glypicans and other GPI-anchored proteins from the cell surface. Biochem J 410:503-11.

Tremble PM, Lane TF, Sage EH, Werb Z (1993) SPARC, a secreted protein associated with morphogenesis and tissue remodeling, induces expression of metalloproteinases in fibroblasts through a novel extracellular matrix-dependent pathway. J Cell Biol 121(6):1433-44.

Uruno T, Liu J, Zhang P, Fan Yx, Egile C, Li R, Mueller SC, Zhan X (2001) Activation of Arp2/3 complex-mediated actin polymerization by cortactin. Nat Cell Biol 3:259-66.

Vannahme C, Schübel S, Herud M, Gösling S, Hülsmann H, Paulsson M, Hartmann U, Maurer P (1999) Molecular Cloning of Testican-2: Defining a Novel Calcium-Binding Proteoglycan Family Expressed in Brain. J Neurochem 73(1):12-20.

Vijayakrishnan N, Woodruff, EA III, Broadie K (2009) Rolling blackout is required for bulk endocytosis in non-neuronal cells and neuronal synapses. J Cell Sci 122:114-25.

Wang Shouwen, Krinks M, Lin K, Luyten FP, Moos M Jr (1997) Frzb, a Secreted Protein Expressed in the Spemann Organizer, Binds and Inhibits Wnt-8. Cell 88(6):757-66.

Yan D, Wu Y, Feng Y, Lin S-C, Lin X (2009) The core protein of glypican Dally-like determines its biphasic activity in wingless morphogen signaling. Dev Cell 17:470-81.

Yook KJ, Proulx SR, Jorgensen EM (2001) Rules of Nonallelic Noncomplementation at the Synapse in Caenorhabditis elegans. Genetics 158(1):209-20.

Zecca M, Basler K, Struhl G (1996) Direct and Long-Range Action of a Wingless Morphogen Gradient. Cell 87(5):833-44.

Zhai L, Chaturvedi D, Cumberledge S (2004) *Drosophila* Wnt-1 Undergoes a Hydrophobic Modification and Is Targeted to Lipid Rafts, a Process That Requires Porcupine. J Biol Chem 279(32):33220-7

Wg Overexpression	Notum Mutant	Cow Mutant
NMJ area	NMJ area	NMJ area
Type 1b boutons	Type 1b boutons	Type 1b boutons
Satellite boutons	Satellite boutons	Satellite boutons
Clustered boutons	Clustered boutons	Clustered boutons
Branches	Branches	Branches
Evoked neurotransmission strength	Evoked neurotransmission strength	Evoked neurotransmission strength
Extracellular Wg ligand	Extracellular Wg ligand	Extracellular Wg ligand
Brp	Brp	Brp
GluRs	GluRs	GluRs
Mini neurotransmission frequency	Mini neurotransmission frequency	Mini neurotransmission frequency
Mini neurotransmission amplitude	Mini neurotransmission amplitude	Mini neurotransmission amplitude
Futsch loops	Futsch loops	Futsch loops
Rollover Time	Rollover Time	Rollover Time
Nuclear Fz2*	Nuclear Fz2	Nuclear Fz2
Synaptic Fz2	Synaptic Fz2	Synaptic Fz2
Enlarged endosomes	Enlarged endosomes	Enlarged endosomes
FM dye loading	FM dye loading	FM dye loading
SV density	SV density	SV density

Table 3: **Comparison of phenotypes observed.**

Wg overexpression, Notum mutants, and Cow mutants have many overlapping phenotypes, but some are separable. Green = the phenotype was increased, Red = the phenotype was decreased, Yellow = the phenotype was unchanged, Blue = the phenotype was not tested. Asterisk* indicates that this finding has been shown in the literature, but not verified in this body of work.

Supplemental Figures

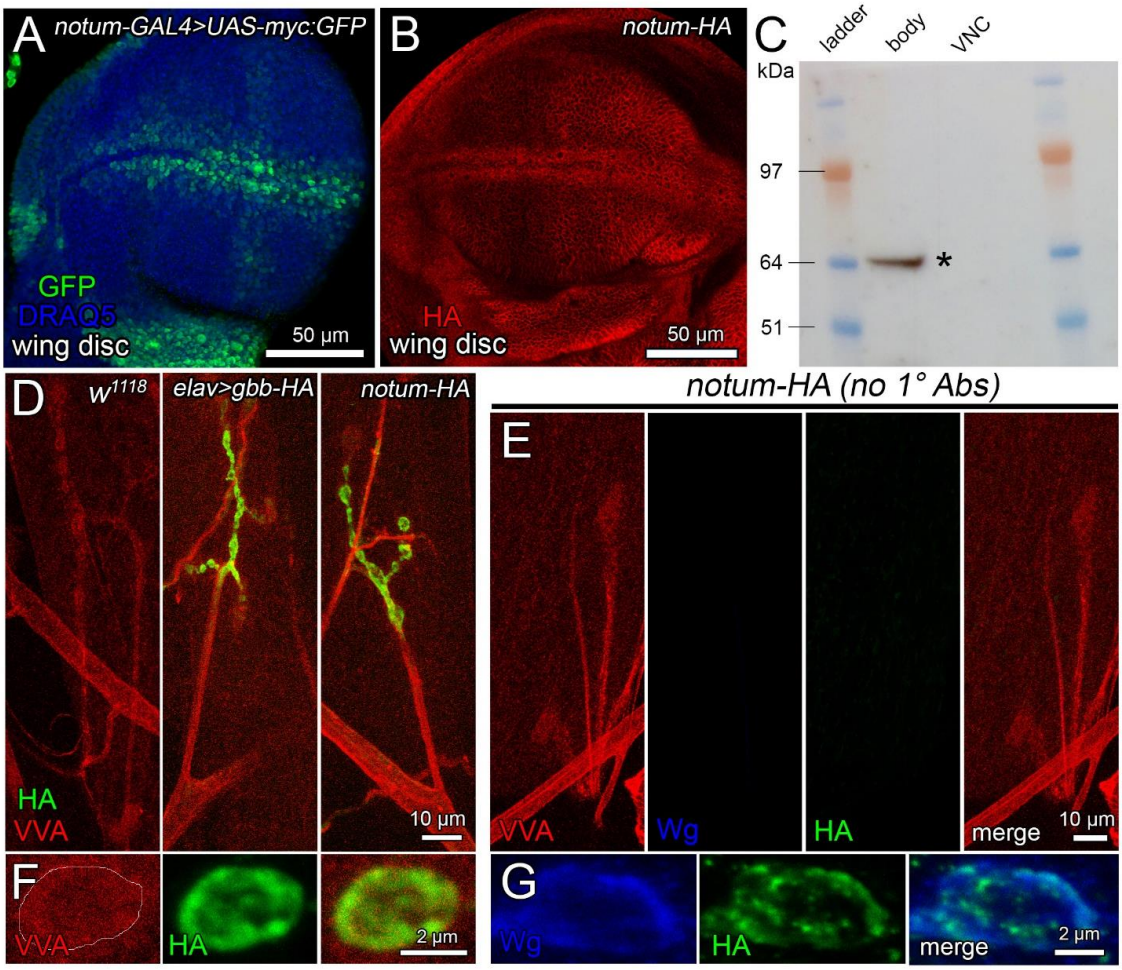

Fig. S1. CRISPR/Cas9 Notum-HA expression and controls

A) Wandering 3rd instar wing disc expressing UAS-myc:GFP under *notum*-Gal4 control labeled with anti-GFP (Notum, green) and DRAQ5 (nuclei, blue). **B**) Wing disc from Notum-HA line labeled with anti-HA (Notum, red). **C**) Anti-HA Western blot of Notum-HA line 3rd instar ventral nerve cord (VNC; neurons) and body (muscles). The Notum-HA predicted molecular weight is 65 kDa (asterisk). **D**) Muscle 4 NMJs detergent-free labels with extracellular VVA-TRITC (red) and anti-HA (green) in w^{1118} (negative control, left), *elav*-Gal4>UAS-Gbb-HA (positive control, middle) and CRISPR Notum-HA line (right). **E**) No primary antibody control of Notum-HA line labeled detergent-free with VVA (red), anti-Wg (blue) and anti-HA (Notum, green). **F**) High magnification single NMJ bouton image of Notum-HA labeled with VVA (red) and anti-HA (green). **G**) High magnification detergent-free single bouton image of anti-Wg (blue) co-labeled with Notum-HA (green).

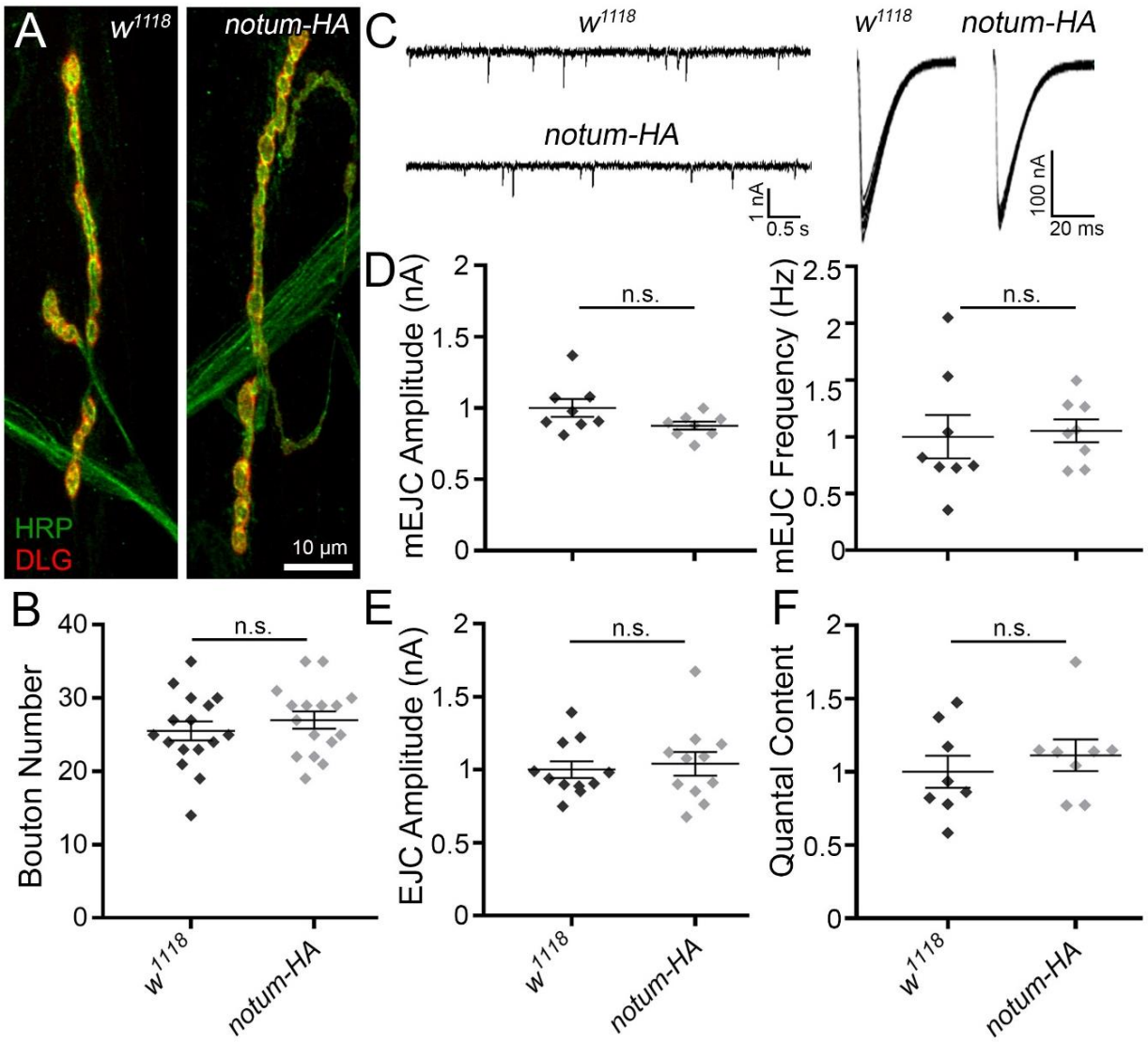

Fig. S2. NMJ structure/function in Notum-HA line indistinguishable from controls

A) Representative confocal images of muscle 4 NMJs co-labeled for the presynaptic membrane marker anti-HRP (green) and postsynaptic scaffold anti-DLG (red) in *w*^{1118} genetic background control (left) and the CRISPR/Cas9 Notum-HA line (right). **B**) The number of type 1b synaptic boutons quantified in each genotype, showing no significant difference (n=16). **C**) Sample miniature excitatory junctional current (mEJC; left) and nerve stimulation-evoked excitatory junctional current (EJC; right) traces (1.0 mM Ca^{2+}) from *w*^{1118} background control and Notum-HA line. **D**) Quantification of mEJC amplitude and frequency (n=8). **E**) Quantification of EJC amplitude (n=11). F) Quantification of quantal content (n=8). There is no significant difference in any parameter (ns=p>0.05).

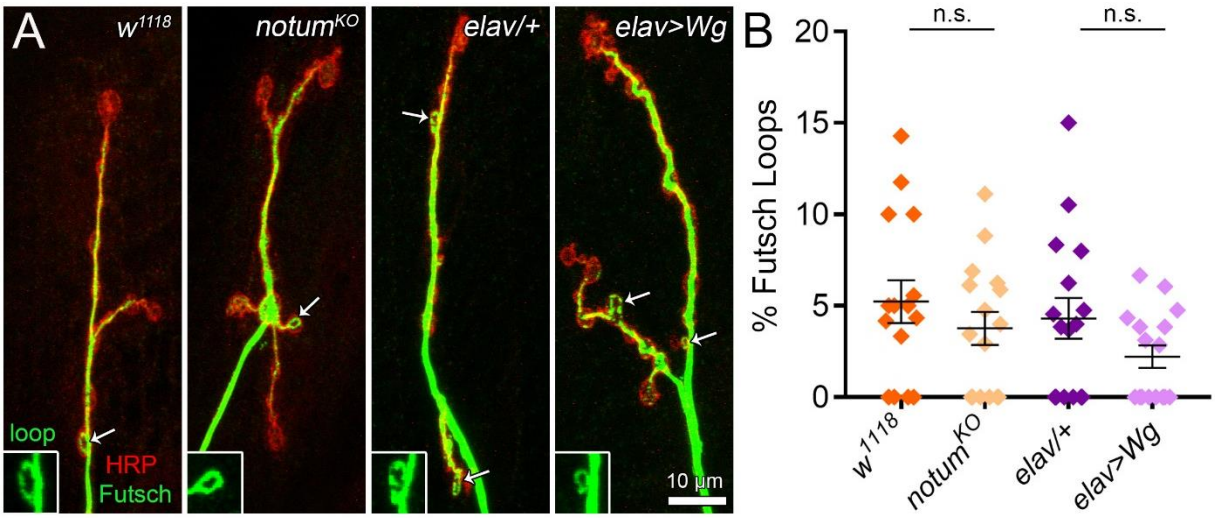

Fig. S3. NMJ Futsch loops are not altered by Wg overexpression or *notum^{KO}*

A) Representative muscle 4 NMJs co-labeled for the presynaptic membrane marker anti-HRP (red) and microtubule associated anti-Futsch/MAP1B (green) in *w^{1118}* genetic background control vs. *notum^{KO}* null mutant (left) and *elav*-Gal4/+ transgenic control vs. *elav*-Gal4>UAS-*Wg* overexpression (right). Lower panel insets show high magnification examples of Futsch-positive microtubule loops for each genotype. **B**) Quantification of the percentage of Futsch-positive microtubule loop containing synaptic boutons per NMJ terminal in all four above genotypes (n≥15; ns=p>0.05).

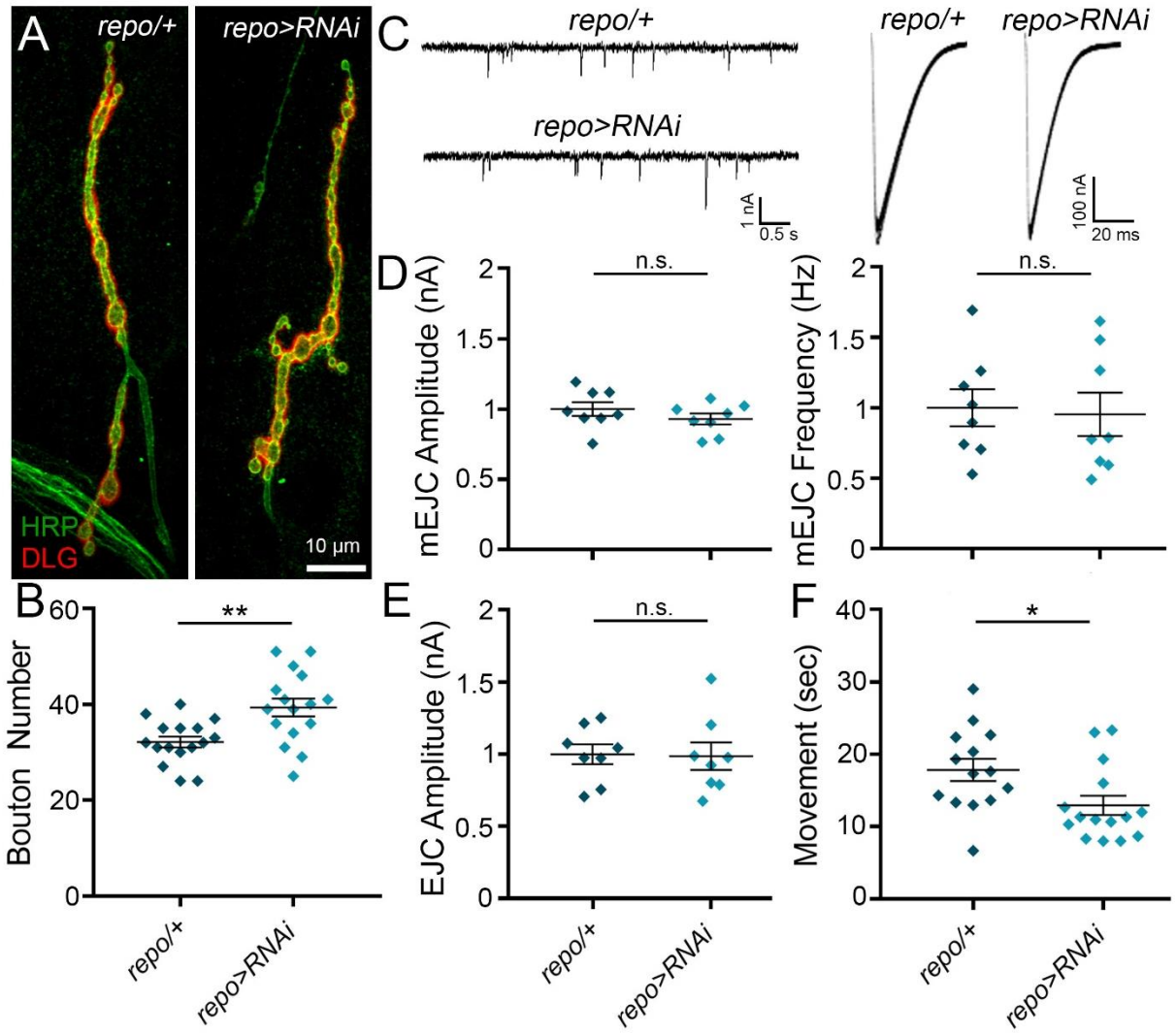

Fig. S4. Glial-secreted Notum regulates NMJ development and motor output

A) Representative confocal images of muscle 4 NMJs co-labeled for presynaptic anti-HRP (green) and postsynaptic anti-DLG (red) in glial driver control (*repo*-Gal4/+) and glial RNAi *notum* knockdown (*repo*-Gal4>*notum:RNAi*). **B**) Quantified synaptic bouton number shows a significant increase with the glial notum knockdown (n=16; p=0.003). **C**) Sample miniature excitatory junctional current (mEJC) and nerve stimulation-evoked excitatory junctional current (EJC; right) traces (1.0 mM Ca2+) from *repo*-Gal4/+ control vs. *repo*-Gal4>*notum:RNAi*. Quantification of mEJC amplitude and frequency (n=8) (**D**), and EJC amplitude (n=8) (**E**), showing no significant difference in any parameter (ns=p>0.05). **F**) Quantification of coordinated movement rollover reaction time shows a significantly faster response with glial RNAi *notum* knockdown (n≥15, p=0.022).

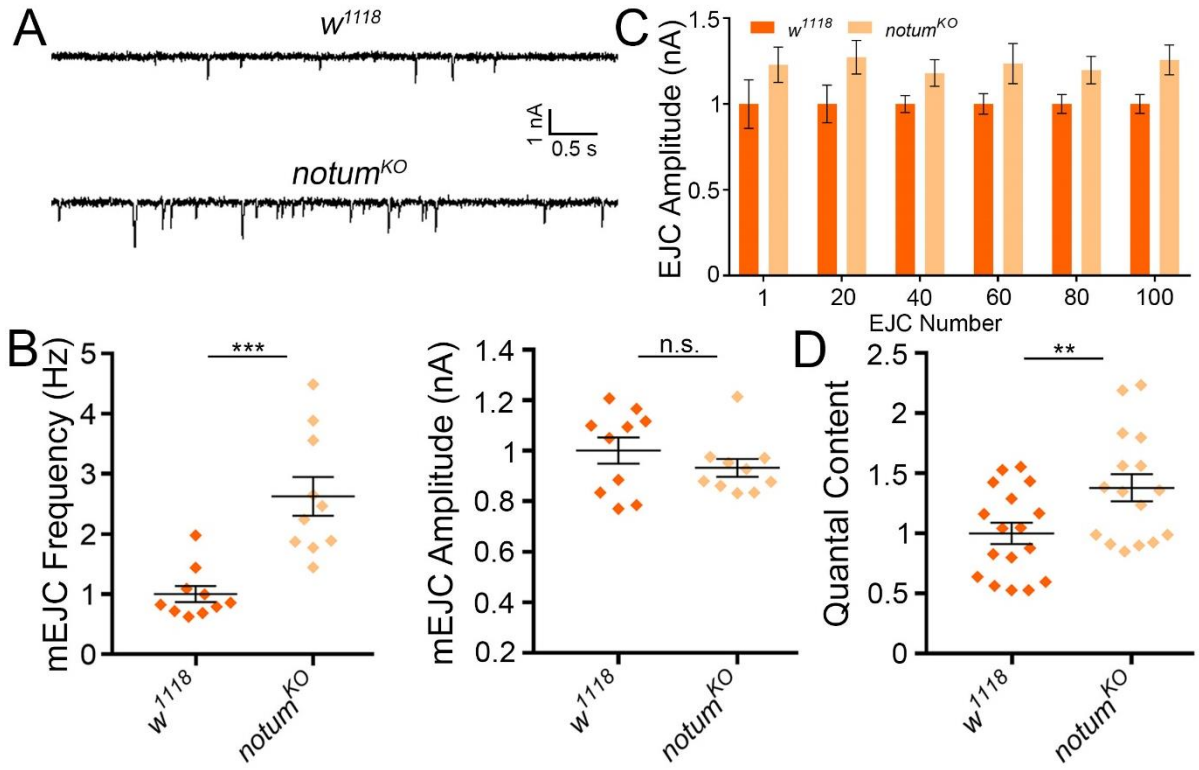

Fig. S5. Functional electrophysiology changes in *notum*^{KO} NMJ synapses

A) Sample miniature excitatory junctional current (mEJC) traces (1.0 mM Ca2+) in *w*^{1118} genetic background control vs. the *notum*^{KO} null mutant. **B**) Quantification of mEJC frequency (left; n=10, p=0.0002) and amplitude (right; n=10, p=0.295). **C**) Quantification of nerve stimulation-evoked excitatory junctional current (EJC) amplitudes in *w*^{1118} vs. *notum*^{KO} during high frequency 20Hz stimuli trains, showing maintained transmission elevation in *notum*^{KO} for 100 responses. **D**) Quantification of the EJC quantal content in *w*^{1118} vs. *notum*^{KO} shows a highly significant increase in the mutant (n≥17, p=0.012).

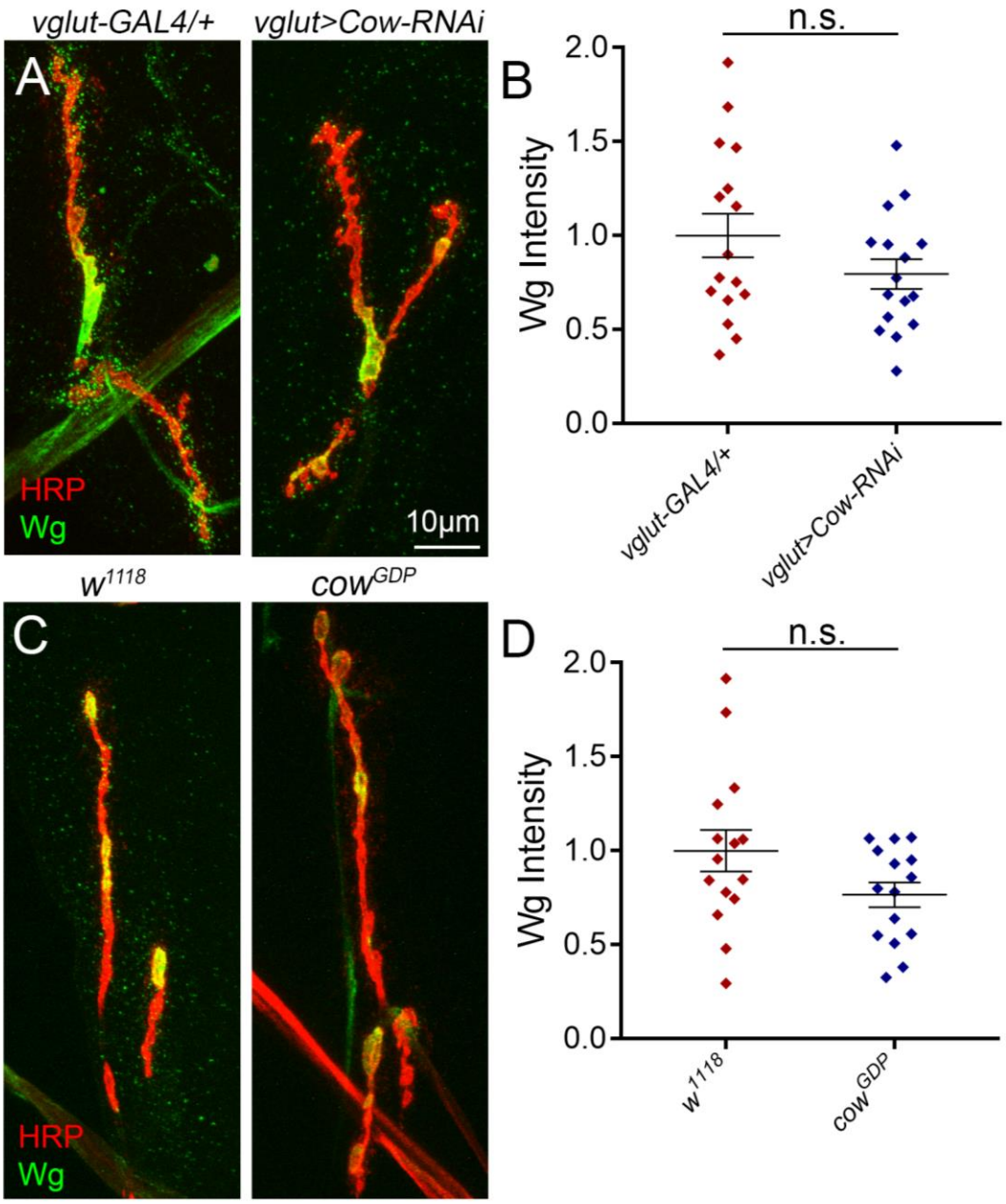

Fig. S6: Extracellular Wg is unchanged in *cow* mutants

(A) Confocal images of the muscle 4 NMJ co-labeled with presynaptic HRP marker (red) and Wg (green) in the vglut-GAL4/+ genetic background control and vglut-GAL4 driving a UAS-Cow-RNAi construct. (B) Quantified fluorescence Wg intensity of images from A, normalized to control. (C) NMJs in the genetic background control (w^{1118}) and *cow* null (cow^{GDP}). (D) Quantified fluorescence Wg intensity of images from C, normalized to control. Significance: not significant (n.s.).

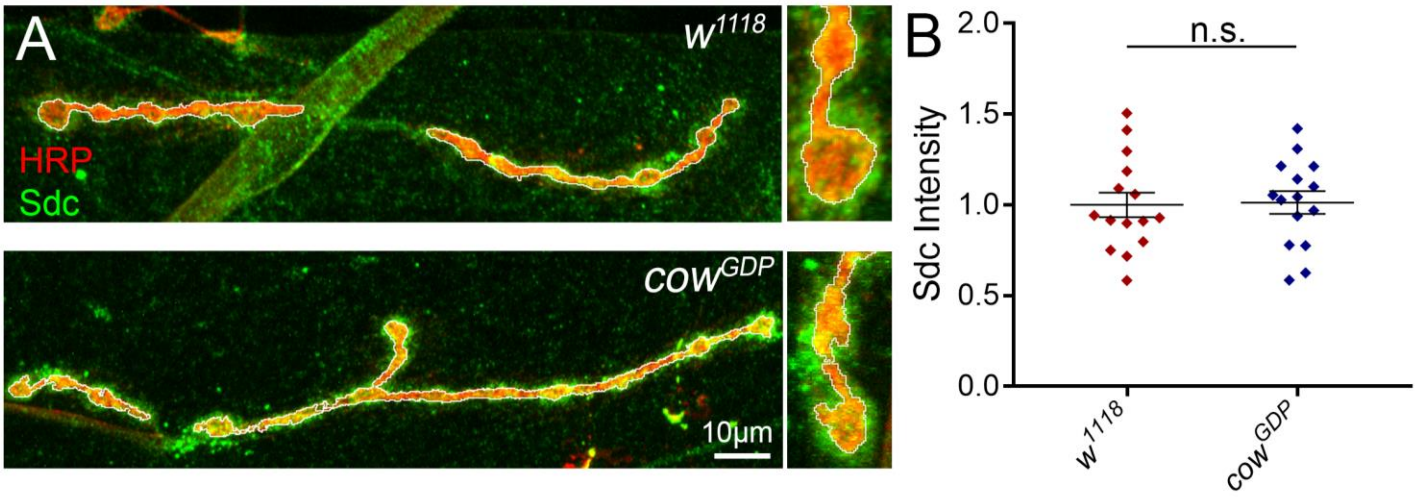

Fig. S7: Extracellular neuronal-associated Sdc is unchanged in *cow* mutants

(A) Confocal images of the muscle 4 NMJ co-labeled with presynaptic HRP marker (red) and Sdc (green) in the genetic background control (w^{1118}) and *cow* null (cow^{GDP}). The white line around the synaptic boutons is where the signal was measured. Insets show that the distribution of Sdc signal surrounding boutons may be changed in the cow^{GDP} condition relative to the w^{1118} control. (B) Quantified fluorescence Sdc intensity of images from A, normalized to control. Significance: not significant (n.s.).

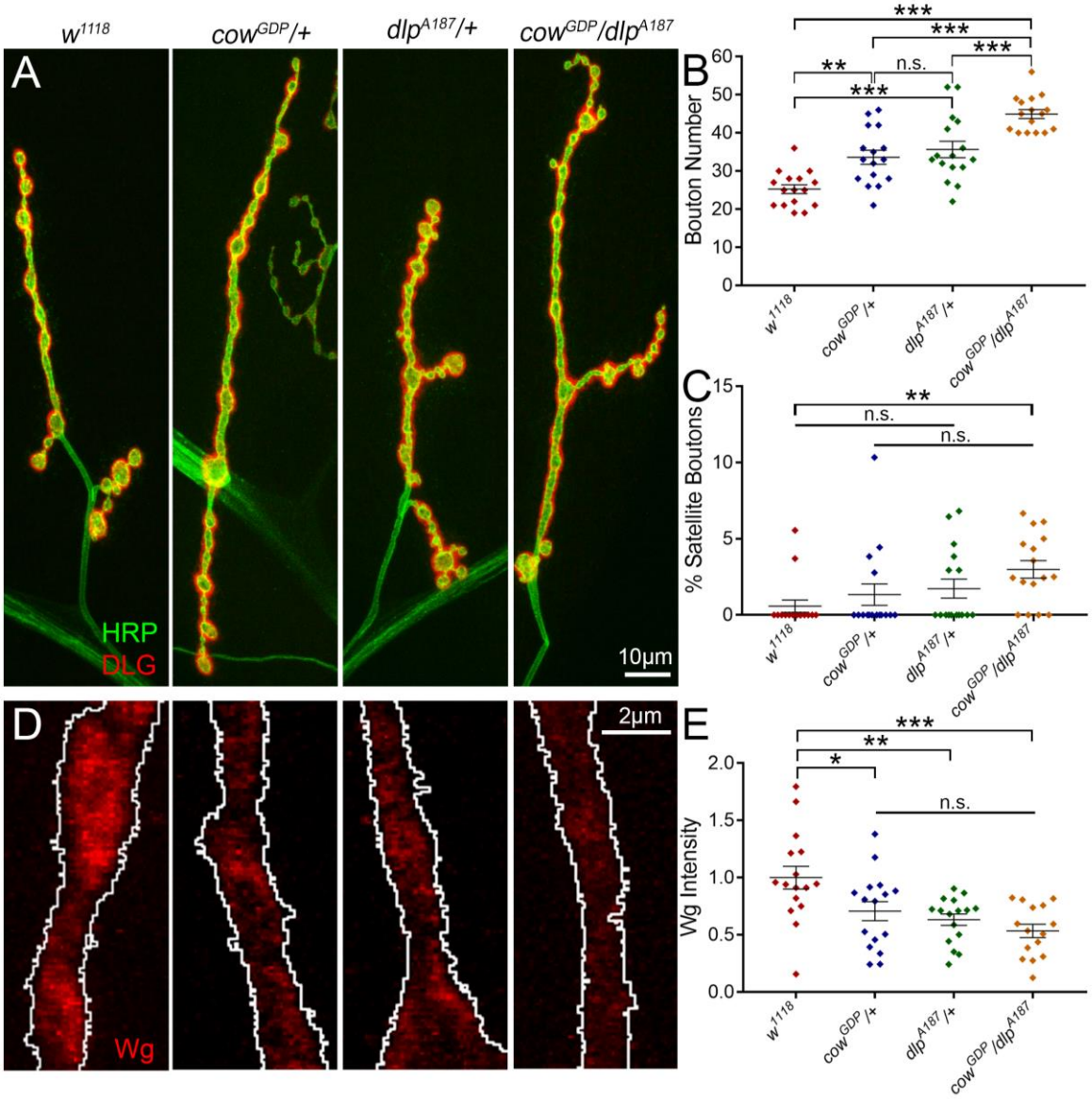

Fig. S8: Cow and Dlp act on functionally related processes to regulate bouton number

(A) Confocal images of the muscle 4 NMJ co-labeled with presynaptic HRP marker (green) and postsynaptic DLG (red) in the genetic background control (w^{1118}), a *cow* null heterozygote (cow^{GDP}/+), a *dlp* null heterozygote (dlp^{A187}/+), and a transheterozygote (cow^{GDP}/dlp^{A187}). (B) Quantified bouton number from the indicated genotypes. (C) Quantified percentage of satellite boutons from the indicated genotypes. (D) Muscle 4 NMJs labeled with Wg (red). The white line around the synaptic boutons is where the signal was measured. (E) Quantified fluorescence Wg intensity of images from D, normalized to control. Significance: *$P \leq 0.05$, **$P \leq 0.01$, ***$P \leq 0.001$ and $P > 0.05$ (not significant, n.s.).

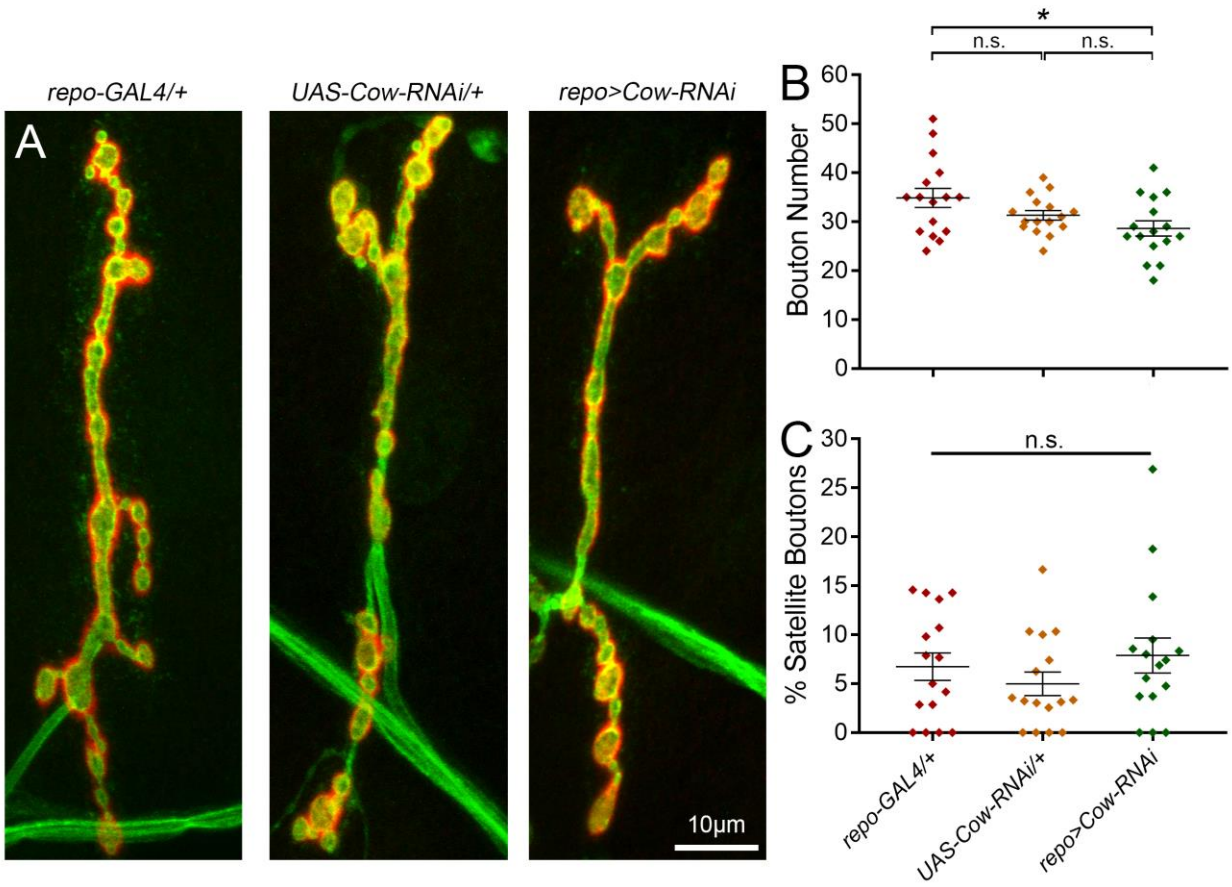

Fig. S9: Glial-specific Cow KD doesn't affect bouton number or size

(A) Confocal images of the muscle 4 NMJ co-labeled with presynaptic HRP marker (green) and postsynaptic DLG (red) in the genetic background GAL4 driver control (*repo-GAL4/+*), UAS responder control (*UAS-Cow-RNAi/+*), and a glial cow KD (*repo-GAL4>UAS-Cow-RNAi*). (B) Quantified bouton number from the indicated genotypes. (C) Quantified percentage of satellite boutons from the indicated genotypes. Significance: **P*≤0.05 and *P*>0.05 (not significant, n.s.).